



*The Stabilisation Process in Mesophase Pitch Based Carbon
Materials*

By

James Anthony Sansom

Submitted in accordance with the requirements for the degree of
Doctor of Philosophy

The University of Leeds
Institute for Materials Research

August 2008

The candidate confirms that the work submitted is his own and that appropriate credit has
been given where reference has been made to the work of others

This copy has been supplied on the understanding that this is copyright material and that
no quotation from the thesis may be published without proper acknowledgement



Acknowledgement

I wish to express my gratitude to my supervisor, Professor Brian Rand, for his constructive advice and support. I would also like to thank Dr Aidan Westwood for his technical guidance and help through out the course of my study.

I want thank my parents for the sacrifices they made to afford me this opportunity to study towards my doctorate, with out them I would not have been able to write this thesis. I also like to extend my undying gratitude to my grandparents who have always been a constant source of inspiration throughout my life, without them I would not be the man I am today.

I want to thank my friends for providing me with encouragement and support. I also want to express my sincere thanks to all the members of the Leeds carbon group and the members of the Leeds Institute for Materials Research for their assistance throughout this study. With special thanks going to Dr Anton Anton –Arulrajah, Donald Forder, Dr Andy Ross, Dr Eric Condliffe, Peter Thompson, Martin Huscroft and Robert Marshall.

Final I would like to also thank Morgan Carbon for their financial support and guidance throughout my study, in particular Dr Chris Stirling and Dr Robert Davies.

Abstract

The primary aim of this work is to investigate the stabilisation process and how it impacts on mesophase products. The stabilisation step in the production of mesophase products has long been of great interest. This study will be broken down to assess the physical and chemical changes that occur during the stabilisation of mesophase products (in particular highly orientated mesophase pitch-based tapes); the transport mechanisms involved in the stabilisation process, how subsequent carbonisation of the mesophase pitch-based products are affected by the stabilisation conditions and how stabilisation affects the optical and mechanical properties of the mesophase pitch-based tapes.

Highly oriented mesophase pitch-based (ARMPH) carbon tapes were oxidatively stabilised at 160°C, 240°C and 300°C for 5hrs and 25hrs. A weight gain as a result of the incorporation of oxygen was observed with increasing temperature and time. Improved structural ordering of the tapes was also noticed with increased stabilisation time and temperature.

A clear correlation between the softening point and oxygen content of the mesophase pitch-based tapes was evident, as oxygen content increases so does the softening point of the mesophase pitch-based tapes influenced by the distribution of oxygen through out the tapes.

Carbonisation of the stabilised material showed the bulk of the weight loss takes place between 400-700°C in the form of evolved CO, CO₂ and hydrocarbons. Improved dimensional stability and morphology was also demonstrated in mesophase pitch-based tapes which were stabilised to greater degrees.

Stabilisation conditions were also seen to play a key role in determining the final mechanical properties of the mesophase pitch-based tapes. Higher temperatures of stabilisation were seen to greatly improve the tensile strength of the tapes. The maximum values of strain to failure were recorded for tapes stabilised to 240°C for 25hrs. The mechanical reliability of the tapes was also seen to improve with increasing temperature of stabilisation.

Table of contents

| | | |
|------|---|----|
| 1 | Introduction | 1 |
| 2 | Literature Review | 4 |
| 2.1 | Forms of carbon | 4 |
| 2.2 | What is pitch? | 5 |
| 2.3 | Pitch production | 5 |
| 2.4 | Mesophase pitch | 8 |
| 2.5 | Mesophase formation | 9 |
| 2.6 | History of mesophase production | 12 |
| 2.7 | Synthesis of mesophase pitch | 13 |
| 2.8 | Mesophase modification | 16 |
| 2.9 | Aspects of Carbon Fibre/Tapes Manufacturing | 18 |
| 2.10 | Production of mesophase carbon fibres/tapes | 19 |
| 2.11 | Orientation of carbon fibres/tapes | 20 |
| 2.12 | Conventional method of stabilisation | 24 |
| 2.13 | Oxidative stabilisation | 24 |
| 2.14 | Alternative methods of stabilisation | 25 |
| 2.15 | Chemistry of stabilisation | 27 |
| 2.16 | Weight gain/loss during stabilisation | 30 |
| 2.17 | Diffusion of oxygen | 34 |
| 2.18 | Factors affecting stabilisation | 38 |
| 2.19 | Stabilisation summary | 40 |
| 3 | Aims and objectives | 42 |
| 3.1 | Aims | 42 |
| 3.2 | Objectives | 43 |
| 3.3 | Stabilisation chemistry | 43 |
| 3.4 | Diffusion of oxygen during stabilisation | 44 |
| 3.5 | Mechanical effects of stabilisation | 44 |
| 4 | Characterisation Techniques | 45 |
| 4.1 | Scanning Electron Microscope (SEM) | 45 |
| 4.2 | XRD (Pole figures) | 47 |
| 4.3 | Thermo-gravimetric Analysis (TGA) | 49 |
| 4.4 | Fourier Transform Infrared (FTIR) Spectroscopy | 51 |
| 4.5 | Thermo-gravimetric – Fourier Transform Infrared (TGA-FTIR) Spectroscopy | 53 |
| 4.6 | CHNO Chemical Analysis | 55 |
| 4.7 | Optical Microscopy | 57 |
| 4.8 | Atomic Force Microscopy (AFM) (Micro-thermal Analysis) | 60 |
| 4.9 | Electron Probe Microanalysis (EPMA) | 62 |
| 4.10 | Pyrolysis-Gas Chromatography-Mass Spectrometry (Py-GC-MS) | 63 |
| 4.11 | X-ray Photoelectron Spectroscopy (XPS) | 64 |
| 4.12 | Raman Microscopy | 67 |
| 4.13 | Mechanical Testing | 69 |
| 5 | Processing of mesophase pitch-based tapes | 75 |
| 5.1 | Pitch comparison | 75 |
| 5.2 | Preparation of mesophase pitch based carbon tapes for stabilisation | 77 |

| | |
|--|-----|
| 5.3 Examination of spun tapes | 83 |
| 5.4 Stabilisation of tapes | 85 |
| 6 Stabilisation | 88 |
| 6.1 Weight change upon stabilisation of tapes | 88 |
| 6.2 Evolution of gases during the stabilisation step | 93 |
| 6.3 Change in chemistry during the stabilisation step | 96 |
| 6.4 FTIR characterisation of stabilised mesophase pitch-based tapes | 106 |
| 6.5 XPS characterisation of stabilised mesophase pitch based tapes | 113 |
| 6.6 Py-GC-MS characterisation of mesophase pitch-based carbon tapes | 123 |
| 6.8 Stabilisation of mesophase pitch-based tapes weight change and chemistry conclusion..... | 133 |
| 7 Oxygen transport study | 137 |
| 7.1 The effect of stabilisation on molecular ordering of mesophase pitch-based tapes | 137 |
| 7.2 Characterisation of stabilised mesophase pitch-based tapes using Micro-thermal Analysis Atomic Force Microscope | 141 |
| 7.3 Electron probe micro analysis (EPMA) | 151 |
| 7.4 Oxygen transport conclusion..... | 155 |
| 8 Carbonisation of stabilised tapes..... | 157 |
| 8.1 Weight change upon carbonisation | 157 |
| 8.2 Evolution of gases during carbonisation of stabilised mesophase pitch-based tapes | 162 |
| 8.3 Examination of the gases evolved during carbonisation of stabilised mesophase pitch-based tapes. | 175 |
| 8.4 Pyrolysis-gas chromatography-mass spectrometry characterisation of carbonised mesophase pitch-based tapes..... | 178 |
| 8.5 Raman characterisation of carbonised mesophase pitch-based carbon tapes..... | 184 |
| 8.6 Carbonisation of stabilised mesophase pitch-based tapes weight change and chemistry conclusion..... | 188 |
| 9 Optical characterisation of stabilised tapes | 192 |
| 9.1 Optical conclusion..... | 201 |
| 10 Mechanical properties | 203 |
| 10.1 Strength and engineering Young's modulus of mesophase pitch -based carbon tapes..... | 203 |
| 10.2 Weibull Analysis..... | 216 |
| 10.3 Mechanical properties: conclusion..... | 220 |
| 11 Overall conclusion..... | 222 |
| 12 Future work | 224 |
| 13 References | 226 |
| 14 Publications resulting from this work | 232 |
| 15 Appendix | 233 |

List of figures

| | |
|---|----|
| Figure 1 A Carbon Atom (www.eia.doe.gov/.../sources/electricity.html) | 4 |
| Figure 2 Concept design of an SCF extraction process for fractionating petroleum pitch (Hutchenson, Roebbers et al. 1991) | 7 |
| Figure 3 Definition of director orientation of a uniaxial discotic nematic liquid crystalline material; the direction n is the average orientation of the units normal to the disc-like molecules in a discotic nematic phase. (Yan and Rey et al 2002) | 8 |
| Figure 4 Spider Wedge molecule of mesophase constituent molecules, (Mochida, Korai et al. 2000)..... | 9 |
| Figure 5 Mesophase nucleation, growth and coalescence (Benn 1989)..... | 11 |
| Figure 6 Catalytic condensation of aromatic hydrocarbon with HF/BF ₃ (Mochida, Korai et al. 2000)..... | 14 |
| Figure 7 Process flow diagram for commercial production of naphthalene-derived AR pitch (Mochida 1995) | 15 |
| Figure 8 Flow diagram representing the route to carbon fibre/tape and its bulk material | 18 |
| Figure 9 Schematic representation of melt spinning apparatus (Edie et al 1998)..... | 19 |
| Figure 10 Summary of the effects of process and material parameters on the tensile stress in the filament (Edie, Fox et al. 1986)..... | 20 |
| Figure 11 Schematic diagram of mesophase pitch based fibre formation (Galanopoulos 2003)..... | 21 |
| Figure 12 transverse textures of mesophase pitch carbon fibres (Edie et al 1998)..... | 22 |
| Figure 13 Preferred orientation of the as-spun circular fibres and tapes as a function of transverse areas. Full peak width at half maximum intensity (FWHM value(°)) is a measure of the preferred degree of orientation on the fibres and tapes calculated using XRD pole figures, the lower the FWHM value (°) the higher the degree of preferred orientation, Transverse area (µm) ² refers of the transverse cross-sectional area of the fibres and tapes. (Lu et al 2002)..... | 23 |
| Figure 14 Change in relative concentration of functional groups during stabilisation at the heating rate of 0.5 deg/min based on solid state ¹³ C NMR spectra of oxidised fibres in the aromatic and aliphatic regions (Matsumoto et al 1992)..... | 29 |
| Figure 15 Weight change curves for mesophase pitch oxidation: filled circles = 240 deg/C. filled squares = 270 deg/C. filled diamonds = 290 deg/C. filled triangle = 320 deg/C. filled cross = 340 deg/C (Drbohlav and Stevenson et al 1995) | 30 |
| Figure 16 Variation in oxygen uptake and hydrogen loss with weight gain during the oxidation stabilisation of mesophase in the temperature range of 200-300 °C (Fanjul, Granda et al. 2001) | 31 |
| Figure 17 Variation of oxygen uptake and hydrogen loss with weight gain during oxidative stabilisation of (a) coal tar derived mesophase (b) naphthalene derived mesophase in the temperature range 200-300 °C (Fanjul, Granda et al. 2002)..... | 32 |
| Figure 18 The weight change for 100% mesophase heat-treatment at various temperatures (Kowbel, Wapner et al. 1988) | 33 |

| | |
|--|----|
| Figure 19 Effect of oxidation temperature and heating rate on the oxygen content of oxidised fibres. Heating rate; O = 0.5°C/min Δ=1.0°C/min, □= 2.0°C/min (Matsumoto and Mochida et al 1992)..... | 33 |
| Figure 20 Oxygen distribution profiles in fibres, as-spun and after oxidation to 250°C at a heating rate of 0.5°C/min pf: as-spun fiber (Matsumoto and Mochida et al 1993) | 36 |
| Figure 21 Oxygen distribution profiles in fibres oxidised at a heating rate of 0.5/min to 250°C and 350°C (Matsumoto and Mochida et al 1993)..... | 36 |
| Figure 22 Stabilisation achieved in carbon fibres when heat treated to (a) 270°C and (b) 160°C and maintained there for 10 hrs (Galanopoulos 2003)..... | 39 |
| Figure 23 Schematic Diagram of Sample Prep for ESEM..... | 46 |
| Figure 24 Schematic diagram of pole figure sample prep | 48 |
| Figure 25 Schematic representation of the Thermo Gravimetric Analysis equipment..... | 50 |
| Figure 26 Illustration of TGA-FTIR | 55 |
| Figure 27 Library IR spectra of specific molecules (CH ₄ , C ₂ H ₆ , CO, CO ₂ and H ₂ O)..... | 55 |
| Figure 28 Polarised light optical microscopy and interference colours (Marsh 1989)..... | 58 |
| Figure 29 Schematical representation of tape sample prep for optical mounting..... | 59 |
| Figure 30 Schematic diagram of the micro-thermal analyser | 62 |
| Figure 31 Conventional XPS hemispherical spectrometer with input lens (Coxon, Krizek et al. 1990)..... | 64 |
| Figure 32 The photoemission process | 65 |
| Figure 33 schematic cross section of a concentric hemispherical analyser (CHA) | 65 |
| Figure 34 Raman spectra for various carbons, taken at room temperature (Pelletier 1999) | 68 |
| Figure 35 Schematical diagram of the original tensile sample showing gauge length of 20mm..... | 71 |
| Figure 36 Pneumatic grips used to hold tensile samples..... | 73 |
| Figure 37 Typical example of an original stress strain curve produced when mechanically testing the mesophase pitch based tapes which have under gone stabilisation (300°C for 25hrs in Oxygen)..... | 73 |
| Figure 38 Weight loss patterns upon carbonisation in nitrogen for different batches of pitch..... | 76 |
| Figure 39 Schematical diagram of spinning apparatus | 77 |
| Figure 40 Graphical representation of the de-gassing route..... | 79 |
| Figure 41 Schematic of pressure vessel showing where CHNO degas samples where obtained from | 80 |
| Figure 42 Schematical diagram of spinning operation..... | 81 |
| Figure 43 (a) Mesophase tape extruding through die, (b) Spinning apparatus | 82 |
| Figure 44 SEM images showing different tape textures available with controlled shear rate 1-2 tape texture produced at a shear rate of shear rate 494 s ⁻¹ , 1-3 tape texture produced at a shear rate of shear rate of 783 s ⁻¹ | 83 |
| Figure 45 (a) Defected mesophase pitch tape, (b) undefected mesophase pitch tape | 84 |
| Figure 46 Pole figure of 240°C 5hrs stabilised mesophase pitch carbon tape spun at 1.5bar and 295°C | 84 |
| Figure 47 3D representation of a pole figure for a tape which has been carbonised to 1600°C | 85 |

| | |
|--|-----|
| Figure 48 schematical representation of the "stabilisation sled"..... | 86 |
| Figure 49 Weight gain experienced by tapes during stabilisation by heating in air to various final temperatures | 88 |
| Figure 50 Weight gain experienced by tapes during stabilisation by heating in oxygen to various final temperatures | 89 |
| Figure 51 Evolution of evolved gases during stabilisation (a) 160°C 5hrs in air (b) 240°C 5hrs in air (c) 300°C 5hrs in air (d) 160°C 5hrs in oxygen (e) 240°C 5hrs in oxygen (f) 300°C 5hrs in oxygen, all samples heated at 2°C min ⁻¹ . Data acquired using TGA-FTIR, wavenumber range used for CO ₂ analysis 2250-2350 cm ⁻¹ | 95 |
| Figure 52 Master Van Krevelen Plot (Van Krevelen 1957)..... | 97 |
| Figure 53 Van Krevelen plot for samples stabilised over a range of time and temperatures in air and oxygen | 98 |
| Figure 54 Van Krevelen plot for all stabilisation data at varying time and temperatures in oxygen | 99 |
| Figure 55 CHO elemental weight change with stabilisation at 160°C with respect to time for oxygen stabilised samples | 100 |
| Figure 56 CHO elemental weight change with stabilisation at 180°C with respect to time for oxygen stabilised samples | 100 |
| Figure 57 % CHO weight change for stabilisation at 200°C with respect to time for oxygen stabilised samples | 101 |
| Figure 58 % CHO weight change for stabilisation at 240°C with respect to time for oxygen stabilised samples | 101 |
| Figure 59 % CHO weight change for stabilisation at 300°C with respect to time for oxygen stabilised samples | 102 |
| Figure 60 Effect of stabilisation at 160°C in oxygen on C/H and C/O atomic ratio..... | 103 |
| Figure 61 Effect of stabilisation at 180°C in oxygen on C/H and C/O atomic ratio..... | 103 |
| Figure 62 Effect of stabilisation at 200°C in oxygen on C/H and C/O atomic ratio..... | 104 |
| Figure 63 Effect of stabilisation at 240°C in oxygen on C/H and C/O atomic ratio..... | 104 |
| Figure 64 Effect of stabilisation at 300°C in oxygen on C/H and C/O atomic ratio..... | 105 |
| Figure 65 FTIR Spectra for 160°C stabilised tape in oxygen (a) Green (b) 160°C 1hr (c) 160°C 2hrs (d) 160°C 3hrs (e) 160°C 4hrs (f) 160°C 5hrs..... | 108 |
| Figure 66 FTIR spectra for 240°C stabilised tapes in oxygen (a) Green (b) 240°C 1hr (c) 240°C 2hrs (d) 240°C 3hrs (e) 240°C 4hrs (f) 240°C 5hrs..... | 108 |
| Figure 67 FTIR Spectra between 1200 - 2000 cm ⁻¹ for samples stabilised in oxygen (Graph A) (a) Green (b) 160°C 1hr (c) 160°C 2hrs (d) 160°C 3hrs (e) 160°C 4hrs (f) 160°C 5hrs and (Graph B) (a) Green (b) 240°C 1hr (c) 240°C 2hrs (d) 240°C 3hrs (e) 240°C 4hrs (f) 240°C 5hrs | 109 |
| Figure 68 (Graph A) FTIR spectra for tapes stabilised in air for 5 hrs over a range of temperatures, line; (a) Green (b) 160°C 5hrs in air (c) 240°C 5hrs in air (d) 300°C 5hrs in air. (Graph B) FTIR spectra for tapes stabilised in oxygen for 5 hrs over a range of temperatures, line; (a) Green (b) 160°C 5hrs in oxygen (c) 240°C 5hrs in oxygen (d) 300°C 5hrs in oxygen. | 110 |
| Figure 69 FTIR Spectra between 1200 - 2000 cm ⁻¹ for samples stabilised in oxygen (Graph A) (a) Green (b) 160°C 5hr in air (c) 240°C 5hrs in air (d) 300°C 5hrs air. (Graph | |

B) (a) Green (b) 160°C 5hrs in oxygen (c) 240°C 5hrs in oxygen (d) 300°C 5hrs in oxygen. 111

Figure 70 (Graph A) FTIR spectra for tapes stabilised in air for 25 hrs over a range of temperatures, line; (a) Green (b) 160°C 25hrs in air (c) 240°C 25hrs in air. (Graph B) FTIR spectra for tapes stabilised in oxygen for 5 hrs over a range of temperatures, line; (a) Green (b) 160°C 25hrs in oxygen (c) 240°C 25hrs in oxygen (d) 300°C 25hrs in oxygen 111

Figure 71 FTIR Spectra between 1200 - 2000 cm^{-1} for samples stabilised in oxygen (Graph A) (a) Green (b) 160°C 25hr in air (c) 240°C 25hrs in air (. (Graph B) (a) Green (b) 160°C 25hrs in oxygen (c) 240°C 25hrs in oxygen (d) 300°C 25hrs in oxygen. 112

Figure 72 XPS survey scan of Mesophase tapes which have been stabilised to (a) green tape (b) 160°C for 5hrs in oxygen (c) 160°C for 25hrs in oxygen (d) 240°C for 5hrs in oxygen (e) 240°C for 25hrs in oxygen (f) 300°C for 5hrs in oxygen (g) 300°C for 25hrs in oxygen. note small sulphur peaks can be observed at approximately 163.3eV in some survey scans..... 114

Figure 73 XPS C1s scan of Mesophase tapes which have been stabilised to (a) green tape (b) 160°C for 5hrs in oxygen (c) 160°C for 25hrs in oxygen (d) 240°C for 5hrs in oxygen (e) 240°C for 25hrs in oxygen (f) 300°C for 5hrs in oxygen (g) 300°C for 25hrs in oxygen 117

Figure 74 change in relative concentrations of C1s carbon-oxygen surface functional groups for mesophase pitch-based tape samples stabilised under various conditions for 5hrs. Oxide 1 corresponds to alcohol and / or ether groups, Oxide 2 to carbonyl groups, Oxide 3 to carboxyl and / or ester groups and Oxide 4 to carbonate groups 118

Figure 75 change in relative concentrations of C1s carbon-oxygen surface functional groups for mesophase pitch-based tape samples stabilised under various conditions for 25hrs. Oxide 1 corresponds to alcohol and / or ether groups, Oxide 2 to carbonyl groups, Oxide 3 to carboxyl and / or ester groups and Oxide 4 to carbonate groups 118

Figure 76 XPS O1s scan of Mesophase tapes which have been stabilised to (a) 160°C for 5hrs in oxygen (b) 160°C for 25hrs in oxygen (c) 240°C for 5hrs in oxygen (d) 240°C for 25hrs in oxygen (e) 300°C for 5hrs in oxygen (f) 300°C for 25hrs in oxygen 120

Figure 77 Valence band spectra showing separation between O2s (at higher binding energy) and C2s peaks for samples of mesophase pitch-derived tapes following exposure to oxygen for various temperatures and times (a) green tape (untreated), (b) treated in O₂ for 5hrs at 160°C, (c) treated in O₂ for 25hrs at 160°C, (d) treated in O₂ for 5hrs at 240°C, (e) treated in O₂ for 25hrs at 240°C & (f) treated in O₂ for 5hrs at 300°C (g) treated in O₂ for 25hrs at 300°C..... 123

Figure 78 (a) Sample unsuccessfully stabilised in situ has softened and flowed (b) Sample successfully stabilised in situ retains original shape 124

Figure 79 Fragment retention time (x-axis) vs. abundance (y-axis) results from Py-GC-MS of green tape in reactive mode at 160 °C for 5 hours in 100% O₂ 125

Figure 80 Fragment retention time (x-axis) vs. abundance (y-axis) results from Py-GC-MS of a green tape in reactive mode at 240 °C for 5 hours in 100% O₂ 125

Figure 81 Fragment retention time (x-axis) vs. abundance (y-axis) results from Py-GC-MS of a green tape in reactive mode at 300 °C for 5 hours in 100% O₂ 126

| | |
|---|-----|
| Figure 82 Position which Raman microscope was focused on mesophase pitch-based tape in order to obtain Raman Spectra..... | 128 |
| Figure 83 Raman Spectrum of green mesophase pitch..... | 128 |
| Figure 84 Raman spectra for tapes stabilised at 160°C for 5 and 25hrs..... | 130 |
| Figure 85 Raman spectra for tapes stabilised at 240°C for 5 and 25hrs..... | 130 |
| Figure 86 Raman spectra for tapes stabilised at 300°C for 5 and 25hrs..... | 131 |
| Figure 87 Raman D/G peak ratio plotted against stabilisation temperature for tapes stabilised for 5hrs and 25hrs..... | 132 |
| Figure 88 Raman D/G peak ratio plotted against % Oxygen content for tapes stabilised for 5hrs and 25hrs..... | 133 |
| Figure 89 Illustration of positions Raman microscope was focused on in order to obtain a Raman spectra for both the edge and middle of the stabilised mesophase pitch-based carbon tapes..... | 138 |
| Figure 90 Raman Spectra of scans made through the cross-section of mesophase pitch-based tapes which have been stabilised to varying degrees in oxygen; (a) 160°C for 5hrs, (b) 160°C for 25hrs (c) 240°C for 5hrs, (d) 240°C for 25hrs, (e) 300°C for 5hrs, (f) 300°C for 25hrs..... | 139 |
| Figure 91 Micro-thermal analysis of a green tape..... | 141 |
| Figure 92 Thermal image of a tape stabilised at 160°C for 5hrs showing micro-thermal analysis sample position (edge of the tape indicated by the red dashed line)..... | 143 |
| Figure 93 Micro-thermal analysis of tape stabilised at 160°C for 5hrs at varying positions throughout its cross-section..... | 143 |
| Figure 94 Thermal image of a tape stabilised at 240°C for 5hrs showing micro-thermal analysis sample position (edge of the tape indicated by the red dashed line)..... | 144 |
| Figure 95 Micro-thermal analysis of tape stabilised at 240°C for 5hrs at varying positions throughout its cross-section..... | 144 |
| Figure 96 Thermal image of a tape stabilised at 300°C for 5hrs showing micro-thermal analysis sample position (edge of the tape indicated by the red dashed line)..... | 145 |
| Figure 97 Micro-thermal analysis of tape stabilised at 300°C for 5hrs at varying positions throughout its cross-section..... | 145 |
| Figure 98 Thermal image of a tape stabilised at 160°C for 25hrs showing micro-thermal analysis sample position (edge of the tape indicated by the red dashed line)..... | 146 |
| Figure 99 Micro-thermal analysis of tape stabilised at 160°C for 25hrs at varying positions throughout its cross-section..... | 147 |
| Figure 100 Thermal image of a tape stabilised at 240°C for 25hrs showing micro-thermal analysis sample position (edge of the tape indicated by the red dashed line)..... | 147 |
| Figure 101 Micro-thermal analysis of tape stabilised at 240°C for 25hrs at varying positions throughout its cross-section..... | 148 |
| Figure 102 Thermal image of a tape stabilised at 300°C for 25hrs showing micro-thermal analysis sample position (edge of the tape indicated by the red dashed line)..... | 148 |
| Figure 103 Micro-thermal analysis of tape stabilised at 300°C for 25hrs at varying positions throughout its cross-section..... | 149 |
| Figure 104 Variation of softening temperature with distance from the tape surface as a function of stabilisation temperature after 5hrs..... | 150 |

| | |
|--|-----|
| Figure 105 Variation of softening temperature with distance from the tape surface as a function of stabilisation temperature after 25hrs..... | 150 |
| Figure 106 Semi-quantitative analysis of tape oxygen content carried out using an EPMA for 160, 240 and 300°C over 5hrs..... | 152 |
| Figure 107 Semi-quantitative analysis of tape oxygen content carried out using an EPMA for 160, 240 and 300°C over 25hrs..... | 152 |
| Figure 108 Variation of the softening temperature with oxygen content | 154 |
| Figure 109 Change in weight of sample tapes which have undergone varying temperatures of stabilisation over a 25hr period upon subsequent carbonisation..... | 157 |
| Figure 110 Graph showing how stabilisation time at 160°C can affect the weight loss... | 159 |
| Figure 111 Weight gain/loss and final carbon yield for samples stabilised in O ₂ for 5hrs at 160 and 240°C..... | 160 |
| Figure 112 Weight gain/loss and final carbon yield for samples stabilised in O ₂ for 25hrs in O ₂ at 160 and 240°C..... | 160 |
| Figure 113 Weight gain/loss and final carbon yield for tapes stabilised for 5hrs in O ₂ at 300°C..... | 161 |
| Figure 114 Weight gain/loss and final carbon yield for tapes stabilised for 25hrs in O ₂ at 300°C..... | 162 |
| Figure 115 TGA-FITR results for the carbonisation of a green tape | 163 |
| Figure 116 Library IR spectra of specific molecules | 163 |
| Figure 117 IR time stack for carbonisation of tape stabilised in oxygen at 160°C for 5hrs, heating rate of 15°C min ⁻¹ to 1000°C..... | 164 |
| Figure 118 IR time stack for carbonisation of tape stabilised in air at 160°C for 5hrs, heating rate of 15°C min ⁻¹ to 1000°C..... | 164 |
| Figure 119 IR time stack for carbonisation of tape stabilised in oxygen at 240°C for 25hrs, heating rate of 15°C min ⁻¹ to 1000°C..... | 165 |
| Figure 120 IR time stack for carbonisation of tape stabilised in air at 240°C for 25hrs, heating rate of 15°C min ⁻¹ to 1000°C..... | 165 |
| Figure 121 weight changes pattern upon carbonisation for tapes stabilised in oxygen for a range of times and temperatures..... | 166 |
| Figure 122 Evolution of hydrocarbons with increasing stabilisation time and temperature in oxygen upon carbonisation | 167 |
| Figure 123 Evolution of CO with increasing stabilisation time and temperature in oxygen upon carbonisation | 169 |
| Figure 124 Evolution of CO ₂ with increasing stabilisation time and temperature in oxygen upon carbonisation..... | 169 |
| Figure 125 TGA weight changes pattern upon carbonisation for tapes stabilised in air for a range of times and temperature | 171 |
| Figure 126 Evolution of hydrocarbons with increasing stabilisation time and temperature in air upon carbonisation | 172 |
| Figure 127 Evolution of CO with increasing stabilisation time and temperature in air upon carbonisation | 173 |
| Figure 128 Evolution of CO ₂ with increasing stabilisation time and temperature in air upon | 174 |



| | |
|--|-----|
| Figure 129 Deconvolution of CO evolution peak for samples stabilised at 240°C in O ₂ for 25hrs | 176 |
| Figure 130 Deconvolution of CO evolution peak for samples stabilised at 300°C in air for 25hrs | 177 |
| Figure 131 Deconvolution of CO ₂ evolution peak for a sample stabilised at 240°C in O ₂ for 25hrs | 177 |
| Figure 132 Deconvolution of CO ₂ evolution peak for a sample stabilised at 300°C in air for 25hrs | 178 |
| Figure 133 Fragment retention time (x-axis) vs. abundance (y-axis) results from Py-GC-MS at 1000°C of a green mesophase pitch tape;..... | 179 |
| Figure 134 Fragment retention time (x-axis) vs. abundance (y-axis) results from Py-GC-MS at 1000°C of mesophase pitch tape; stabilised at 160°C for 5hrs..... | 180 |
| Figure 135 Fragment retention time (x-axis) vs. abundance (y-axis) results from Py-GC-MS at 1000°C of mesophase pitch tape; stabilised at 160°C for 25hrs..... | 180 |
| Figure 136 Fragment retention time (x-axis) vs. abundance (y-axis) results from Py-GC-MS at 1000°C of mesophase pitch tape; stabilised at 240°C for 5hrs..... | 181 |
| Figure 137 Fragment retention time (x-axis) vs. abundance (y-axis) results from Py-GC-MS at 1000°C of mesophase pitch tape; stabilised at 240°C for 25hrs..... | 181 |
| Figure 138 Fragment retention time (x-axis) vs. abundance (y-axis) results from Py-GC-MS at 1000°C of mesophase pitch tape; stabilised at 300°C for 5hrs..... | 182 |
| Figure 139 Fragment retention time (x-axis) vs. abundance (y-axis) results from Py-GC-MS at 1000°C of mesophase pitch tape; stabilised at 300°C for 25hrs..... | 182 |
| Figure 140 O/C ratio for samples stabilised to various conditions vs. the phthalic anhydride (peak area) signals produced upon carbonisation..... | 183 |
| Figure 141 Raman spectra of tape stabilised at 160°C for 25hrs and tape stabilised at 160°C for 25hrs and subsequently heat treated to 450°C | 185 |
| Figure 142 Raman spectra of tape stabilised at 240°C for 25hrs and tape stabilised at 240°C for 25hrs and subsequently heat treated to 450°C | 185 |
| Figure 143 Raman spectra of tape stabilised at 300°C for 25hrs and tape stabilised at 300°C for 25hrs and subsequently heat treated to 450°C | 186 |
| Figure 144 Pole figure for mesophase pitch based tape stabilised at 240°C for 5hrs | 187 |
| Figure 145 Pole figure for mesophase pitch based tape stabilised at 240°C for 25hrs ... | 187 |
| Figure 146 Pole figure for mesophase pitch based tape stabilised at 240°C for 25hrs and heat treated to 450°C | 188 |
| Figure 147 Optical image of tape (a) stabilised at 160°C for 5hrs in O ₂ (b) stabilised at 160°C for 25hrs in O | 192 |
| Figure 148 Optical image of tape (a) stabilised at 240°C for 5hrs in O ₂ (b) stabilised at 240°C for 25hrs in O ₂ | 192 |
| Figure 149 Optical image of tape (a) stabilised at 300°C for 5hrs in O ₂ (b) stabilised at 300°C for 25hrs in O ₂ | 193 |
| Figure 150 Optical images of samples stabilised at 160°C for 5hrs and carbonised to 1000°C | 194 |
| Figure 151 Optical images of samples stabilised at 160°C for 25hrs and carbonised to 1000°C | 195 |



Figure 152 (a) SEM image (b) optical images, of a tape stabilised to 160°C for 25hrs and carbonised to 1000°C..... 195

Figure 153 Optical images of samples stabilised at 240°C for 5hrs and carbonised to 1000°C..... 196

Figure 154 (a) SEM image (b) optical image of a tape stabilised at 240°C for 5hrs and carbonised to 1000°C..... 197

Figure 155 Optical images of samples stabilised at 240°C for 25hrs and carbonised to 1000°C..... 198

Figure 156 Optical image of a tape stabilised at 240°C for 25hrs and carbonised to 1000°C showing the alignment of the mesophase micro domains 198

Figure 157 Optical images of samples stabilised at 300°C for 5hrs and carbonised to 1000°C..... 199

Figure 158 Optical images of samples stabilised at 300°C for 25hrs and carbonised to 1000°C..... 200

Figure 159 (a) SEM image (b) optical image of a tape stabilised at 300°C for 25hrs and carbonised to 1000°C..... 201

Figure 160 Typical example of an original load displacement curve produced when mechanically testing mesophase pitch based tapes which have under gone stabilisation at 240°C for 5hrs in Oxygen and subsequently been heat treated to 400°C (Sansom 2004). 203

Figure 161 Typical example of an original stress-strain curve produced when mechanically testing mesophase pitch based tapes which have under gone stabilisation at 240°C for 5hrs in Oxygen and subsequently been heat treated to 450°C (Sansom 2004). 204

Figure 162 Tensile strength of the tape in relation to heat treatment temperature (Sansom 2004)..... 205

Figure 163 Average engineering Young’s modulus in relation to heat treatment temperature (Sansom 2004) 206

Figure 164 Change in tensile strength with stabilisation conditions, time, temperature and 450°C heat treatment temperature 211

Figure 165 Change in average engineering Young’s modulus with stabilisation conditions, time, temperature and 450°C heat treatment temperature..... 212

Figure 166 Tensile strength versus % oxygen content of mesophase tapes which have been stabilised over range of stabilisation times and temperatures..... 213

Figure 167 Tensile strength versus % oxygen content of mesophase tapes which have been stabilised over range of stabilisation times and temperatures and subsequently heat treated to 450°C 213

Figure 168 Average engineering Young’s modulus versus % oxygen content of mesophase tapes which have been stabilised over range of stabilisation times and temperatures 214

Figure 169 Average engineering Young’s modulus versus % oxygen content of mesophase tapes which have been stabilised over range of stabilisation times and temperatures and subsequently heat treated to 450°..... 215

Figure 170 Weibull plot of tensile strength of Green mesophase pitch based carbon tapes 219

List of Tables

| | |
|--|-----|
| Table 1 Some properties of mesophase pitch (Mochida, Zeng et al. 1991)..... | 2 |
| Table 2 Diffusion time ($t_{0.5}$ & $t_{0.9}$) required for mesophase pitch fibres to attain 50% and 90% of their oxygen sorption capacity (Singer and Mitchell et al 1997)..... | 37 |
| Table 3 Change in CHNO composition with pitch batch..... | 75 |
| Table 4 Typical Properties of ARMP Mesophase Pitch (taken from www.mgc-a.com/newProducts/media/ARBrochure.pdf) | 78 |
| Table 5 CHNO results for pitch degas | 80 |
| Table 6 % mass gain for samples stabilised at varying degrees of temperature and time in air..... | 91 |
| Table 7 % mass gain for samples stabilised at varying degrees of temperature and time in oxygen | 91 |
| Table 8 Table of evolved gas data for isothermally stabilised tapes in both air and oxygen | 96 |
| Table 9 CHNO Chemical analysis for samples stabilised over a range of temperatures in air and oxygen | 96 |
| Table 10 Atomic compositions ratios for samples stabilised in oxygen at varying times and temperatures | 105 |
| Table 11 Aromatic index determined by FTIR for samples stabilised at 160°C and 240°C between 1-5 hrs in oxygen | 109 |
| Table 12 Aromatic index determined by FTIR for samples stabilised at 160°C, 240°C and 300°C in air and oxygen for 5 and 25 hrs..... | 112 |
| Table 13 Relative concentrations of C1s carbon-oxygen surface functional groups for mesophase pitch-based tape samples stabilised under various conditions. Oxide 1 corresponds to alcohol and / or ether groups, Oxide 2 to carbonyl groups, Oxide 3 to carboxyl and / or ester groups and Oxide 4 to carbonate group..... | 117 |
| Table 14 Relative concentrations of O1s carbon-oxygen surface functional groups for mesophase pitch-based tape samples stabilised under various conditions. Oxide 1 corresponds to carbonyl (C=O) groups (531.6 - 532.0 eV), Oxide 2 to alcohol (C-OH) and / or ether (C-O-C) groups (533.2 - 533.5 eV), Oxide 3 to chemisorbed oxygen and / or adsorbed water (535.8 - 536.2 eV)..... | 121 |
| Table 15 showing the values of C2s and O2s peak positions and the O2s-C2s peak separation for tapes oxidatively treated at different temperatures for 5 and 25 hours | 123 |
| Table 16 Raman D and G peak intensity and D/G ratio for tapes stabilised under various conditions | 131 |
| Table 17 Raman D and G peak intensity and D/G ratio for tapes stabilised under various conditions, scanned on both edge and middle sites on the tape | 140 |
| Table 18 Carbonisation TG curve information for tapes stabilised at varying temperatures for 25hrs | 158 |




| | |
|--|-----|
| Table 19 Peak areas and maximum peak positions for evolved gases during carbonisation of tapes which have seen varying degrees of stabilisation in oxygen (all experiments carried out using 95mg of sample) | 170 |
| Table 20 Peak areas and maximum peak positions for evolved gases during carbonisation of tapes which have seen varying degrees of stabilisation in air (all experiments carried out using 95mg of sample) | 174 |
| Table 21 Desorption temperatures T_{des} and gaseous decomposition products (Collins 2005)..... | 175 |
| Table 22 Some oxygen surface groups and corresponding decomposition products (Collins 2005)..... | 175 |
| Table 23 Phthalic anhydride peak area and O/C ratio for tapes stabilised to varying degrees (all experiments carried out using a 2mg sample mass) | 183 |
| Table 24 Raman D and G peak intensity and D/G ratio for tapes stabilised under various condition and subsequently heat treated to 450°C | 186 |
| Table 25 Average load displacement table for tapes heat treated to different temperatures after stabilisation at 240°C for 5hrs (Sansom 2004) average results are an average of 10 samples. | 204 |
| Table 26 Stress strain table for tapes stabilised at 240°C for 5hrs and subsequently heat treated to a variety of temperatures (Sansom 2004)..... | 205 |
| Table 27 Average load-displacement table for mesophase tapes which have experienced a variety of stabilisation conditions | 207 |
| Table 28 Table displaying the Stress strain and engineering Young's modulus data for tape samples stabilised at 160°C, 240 °C and 300 °C for 5 and 25 hrs and then subsequent heat treatment to 450°C | 210 |
| Table 29 X-Y Co-ordinate parameters of Weibull plot..... | 218 |
| Table 30 Average mechanical test values for tapes stabilised under a variety of conditions and tapes which have been stabilised and heat treated to 450°C..... | 219 |
| Table 31 Raw data for CHO weight change for stabilisation at 160°C with respect to time of oxygen stabilised samples..... | 233 |
| Table 32 Raw data for CHO weight change for stabilisation at 180°C with respect to time of oxygen stabilised samples..... | 233 |
| Table 33 Raw data for CHO weight change for stabilisation at 200°C with respect to time of oxygen stabilised samples..... | 234 |
| Table 34 Raw data for CHO weight change for stabilisation at 240°C with respect to time of oxygen stabilised samples..... | 234 |
| Table 35 Raw data for CHO weight change for stabilisation at 300°C with respect to time of oxygen stabilised samples..... | 234 |

List of Equations

| | |
|--|-----|
| Equation 1 Presumed mechanism of the stabilisation reaction (Miura, Nakagawa et al. 1995)..... | 25 |
| Equation 2 Bragg's Law..... | 47 |
| Equation 3 Lambert-Beer equation | 52 |
| Equation 4 Aromatic index ratio equation | 52 |
| Equation 5 Potential of mean path through the analyser..... | 66 |
| Equation 6 Tensile strength equation | 70 |
| Equation 7 engineering Young's modulus equation | 70 |
| Equation 8 Weibull Equation | 216 |
| Equation 9 Weibull modulus equation | 216 |
| Equation 10 Weibull modulus equation | 217 |
| Equation 11 Weibull modulus equation | 217 |
| Equation 12 Weibull modulus equation in form suitable for plotting..... | 217 |
| Equation 13 Probability of tape survival..... | 218 |

List of abbreviations

| | |
|-----------|---|
| ➤ A | Area (for all calculations) |
| ➤ ACF | Activated Carbon Fibre |
| ➤ AFM | Atomic Force Microscopy |
| ➤ AR-MP | Arocarb Mesophase pitch |
| ➤ As-spun | Wound onto a spool |
| ➤ ASTM | American Society for Testing Materials |
| ➤ Bar | Pressure |
| ➤ BSI | British Standard Institute |
| ➤ Bi | Benzene Insoluble |
| ➤ °C | Degrees Celsius |
| ➤ CHA | Concentric Hemispherical Analyser |
| ➤ DMTA | Dynamic Mechanical Thermal Analysis |
| ➤ DSC | Differential Scanning Calorimetry |
| ➤ dwell | Period of maintaining the temperature at the same level |
| ➤ E | engineering Young's modulus |

- FWHM Full Width Half Maximum
- FTIR Fourier Transform Infra-red
- GPCF General Purpose Carbon Fibre
- HOMG Highly Oriented Mesophase Graphite-based
- HOPG Highly Oriented Pitch Graphite-based
- Horizontal orientation (1-2) 

- hr Hour
- HPCF High Performance Carbon Fibre
- HTT Heat Treatment Temperature
- K Consistency Coefficient
- kg Kilogram
- l length (for all calculations)
- LTCTP Low Temperature Coal Tar Pitch
- m Meter
- N Newton
- NP Naphthalene
- NMP Naphthalene Mesophase Pitch
- P Pressure
- PAN Polyacrylonitrile
- Pa Pascal
- PAH Polycyclic aromatic anhydride
- rpm Revolutions Per Minute
- SEM Scanning Electron Microscope
- T_a Ambient temperature
- TEM Transmission Electron Microscope
- THQ Tetrahydroquinoline
- TGA Thermo-Gravimetric-Analysis
- ThAFM Thermal Atomic Force Microscopy
- TM Tensile-testing Machine

- › Vertical orientation (1-3)



- › XPS X-ray Photoelectron Spectroscopy
- › XRD X-ray Diffraction

Greek Symbols

- › ϵ Strain
- › θ Bragg angle
- › λ Wavelength
- › ρ Density
- › σ Tensile stress
- › ψ Range of angle used in X-ray topography

1 Introduction

Carbon fibres/tapes are materials which are relatively new but are of great industrial importance. It is said that they are perhaps the most successful new carbon product to be commercialised in the past 35 years (Edie et al 1998). Their industrial importance comes about due to their unique properties; carbon fibres exhibit high specific strength and stiffness combined with a low weight; properties that some fibres/tapes demonstrate can be superior to steel whilst being up to 70% lighter (Donnet et al 1984). Carbon fibres also display properties such as thermal stability, thermal conductivity of up to three times that of copper, electrical conductivity and corrosion resistance, which are all controlled by the processing conditions used in their preparation. As a result of the unique and versatile properties of carbon fibres/tapes they are suitable for a wide range of products. From use in structural composites, printed circuits substrates (Mchugh and Edie et al 1996) and sporting equipment to high end aerospace applications (Fitzer et al 1989) along with satellite structures and other thermal management applications (Cato and Edie et al 2003). When combined with a matrix material these carbon fibres/tapes impart their physical properties to the composite providing a high performance, low density option for design engineers.

In the past the high cost of carbon fibres from PAN (Polyacrylonitrile) made their use uneconomical for non-high end application (Edie, Robinson et al. 1994). Initially it was felt that mesophase pitch based fibres would provide a low cost alternative to PAN based carbon fibres (Edie et al 1998). However, the expense of mesophase pitch fibres in high volume applications limits their use, primarily due to the large cost of the high temperature processing needed for graphitisation ($\sim 3000^{\circ}\text{C}$) (Gallego, Edie et al. 2000) and post spinning processes such as stabilisation and carbonisation (Hamada, Nishida et al. 1988).

Many new carbon fibre/tape materials are produced from a mesophase pitch precursor due to excellent physical, electrical and thermal properties and its relatively low cost. Carbonaceous mesophase can be obtained from a number of sources such as polycyclic aromatic hydrocarbons and pitches, giving it good inherent properties such as

a high softening point, high carbon yield and excellent graphitisation (table 1). These make it suitable for the preparation of polygranular carbon materials (Fanjul, Granda et al. 2002) owing to the fact that mesophase is a plastic material which has self-sintering capabilities upon carbonisation without the aid of an external binder.

Table 1 Some properties of mesophase pitch (Mochida, Zeng et al. 1991)

| | Wt (%) | | | | H/C | T _g ^a (°C) | SP ^b (°C) | AP ^c (%) | Solubilities % | | |
|----|--------|------|-----|------|-----|-------------------------------------|-------------------------|------------------------|----------------|------|------|
| | H | C | N | diff | | | | | BS | B-QS | Q |
| MP | 3.1 | 94.9 | 1.0 | 1.0 | 0.4 | 207.0 | 275.0 | 95.0 | 5.5 | 67.0 | 27.5 |

^aglass transition temperature DSC

^bsoftening point by hot plate

^canisotropic percentage

The stabilisation step is essential in ensuring the quality of the finished fibre/tape, giving the carbon fibres/tapes their dimensional stability, preventing melting when the fibres/tapes are carbonised, by raising the glass transition temperature (T_g) of the material so that decomposition occurs before softening. The stabilisation step also helps preserve the orientation of the fibres/tapes produced during spinning.

Stabilisation is a vital step in the preparation of pitch based carbon fibres/tapes; the optimisation of this process for the production of carbon fibres/tapes is of the utmost interest as it could lead to improvements in the mechanical and thermal transport properties of the final fibres/tapes. Although the actual production of fibres/tapes is relatively cheap, as petroleum pitch is a very cost effective raw material (about \$0.25/kg) (Hutchenson, Roebbers et al. 1991), it is the resultant heat treatment processes such as the stabilisation, which increase the production costs. If the stabilisation of the fibres/tapes was better understood it is likely that the costs of production could be dramatically reduced.

The optimisation of the stabilisation step is difficult as the mechanisms involved in the reaction are complex and not fully understood. Some of the mechanisms that are described in previous literature refer to the addition of oxygen, forming oxygen-containing molecules, the promotion of cross-linking between molecules and the removal of smaller molecules by decomposition (Blanco, Lu et al. 2003). The cross-linking that occurs during stabilisation is thought to take place at sites with oxygen functional groups. As a result of this it is believed that the extent of the stabilisation (When considering



stabilisation there are three main categories which should be taken into account; maintaining the morphology imparted to the samples during its initial processing step, minimisation of weight loss upon subsequent carbonisation and maximising the homogeneity of the sample) taking place is closely linked to the number of oxygen functional groups which are formed during stabilisation. Mesophase pitch has high stabilisation reactivity due to its abundance of naphthenic rings, aliphatic carbons and hydrogens. It is suspected that the initial stage of oxidative stabilisation involves the addition of oxygen into naphthenic rings as ketone functionality and the loss of methylene hydrogen forming water.

In recent years the development of mesophase pitch based carbon tapes, a product which can be adapted for a wide range of applications; from potential biocompatible endovascular stents to laminates for use in high end thermal applications has led to the need for a better understanding of the stabilisation process. However, it should be noted that a more complete understanding of the stabilisation process will not only aid in the production of fibres and tapes but all mesophase products across the board.

2 Literature Review

2.1 Forms of carbon

Carbon is the only element which is capable of forming the complex ring and long chain compounds which are the prerequisites of life itself. Carbon has an atomic number of 6 and an atomic mass of 12 amu. Of the six electrons present four of these are in the atom's outer shell and are capable of forming chemical bonds with other atoms (figure 1). The valence electron configuration of the carbon atom is $1s^2 2p^2 2p^2$ as a result of this half filled valence shell carbon has special properties that straddle the line between metals and non-metals. Carbon can form covalent compounds with non-metallic compounds and ionic compounds with metals; the oxides of carbon are acidic.

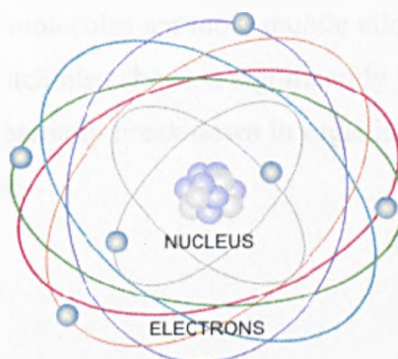


Figure 1 A Carbon Atom (www.eia.doe.gov/.../sources/electricity.html)

As a solid element carbon exists in the earth's crust as the amorphous solid anthracite and in the crystalline form as graphite and diamond. In recent years carbon has also been seen to exist in the form of fullerenes and nanotubes. Graphite is the most thermodynamically stable of all the allotropes of carbon. The diversity in the properties of different carbon allotropes can be explained by the difference in their bonding, whether it is by van der Waals forces or strong covalent bonds.

2.2 What is pitch?

Pitches are the main precursor for the production of graphitisable carbons. Pitch is a mixture of hundreds of different molecules made up mostly of lots of aromatic polynuclear compounds. The molecules in the pitch tend towards a planar morphology and some have aliphatic side chains. Most pitches are produced from coal tar, petroleum residue or are synthetically derived. The most commonly used pitches in industry are those that originate from coal tar (preferred as a binder material) and petroleum (more aliphatic than coal tar pitches). The largest user of coal tar pitch is the aluminium industry in the manufacturing of electrodes. A wide variety of pitches are used with a correspondingly wide range of glass transition temperatures T_g , however all of these pitches behave thermoplastically. This is a key parameter of the pitch's thermoplastic behaviour. Below T_g the molecular mobility is slow and limited causing it to be hard and brittle whereas above T_g the molecules are more mobile allowing the pitch to be soft and flow at high temperatures. Pitch also shows a significantly wide variation in distribution of molecular mass and may partially break down in organic solvents. Furthermore, it can exhibit colloidal characteristics.

2.3 Pitch production

Three primary steps or a mixture of these steps are taken in order to produce pitches which are suitable for spinning and other applications; heat soaking, gas sparing and solvent extraction. In the heat soaking process an isotropic pitch is heated to around 400°C for a prolonged period of time (usually days). This allows the pitch to convert to around 40 – 90 wt% mesophase as a result of molecular condensation increasing the mesophase pitch molecular weight. Gas sparing is a variation of the heat soaking process; an inert gas is bubbled through the pitch during the formation of the mesophase resulting in enhanced removal of low molecular weight compounds. Using gas sparing a comparable amount of mesophase can be produced as using heat soaking but the formation time is greatly reduced (Hutchenson, Roebers et al. 1991). Mesophase pitch can also be produced using solvent extraction to concentrate the mesogens due to

isotropic pitch containing separable fractions. It was discovered that the isotropic phase of the pitch developed an anisotropic phase on heating that could be concentrated by a solvent extraction process. The advantages of using this method is that the pitches produced have a typically high molecular weight negligible quinoline insoluble content, and it is a particularly effective way of making a very high strength/modulus fibre (Lavin et al 1992).

Supercritical fluid extraction can also be used to produce mesophase pitch in a continuous operation (Hutchenson, Roebbers et al. 1991) (figure 2). One advantage of this process is that the pitch can be separated into any desired number of fractions until the solvent density becomes too low to dissolve, allowing the production of pitch with a narrower molecular weight range than its parent pitch. This offers greater control over the final properties of the resulting fibres and improved reproducibility of the pitch properties from batch to batch (Hutchenson, Roebbers et al. 1991).

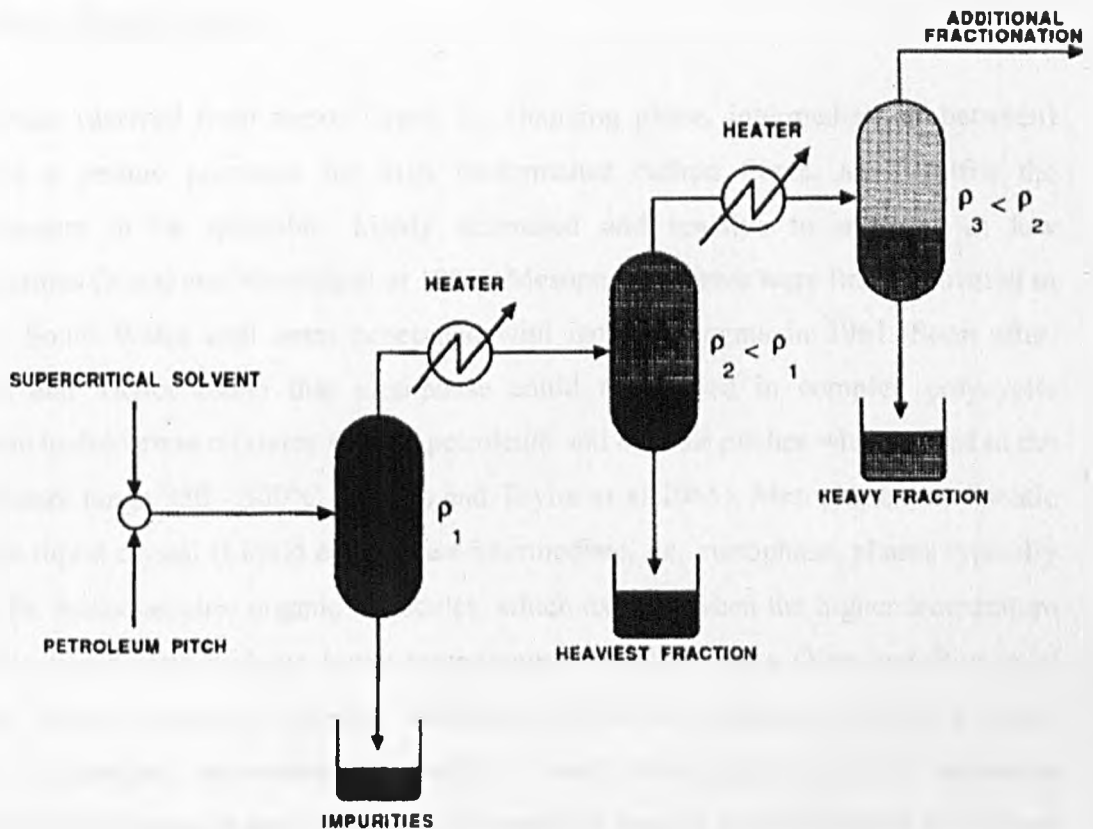


Figure 2 Concept design of an SCF extraction process for fractionating petroleum pitch (Hutchenson, Roebbers et al. 1991)

Air blowing can also be successfully used to produce pitch precursors for isotropic carbon (Maeda, Ming Zeng et al. 1993), which are typically used in the production of general purpose carbon fibres (GPCF). Whilst GPCFs exhibit moderate mechanical properties the resultant carbon fibres can be produced at a much lower cost than high performance carbon fibres (HPCF) as no time consuming pre-treatments are required. Air blowing works by raising the softening point of the original pitch feedstock, giving rise to the development of larger molecules in the pitch such as the benzene insoluble fraction (BI) (Maeda, Ming Zeng et al. 1993). A resultant cross-linking reaction ensues which suppresses the growth of mesophase spheres in the isotropic matrix.

2.4 Mesophase pitch

Mesophase (derived from mesos Greek for changing phase, intermediate or between) pitch is a unique precursor for high performance carbon fibres, as it fulfils the requirements to be spinnable, highly orientated and reactive to oxidants at low temperatures (Korai and Mochida et al 1985). Mesophase spheres were first discovered in a New South Wales coal seam penetrated with igneous magma in 1961. Soon after, Brooks and Taylor found that mesophase could be formed in complex polycyclic aromatic hydrocarbon mixtures such as petroleum and coal tar pitches when heated in the temperature range 350 - 500°C (Brooks and Taylor et al 1965). Mesophase is a discotic nematic liquid crystal (Liquid crystals are intermediate, i.e. mesophase, phases typically found for anisodiametric organic molecules, which exist between the higher temperature isotropic liquid state and the lower temperature crystalline state (Yan and Rey et al 2002)), which consists of aromatic oligomers (disc-like molecules), where aromatic planes are stacked approximately parallel to each other (figure 3); this molecular alignment of mesophase can be changed by applying heat or a stress field to it. These aromatic planes carry alkyl and naphthenic groups that help the mesophase pitch with its solubility and fusibility (figure 4).

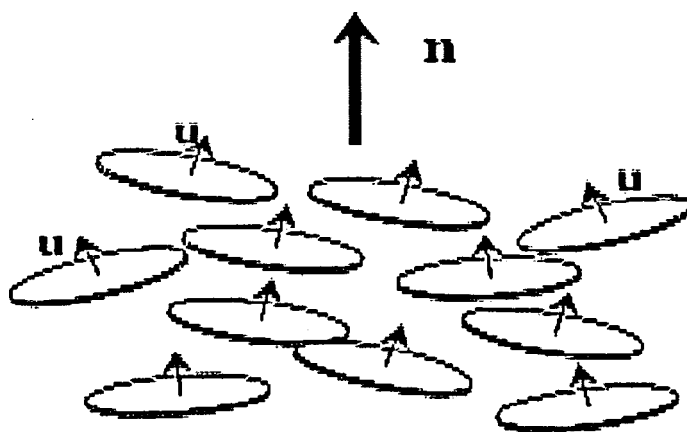


Figure 3 Definition of director orientation of a uniaxial discotic nematic liquid crystalline material; the direction n is the average orientation of the units normal to the disc-like molecules in a discotic nematic phase. (Yan and Rey et al 2002)

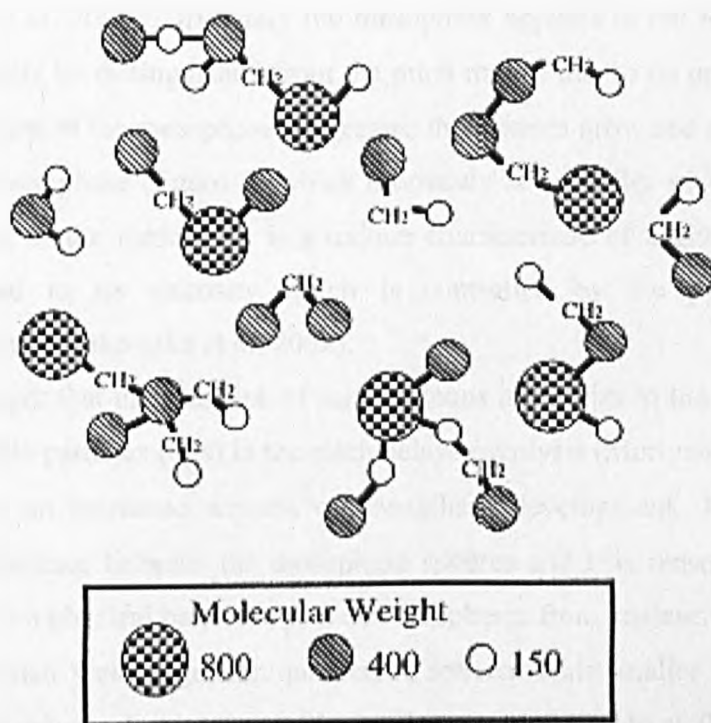


Figure 4 Spider Wedge molecule of mesophase constituent molecules, (Mochida, Korai et al. 2000)

2.5 Mesophase formation

The chemical reaction which can be attributed to the pyrolytic conversion of pitch to a carbonaceous residue is a radical condensation of aromatic and heteroaromatic constituents occurring at a reasonable rate above 400°C. During this heat treatment in an inert atmosphere, large polycondensed aromatic hydrocarbons (PAH) are formed due to thermal decomposition and polymerisation reactions (Montes-Moran, Crespo et al. 2002). However it has been indicated in previous studies that the formation of mesophase not only takes place upon heating but also upon cooling. This is consistent with the general mechanism of crystalline solid/liquid formation from a solution, in which nucleation is driven by super-saturation of solute and of super-cooling of solution (Moriyama, Hayashi et al. 2002). The formation of mesophase spheres generally involves three elemental rate processes; generation (nucleation) where the rate is dictated by the concentration of the precursor and is a function of temperature; growth which occurs at a steady rate and; the

coalescence of spheres which obeys second order kinetics (Machnikowski, Machnikowska et al. 2002). Originally the mesophase appears in the form of spherical units that can easily be distinguished from the pitch matrix due to its optical anisotropy. As the development of the mesophase progresses the spheres grow and coalesce in order to form a bulk mesophase (figure 5) which ultimately re-solidifies giving a semi-coke. The development of the mesophase is a unique characteristic of a given carbonisation system correlated to its viscosity which is controlled by the pitch constituents (Machnikowski, Machnikowska et al. 2002).

It is thought that the presence of carbonaceous impurities in the form of primary quinoline-insoluble particles (QIs) in the pitch delays pyrolysis (Moriyama, Hayashi et al. 2004) shown by an increased amount of mesophase development. The primary QIs control the coalescence between the mesophase spheres and it is reasonable to assume that the QIs act as a physical barrier to prevent the spheres from coalescing. The presence of QIs in pitch also yield a greater number of spheres with smaller radii as the QIs suppresses linear growth of mesophase spheres (Moriyama, Hayashi et al. 2004). In pitch, which is free of primary QIs, the nucleation occurs continuously throughout the heat treatment. If a significant amount of QI is present then only a short period of nucleation occurs up to a point until it becomes inhibited by the QI (Mora, Santamaria et al. 2003).

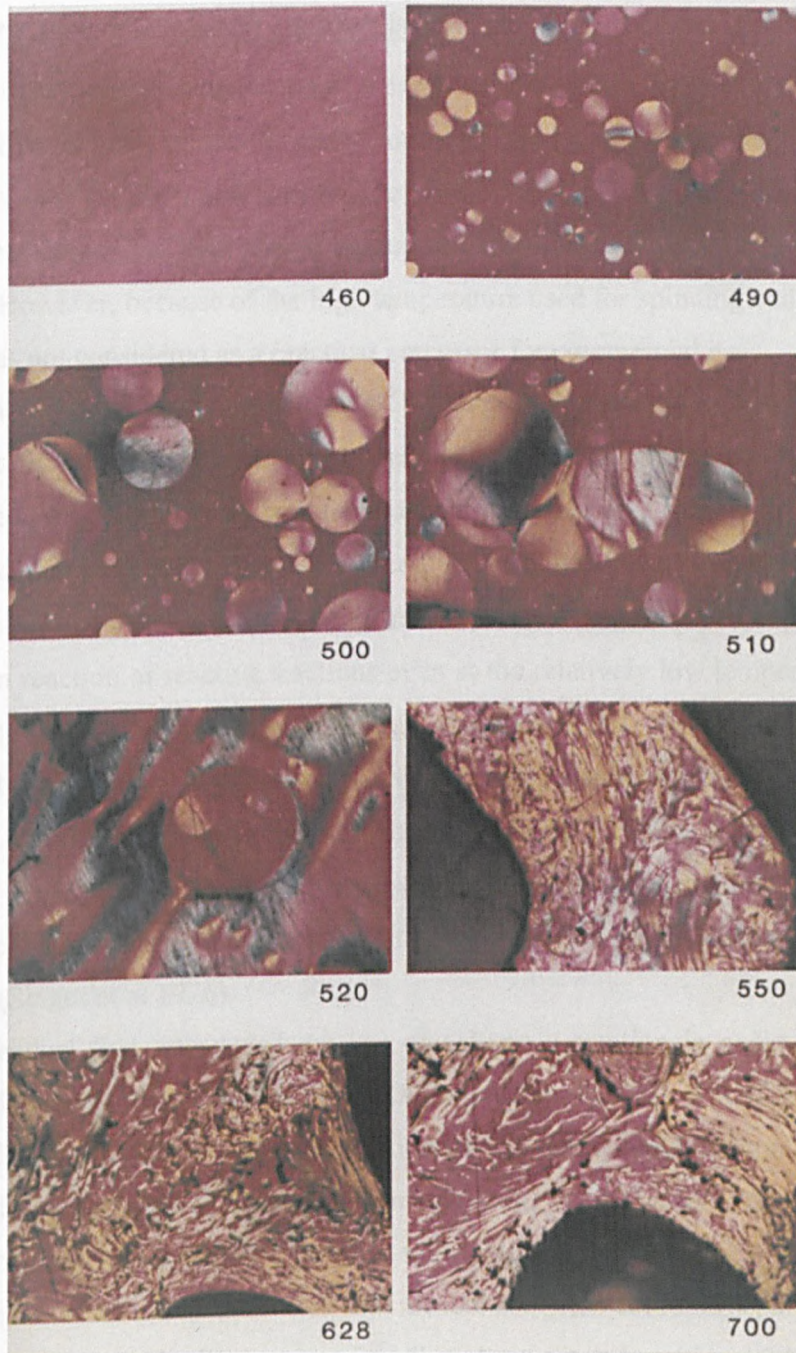


Figure 5 Mesophase nucleation, growth and coalescence (Benn 1989)

2.6 History of mesophase production

A summary of mesophase preparation as a precursor for carbon fibres is discussed below. It was discovered that spinnable pitch could be produced by the heat treatment of tetrabenzophenazine (TBP) at a temperature above 500°C. This pitch could be spun into large diameter fibres with high tensile moduli at temperatures between 410-440°C (Otain et al 1970). However, because of the high temperature used for spinning and the high cost of TBP it was not considered as a practical precursor for commercial use.

Pitch with a softening point below 350°C can be produced by heating petroleum pitch in a rapid flowing nitrogen atmosphere which acts to remove the low molecular weight molecules. This process was developed by the Union Carbide Co (UCC); they claimed that the mesophase pitch produced showed improved spinability and some solubility in solvents. In contrast, a long heat treatment time can not avoid the excess condensation reaction of reactive fractions even at the relatively low temperature of 380-430°C producing a fraction of very large molecules and a high softening point. Consequently the resultant mesophase pitch had to be spun at around 350°C (Mochida, Korai et al. 2000). At the spinning temperature of 350°C using this pitch, pyrolytic reactions of constituent molecules occur resulting in an unstable spinning caused by the production of infusible solids as a result of the condensation of the aromatic constituents of the pitch (Singer et al 1976).

Diefendorf first introduced the use of solvent extraction in order to produce a concentrated fraction of mesophase pitch (Diefendorf et al 2000). It was discovered that an intermediate molecular weight distribution of the pitch could be controlled by the extraction of two extremes of the components by using solvent with different dissolving abilities, allowing the properties of the pitch to be controlled .

Strehlow and Tonen discovered that mesophase pitch could be separated from the isotropic phase during the heat treatment of coal tar pitch by using high temperature centrifugation. As a result of the mesophase being denser than the isotropic phase, the mesophase can be can be precipitated slowly to the bottom of a vessel from the isotropic matrix in the fused state (Strehlow et al 1970) (Mochida, Korai et al. 2000).

Mochida found that naphthenic and short alkyl chain groups are essential in order to give the mesophase pitch a lower softening point for stable fibre/tape spinning and reasonable stabilisation reactivity (Mochida, Korai et al. 2000). As a result of this, hydrogenation of pitch was carried out by Mochida and Yamada in order to enhance the mesophase pitch by introducing naphthenic groups into it using a hydrogen donor solvent (tetrahydroquinoline) THQ prior to the preparation (Mochida, Kudo et al. 1975) (Yamada 1981). Nonetheless the problem with aromatic hydrogenation of the pitch is its high cost making it unattractive for use on a commercial scale.

Park and Mochida (1988) (Park, Mochida et al 1988) proposed a two-stage production process for mesophase pitch to increase the yield where mesogen molecules are produced under pressure at high temperatures and then are efficiently concentrated under vacuum in the second stage (Mochida, Korai et al. 2000).

2.7 Synthesis of mesophase pitch

Production of mesophase pitch via a synthetic process has become the newest way in which to prepare it. It has been reported that mesophase pitch can be produced by the condensation with formaldehyde of the C₉ alkylbenzene in the naphtha followed by the successive heat treatments, which involve alkylbenzene molecules being converted mesogenic aromatic oligomers (Yanagida et al 1989). This synthetic mesophase is believed to have a structure with several bends in its aromatic skeleton on the nine rings. This structure of mesophase is thought to be responsible for the low softening point and the low melt viscosity along with the highly ordered stacking in the spun fibre. Synthetic mesophase does require a much longer stabilisation time for spun fibres than that for the mesophase pitches mentioned in the previous section, which is most likely to be as a result of their lower softening points.

Spinnable mesophase pitch precursor can also be synthesized using naphthalene, ethylene tar and an aluminium chloride (AlCl₃) catalyst. In this process the AlCl₃ catalyst is removed as a hydroxide by washing it with acid leaving the precursor pitch to be further heat treated into a mesophase pitch. This pitch however still contains a lot of naphthenic groups, exhibiting a low softening point and high solubility compared

with those pitches produced using conventional methods. Nevertheless one problem with this method of production is that it is incredibly difficult to remove all aluminium hydroxide from the mesophase pitch leading to an unacceptable degradation of the final fibre properties (Mochida, Korai et al. 2000).

The most popular and successful method for the synthesis of mesophase pitch on an industrial scale is with the use of HF-BF₃ as a catalyst (figure 6). Using this process spinnable mesophase has effectively been produced from aromatic hydrocarbons. The HF-BF₃ catalyst produces protonated complex aromatic hydrocarbons such as naphthalene (Mochida, Korai et al. 2000). The mesophase produced has been seen to have a very high yield due to the catalytic reaction of the naphthalene that takes place; another benefit of this process is that the HF-BF₃ catalyst can be recycled using atmospheric distillation. The acids HF and BF₃ have boiling points of 19.9 and -101.1°C respectively.

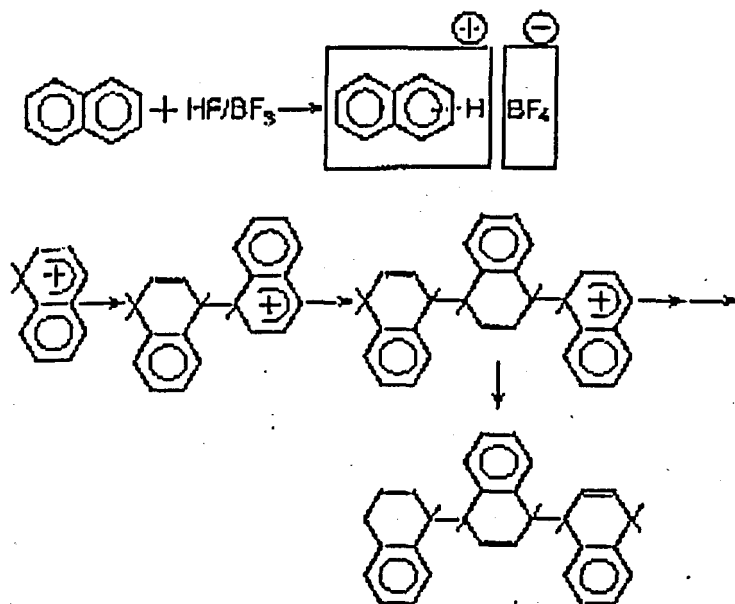


Figure 6 Catalytic condensation of aromatic hydrocarbon with HF/BF₃ (Mochida, Korai et al. 2000)

AR (aromatic) pitch is also synthesized from a pure aromatic hydrocarbon (naphthalene) with HF-BF_3 catalyst and can be produced on an industrial scale in a batch wise process (figure 7). The reaction takes place in two reactors and a purification tank. In the first reactor a small proportion of naphthalene feed is combined with a stoichiometric amount of HF-BF_3 in order to form the catalyst complex, which is then recovered to the bulk feed in the second reactor in order to produce the mesophase pitch. When the reaction is completed the reactor is heated to drive off the HF-BF_3 so that it can be recycled. The pitch product is then transferred to a purification tank to be purged with nitrogen to remove any volatile compound (Mochida 1995)

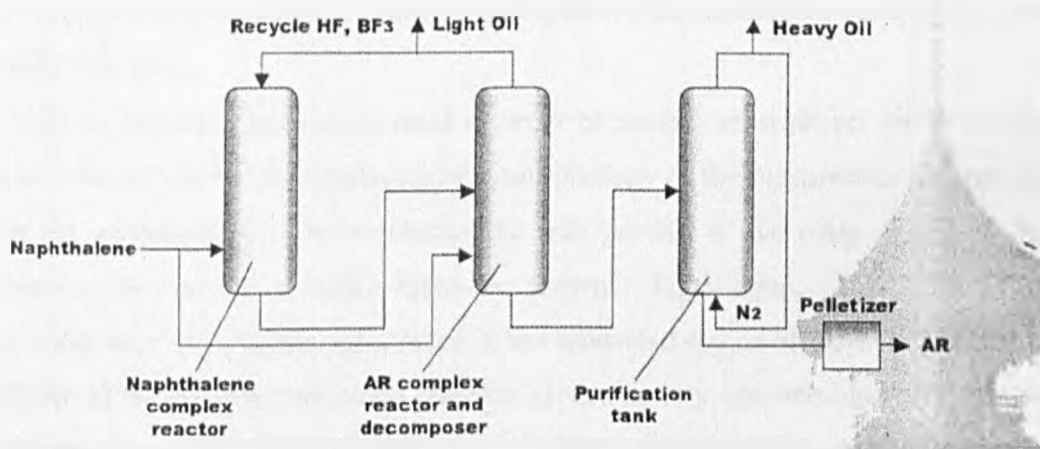


Figure 7 Process flow diagram for commercial production of naphthalene-derived AR pitch (Mochida 1995)

Mesophase can also be developed rapidly by using low temperature coal tar pitches (LTCTP), as a result of its high content of heteroatom and aliphatic groups. The mesophase which is produced from the LTCTP has a high tendency to coalesce due to its low viscosity and low primary quinoline insoluble content (Crespo, Arenillas et al. 2004). It also displays a low carbon yield which can be attributed to the pitch's low aromaticity. Polymerisation of the LTCTP can be carried out in order to increase the viscosity of the pitch by the creation of methylene bridges through the formation of methyl groups which gives rise to larger aromatic molecules. Another effect of polymerisation with the formaldehyde is to increase the amount of mesophase formed during the first stages of carbonisation of the pitch. In addition the formaldehyde enhances the reaction of the phenolic compounds to form β -resins that increases the semi-

coke yields and decreases the coalescence tendency of the mesophase. Further more the formation of additional bulk mesophase is also promoted by the polymerisation. However, most of the mesophase produced using the formaldehyde polymerisation process has rather irregular shaped mesophase particles (Crespo, Arenillas et al. 2004).

2.8 Mesophase modification

Mesophase pitch has been modified with a wide variety of different additives in order to alter and improve its properties, ranging from polymers to iron oxide. Additions to the mesophase can help to improve the yield of its insoluble fraction, inhibit the expansion of the pitch during subsequent heat treatments and improve the successive carbonisation of the insoluble fraction.

Various polymers have been used in order to modify mesophase; the polymers modify the kinetics of the conversion and the morphology of the mesophase. A common effect of the modification is to accelerate the unit growth in the early stages of the transformation as a result of dehydrogenative polymer degradation. This leads to an increase in the area of isotropic appearance in the advanced stages of the transformation. The addition of the polymer polyvinyl chloride gives rise to a non-homogeneous texture of mesophase as a result of early separation of the particulate quinoline insoluble. On the other hand the addition of polyethylene glycol hinders the coalescence of the mesophase leading to an enhanced proportion of spherical mesophase (Machnikowski, Machnikowska et al. 2002).

Iron oxide Fe_2O_3 is another additive, which is used to alter the properties of mesophase. The iron oxide enhances the dehydrogenative polymerisation of the pitch, giving rise to an increase in the yield of the extracted insoluble fraction and a decrease in the hydrogen content of the mesophase. The iron oxide additive tends to lead to a semi-coke material with a mosaic structure offering enhanced reactivity of the constituent molecules within the mesophase. However the extent of graphitisation which the mesophase undergoes at high temperature 3000°C is limited by the presence of iron oxide (Wang, Korai et al. 2001).

Naphthalene derived mesophase pitch modified with benzoquinone can be seen to lower the solubility and fusibility of the NMP (naphthalene mesophase pitch), increase the isotropy and yield of the carbon with lowered swelling and graphitisation. Increasing the size of the constituent molecules with the modification contributes to reduce the amount of gasification the pitch requires, on account of the larger molecules giving enough free volume for the evolved gas to escape resulting in a lowering of the swelling. Modification such as this also improves the carbonisation of the pitch, owing to modifications to the structure of the component molecules. Large peri type rings obtained through condensation and hydrogen bonding between components after the modification restricts the fusibility essential for the anisotropic development in the carbonisation (Yang, Kim et al. 1997).

The modification of mesophase can also be carried out using nanotube-reinforcement. Mesophase pitch is a thermotropic liquid crystalline precursor with a multi-domain structure. When the mesophase is modified with nanotubes the pitch nucleates to a larger number of smaller-size domains altering the final morphology of resulting fibres. Pure mesophase pitch fibres exhibit a radial texture where as fibres produced using the nanotube modified mesophase pitch show a more random texture. It has been shown that textural changes to mesophase carbon fibres can be altered by compositional changes not just changes to die design (Cho, Lee et al. 2003).

Mesophase has also been modified with the addition of naphthalene derived partially isotropic pitch. This acts to lower the melting viscosity of the pitch and improve the alignment of the mesophase molecules when spun. Carbon black is another additive which has been used in order to alter the properties of the mesophase pitch, effectively reducing the swelling of the pitch which takes place upon subsequent carbonisation (Kanno, Fernandez et al. 1997).

2.9 Aspects of Carbon Fibre/Tapes Manufacturing

The process of preparing carbon fibres from mesophase pitch is illustrated in (Figure 8). The starting pitch is processed to mesophase pitch which is melt spun, oxidized at low temperatures to render the fibres/tapes infusible; the tapes are then heat treated to higher temperatures in order to develop their final properties (Rand 1986).

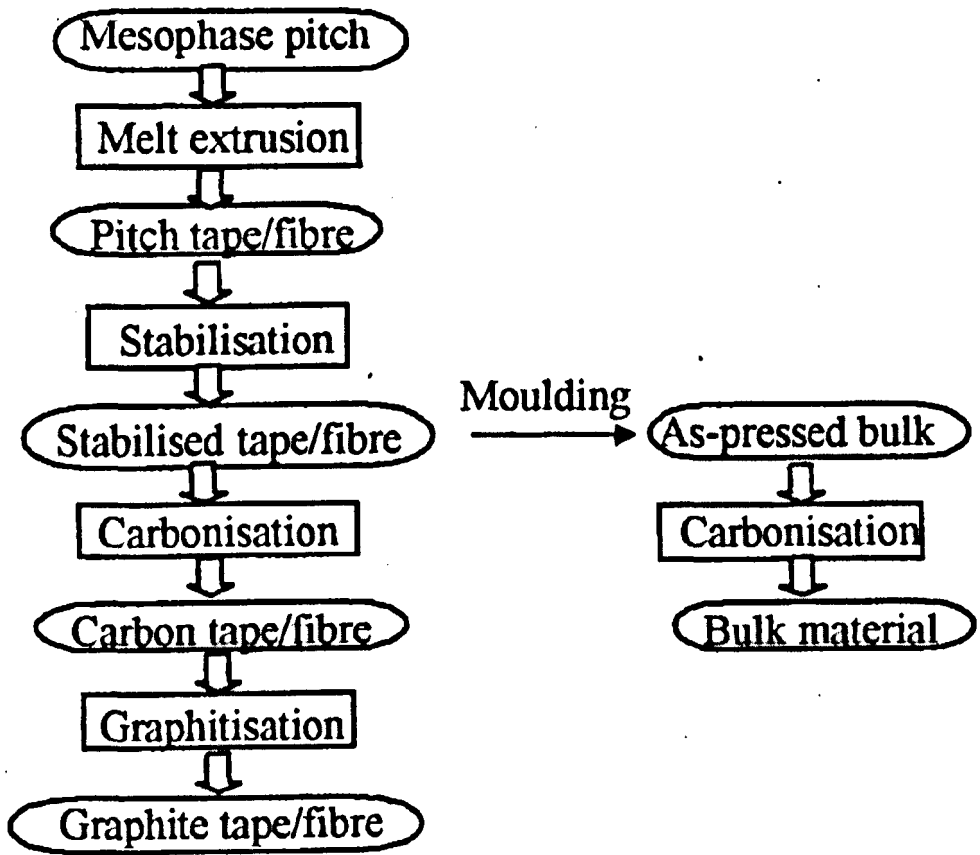


Figure 8 Flow diagram representing the route to carbon fibre/tape and its bulk material

2.10 Production of mesophase carbon fibres/tapes

The as-spun fibres/tapes are prepared from a naphthalene derived mesophase pitch using a bench-scale melt-spinning apparatus (figure 9). The molten mesophase pitch is melt-extruded at 230-300°C. It is extruded through a single hole spinneret or a slot shaped hole then a roller on a variable speed motor is used to collect the fibres .

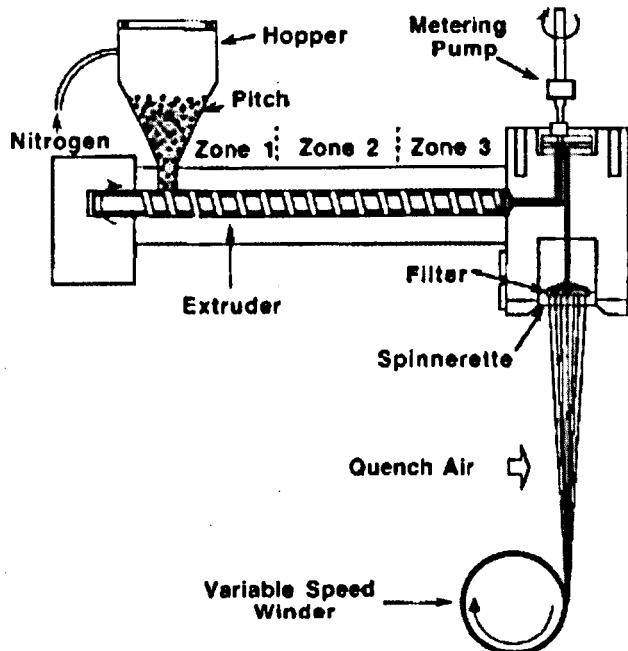


Figure 9 Schematic representation of melt spinning apparatus (Edie et al 1998)

At first glance this operation appears to be relatively simple (Edie et al 1998). However it is a rather difficult process to perform due to the flow characteristics of mesophase pitch. The pitch can be non-Newtonian but still be significantly temperature susceptible, more than most melt-spun materials. This temperature dependence of the viscosity of mesophase can create stresses near to the ultimate tensile strength of the filament, which is why the control of the heat transfer rate and the temperature is extremely important when forming pitch based carbon fibres or tapes (figure 10) (Edie, Fox et al. 1986). Edie By applying heat, mass and momentum balances, Edie and Dunham (Edie et al 1989) showed that the mesophase melt-spinning process is extremely sensitive in changes in process conditions.

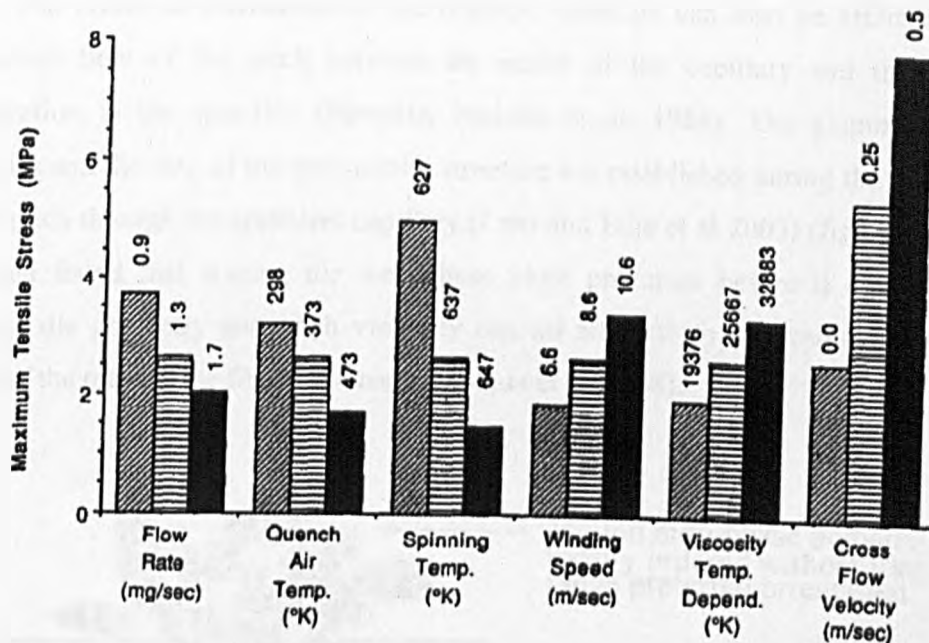


Figure 10 Summary of the effects of process and material parameters on the tensile stress in the filament (Edie, Fox et al. 1986)

Carbon fibres can be prepared from mesophase pitch by spinning using several different types of nozzles of different sizes and cross sections. It has been found that the mechanical properties are better in fibres from unconventional shaped nozzles, than those fibres which have originated from conventional circular nozzles (Fortin, Yoon et al. 1994).

2.11 Orientation of carbon fibres/tapes

The potential properties of mesophase pitch-based carbon fibres have not been fully realised. The internal structure and therefore the final properties of the pitch based carbon fibres are highly dependent on the processing conditions (Cato and Edie et al 2003). The control of processing conditions during fibre spinning allows the control of preferred orientation and transverse arrangement of the discotic liquid crystalline mesophase molecules, resulting in mesophase pitch-based carbon fibres with enhanced mechanical transport properties (Lu, Blanco et al. 2002). The high thermal conductivity value is a direct result of the highly orientated crystalline graphitic structure and its high degree of orientation parallel to the fibre axis (Rand 1986) (Adams, Katzman et al. 1998).

The preferred orientation of the discotic molecule can also be affected by the extensional flow of the pitch between the outlet of the capillary and the point of solidification in the spin-line (Hamada, Nishida et al. 1988). The alignment of the molecules and the size of the polynomial structure are established during the flow of the molten pitch through the spinneret capillary (Cato and Edie et al 2003) (figure 11). It has also been found that stirring the mesophase pitch precursor before it enters the die capillary, die geometry and pitch viscosity can all attribute to the resultant transverse texture of the mesophase fibres (Hamada, Nishida et al. 1988).

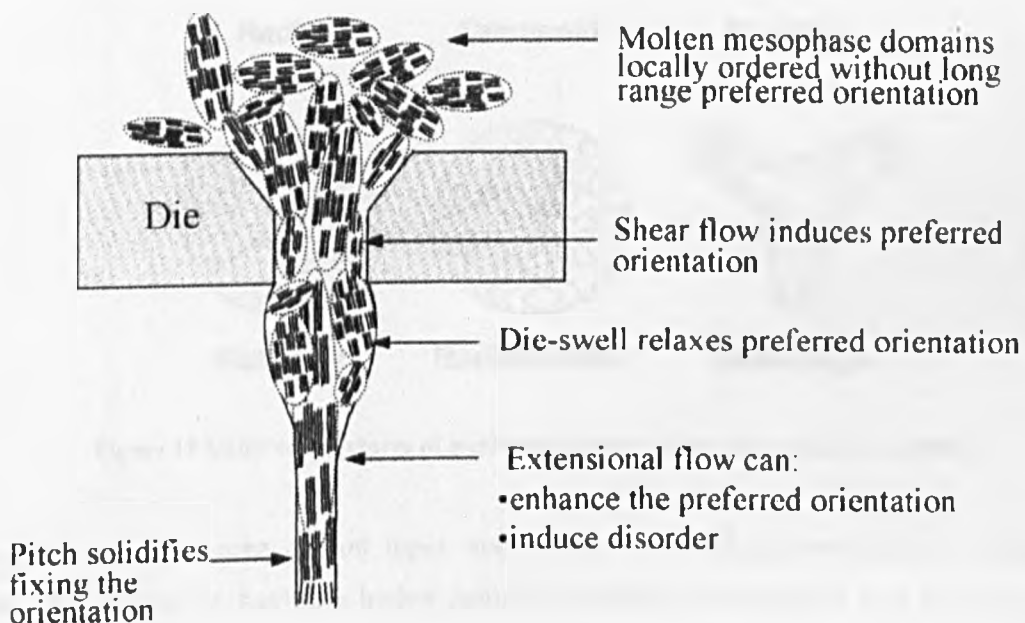


Figure 11 Schematic diagram of mesophase pitch based fibre formation (Galanopoulos 2003)

It has been established that the preferred orientation of the mesophase molecules along the fibre axis is a function of the fibre diameter. The orientation increases as the diameter of the fibre increases i.e. as the winding speed decreases. This is beneficial to the spinning process of the mesophase pitch as excessive winding speeds can introduce disorders in the tape (Hamada and Tomioka et al 1993).

Several transverse textures of mesophase pitch based carbon fibres have been reported, among which the radial, flat-layer, onion-skin and random are typical (figure 12). It is also known that fibres having a more planar texture, e.g. radial and flat-layer, exhibit higher graphitizability.

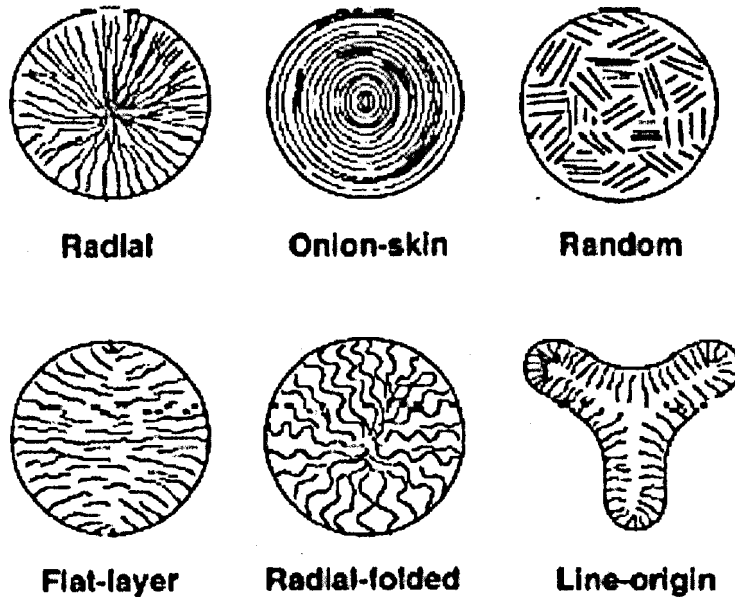


Figure 12 transverse textures of mesophase pitch carbon fibres (Edie et al 1998)

Larger transverse area carbon tapes may allow the development of more extensive graphitic planes, i.e. having a higher degree of preferred orientation. It is interesting to note that the preferred orientation of a typical mesophase pitch tape is comparable to the largest possible diameter mesophase pitch-based fibres. Figure 13 illustrates the degree of preferred orientation Full peak width at half maximum intensity (FWHM value) of as-spun mesophase pitch fibres and tapes as a function of their average transverse areas. This improvement in preferred orientation of the mesophase pitch-based tapes in turn improves the thermal transport properties (Lu et al 2002).

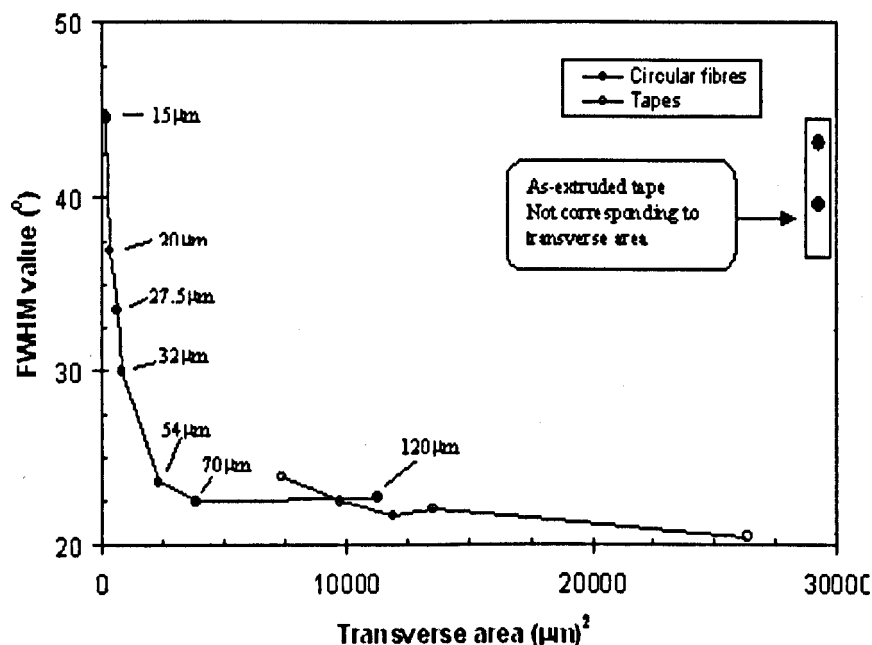


Figure 13 Preferred orientation of the as-spun circular fibres and tapes as a function of transverse areas. Full peak width at half maximum intensity (FWHM value($^\circ$)) is a measure of the preferred degree of orientation on the fibres and tapes calculated using XRD pole figures, the lower the FWHM value ($^\circ$) the higher the degree of preferred orientation, Transverse area (μm^2) refers of the transverse cross-sectional area of the fibres and tapes. (Lu et al 2002)

Stabilisation of larger diameter mesophase carbon fibres is also restricted by the time-consuming diffusion process. This is due to the formation of a diffusion barrier on the periphery of the fibre, which slows down the penetration of the oxidant to the centre of the fibre; this makes it difficult to lockdown the ordered molecular arrangement leading to a relaxation of the axial orientation during heat treatment (Lu et al 2002). It has been discovered that the ribbon shaped carbon fibres with graphitic layers predominantly orientated perpendicular to the ribbon surface show high graphitisability. This has been backed up by the work carried out on the development of the graphitic material termed Highly Orientated Mesophase-based Graphite (HOMG)(Lu et al 2002), proving the layer structure of the material can orientate parallel to the ribbon surface thus extending the planar structure and leading to a higher graphitisability (Korai, Hong et al. 1999).

2.12 Conventional method of stabilisation

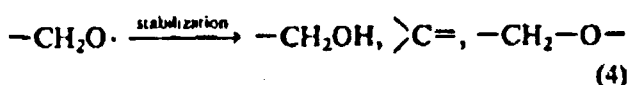
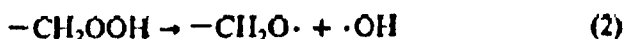
For most fibres/tapes to be stabilised they are heated in a furnace either in air or oxygen to a temperature below their glass transition temperature (T_g). The length of time that the samples are heat treated in order to stabilise them is dimension dependent. Larger diameter fibres and larger tapes will take a much longer heat treatment time than smaller fibres/tapes, as the oxygen has to diffuse much greater distances into the sample for enough stabilisation to take place to prevent softening or melting. The atmosphere in which the samples are stabilised can also effect the stabilisation time. Although stabilisation can take place in air it is a much slower process than if the sample is heated in an oxygen rich environment.

2.13 Oxidative stabilisation

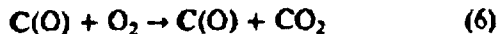
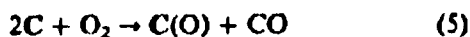
The optimisation of the stabilisation condition is important in order to maximise the mechanical and transport properties of the resultant fibres/tapes and ensure dimensional stability. Stabilisation is usually carried out between 200-300°C in air or oxygen for the as spun fibres (Lu, Blanco et al. 2002) but the thermal oxidation of the precursor carbon fibre/tape is accelerated especially when the stabilisation temperature exceeds 249°C (Yang and Simms et al 1993). The mechanisms for this oxidative stabilisation are still not fully understood. Previous research has indicated that the oxidation history of a mesophase sample does have a significant effect on the mechanical merits of the finished carbon product (Paiva, Bernardo et al. 2000). Studies of the chemical reactions that take place during the stabilisation of mesophase pitch-based carbon fibre reveal that methyl- and hydro- groups are found to accelerate the oxidation reaction and react with carbonyl groups (Kowbel, Wapner et al. 1988).

The stabilisation of pitch-based fibre showed that gases given off were limited to H_2O , CO_2 , and CO . At a given temperature the evolution of H_2O would eventually diminish to zero although its evolution could be re-started by increasing the temperature indicating a bulk dehydrogenation reaction with a number of steps available at each temperature (Lavin et al 1992). Even though, as previously mentioned, not a lot is known about the reaction sequence of stabilisation, work carried out by Miura, Nakagawa and

Hashimoto from Kyoto University has led to a plausible presumed mechanism of stabilisation (equation 1) (Miura, Nakagawa et al. 1995). As only functional groups of the fibre are expected to react with the oxygen to produce H₂O, the fibre is represented by -CH₃, the reaction sequence will be represented by:



where part (4) is not a stoichiometric equation. The sequences to form CO and CO₂ are written as follows:



Equation 1 Presumed mechanism of the stabilisation reaction (Miura, Nakagawa et al. 1995)

where C represents a carbon atom in the yarn, and C (O) represents an oxygen atom chemisorbed on C (Miura, Nakagawa et al. 1995).

2.14 Alternative methods of stabilisation

Stabilisation cannot only be carried out using the conventional oxidative technique it can also take place via several different methods such as multi-step thermal oxidation to extractive stabilisation. Multi-step thermal oxidation stabilisation was experimented with by Hayashi and Nakashima. Coal tar pitch derived fibre samples were heated to a temperature of 220°C in 1 minute and held there isothermally for 4 minutes before the

temperature was increased in the same manner to 250 and 300°C in a three step program. The stabilisation of the samples without fusion only took 15 minutes to complete. Yet the samples stabilised in this way saw a huge reduction in the final tensile properties of the fibre with up to 70% less than fibres stabilised using the slower more conventional method. A four step method was then introduced which took 20 minutes heating the sample as before to 220-250-300-350°C giving the fibres a final tensile strength of 88% compared to fibres conventionally stabilised (Hayashi, Nakashima et al. 1995). Differential scanning calorimetry (DSC) was then used to investigate the reactions that had taken place, the three-step program saw a decrease in the heat capacity of the fibre but ultimately did not completely stabilise the microstructure of the fibre. The four step program showed results very close to the samples which had been prepared using the slower heating method (Hayashi, Nakashima et al. 1995)

Extractive stabilisation, a popular alternative method of stabilisation, can be used on its own as it is proposed that deep extraction alone could provide sufficient stabilisation of fibres (Park, Mochida et al 1988) or it can be used in conjunction with oxidative stabilisation though this has been seen to give rise to a skin core structure (Mochida, Zeng et al. 1990). Extractive stabilisation is usually carried out by washing the fibre with either benzene or tetrahydrofuran (THF) (Park, Mochida et al. 1988) for about 30 minutes. The benefit of using extractive stabilisation is that it helps remove soluble fractions in the mesophase pitch by raising its softening temperature. This allows stabilisation at a higher temperature with less oxidation required for complete stabilisation. Yet as with the multi-stage thermal oxidation the resultant properties of the fibres were not excellent.

Nitric acid has been used as an effective oxidising agent at room temperature for low softening point pitch fibres. The treatment with nitric acid was carried out by contacting the fibres with a nitric acid solution. The concentration of this solution had to be carefully controlled to avoid the destruction of the fibre. It has been suggested that as a result of the oxidation caused by nitric acid it is reasonable to assume that it facilitates the stabilisation reaction. The treatment of the low softening point pitch fibres with nitric acid allows their stabilisation time to be reduced from hours to minutes (Vilaplana-

Ortego, Alcaniz-Monge et al. 2003). The nitric acid has been seen to decrease the hydrogen content in the pitch as a result of the oxidation of the pitch fibre molecules. This interaction produces some oxygenated groups of NO₂ and NO which help promote the polymerisation reactions taking place during the carbonisation, allowing the stabilisation of the pitch fibres (Vilaplana-Ortego, Alcaniz-Monge et al. 2003).

Radiation has also been used in attempts to stabilise samples. One such radiation is UV light (Paiva, Kotasthane et al. 2003). Samples of PAN fibres were exposed to UV leading to the evolution of hydrogen, methane, acrylonitrile and hydrogen cyanide, promoting simultaneous scission of chains and cross-linking reactions. A study carried out by Paiva established that UV irradiation could effectively cross-link any copolymers and enable subsequent thermal oxidation. However as with all the alternative methods mentioned low mechanical properties were exhibited using this stabilisation method (Paiva, Kotasthane et al. 2003).

2.15 Chemistry of stabilisation

Three types of oxidation reactions were recognised in the stabilisation of mesophase pitch (Fanjul, Granda et al. 2002). This can be seen in FTIR work carried out by Fanjul (2002); the first is used effectively to raise the glass transition temperature by oxygenation at lower temperatures to form alcohol, phenol, alkyl ether, aldehyde, ketone and carboxylic acid groups via dehydrogenation. These reactions are effective only for preventing sticking during stabilisation and have no contribution to the final properties of the fibre/tape.

The second is the cross-linking formation of aryether, aryester or condensation (removal of hydrogen, which is mostly aliphatic in the form of water). This improves the molecular structure of the final fibre/tape. It is this uptake of oxygen and the dehydrogenation which produces a significant change in the composition of the mesophase leading to the development of aromatic rings (Matsumoto et al 1992). As the severity of the stabilisation increases a drop in the hydrogen content is evident due to the

condensation reaction becoming more efficient. At higher temperatures it has been observed that oxygen diffuses into the core of the fibre/tape and forms cross-linking.

The third process is the gasification of the functional groups on the periphery of the aromatic rings which takes place, producing CO and CO₂. Matsumoto and co-workers (Matsumoto et al 1992) stated that it is the decomposition of the aromatic rings which releases CO and CO₂ leading to the formation of carboxylic acids, phenols and aldehydes. These, they suggested, come about due to the cleavage of carbon-carbon bonds that result in defects in the final fibre/tape (Matsumoto et al 1992). It is however unlikely that CO and CO₂ is produced via the decomposition of the aromatic rings as a result of their stability, it is more probable that the evolution of the CO and CO₂ is produced as a result of the decomposition of alkyl functional groups of the periphery of the aromatic rings.

The major reactions which take place in oxidative stabilisation occur initially around 250°C, where the oxygenation of methylene takes place, forming conjugated carbonyls on the surface of the fibres which increases the fiber weight via oxygen uptake. The second major reaction takes place around 300-400°C where oxygen diffuses into the fibre/tape cross-linking the aromatic systems by such groups as ethers and esters. Also at this temperature the oxidation of alkyl and carbonyl groups takes place to form carboxylic acids and esters. Figure 14 shows the functional groups, such as Ar-O (phenol, ether, ester), carboxyl (acids, ester), aliphatic alcohols and/or ethers, and ketones and/or aldehydes that are introduced during stabilisation. The results show a marked increase in Ar-O and unconjugated carbonyls, which were observed at 300 and 350°C. The results also show that aliphatic alcohols and ethers appeared to increase first up to 200-250°C, then probably decreased slightly up to 250°C, above 250°C it is most likely being converted into alcohol at lower temperatures and carbonyl and carboxyl groups at higher temperatures (Matsumoto et al 1992).

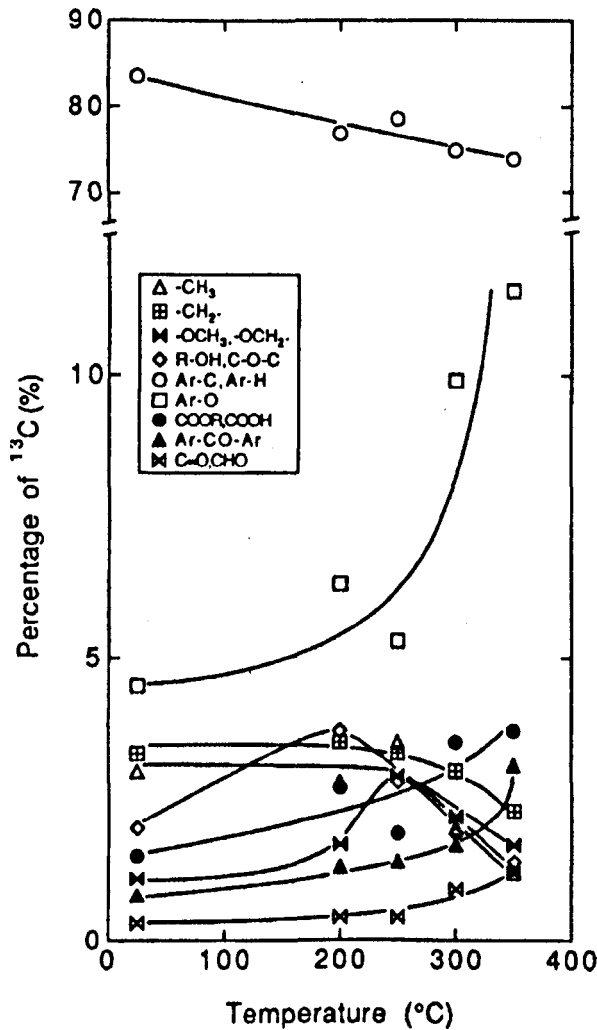


Figure 14 Change in relative concentration of functional groups during stabilisation at the heating rate of 0.5 deg/min based on solid state ¹³C NMR spectra of oxidised fibres in the aromatic and aliphatic regions (Matsumoto et al 1992)

Naphthalene derived mesophase has a more abundant and varied amount of the functional groups required for oxidative stabilisation to take place than coal tar derived mesophase. However in both cases it is the oxygen functional groups which are responsible for the massive release of volatiles promoting the formation of cross-linking bonds (Fanjul, Granda et al. 2002). It must be noted that naphthalene derived mesophase sees a greater weight gain than that of the coal tar derived mesophase during stabilisation. As a result of this the stabilisation of naphthalene derived pitch is more difficult to control and occurs within a narrow temperature range.

2.16 Weight gain/loss during stabilisation

During the oxidation process a characteristic weight gain/loss can take place; the weight gain has been attributed to a loss of aliphatic content in the pitch, with a simultaneous increase in the oxygen content as predominately ester and anhydride. The weight loss is characterised by the loss of aromatic carbon content from the pitch and further increase in the relative oxygen content in the pitch. Drbohlav (figure 15) proposed that net weight gain is dominant at lower temperatures of oxidation over short time periods while net weight loss is dominant at higher temperatures of oxidation and over a longer period of time (Drbohlav and Stevenson et al 1995). However, Cho and co-workers concluded that the net weight loss of the material is caused by decomposition of surface oxidation groups (Cho, Ha et al. 1996). Examination of the oxidation off-gas shows a relationship between the weight gain and the production of H₂O and weight loss, and also between the production of CO and CO₂ (Lu, Blanco et al. 2002).

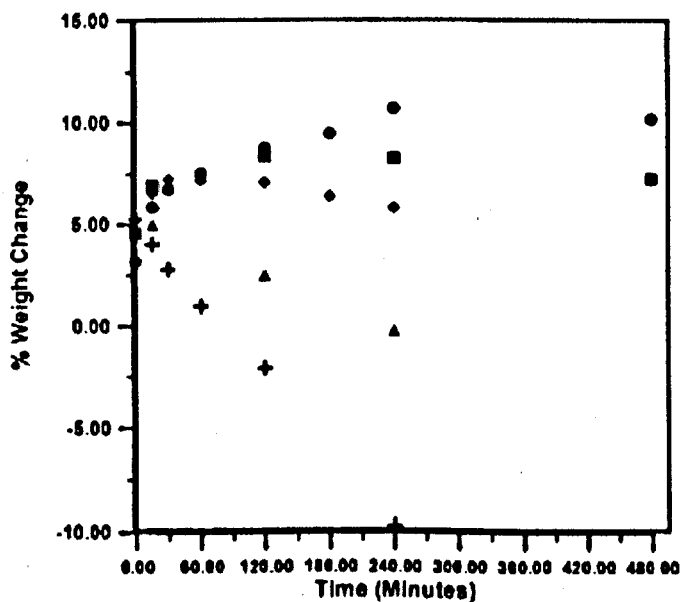


Figure 15 Weight change curves for mesophase pitch oxidation: filled circles = 240 deg/C, filled squares = 270 deg/C, filled diamonds = 290 deg/C, filled triangle = 320 deg/C, filled cross = 340 deg/C (Drbohlav and Stevenson et al 1995)

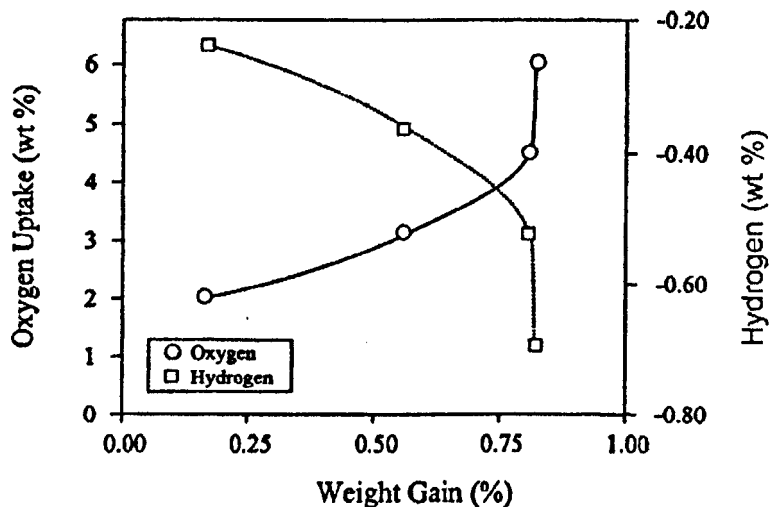


Figure 16 Variation in oxygen uptake and hydrogen loss with weight gain during the oxidation stabilisation of mesophase in the temperature range of 200-300 °C (Fanjul, Granda et al. 2001)

Figure 16 shows that up to 275°C both a continuous increase in oxygen content and a continuous decrease in hydrogen content accompanies the gain in weight (Fanjul, Granda et al. 2001). However, it can be seen that between 275°C and 300°C the weight gain is practically zero, while the oxygen and hydrogen contents undergo a significant variation suggesting that the oxygen uptake is competing with the degradation of the material.

As the change in weight of the mesophase occurs as a result of the stabilisation process, there is a variation in the hydrogen and oxygen content. These variations can be seen in (figure 17). Up to 275°C there is a clear weight gain in the coal tar pitch based mesophase (figure 17(a)), showing a continuous increase in the oxygen content with a decrease in the hydrogen content. However, it can be seen that between 275 and 300°C the weight remains almost constant whilst the oxygen and hydrogen content undergoes a substantial change (Fanjul, Granda et al. 2002). A similar trend can be seen in the naphthalene derived mesophase (figure 17(b)) although the variation in weight of the hydrogen and oxygen content is much higher. It can also be seen in (figure 17(b)) that between 275 and 300°C the naphthalene derived mesophase oxygen content increases

and the hydrogen content decreases at the same time that the weight of the sample decreases.

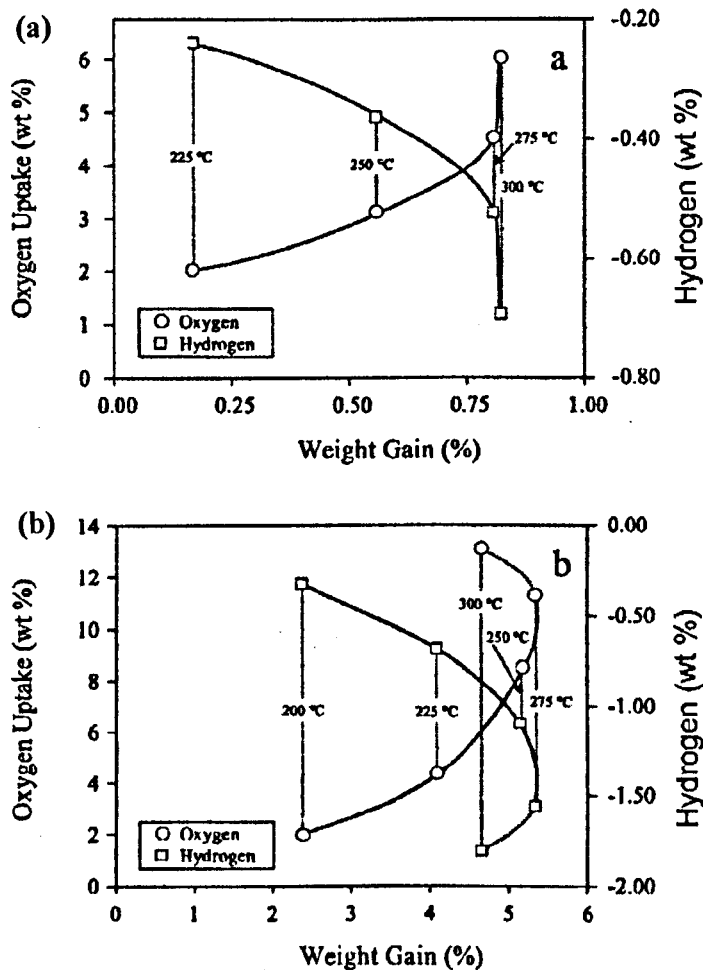


Figure 17 Variation of oxygen uptake and hydrogen loss with weight gain during oxidative stabilisation of (a) coal tar derived mesophase (b) naphthalene derived mesophase in the temperature range 200-300 °C (Fanjul, Granda et al. 2002)

During the oxidation of mesophase an initial weight gain can be seen which reaches a maximum after a time which is dependent on the temperature or atmosphere at which the stabilisation of the sample takes place, after the given time weight loss then begins to occur at a rate which is also dependent on the temperature or atmosphere with higher temperatures exhibiting a greater rate of weight loss (figure 18) (Kowbel, Wapner et al. 1988).

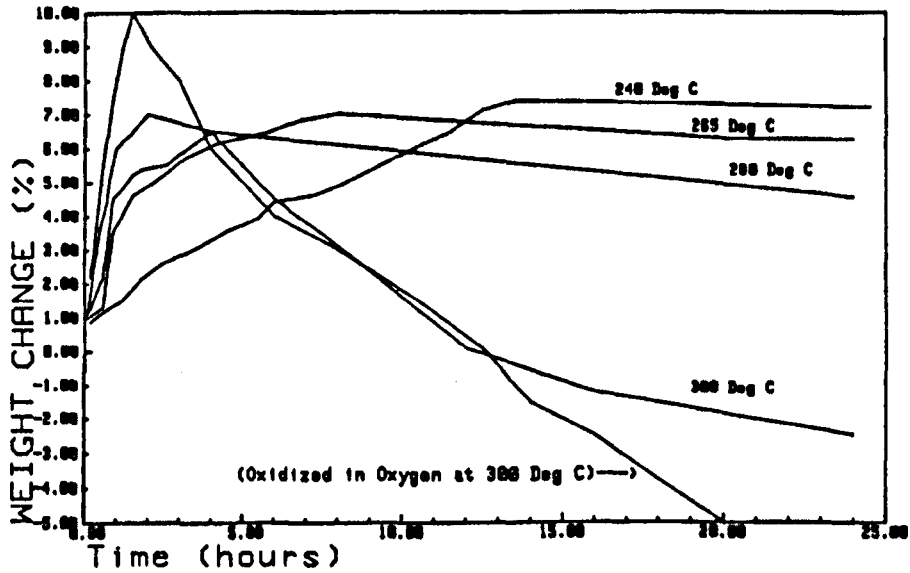


Figure 18 The weight change for 100% mesophase heat-treatment at various temperatures (Kowbel, Wapner et al. 1988)

It should also be noted that work carried out by Matsumoto and Mochida in 1992 showed that the optimum oxidation conditions provided the largest weight gain (6 wt%) of the oxidised fibres with 12 wt% of oxygen uptake, independent of the heating rate (figure 19) (Matsumoto and Mochida et al 1992).

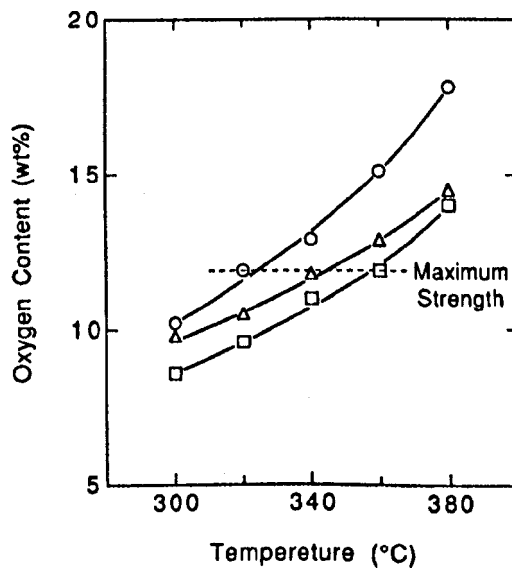


Figure 19 Effect of oxidation temperature and heating rate on the oxygen content of oxidised fibres. Heating rate; O = 0.5°C/min Δ=1.0°C/min, □= 2.0°C/min (Matsumoto and Mochida et al 1992)

It is believed that the overall weight gain that takes place during stabilisation at lower temperatures is as a result of an increase in the oxygen content in the form of ester and anhydride functionality accompanied by a loss of hydrogen in the form of water.

The weight loss experienced by the pitch comes about due to a loss of aromatic carbon content. This takes place in the form CO and CO₂ over a long period of time. The formation of aldehydes, carboxylic acids, esters and anhydrides also contribute to the weight loss along with promoting cross-linking in the pitch. The weight loss that takes place in the mesophase can be seen to take place at two distinct points. The first is around 293°C which can be attributed to the loss (distillation) of light compounds and the second ~ 457 - 480°C which can be assigned to the elimination of lighter compounds.

2.17 Diffusion of oxygen

The physical diffusion of molecular oxygen into pitch is the first step in the cross-linking and polymerisation process which leads to a thermosetting of pitch by oxygen or air. However, low oxygen uptake during stabilisation is preferred to minimise the stabilisation time, energy consumption and unfavorable influences on the properties and yield of the resultant carbon fibres. On the other hand, insufficient oxygen uptake at the core of the fibre can lead to sticking of the fibres, due to insufficient formation of oxidised molecules that can diffuse to the surface of the fibres during carbonisation (Matsumoto and Mochida et al 1993).

It is known that increasing the temperature of stabilisation accelerates the oxidation reaction. This leads to a reduction in the tensile properties of the final fibre/tape as quicker oxidation results in defects in the final fibre/tape owing to burn off taking place on their surface (Matsumoto and Mochida et al 1993). Faster heating rates allow the progress of exothermic oxidation which can exceed the rate of heat released and therefore leads to an overheated temperature that exceeds the T_g . It is for this reason that the diffusion of oxygen and its distribution in fibres/tapes should be carefully controlled via the stabilisation conditions. Matsumoto recommended that the heating rate for stabilisation of pitch should not exceed 2.0°C/min (Matsumoto and Mochida et al 1993). However, if excessive stabilisation takes place it can lead to more extensive disorder in

the carbon fibre/tape due the widespread volatilisation of CO and CO₂.

The heating rate during stabilisation is also recognised to be important, as it has been found to influence the distribution of oxygen on the surface of the fibres. In an experiment using secondary ion mass spectrometry (SIMS) the oxygen profile was measured along the radial direction in mesophase pitch fibres of 10 μm diameter heated at a constant rate of 0.5°C/min in air. Figure 20 exhibits a gradual decrease of oxygen content as the depth from the surface increases. It is also of note that Matsumoto detected more oxygen in the as-spun fibres than in the starting pitch, pointing to oxidation taking place during the melt spinning process

The oxygen profile was found to be distributed homogeneously along the radial direction in fibres oxidised to 350°C where the fiber oxidised to 250°C was found to possess a gradient of oxygen distribution from the surface to 2.5μm in depth and a flat distribution at greater depths (figure 21), Matsumoto and co workers stated that the 350°C fiber illustrated a oxygen distribution sufficient to complete stabilisation where as the distribution observed in the 250°C fiber indicating a limited diffusion of oxygen is reflects that of an incomplete stabilisation profile showing an insufficiently oxidised core from which volatile components may diffuse to the surface thus causing sticking of adjacent filaments during successive carbonisation (Matsumoto and Mochida et al 1993). Matsumoto also stated that the fibres which exhibited a more homogeneous oxygen distribution (350°C) also exhibited the maximum tensile strength and elongation (Matsumoto and Mochida et al 1993).

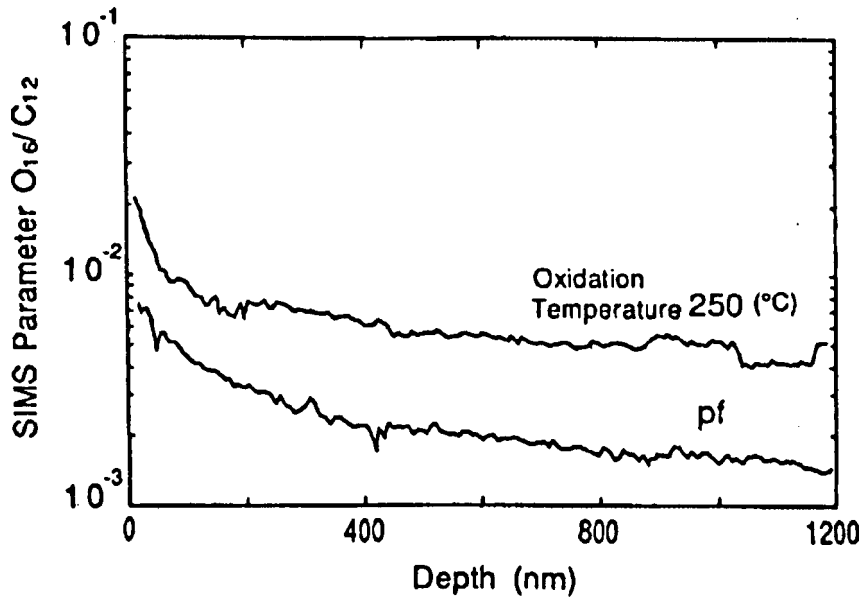


Figure 20 Oxygen distribution profiles in fibres, as-spun and after oxidation to 250°C at a heating rate of 0.5°C/min pf: as-spun fiber (Matsumoto and Mochida et al 1993)

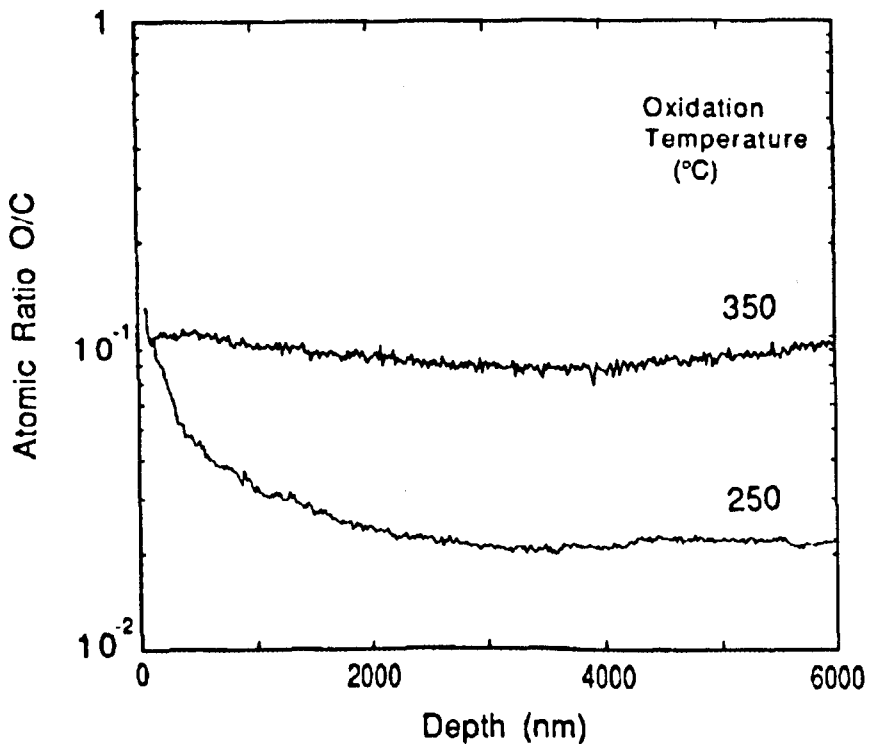


Figure 21 Oxygen distribution profiles in fibres oxidised at a heating rate of 0.5/min to 250°C and 350°C (Matsumoto and Mochida et al 1993)

Work carried out by Singer and Mitchell in (1997) produced table 2 showing the diffusion times required for mesophase pitch fibres to attain 50% and 90% of their oxygen sorption capacity (Singer and Mitchell et al 1997).

Table 2 Diffusion time ($t_{0.5}$ & $t_{0.9}$) required for mesophase pitch fibres to attain 50% and 90% of their oxygen sorption capacity (Singer and Mitchell et al 1997)

| r_s (μm) | T ($^{\circ}\text{C}$) | D ($\text{cm}^2 \text{s}^{-1}$) | $t_{0.5}$ | $t_{0.9}$ |
|-------------------------|----------------------------|-------------------------------------|--------------|-------------|
| 10 | 25 | 1.9×10^{-9} | 36 seconds | 190 seconds |
| 100 | 25 | 1.9×10^{-9} | 60 minutes | 313 minutes |
| 1000 | 25 | 1.9×10^{-9} | 100 hours | 522 hours |
| 10 | 100 | 3.2×10^{-8} | 2.1 seconds | 11 seconds |
| 100 | 100 | 3.2×10^{-8} | 3.5 minutes | 18 minutes |
| 1000 | 100 | 3.2×10^{-8} | 5.8 hours | 30 hours |
| 10 | 150 | 1.3×10^{-7} | 0.52 seconds | 2.7 seconds |
| 100 | 150 | 1.3×10^{-7} | 0.87 minutes | 4.5 minutes |
| 1000 | 150 | 1.3×10^{-7} | 1.5 hours | 7.8 hours |

The results in table 2 are in keeping with the findings of Lewis (Lewis et al 1993) who concluded that for small diameter fibres ($<10\mu\text{m}$) the process of thermosetting was a reaction controlled process and not diffusion controlled. It is for this reason that fibres with a diameter greater than $10\mu\text{m}$ are rarely produced commercially, as they are difficult to stabilise due to slow oxygen diffusion (Ko, Chiranjiradul et al. 1992). More over it must be pointed out that the time recorded for the complete stabilisation i.e. $t_{0.9}$ of the larger diameter fibres in table 2 seem to be rather short when compared to the 64 hours at 300°C in pure oxygen, which only achieved a stabilisation depth of $45\mu\text{m}$ (Smith, White et al. 1985).

This discrepancy in the findings may be because below the reaction temperatures for petroleum (180°C) and for coal tar derived pitch ($\sim 165^{\circ}\text{C}$) the results are in keeping with Lewis (Lewis et al 1993) and Cornec (Cornec et al 1992), who stated "at low temperatures a physical absorption diffusion process dominates stabilisation, allowing greater depth of penetration and a more uniform concentration profile.", at lower

temperatures diffusion of oxygen into the fibres is considered to be reversible, hence oxygen can be introduced at lower temperatures and then processed at higher temperatures (Cornec et al 1992). Above the reaction temperature the outward diffusion of reaction products prevents the penetration of the oxygen in to the fibres/tapes. It could be that the oxidation reaction products occupy micro pores and channels in the pitch and this blocks the access route of the oxygen (Singer and Mitchell et al 1997). It is also thought that the ultimate stabilisation depth of fibres/tapes maybe inhibited due to a thermosetting impermeable skin on the outer surface of larger diameter fibres/tapes preventing deeper diffusion of oxygen. As oxidative stabilisation of larger diameter fibres/tapes is a diffusion controlled process, sheath core structures in pitch based carbon fibres can form if the stabilisation at the core of the fibre is insufficient. This can also occur if the degree of stabilisation that has taken place is less than the optimum; in this, fewer oxygen atoms are permitted to diffuse into the centre core of the fibre and cross-link.

Increasing the stabilisation temperature has also been found to have an effect on the diffusion of the oxygen within the fibre/tape by accelerating the oxidation reaction. This however results in an adverse effect on the final product and is why the distribution of oxygen within the fibres/tapes should be carefully controlled by a slower stabilisation rate.

2.18 Factors affecting stabilisation

There are many factors that affect the stabilisation: the nature of the pitch, temperature, gaseous environment and time. The thermosetting of the pitch requires a careful balance of pitch properties; the pitch must be stable at the spinning temperature to prevent bubbles from forming whilst at the same time it must be able to react sufficiently with oxygen to allow a rapid stabilisation process.

The diffusion, chemical reaction and the number of reactive sites within a fibre/tape also contribute to determining the rate of stabilisation. Previous experimental work carried out by Stevens and Diefendorf (Stevens et al 1986) and Singer and Mitchell (Singer and Mitchell et al 1997) indicates that the stabilisation rate is restricted to a

degree by both diffusion and reaction rate. At temperatures lower than 200°C, oxygen profiles show that stabilisation is more reaction rate limited, while at higher temperatures (around 300°C), diffusion is the limiting factor showing a lower diffusivity for oxygen and other product gases (Stevens et al 1986) (Diefendorf et al 2000).

The formation of a sheath core structure also hinders the stabilisation process as the sheath acts as a diffusion barrier preventing oxygen uptake (Dhami, Manocha et al. 1991). The microstructure of mesophase carbon fibres has been studied using SEM Optical Microscopy and x-ray diffractometry after graphitisation. This led to the discovery that some mesophase pitch based carbon fibres have a sheath core type microstructure, the sheath being made of sheet like graphitic layers parallel to the fibres axis while others exhibit uniform structure wherein the graphitic sheets are parallel to the radius or diameter of the fibres and run along its length. The oxidation behaviour of these fibres has been correlated with their microstructure and crystallite parameters. In the case of the sheath and core microstructure the oxidation of the core starts at a relatively lower temperature than that of the sheath. Carbon fibres having higher L_a (mean x-ray coherence length in the crystallographic 'a' direction) values are found to have higher oxidation resistance (Dhami, Manocha et al. 1991).

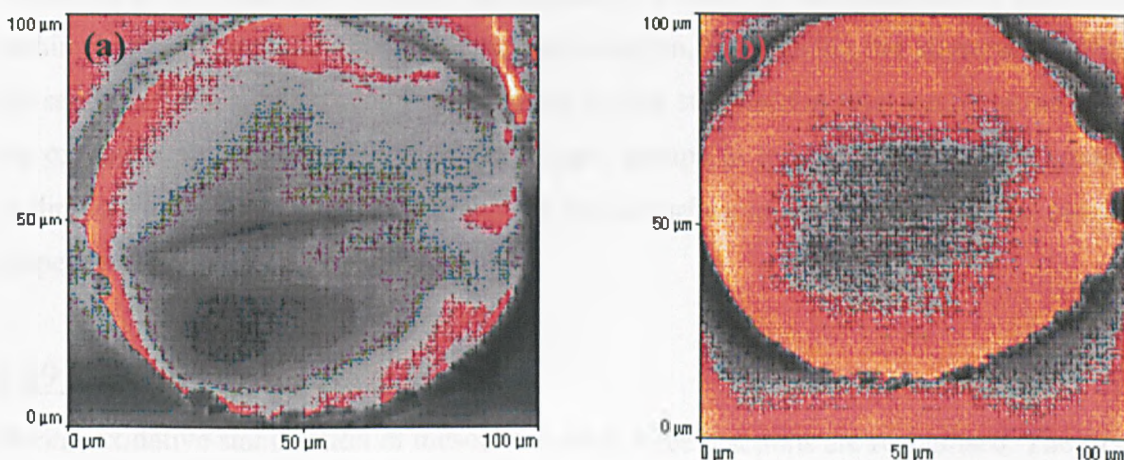


Figure 22 Stabilisation achieved in carbon fibres when heat treated to (a) 270°C and (b) 160°C and maintained there for 10 hrs (Galanopoulos 2003)

Figure 22(a) illustrates the stabilisation achieved for carbon fibres (derived from AR240) when heat-treated straight up to 270°C and maintained there for 10hrs. It can be seen that the carbon fibre has been stabilised around its surface, whereas in the centre it has not been fully stabilised. This has a dramatic affect on the properties of the carbon fibre. However (figure 22(b)) illustrates that better stabilisation is achieved when holding the stabilisation temperature at 160°C for 10hrs. This surprising behaviour has not yet been fully understood (Galanopoulos 2003) . Work was also carried out on the formation of Skin-core structure with at varying stabilisation temperatures by Blanco and co-workers using a (Thermal Atomic Force Microscope) ThAFM to show how stabilisation condition affected the oxygen profiles in carbon fibres (Blanco, Lu et al. 2002; Blanco, Lu et al. 2003).

Work carried out by Singer and Mitchell (Singer and Mitchell et al 1997), suggested that the out flow of the product gases from the fibre produced during stabilisation increases at higher temperatures. This slows the stabilisation reaction as the product gases that are released take up the voids and channels, which the oxygen would usually diffuse down.

The rate at which stabilisation occurs is also a critical factor influencing the ultimate properties of the final product. If insufficient stabilisation takes place the tensile properties of the final fibre/tape can be reduced as a result of the deformation occurring within the final fibre/tape after resultant carbonisation, by reducing the alignment within the samples. On the other hand if the sample is over stabilised at high temperatures then the oxidation and decomposition of the oxygen groups in the tape/fibre are accelerated leading to defects in the sample prominent on its surface and acts to reduce the tensile properties of the sample.

2.19 Stabilisation summary

During oxidative stabilisation of mesophase pitch three reactions are recognised. The first sees a rise in the T_g at lower temperature by oxygenation to form alcohol, phenol, alkyl ether, aldehyde, ketone and carboxylic acid groups; in this step dehydrogenation also



takes place. This reaction prevents the sticking and melting of fibres/tapes during the stabilisation process. The second forms cross-links between the pitch molecules via the formation of aryether, arylester or condensation. This results in an improvement in the structure of the final fibre/tape. The third reaction is a decomposition of aromatic rings that releases CO and CO₂ leading to carboxylic acids, phenols and aldehydes, causing defects in the final fibres/tapes.

The weight gain experienced during stabilisation takes place at lower temperatures due to an increase in the oxygen content in the form of ester and anhydride functionality accompanied by a loss in hydrogen in the form of H₂O. The weight loss occurs due to the loss of aromatic carbon content in the form of CO and CO₂, taking place over a prolonged period of time. The formation of aldehydes, carboxylic acids, esters and anhydrides also contribute to the loss in weight.

Oxygen diffusing into the pitch is the first step in the formation of cross-links between its molecules and should be carefully controlled. It has been recognised that too much oxygen uptake can adversely affect stabilisation time along with reducing the final properties of the fibre/tape. Not enough oxygen diffusion and the pitch will not stabilise sufficiently leading to melting and sticking of the fibres/tapes upon further heat treatment. It has also been noted that the kinetics of oxygen uptake on to the other surface of the samples appears to be a reaction-controlled process, and that the diffusion of oxygen into the centre of the sample is believed to be a physically controlled process.

Stabilisation can be affected by many different factors such as the properties of the pitch being used and the degree of oxygen diffusion taking place as mentioned above. The diffusion of oxygen into the fibres/tapes is believed to be hindered by the formation of a sheath-core structure which acts as a diffusion barrier and the evolution of product gases during the oxidative stabilisation process resulting in a slower, less comprehensive stabilisation. If insufficient stabilisation takes place the mechanical properties of the final fibre/tape can adversely be affected. Similarly if the stabilisation rate is too high then the oxidation and decomposition of oxygen groups are accelerated leading to surface defects on the fibre/tape, ultimately reducing its final properties. It must also be documented that

other methods of stabilisation are available but all have a detrimental effect on the final mechanical properties of the product.

3 Aims and objectives

3.1 Aims

As a result of the excellent physical, thermal and electrical properties of carbon fibres/tapes they have become of great importance in a wide range of applications: from use in the construction industry to high end thermal management, electrical and aerospace applications. Although the raw precursor is relatively inexpensive it is the resulting heat treatments which incur the bulk of the expense when producing the fibres/tapes.

Firstly stabilisation must be defined and what is to be achieved by a successful stabilisation. The general approach to stabilisation of mesophase products is to heat them to a given temperature; in most cases between 200-300°C, here they are left in an oxidising atmosphere for a pre-determined period of time usually several days. The success of the stabilisation is then judged by whether the sample melts upon carbonisation. This however is not an accurate assessment of a successful stabilisation step. When considering stabilisation there are three main categories which should be taken into account; maintaining the morphology imparted to the samples during its initial processing step (in the cases of the mesophase tapes the alignment of the discotic planes during the spinning process), minimisation of weight loss upon subsequent carbonisation and maximising the homogeneity of the sample.

The primary aim of this study is to understand further the stabilisation step which mesophase products must undergo in order to maintain their dimensional stability upon further heat treatment processes such as carbonisation and graphitisation. A greater understanding of the processes taking place during stabilisation will offer information which may be instrumental in tailoring the stabilisation step leading to a dramatic reduction in the cost associated with the heat treatment step by refining the temperature and time required to completely stabilise a mesophase pitch based carbon product.

3.2 Objectives

In order to carry out this study the difference between low and high temperature stabilisation will be investigated, concentrating on the effects different treatments have on the resultant chemistry and properties of the fibres/tapes. In this study mesophase pitch based tapes will be produced from ARMPH mesophase pitch (supplied by the Mitsubishi chemical company) via a controlled melt spinning process.

3.3 Stabilisation chemistry

From the literature the mechanism of stabilisation appears to be open to conjecture. As a result of this the chemistry of the stabilisation step will be further scrutinised in this project, focusing on the differences between low (160°C) and high (300°C) temperature stabilisation and the mechanisms involved. The chemistry of the mesophase products stabilised to varying degrees will be examined using CHNO chemical analysis and Fourier Transform Infrared Spectroscopy (FTIR) to investigate the effect of time and temperature on the carbon content (higher carbon content more favourable stabilisation indicating less decomposition) and oxygen functionalities (considered vital in the cross-linking step).

The weight change that occurs during stabilisation appears to be a key step in understanding stabilisation. A Thermo-gravimetric Analysis (TGA) instrument will be used to investigate the effect of different stabilisation times and temperatures on the weight change; carbonisation weight change of stabilised samples will also be considered. In addition using TGA-FTIR the various weight changes experienced by the mesophase product can be linked to gases evolved during the stabilisation and carbonisation steps.

Pyrolysis Gas Chromatography Mass Spectroscopy (Py-GC-MS) will also be employed to examine the effect different stabilisation conditions have on the evolution of any lower molecular weight products during the oxidative stabilisation process and subsequent carbonisations. A study on what effect varying degrees of stabilisation has on

the surface functionality will also be undertaken using XPS (X-ray photoelectron spectroscopy). This will yield important information that can not only be used to help decipher the chemistry and mechanistic routes of the stabilisation step but could also be linked to aid work on the production of laminates derived from the mesophase pitch tapes. Used along side work carried out investigating the effect of stabilisation on the mechanical properties should offer a better understanding of the most efficient stabilisation conditions to process a laminate.

3.4 Diffusion of oxygen during stabilisation

Oxygen is considered to be the key component in the stabilisation mechanism as it promotes the cross-linking reaction which ultimately leads to the thermosetting of the pitch. As a result of this it can be assumed that better oxygen diffusion will offer an improved stabilisation. In order to determine this effect Electron Probe Micro-Analysis (EPMA) and Atomic Force Micro-thermal Analysis (ThAFM) will be adopted to investigate variations in oxygen and softening profiles with stabilisation conditions.

3.5 Mechanical effects of stabilisation

The mechanical implications of stabilisation will also be explored; samples which have seen a range of stabilisation conditions will undergo tensile examination. This could lead to information which is critical to the production and development of a wide range of new mesophase products. In order to study the effect of stabilisation of the mesophase pitch-based tapes on the mechanical properties of the resultant carbon tapes, mechanical testing will be carried out using a Mayes SM50 tensile testing machine. An Environmental Scanning Electron Microscope (ESEM) will also be used to examine the tapes' fracture surfaces and to measure the surface areas.

4 Characterisation Techniques

In order to characterise the extent and affect of stabilisation of the mesophase tapes several different techniques will have to be adopted; Scanning Electron Microscopy (SEM), X-ray Diffraction (XRD), Thermo-gravimetric Analysis (TGA), Fourier Transform Infra Red (FTIR) Spectroscopy, Thermo-gravimetric – Fourier Transform Infra Red (TGA-FTIR) Spectroscopy, CHNO chemical analysis, Raman Microscopy, Optical microscopy, Atomic Force Microscopy (AFM) micro-thermal analysis, Electron Probe Micro Analysis (EPMA), X-ray Photoelectron Spectroscopy (XPS), Pyrolysis Gas Calorimetry Mass Spectroscopy (Py-GCMS), and Mechanical Testing.

4.1 Scanning Electron Microscope (SEM)

The concept of producing an image by scanning was perhaps first conceived in 1842 when Alexander Bain invented the first fax machine; however it was not till 1929 when Stintzing patented the idea of using charged particle beams for scanning and it was not until 1952 that Sir Charles Oatley invented the scanning electron microscope as we know it today.

The scanning electron microscope (SEM) operates by scanning a beam of electrons over a sample. The electrons interact with the sample's surface. As they hit the surface weakly bound electrons are emitted producing secondary electrons. It is the secondary electrons that can be measured by a detector, and used to calculate the intensity for each pixel of an SEM image. As secondary electrons are of low energy their trajectory can easily be influenced by an electromagnetic field. In order to avoid a charge build up on the sample's surface, which would influence the path of the secondary electrons, the sample surface must be conductive. Several techniques have been developed to do this such as coating the surface of a non conducting sample with a thin layer of metal or carbon.

SEM was used to examine the microstructure and surface topography of the mesophase carbon tapes. One of the main advantages of this technique is its large depth

of focus which is vital for the examination of the tapes' fracture surfaces (Edie et al 1993).

The tapes were examined using a Philips XL30 environmental SEM (ESEM) equipped with electron dispersive X-ray (EDX) analysis. Samples were prepared for use in the ESEM by cutting a carbon sticky pad in half. One half of the pad was then folded to form a right angle and stuck to the sample platform; this process was repeated on the other half of the sample platform. This allowed the mesophase carbon tapes to be stuck in a vertical position so images and measurements of the width and thickness could be obtained (figure 23). Once the tapes had been attached to the sticky carbon pads they were coated with carbon contact paint to ensure a good contact and conductivity.

SEM was utilised for several different characterisations during this investigation; firstly it was employed to determine the quality of the degassing route and tape spinning step by characterising a cross-section of a tape, post spinning session. Secondly the method was used to examine the microstructure and topography of tapes which had undergone a range of stabilisation treatments and subsequent carbonisations. Thirdly the technique was used to investigate the fracture surfaces of the tapes which had undergone mechanical testing after a range of stabilisation conditions and heat treatments and take measurements of the stabilised tapes cross section using image analysis software built into the SEM.

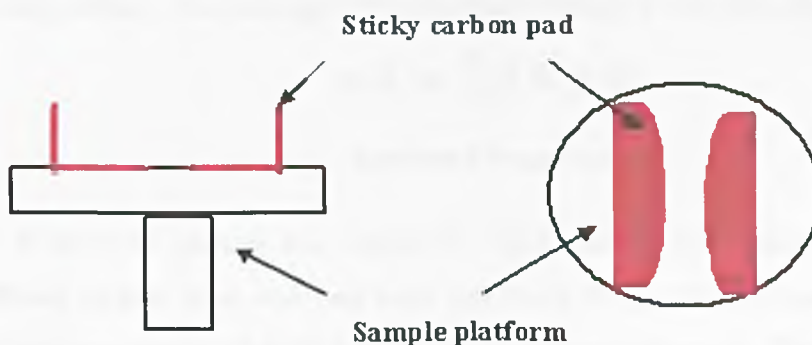


Figure 23 Schematic Diagram of Sample Prep for ESEM

In order to examine the tapes once the samples had been prepared as described above, the Philips XL30 ESEM was used in Low vacuum mode with the sample chamber operating

at a pressure of 0.5 Tor. The tapes could be examined without being coated because they had sufficient electrical conductivity to conduct away any charged electrons accumulating on their surface. The electron beam was accelerated using a 20Kv voltage and a spot size of 5, a working distance (WD) of 11mm was also set. The images were collected in Secondary Electron mode which allowed the topographic contrast of the tapes to be detected using the Gaseous Secondary Electron (GSE) detector. Knowing the working distance used in the ESEM precise measurements of the tapes dimensions were able to be made using the ESEM software by annotating the images

4.2 XRD (Pole figures)

Interested in the diffraction of light by crystals, it was in 1912 that Max von Laue demonstrated the wave nature of X-rays, diffracting them using copper sulphate crystals. Upon hearing of Laue's work William Henry Bragg along with his son, William Laurence Bragg, abandoned the notion of X-rays being electromagnetic particles, then during 1913-1914 went on to establish the use of X-ray diffraction (XRD) as a means by which to investigate crystal structures. Both father and son's achievements were simultaneously recognised by the joint award of a Nobel Prize in 1915. It was the younger, W.L. Bragg who must be credited with the concept of planes of atoms acting as 'reflecting planes', thus leading to the renowned 'Bragg's law' (Daniles 2003).

$$n\lambda = 2d \sin \theta$$

Equation 2 Bragg's Law

In order to prepare the sample for XRD pole figures a selection of mesophase pitch-based carbon tapes that had been stabilised for a selected time and temperature, were glued to a glass slide with their major surfaces parallel to it. The tapes were aligned and glued in parallel on to the glass slide to cover an area of about a 2cm² (figure 24).

XRD pole figures were used in this work to determine the quality of the alignment of the tapes after the spinning process to ensure a high alignment of the mesophase micro

domains had been achieved. The sample arrangement with respect to the X-ray beam and corresponding pole figures is illustrated in figure 24.

To produce the pole figures x-ray texture scans were carried out on a Philips X'pert texture goniometer using Cu K_{α} radiation with a Schultz reflection specimen holder with the source detector being positioned and fixed at 2θ Bragg angle for the reflection from the (0002) planes. This 2θ value was determined in a separate Bragg scan. The samples prepared as described above were then rotated around the Φ -axis at a speed of $72^{\circ}\text{min}^{-1}$. The samples was tilted by 2.5° with respect to the ψ -axis for every revolution around ϕ . The intensity from the 0002 graphite plane lying in a spiral of 2.5° pitch was recorded. The cycle of rotation around the ϕ axis was continued up to a ψ value of 85° and the data were plotted on a stereographic projection (Pole Figure) presenting the intensity data in terms of contours. Note that the data can also be presented more quantitatively as an orientation distribution function. The preferred orientation distribution is reported as the mis-orientation angle of (0002) planes along the chosen axis. This is taken as full width at half maximum (FWHM) which can be obtained from a plot of relative intensity as a function of ψ . The better the layer plane orientation parallel to the chosen sample axis, the lower the spread intensity along the ψ axis and the smaller the FWHM value will be. The orientation distribution functions were curve fitted to a Gaussian function to obtain the FWHM values; the experimental errors of FWHM values were within $\pm 1^{\circ}$.

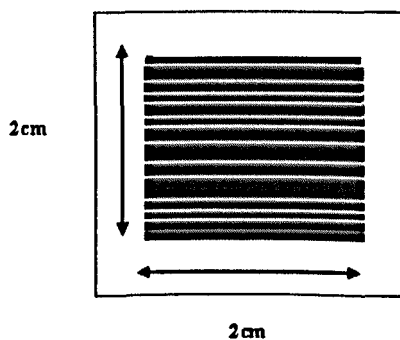


Figure 24 Schematic diagram of pole figure sample prep

4.3 Thermo-gravimetric Analysis (TGA)

A Thermo-gravimetric Analysis (TGA) was adopted as a technique to investigate the weight gain experienced by the tape samples stabilised in either an oxygen or air atmosphere over a range of times and temperatures. It was also used to track the weight loss experienced during carbonisation of tape samples which had seen a variety of stabilisation conditions and determine their final carbon yield.

A small amount of tape 95mg was accurately measured to ± 0.1 mg either green or stabilised was placed in a silica glass crucible which was supported by a wire that in turn was suspended from a microbalance. This was then enclosed within a silica tube, which was sealed and oxygen/nitrogen/air gas as appropriate was pumped into the top of the tube and expelled through the bottom. To heat the sample a vertical tube furnace was used which could be adjusted up and down the tube so that it could be positioned to best heat the sample. A type K thermocouple was then inserted to track the temperature of the sample crucible. The data from the thermocouple and the microbalance (figure 25) were fed into a Pico TC-08 digital data logger, which was connected to a computer for analysing.

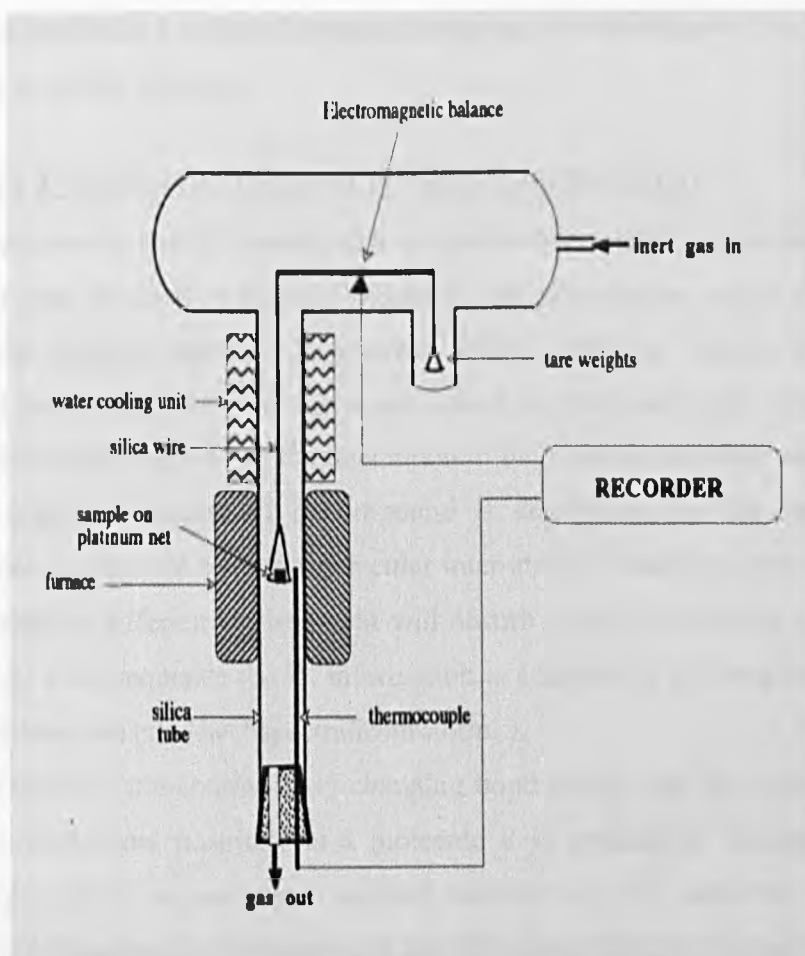


Figure 25 Schematic representation of the Thermo Gravimetric Analysis equipment

When using the TGA to examine the weight change experienced during the stabilisation of the mesophase pitch-based tapes 95 \pm 0.1 mg of green tape was placed in the TGA crucible. The sample was then sealed in the TGA furnace and nitrogen gas passed through it. A heating rate of 2°C min⁻¹ was used until the desired temperature of stabilisation was reached 160°C, 240°C or 300°C. Once at the required stabilisation temperature the atmosphere in the TGA was changed to the stabilising atmosphere, either oxygen or air and the furnace held isothermally for a period of 25hrs. The weight change of the samples was recorded at one minute intervals.

To examine the change in weight upon carbonisation 95mg \pm 0.1 mg of stabilised tapes was placed in the TGA crucible. The stabilised tapes were then heated at 15°C min⁻¹ to 1000°C in a nitrogen atmosphere and immediately cooled; the change in weight was

constantly monitored at 1 minute intervals throughout the experiment. The TGA balance was accurate to within ± 0.1 mg.

4.4 Fourier Transform Infrared (FTIR) Spectroscopy

Infrared spectroscopy is an invaluable tool as spectra information can be obtained from a sample whatever phase it is in solid, liquid or gas. The region which is of the most interest in the infrared spectrum is between $4000 - 600 \text{ cm}^{-1}$ (wave number is the reciprocal of wavelength), as it is the region which is most useful for organic analysis. Infrared spectroscopy depends on the interaction of the infrared radiation with matter.

The organic structure of a compound is determined by the electromagnetic infrared radiation absorbed by inter-molecular inter-atomic bonds in organic compounds. Chemical bonds in different environment will absorb varying intensities and at varying frequencies, as a consequence the IR information is analysed in the form of a spectrum (<http://www.chem.ucla.edu/~webspectra/irintro.html>).

As a result of the continuously changing bond angles and bond lengths of atoms oscillating around fixed positions in a molecule it is possible to distinguish between different molecules in a compound. Infrared radiation is only absorbed by molecules when the oscillating electric field produced by the atoms vibration is exactly the same as the infrared frequency. The atomic vibration which produces the oscillating electric field can be as a result of stretching (which can be either symmetric or asymmetric) or bending (in or out of plane of the molecule) of bonds. Stretching can be seen at both high and low wavenumbers whereas bending can only be detected at lower wavenumbers. As a result of this it is possible that many primary vibrations which take place in the molecule are undetected. FTIR is a useful technique as it can be used to identify the major structural features of a molecule.

FTIR was used to characterise any chemical changes that arose in the tape samples as a result of the variety of the stabilisation conditions and partial carbonisation i.e. heat treatment at 450°C . FTIR characterisations of the tapes were carried out using a Burker Vertex 70 DRIFTS spectrometer fitted with a mid-IR source; in reflection mode. Tape samples which had undergone a range of stabilisation temperatures 160°C , 240°C

and 300°C in both air and oxygen for 5 and 25 hours and subsequent heat treatment to 450 °C were prepared for examination by grinding the samples into a fine powder using a pestle and mortar. The powder was then sieved to < 100µm (Fanjul, Granda et al. 2002) and then 20g of the sieved powder was then placed on to a glass slide. A background sample was taken using a gold coated 1st surface glass mirror. (98% reflective from 1µm - 14µm or more) once the background scan had been carried out a glass slide with the powdered sample was inserted into the FTIR for analysis. The FTIR data was collected from an average of 100 scans. The spectra were collected using diffuse reflectance (absorbance) and the software then adopted the Lambert-Beer Law (equation 3), which ratios the gold mirror background signal against the signal from the stabilised mesophase pitch-based samples.

$$A = -\log_{10} \left(\frac{I}{I_o} \right)$$

Equation 3 Lambert-Beer equation

A = absorbance

I = the intensity of the light reflected by the gold mirror

I_o = intensity of the light reflected by the stabilised mesophase pitch-based tapes

The aromatic index I_{Ar} , of the samples was determined semi-quantitatively by taking the ratio of the areas corresponding to the aromatic C-H stretching band ($A_{3150-2990 \text{ cm}^{-1}}$) and both the aromatic ($A_{3150-2990 \text{ cm}^{-1}}$) and aliphatic ($A_{2990-2800 \text{ cm}^{-1}}$) C-H stretching bands using the formula (equation 4) (Fanjul, Granda et al. 2002);

$$I_{Ar} = \frac{A_{3150-2990 \text{ cm}^{-1}}}{(A_{3150-2990 \text{ cm}^{-1}}) + (A_{2990-2800 \text{ cm}^{-1}})}$$

Equation 4 Aromatic index ratio equation

4.5 Thermo-gravimetric - Fourier Transform Infrared (TGA-FTIR) Spectroscopy

Thermo-gravimetric - Fourier transform infrared (TGA-FTIR) spectroscopy is the combination of both thermo-gravimetric analysis (TGA) and Fourier transform infrared spectroscopy (FTIR) (figure 26). It can be used to study simultaneous weight change and gas evolution. Gases evolved during the heating of the sample in the TGA are passed through a heated transfer line (180°C) into the path of an IR beam in the FTIR sample compartment. As the evolved gas travels through the flow cell (heated to 300°C) FTIR spectra are collected at intervals and then stored for later processing. The TGA weight change pattern and the FTIR information can be combined to give an overview of how the evolution of specific gases during the heating process affects the overall change in weight

TGA-FTIR was utilised for two distinct investigations in this project. Firstly it was used to simulate the stabilisation process at different temperatures over a 5hr period in both air and oxygen atmospheres to examine the gases evolved during the process. Secondly TGA-FTIR was used to explore how the evolution of gases upon carbonisation varied between samples stabilised over a range of conditions.

In order to simulate the stabilisation conditions 95 ±0.1mg of green tape was placed in the TGA crucible, the sample was then sealed in the TGA furnace and nitrogen gas passed through it. A heating rate of 2°C min⁻¹ was applied until the chosen temperature of stabilisation was reached i.e. 160°C, 240°C or 300°C. Once at the desired temperature the TGA furnace atmosphere was changed to either oxygen or air, the sample was then held isothermally for 5hrs before being allowed to cool. As the stabilisation progressed the compounds that were evolved during the process are continuously swept into the FTIR flow cell. Here an infrared beam scans the gases and the spectral data are recorded.

A similar technique is used to examine the evolved gases during carbonisation. In this case, 95 ±0.1mg of tapes stabilised over a range of conditions were heated at a rate of 15°C min⁻¹ to 1000°C in a nitrogen atmosphere. Again as the sample is carbonised the evolved gas were continuously swept into the FTIR gas cell for analysis. In both

experiments the change in weight and the spectra of the evolved gases were continuously recorded.

In order to examine the gases evolved during the simulated stabilisation and carbonisation of the tapes in the TGA-FTIR (same process used for both experiments) a background reading of the FTIR gas cell was taken prior to each individual experiment. The machine was then calibrated by setting the system to subtract the background reading from any of the evolved spectra collected during the experimental runs.

The evolved gases from each sample were scanned 75 times during their respective experimental runs. Each scan generated infrared spectra for the evolved gases between 400–4000 cm^{-1} . The software (Omniac) then added the intensity data for these scans together to give an overall response for the experimental run. In order to identify individual evolved gases the instruments IR data library (Figure 27) was used to define wave number range for each one of the component gases (H_2O , CH_4 , C_2H_6 , CO and CO_2) based on a strong and unequivocal vibrational mode for each gas believed to be evolved from the samples. For example, for CO_2 both of the $\nu(\text{C}=\text{O})$ bands were encompassed by the chosen wave number range of 2250–2350 cm^{-1} , CO wave number range 2000–2200 cm^{-1} , CH_4 wave number range 2800–3200 cm^{-1} , C_2H_6 wave number range 2960–3100 cm^{-1} and H_2O wave number range 3100–4000 cm^{-1} . The intensity of infrared absorption within each wave number range then gives a measure of the relative abundance of the corresponding gas at successive stages throughout the experiment. It is possible to sum this intensity data to give a measure of the overall evolution of each gas during the experiment. As only semi-quantitative comparisons were made between samples of equal weight under equivalent experimental conditions of gas flow etc. no calibration of characteristic infrared signal intensity versus standard gas quantity was required. FTIR is only a semi-quantitative experimental method whereas the accuracy of the TGA used in this experiment was $\pm 0.01 \text{ mg}$.

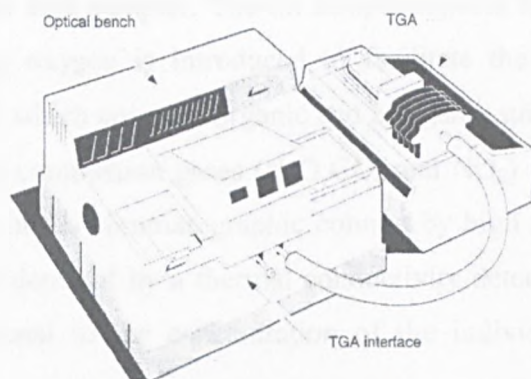
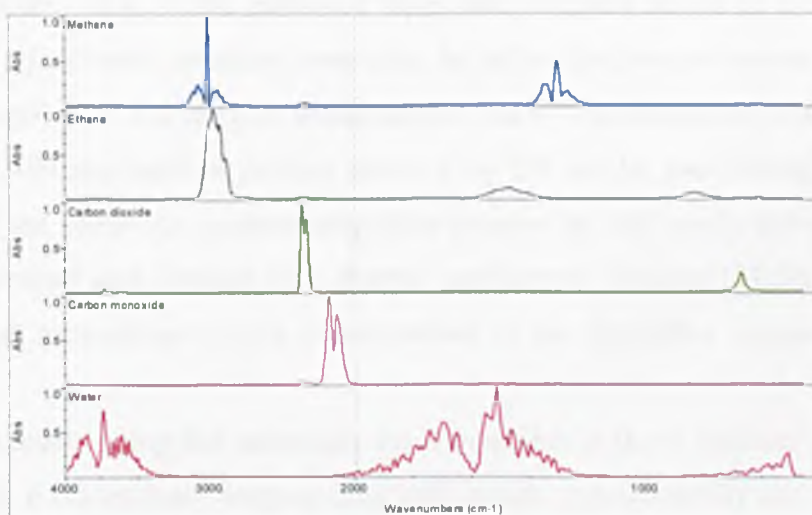


Figure 26 Illustration of TGA-FTIR

Figure 27 Library IR spectra of specific molecules (CH_4 , C_2H_6 , CO , CO_2 and H_2O)

4.6 CHNO Chemical Analysis

The CHNO chemical analysis was carried out using a Thermo Flash EA series 1112 Elemental Analyser. Each sample was measured twice, the first run was for the carbon, nitrogen and hydrogen (CHN) and the second was for oxygen (O) which was measured directly instead of being calculated by difference.

The method used for testing CHN is based on the complete instantaneous oxidation of the sample. Due to the high carbon content of the stabilised mesophase pitch-based tapes, vanadium pentoxide was added to 1 ± 0.01 mg of the stabilised tape sample to ensure complete combustion. The samples were weighed out in a tin capsule

and then placed into an auto sampler. The tin sample capsule then falls into the reactor chamber where excess oxygen is introduced to facilitate the combustion by “flash combustion” at 1700°C which converts organic and inorganic substances into combustion products. The resulting combustion gases (H_2O CO_2 and NO_2) pass through a reduction furnace and are swept into a chromatographic column by high purity helium gas where they are separated and detected by a thermal conductivity detector (TCD) that gives an output signal proportional to the concentration of the individual components of the mixture.

When testing for oxygen directly a very similar technique was adopted with a few minor variations. 1mg of the stabilised tapes was weighed out in to a silver sample capsule and mixed with vanadium pentoxide. As before the sample capsule falls into the reactor chamber where it undergoes instantaneous “flash” combustion at 1060°C. As when testing for CHN the resultant product gases of N_2 CO and H_2 pass through a reduction furnace and are swept into a chromatographic column by high purity helium gas where they are separated and detected by a thermal conductivity detector (TCD) that gives an output signal proportional to the concentration of the individual components of the mixture.

The results using this technique are comparable to those obtained by traditional methods, but it offers faster analysis time with greater reproducibility and accuracy. An extra benefit of the “flash combustion” method is that no hazardous waste is created other than the spent columns that can be used for hundreds of samples.

CHNO chemical analysis was carried out on tape samples which had been stabilised over a range of times, temperatures and atmospheres to evaluate any changes occurring in the chemistry of the tapes as a result of different degrees of stabilisation. The detection limit of this technique ± 0.30 wt% and duplicate analyses showed reproducibilities of within 0.30 wt% or better for carbon, 0.25 wt% or better for hydrogen and 0.30 wt% or better for oxygen.

4.7 Optical Microscopy

In 1665 Robert Hooke published 'Micrographia', the first text to demonstrate the importance of optical microscopy for analysing specimens of scientific interest. Since then, many developments both in the theory and design of optical microscopes have made them invaluable for characterisation of thin or polished specimens (Richardson et al 1971; Daniels 2003). Polarised light microscopy was first performed by G. B. Amici using nicol prism, a technique which imparts contrast to a specimen as a result of variations in refractive indices between different crystallographic axes. This phenomenon of optical anisotropy was further exploited by Henry Clifton Sorby in the mid and late 1800's to observe a thin hard slice of material under polarising conditions in order to distinguish various components of a material and finally establish a value for the technique (Daniels 2003).

Polarised light microscopy relies on the fact the light vibrates in all planes perpendicular to its direction of propagation. In polarised light microscopy a polariser is used which only permits the transmitted light to vibrate in one plane. The light is unaffected by being reflected from the optically isotropic specimen surface. When this unaffected light passes through the second polariser (termed the analyser) the rays enter an optically anisotropic crystal which splits the beam into two components; the ordinary ray (O-ray) and the extraordinary ray (E-ray). This allows the specimen to be observed as now the ray has a component which may pass through the analyser (Daniels 2003). Both the O-ray and E-ray have different velocities which results in them being out of phase with one another when the sample is excited. It is as a result of the interference between the two out of phase components which gives rise to the colours which can be observed when examining optically anisotropic crystals.

Optical microscopy is an important method of characterisation for a wide range of carbon materials as information can be learned from their microstructure. In order to carry out the optical characterisation of the tapes a Nikon optical microscope with a 100W halogen light source was used in reflectance mode linked to a Zeiss AxioCam MRc5 digital camera. The digital camera was connected to a computer using AxioVision

software for image processing. Polarised light and a half λ plate was used to observe the interference colours generated by the different orientations present in the carbon lamellae layers of the tapes blue, yellow and purple which are used in order to interpret the optical texture (figure 28).

In this study polarised light microscopy will be used to investigate any changes in microstructure of the tapes as a result of varying stabilisation conditions and heat treatments.

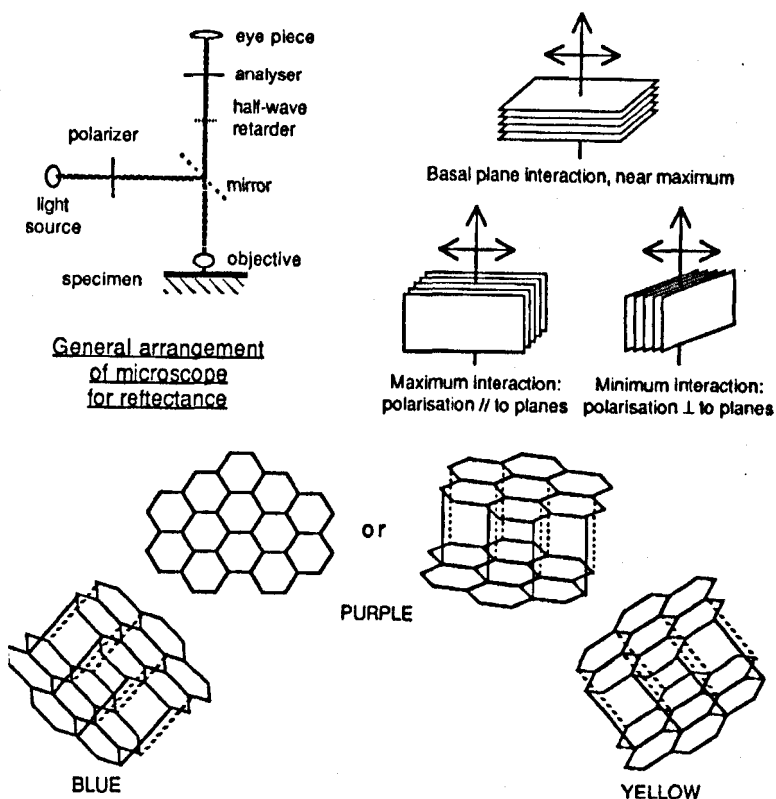


Figure 28 Polarised light optical microscopy and interference colours (Marsh 1989)

Mounting of the tapes proved to be difficult due to their fragile nature. To characterise the tapes in the best possible way they had to be mounted end on. To do this the mounting process had to be broken down into two steps. Firstly the tapes were laid flat and cast into a resin block (figure 29(a)) using a mixture of low viscosity epoxy resin and hardener supplied by Epofix. After allowing them to cure the resin tape blocks were then cut and mounted in a Struers mould (30mm diameter) with the cross-sections of the

tapes parallel with the polishing surface. Again epoxy resin and hardener was poured around the samples and vacuum impregnated (figure 29(b)). The sample was then polished for optical examination.

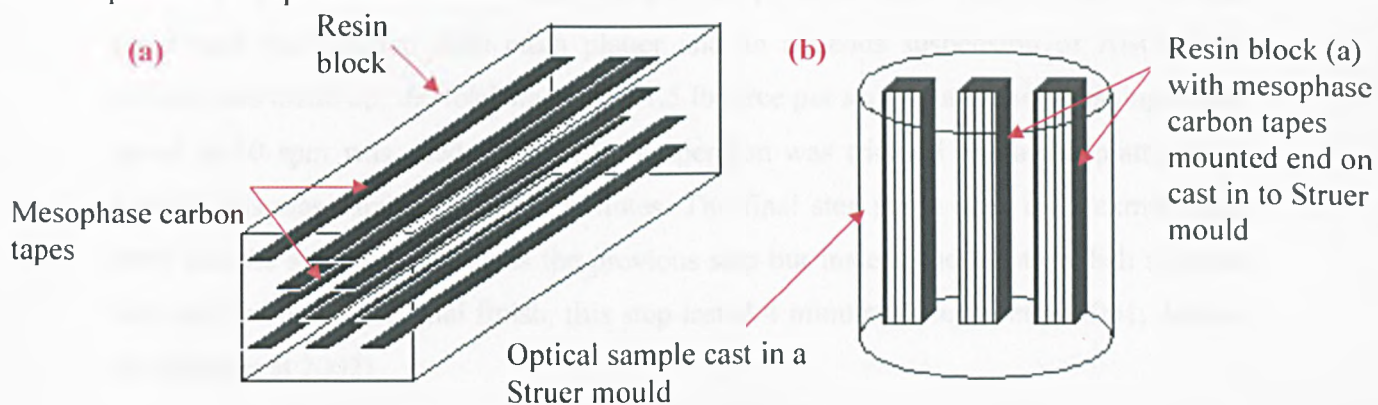


Figure 29 Schematic representation of tape sample prep for optical mounting

Before polishing could commence the samples had to undergo a short grinding procedure so that as many of the tape cross-sections could be exposed as possible. Once the tapes had been exposed a Buehler Metaserv Motopol 12 polisher was used to polish the samples. In order to obtain the best possible finish for the samples a standard polishing route was devised based on several different routes for other carbon pitches and graphite. It must be noted that polishing green tapes or those samples which had only seen a short stabilisation time and low temperature proved to be very difficult due to their soft mechanical properties.

The polishing route used was; the tape edges were exposed by grinding the samples using a SiC P60 grit paper with water, 10 samples were then placed in the Motopol sample holder ensuring all the samples were parallel to the base plane to avoid uneven polishing. A 400 grit SiC paper and water was used at 2lb force per sample for 5 minutes at 60 rpm in order to give a flat reasonable starting condition for polishing to all the samples. Once all the samples had been standardised, a 1200 grit SiC paper was used with water, applying 2lb force per sample and a wheel speed of 60rpm for 4 minutes. The samples were then washed and placed in an ultrasonic bath for 10 minutes to remove any loose particles on the sample surface which may hinder the quality of the final polish. The Motorpol was then fitted with the Buehler Metlap 4 clot platter and a 9 μ m diamond

oil polishing fluid was used at 2lbs force per sample and an rpm of 60 for 4 minutes. The samples were then washed with detergent to remove any oil and again placed in an ultrasonic bath for 10 minutes before being rinsed clean in water. The Motorpol was then fitted with the Texmat 1000 cloth platter and an aqueous suspension of Al_2O_3 $3\mu\text{m}$ powder was made up, the load was set to 1.5 lb force per sample and the polishing wheel speed to 60 rpm was used. The Al_2O_3 suspension was trickled on to the platter as it rotated; this was carried out for 5 minutes. The final step again used the Texmat 1000 cloth and the same conditions as the previous step but instead the Masterpolish solution was used to obtain the final finish, this step lasted 4 minutes (Blanco et al 2001; Anton-Arulrajah et al 2002).

4.8 Atomic Force Microscopy (AFM) (Micro-thermal Analysis)

Scanning thermal microscopy combines an atomic force microscope with a Wollaston thermal probe developed by Dinwiddie (Dinwiddie et al 1994) which has a loop of exposed platinum at its end to form the scanning tip (Hammiche et al 1996). This allows the measurement of the physical and thermal properties of samples with a lateral resolution of micrometers to nanometres (Williams and Wickramasinghe 1986; Wickramasinghe et al 2000). The probe provides a heat source together with associated electronic circuitry and which detects the thermal response. The probe can be used to obtain topographic information about the sample when in conventional atomic force microscopy contact mode. Here the tip rasters across the sample using a pair of piezo elements aligned in the x- and y-axis. With changing sample height the deflection of the tip in the z-axis changes (Majumdar et al 1998). This is monitored by an optical lever formed by a laser beam which is reflected off the mirror on the back of the cantilever into a four-quadrant photodetector. As the scanning tip passes over the sample the tip is moved vertically up and down in line with the topography of the sample by a feedback loop connected to a z-axis piezo which maintains a constant contact force thus providing a height for the sample at a given x and y position. Simultaneously the thermal tip can be used in thermal feedback, an electrical current is passed through the wire tip to heat it to a constant temperature by Joule heating, regardless of any variations in the thermal

properties of the sample (Pollock et al 2001). The probe forms one of the arms of a Wheatstone bridge, whose circuit uses a feed back loop to adjust the bridge voltage to maintain the bridge's balance and thus keep the temperature probe constant. As the tip comes into contact with the sample as it rasters across, heat is lost from the probe into the sample. In the absence of feedback, this flow of heat reduces the temperature of the probe, decreasing its resistance, resulting in an imbalance in the bridge. The feedback senses this shift and increases the voltage applied to the bridge so that the resistance returns to its set point (i.e. corresponding to the set temperature). Using this technique heat flow out of the probe is measured by monitoring the voltage across the bridge, which is then used to create a contrast based on the apparent local thermal conductivity of the sample (Hammiche et al 1996; Blanco et al 2001) thus building up an image of thermal conductivity across the sample.

Using the images obtained topographically and thermally different regions of the sample can be identified and selected for further local thermal analysis. Here the tip is moved into position over the selected area and brought into contact with the sample. The temperature of the probe is then increased using a linear heating rate whilst a small force is applied to the tip (typically around 50nN) (Blanco et al 2001). When the material reaches its softening point the tip will penetrate into the material and the z-axis position is recorded, thus determining the local softening point of the material.

The Micro-thermal analysis is carried out using a Thermomicroscope Explorer AFM fitted with a platinum/10% rhodium thermal probe (figure 30). Samples stabilised under various conditions were mounted in resin and polished using the same route as described for optical characterisation as flatness of the samples is very important factor in using the Atomic Force Microscope 4.7. Before examining each sample the ThAFM was thermally calibrated using a Nylon 6,6 (softening point 55.6°C) and Polycaprolactone (softening point 263.9°C) The samples were then placed in the AFM and the thermal tip was scanned over an area of 50µm² of the sample at a rate of 50 µm/min in order to create a thermal image. Using the thermal image as a reference, local thermal analysis can take place by positioning the thermal tip at specific points on the sample. The temperature of the tip was then increased by increasing the voltage across it. When the

temperature of the tip reached the softening point of the stabilised tape the tip of thermal probe penetrates the surface of the tape. A plot of the sensor depth against temperature was then plotted for each individual point on the sample which offers an indication as to the regions of the sample which have sustained a greater amount of stabilisation by indicating those tapes which have had their softening point raised.

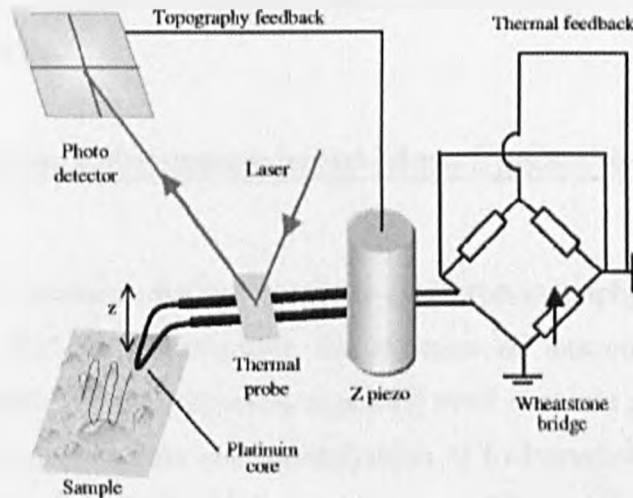


Figure 30 Schematic diagram of the micro-thermal analyser

4.9 Electron Probe Microanalysis (EPMA)

Electron probe microanalysis (EPMA) is a semi-quantitative analytical technique which has been around since the 1930's when major developments were being made in the area of electron optics. One of the advantages of this characterisation technique is that it is non destructive.

Electron probe microanalysis (EPMA) was adopted as a technique to measure the oxygen distribution across the thickness of mesophase tapes which had undergone a range of stabilisation times and temperatures. A Microprobe Cameca SX-50 fitted with a 3 wavelength dispersive spectrometers was used for all quantitative analyses and an Oxford Mirco Analysis Division Link 10/55s EDS was used for reconnaissance and qualitative analysis. Tape samples were mounted and polished using the method described for optical characterisation 4.7 in order to allow for oxygen profiling across the

tapes cross-section. These samples were coated with 15- 20 nm of electrically conductive carbon to avoid a build up of charge on the surface of the sample. Semi-quantitative analyses for oxygen was performed at 10 KV and 10nA beam using a Cameca PC2 multilayer crystal. Oxygen was standardised on alumina, with no determination of peak shift. Count times were 20 sec on the peak and 10 sec on the back ground position (Blanco et al 2001). Analysis of the tape samples was carried out at 1 μ m intervals across the full width of the tape.

4.10 Pyrolysis-Gas Chromatography-Mass Spectrometry (Py-GC-MS)

Analytical pyrolysis methods such as pyrolysis-gas chromatography-mass spectrometry (Py-GC-MS) are ideal for investigating the structure of macromolecular polymeric materials (Jones 2006). Strong inferences regarding pitch structure and composition can be drawn from the identification and quantification of hydrocarbon fragments evolved during pyrolysis of pitch. Py-GC-MS is therefore ideally suited to identification of structural changes occurring in the pitch during oxidative stabilisation. In addition, the use of reactive gas Py-GC-MS offers a method for performing oxidative stabilisation of the pitch on an analytical scale.

Py-GC-MS analysis was performed on a CDS 5000 series pyrolyser connected to a Shimadzu 2010 GC-MS. Simulation of the stabilisation on an analytical scale was performed in reactive pyrolysis mode in 100% O₂ at 160°C, 240 °C and 300°C. 2mg of green tape were held in a quartz tube and heated at a ramp rate of 1 °C min⁻¹ under a flow rate of oxygen at 10ml min⁻¹. Once the required temperature of stabilisation had been reached the samples were held isothermally for a dwell time of 300 minutes. The volatile species evolved during the oxidation were collected onto a Tenax trap and subsequently desorbed at 350°C and analysed by GC-MS.

In order to characterise the stabilised tapes upon carbonisation samples of oxidatively stabilised tape (160°C , 240°C and 300°C for 5 and 25 hrs) (2 mg) were pyrolysed at 1000 °C in He (flow rate of 10ml min⁻¹) at a ramp rate of 20 °C ms⁻¹ with a hold time of 20 sec. The products were separated on an RTX 1701 60 m capillary

column, 0.25 mm i.d., 0.25 μm film thickness, using a temperature program of 40 $^{\circ}\text{C}$ held for 2 minutes then ramped to 250 $^{\circ}\text{C}$ held for 30 minutes. A column head pressure of 30 psi at 40 $^{\circ}\text{C}$ was used.

4.11 X-ray Photoelectron Spectroscopy (XPS)

X-ray photoelectron spectroscopy (XPS) (figure 31) was developed in the mid 1960's by K. Siegbahn and his research group; he was later awarded the Nobel Prize for Physics in 1981 for his work in the field.

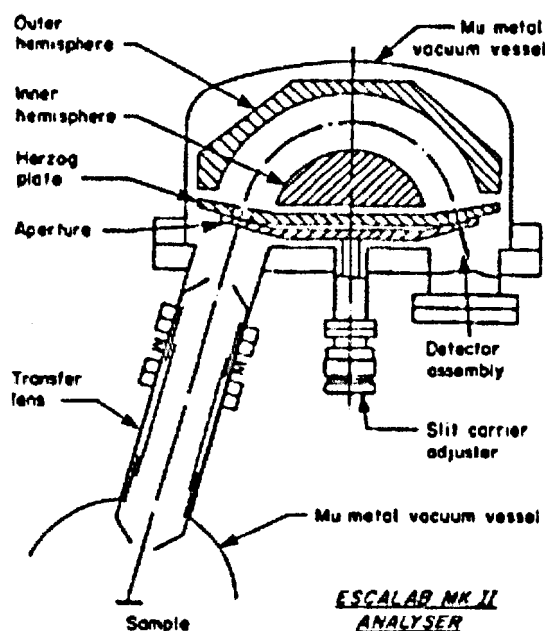


Figure 31 Conventional XPS hemispherical spectrometer with input lens (Coxon, Krizek et al. 1990)

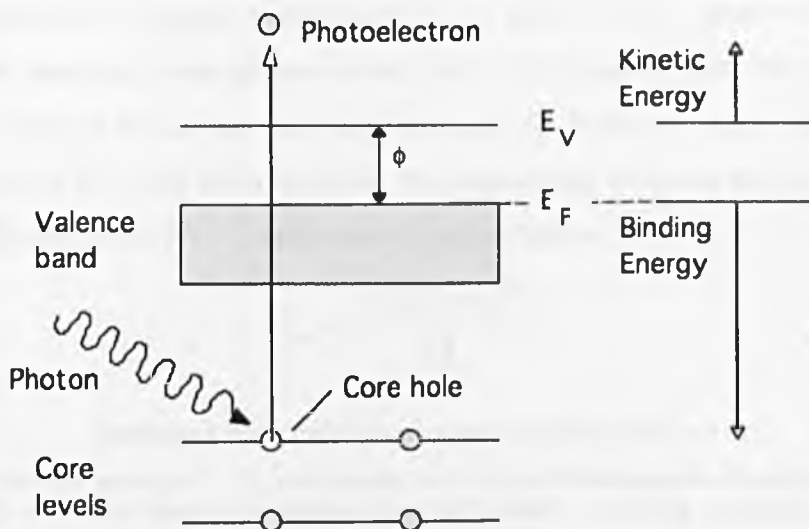


Figure 32 The photoemission process

The phenomenon is based on the photoelectric effect, first proposed by Einstein in 1905, where the concept of the photon was used to describe the ejection of electrons from the surface of a material when a photon (from a monochromatic source in the case of XPS) has impinged on it (figure 32). The technique is highly surface specific as a result of the short range of the photoelectrons which are excited from the solid. The energies of the photoelectrons leaving the sample are determined using a concentric hemispherical analyser (CHA) (figure 33) in order to give a spectrum with a series of peaks.

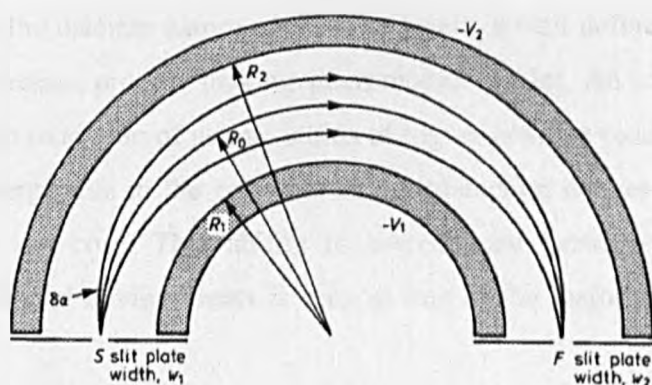


Figure 33 schematic cross section of a concentric hemispherical analyser (CHA)

The CHA works by utilising two hemispheres of radii R_1 (inner) and Radii R_2 (outer), These hemispheres are positioned concentrically to one another, with R_0 the radius of the

medium equipotential surface. Potentials of $-V_1$ and $-V_2$ ($-V_2$ greater than $-V_1$) are applied to the inner and outer spheres respectively. The electrons enter the CHA through a slit with a width of W_1 and an ideal tangential path $\delta\chi$. They exit with a focus of F and through a slit of W_2 . The expression for the relationship between the energy and an electron and the difference V_2-V_1 can be expressed as follows;

$$V_o = \frac{V_1 R_1 + V_2 R_2}{2R_o}$$

Equation 5 Potential of mean path through the analyser

An electron of kinetic energy $eV = V_o$ will travel a circular orbit through the hemispheres at radius R_o . Since R_o , R_1 and R_2 are fixed in principle, changing V_1 and V_2 will allow scanning of electron KE (kinetic energy) following the mean path through the hemisphere

As the binding energies of the peaks produced by the scan are element specific it allows a material to be characterised into its component elements. Also by using the correct sensitivity factors ($C1s = 0.25$, $O1s = 0.66$) the areas under the peaks can be used to determine the composition of the material's surface. The shape of the peak and the binding energy position can also offer up information about the chemical state of the emitting atom. A chemical shift occurs as a result of small changes taking place in the formal oxidation state or the local chemical and physical environment of the emitting atom. These changes result in small shifts in the peak positions of the spectrum. The chemical shifts are interpretable in the XPS spectra due to the technique's high intrinsic resolution (due to the discrete nature of the core levels, a well defined energy level) and that it is a one electron process making interpretation easier. An example of chemical shift can be seen in oxidation of atoms; atoms of higher positive oxidation state exhibit a higher binding energy due to the extra columbic interaction between the photo-emitted electron and the ion core. This ability to discriminate between different states of oxidation and chemical environments is seen as one of the major strengths of the XPS technique.

XPS was employed in this study to track any changes in the surface functionality of the tapes with respect to their stabilisation conditions. XPS analysis was carried out using an ESCLAB 250 XPS with a $Al K\alpha$ (1486.6 eV) photon source. Sample preparation for XPS was straight forward; tapes at varying degrees of stabilisation were placed on the

XPS sample holder and were simply attached to it by painting over the edges of the tapes with carbon dag (conductive carbon paint). The mounted tapes were placed in the XPS sample chamber which had been pumped down to a pressure of 3×10^{-9} mbar by way of an air lock. Once the samples were in place the X-ray beam (spot size $500\mu\text{m}$, take off angle 45°) was positioned at the centre of the mesophase pitch-based tape. A survey scan (between $\sim 0 - 1500$ eV, number of passes 3) was then carried out on the tape at a pass energy of 150eV in order to identify the near surface chemical composition of the tapes. Once the chemical composition of the tapes had been established by the survey scan a narrow more detailed scan (80 passes) was carried out for the C1s (275-300 eV) region and O1s (420-445 eV) region carried out at a pass energy of 20 eV

In order to analyse the spectra produced from the XPS scans a purpose written commercial computer package was used (Casa XPS). As the spectra would need to be deconvoluted to obtain the maximum amount of information a XPS C1s scan was carried out on a pure form of carbon (natural graphite) to determine a reasonable FWHM constraint value. As this FWHM was found to be $\sim 0.7\text{eV}$ it was practical to set the deconvolution limit to be twice this value to account for the strongly non-graphitic nature of the samples analysed. The samples were then baseline corrected using a Shirley line and the samples were curve fitted using a Gaussian fit procedure.

4.12 Raman Microscopy

Raman spectroscopy makes use of the Raman effect. Inelastic scattering occurs when an incident photon has enough energy to cause the atom to make a transition to an excited vibrational state. The energy of the scattered photon (hf') is related to the energy of the incident photon (hf) by the equation $hf' = hf - \Delta E$, where ΔE is the excitation energy. Inelastic scattering of light from molecules was first observed by CV Raman and is therefore referred to as Raman scattering (Aslam 2006)

Raman scattering provides a spectral technique for the identification of the symmetries of the structure and bonding of the carbon atoms and the energies associated with these fundamental excitations in the various forms of carbons. In addition,

information can be gathered about defects present in materials by comparison with an ideal case (Dresselhaus, Jorio et al. 2002; Aslam 2006).

Raman spectra are distinctive for sp^3 , sp^2 and sp carbons, as well as for disordered sp^2 carbons, fullerenes and carbon nanotubes (Dresselhaus, Jorio et al. 2002); thus Raman spectroscopy has been used extensively to study carbon materials as an initial non-intrusive technique. The Raman spectra of carbon consist mainly of two peaks with the relative intensities depending on their structure, as can be seen in (figure 34). The higher frequency peak occurs at $1582\pm 1\text{ cm}^{-1}$ (figure 34(a)) and corresponds to graphitic in-plane stretching mode in the vicinity of the E_{2g2} mode of pristine graphite and is referred to as the 'G' peak. The low frequency peak, at 1360 cm^{-1} in (figure 34(b)), arises from disordered carbon and is referred to as the 'D' peak; the intensity of the peak increases with an increase in defects while the position of this peak is dependent on the energy of the exciting laser (Wang, Alsmeyer et al. 1990) and is shifted by 50 cm^{-1} for 1 eV difference in laser energy (Reich, Thomsen et al. 2004). This has been observed during studies of graphite as well as MWCNTs and SWCNTs (Pimenta, Jorio et al. 2001; Aslam 2006).

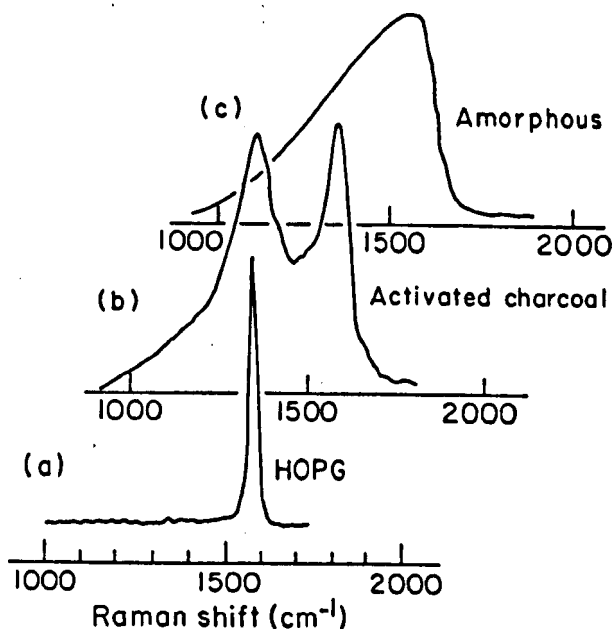


Figure 34 Raman spectra for various carbons, taken at room temperature (Pelletier 1999)

The origin of the D-peak can be understood due to a double resonant Raman scattering; a one-phonon-emission and a second-order Raman process that consists of two scattering processes, one of which is elastic and due to a defect while the other is a phonon emitting/absorbing inelastic scattering process (Dresselhaus, Jorio et al. 2002). The two phonon processes result in the second harmonic D' Raman phonon mode around 2700cm^{-1} (Dresselhaus, Jorio et al. 2002). In double resonant Raman scattering, electron scattering can occur when there are electronic states for both scattered and excited electronic states for photons to go into, resulting in the Raman intensity being doubly enhanced (Aslam 2006)

Raman characterisation was exploited in this study to examine how a range of stabilisation conditions can affect the bonding and structure of the mesophase pitch carbon tapes. A Renishaw InVia Raman microscope using a 514 nm argon ion laser and 1800 grooves per mm grating was used. The experiment was carried out on stabilised and partially stabilised tapes, using the transverse cross sections to study the oxygen transport process and the major surface to characterise the stabilised tapes themselves. For the cross-section examination samples were prepared using the same method as described in the optical characterisation, section 4.7. Changes in the ordering of tapes as a result of variations in stabilisation conditions, and thus oxygen uptake, were examined by comparing Raman spectra taken from tapes' cross-section examining the edge and middle of the tapes. For the tape surface characterisation samples were simply placed on a microscope slide and positioned under the microscope and the instrument was focused on the centre of the major surface of the tape.

4.13 Mechanical Testing

Mechanical tensile testing dates back many years. It is documented that Leonardo da Vinci carried out such an experiment with his famous test on iron wire. Galileo was the first to propose using cross-sectional area as a characterising parameter for strength calculations. However, it was not thought that other dimensions would need to be scaled in order to provide a full insight in to the tensile properties of the material. It was not until



the second half of the nineteenth century that this was realised and mechanical testing began to be carried out on a scientific basis (Curbishley et al 1998).

The mechanical properties of carbon fibres, is an area of particular interest due to the unique properties the material can possess both, thermally and electrically. It has already been discussed in the literature review that these properties arise as a result of the mesophase fiber/tape process route and the processing conditions used. It is important to obtain values of material properties, such as strength in tension, as they are important dynamic in engineering design. Tensile test data can be used for a number of different purposes such as: to design or predict service performance, to compare materials for selection purposes, for quality control, to the control forming or fabrication processes and provide a tool for fundamental studies of material behaviour.

Since the purpose of this research was to compare the effects of various processing conditions on the mechanical properties it was deemed sufficient to measure engineering properties. Hence the values used are as defined below.

The equations used to derive the engineering Young's modulus and tensile strength were

$$\text{Tensile strength} = \frac{\text{Force}}{\text{Area}}$$

Equation 6 Tensile strength equation

$$\text{engineering Young's modulus} = \frac{\sigma}{\epsilon}$$

Equation 7 engineering Young's modulus equation

Where,

σ is the tensile stress

ϵ is the tensile engineering strain = $\frac{\text{change in dimension}}{\text{original dimension}}$

As a result of the homogenous nature of the carbon tapes there are two major hurdles which have to be overcome before uniform stress can be obtained in tensile tests. The first is non-axial loading which results in a bending force being applied to the sample. The second is geometric stress concentrations across the gauge sections of the tapes.

Samples were prepared for testing using a route based on the recommended method by the American Society for Testing and Materials (ASTM) D3379-75⁵, where the filament is mounted on a centre line of a slotted paper and axial alignment is achieved without damage to the filament. After the specimen is mounted in the testing machine the paper tab is cut to allow the filament to elongate so that a load displacement curve can be obtained.

In order to adapt this technique for use with mesophase pitch based carbon tapes a few modifications had to be made. The carbon tapes were stuck in the correct position on the card jig (which has a gauge length of 20mm) (figure 35) using a piece of doubled sided sticky tape. It is of the utmost importance that the tape is stuck as straight as possible. Once the carbon tape was secured to the card jig superglue was added to the point where the card and the tape were in contact. A piece of card was placed over the point at which the tape contacted the card to reinforce and ensure a secure bond during testing, so that no slipping would occur and the best results possible would be obtained. It should also be noted that the card box used had cuts in the sides a feature which was added with the hope that it would make cutting through the card with a hot wire easier without affecting the tape, to allow the sample to elongate.

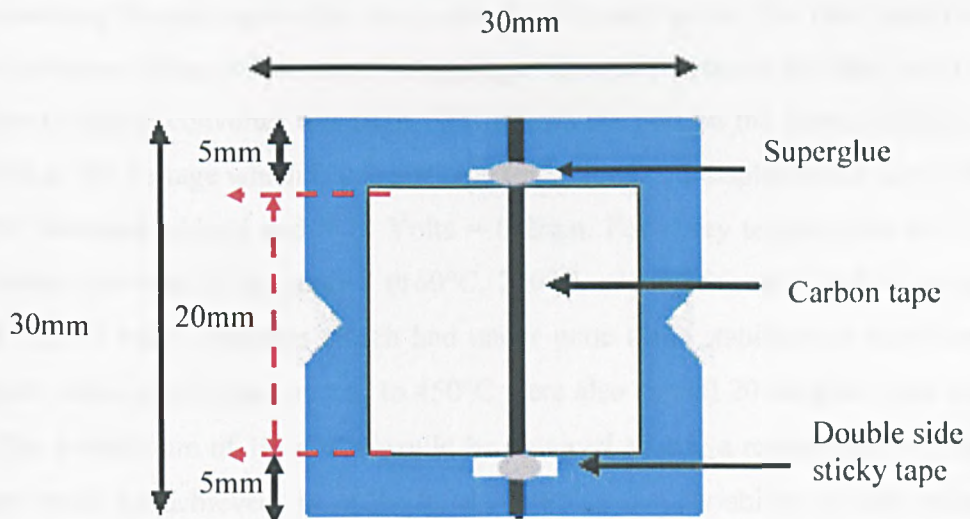


Figure 35 Schematic diagram of the original tensile sample showing gauge length of 20mm

The tensile tests of brittle materials such as carbon fibres are difficult to analyse due to the high scatter observed. This is a consequence of the nature of the test such as the dimensions of the samples and the presence of flaws and other imperfections even with a carefully controlled spinning process. Flaws are randomly distributed within the tapes. The tensile strength of the sample depends on the gauge length of the test sample. The longer the fiber the more flaws that can be present and the higher the probability of several flaws being present in one sample (Paiva, Bernardo et al. 2000; Paiva, Bernardo et al. 2001) This is why a smaller gauge length is beneficial as it keeps the number of flaws to a minimum giving a more consistent set of results however, the shorter gauge lengths are less representative of the fibres/tapes used in practice

The mesophase tape samples which had been treated to a range of stabilisation temperatures and heat treatment temperatures were tested using a Mayes SM50 tensile testing machine. The load cell used in this experiment was set to 2kN (which equated to a 2000N maximum load) and the range was set to 20mm whilst the speed of the experiment was set to move the load cell at a rate of 20 μ m per minute. The Mayes SM50 pneumatic grips were used to hold the tensile samples in place (figure 36). This was a great advantage due to the small size of the tensile samples that were being dealt with and made resetting the apparatus after every sample relatively quick. The data were recorded on to a computer using a Pico recorder package. In order to record the data an ADC 100 analogue to digital converter was used. This allows the port on the Mayes SM50 to send its signal in DC voltage which is proportional to the load and displacement i.e. 0-10 Volts = 0-200 Newtons of load and 0-10 Volts = 0-2mm. For every temperature and time of stabilisation that was being studied (160°C, 240°C, and 300°C stabilised in oxygen for both 5 and 25 hours. Samples which had under gone these stabilisation conditions and then been subsequently heat treated to 450°C were also tested) 20 samples were tested in order that a minimum of 10 results would be obtained so that a representative arithmetic average could be achieved. In order to characterise the variability of the strengths a Weibull analysis was carried out as explained in detail in the results section. Although only a limited number of samples could be measured, this treatment did enable changes in the strength distribution due to different stabilisation or heat treatment conditions to be

detected. In addition, standard deviations were calculated. A typical example of the stress strain curve produced when testing one of the stabilised mesophase pitch-based tapes can be seen in figure 37.

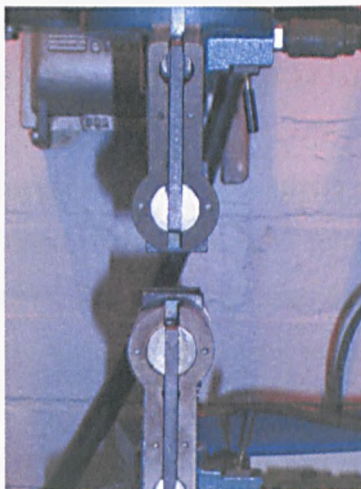


Figure 36 Pneumatic grips used to hold tensile samples

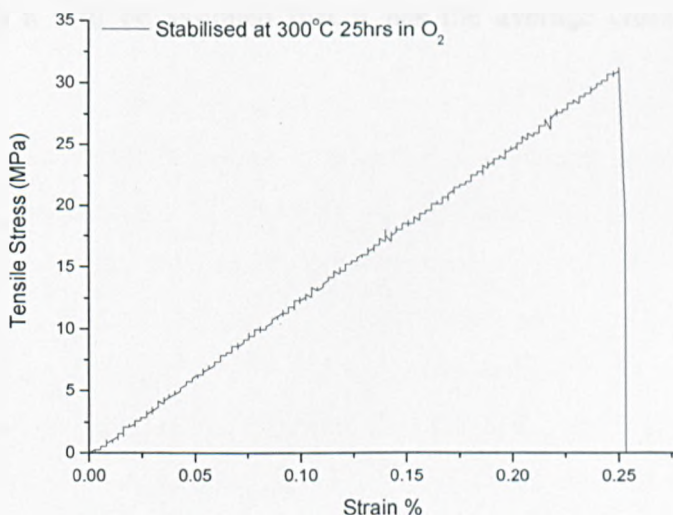


Figure 37 Typical example of an original stress strain curve produced when mechanically testing the mesophase pitch based tapes which have under gone stabilisation (300°C for 25hrs in Oxygen).

In order to obtain an accurate measurement for the tensile stress and therefore the engineering Young's modulus of the tapes, a precise measurement of the cross sectional area of the tapes is required. To gather this information a Philips XL30 ESEM was used as described in the electron microscope section and images of tape cross sectional areas were quantified by using the ESEM software XL microscope control version 6, the measurements were accurate to within 1%. The ESEM was also used to gather fracture surface images of the tapes.

When measuring the dimensions of the mesophase pitch based carbon tapes a non uniform set of results were obtained, showing that the spinning process does not produce exactly dimensionally perfect tapes. The results showed that the width of the tapes varied from 0.754 – 1.4mm and the thickness of the tapes ranged from 0.0151 – 0.0312mm. Calculating the cross sectional area of the tapes provides results ranging from $1.3 \times 10^{-8} \text{ m}^2$ – $3.31 \times 10^{-8} \text{ m}^2$. As not all the samples that were tested were recoverable an average of the tape dimensions had to be acquired in order to process the data for each of the individual tests. In this experiment if the tape was not recovered (fractured into pieces too small to recover) it will be assumed that it has the average cross sectional area of $2.2232 \times 10^{-8} \text{ m}^2$.

5 Processing of mesophase pitch-based tapes

5.1 Pitch comparison

Several different batches of pitch supplied by Mitsubishi were available in the laboratory; which had all been stored in air tight containers. A comparison of the pitches was undertaken to evaluate how the pitch differed from batch to batch. The materials available were; ARA24 from 1994 (a prototype ARMP pitch), ARMP pitch from 1999, 2004 and 2005. In order to compare the pitches samples were analysed by CHNO chemical analysis (table 3) and carbonised in a TGA to determine their final carbon yield and weight loss pattern.

Table 3 Change in CHNO composition with pitch batch

| <i>Sample</i> | <i>Carbon %</i> | <i>Hydrogen %</i> | <i>Nitrogen %</i> | <i>Oxygen %</i> | <i>Difference %</i> |
|------------------|-----------------|-------------------|-------------------|-----------------|---------------------|
| <i>ARA24</i> | <i>94.2</i> | <i>5.1</i> | <i>T/N</i> | <i>T/N</i> | <i>0.7</i> |
| <i>ARMP 1999</i> | <i>94.1</i> | <i>5.0</i> | <i>T/N</i> | <i>T/N</i> | <i>0.7</i> |
| <i>ARMP 2004</i> | <i>94.5</i> | <i>5.4</i> | <i>T/N</i> | <i>T/N</i> | <i>0.1</i> |
| <i>ARMP 2005</i> | <i>94.2</i> | <i>5.2</i> | <i>T/N</i> | <i>T/N</i> | <i>0.6</i> |

T/N = trace or nil < (0.3), elemental analysis error is $\pm 0.3\%$ in all cases.

Note, where the percentage difference in a sample's elemental analysis is greater than that of the experimental error, it can be accounted for by the presence of sulphur (an element which was not tested for in this experiment) in the mesophase pitch supplied by the Mitsubishi Gas Chemical Company. The presence of sulphur in the mesophase pitch is documented in the work of Fanjuil and co-workers (Fanjul, Granda et al. 2002). Its presence is also evident in later characterisation work carried out in this study using x-ray photoelectron spectroscopy (XPS) in figure 72 small peaks identified as sulphur can be observed at approximately 163.3 eV in the XPS survey scans.

All pitches exhibit similar carbon and hydrogen content: ~94% and ~5% respectively (detection limit of ± 0.3 wt %), no readings were obtained for nitrogen or oxygen in any of the supplied batches of pitch. It should be noted that oxygen was tested for directly and not by difference.

Carbonisation TGA curves for different batches of green mesophase pitch (figure 38) again all illustrate similar results, they appear to follow a very similar weight loss pattern and display roughly the same carbon yield of approximately 80%. In light of these results it was decided that the ARMP 2004 pitch would be used as it exhibited a fractionally higher carbon and hydrogen content and there was a plentiful supply.

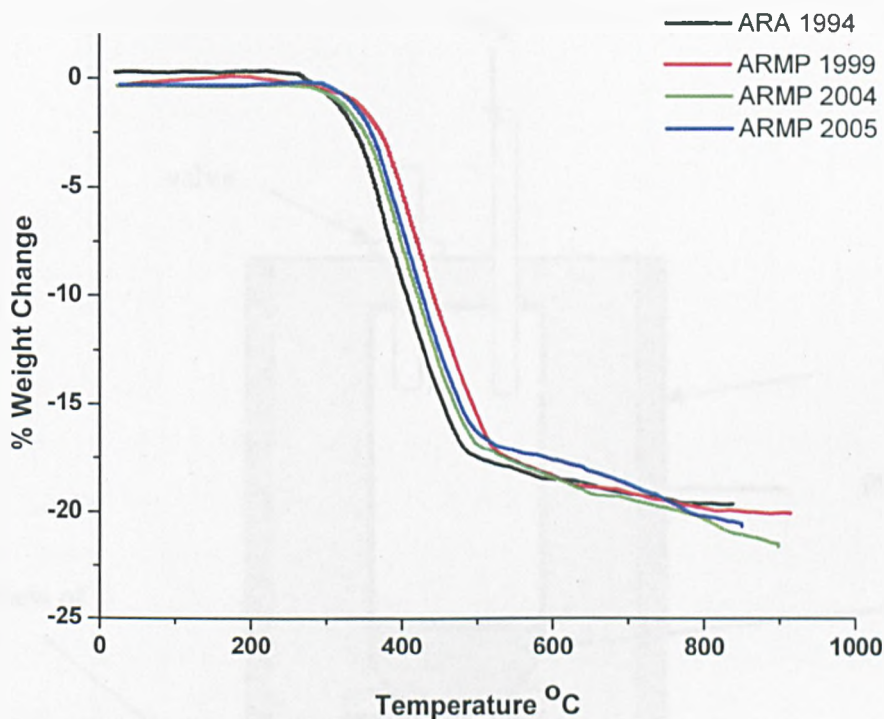


Figure 38 Weight loss patterns upon carbonisation in nitrogen for different batches of pitch

5.2 Preparation of mesophase pitch based carbon tapes for stabilisation

For a successful spinning to be carried out it is essential that the spinning rig apparatus (figure 39) is thoroughly cleaned. Flaws in the fibre can develop as a result of foreign particles contaminating the fibres during the original spinning (Bacon et al 1979). The die was cleaned using THF (Tetrahydrofuran), a solvent which dissolves the pitch making cleaning easier.

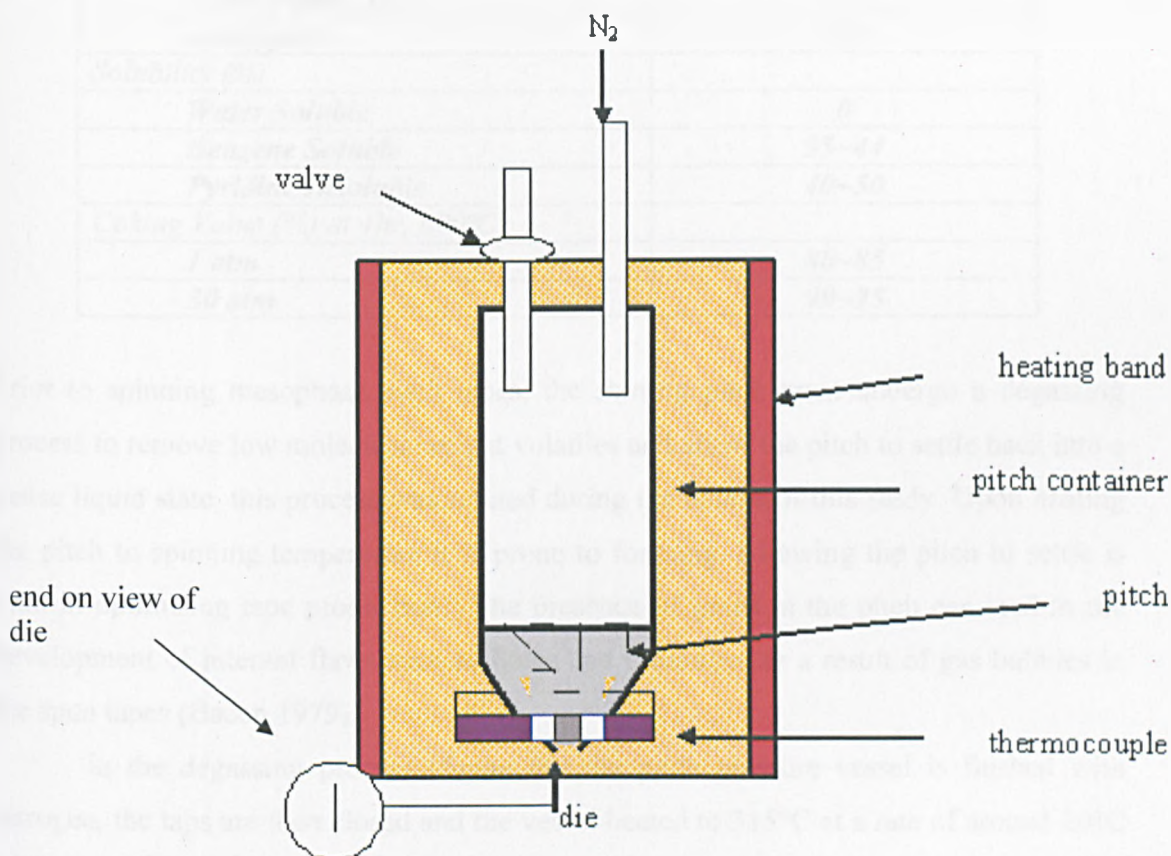


Figure 39 Schematic diagram of spinning apparatus

The particular pitch used in this set of experiments was ARMP (2004 batch) mesophase pitch supplied by the Mitsubishi Gas Chemical Company (table 4). This is a pitch which is already 100% mesophase. One advantage of this pitch is that alignment of the molecules is significantly more straightforward upon spinning.

Table 4 Typical Properties of ARMP Mesophase Pitch (taken from www.mgc-a.com/newProducts/media/ARBrochure.pdf)

| | |
|--|----------------------|
| <i>Physical Properties</i> | |
| <i>Appearance</i> | <i>Black Pellets</i> |
| <i>Bulk Density (g/cm³)</i> | <i>>0.65</i> |
| <i>Specific Gravity (25°C)</i> | <i>1.23</i> |
| <i>Specific Heat (cal/g°C)</i> | <i>0.65</i> |
| <i>Softening point (°C) by Mettler</i> | <i>275</i> |
| <i>Mesophase Content (%)</i> | <i>100</i> |
| <i>Hydrogen/Carbon (atom/atom)</i> | <i>0.58~0.64</i> |
| <i>Flash Point (°C)</i> | <i>>300</i> |
| <i>Ash (ppm)</i> | <i><20</i> |
| <i>Solubility (%)</i> | |
| <i>Water Soluble</i> | <i>0</i> |
| <i>Benzene Soluble</i> | <i>35~44</i> |
| <i>Pyridine Insoluble</i> | <i>40~50</i> |
| <i>Coking Value (%) at 1hr, 600°C</i> | |
| <i>1 atm</i> | <i>80~85</i> |
| <i>30 atm</i> | <i>90~95</i> |

Prior to spinning mesophase pitch tapes, the starting pitch must undergo a degassing process to remove low molecular weight volatiles and allow the pitch to settle back into a dense liquid state, this process was refined during the course of this study. Upon heating the pitch to spinning temperature it is prone to foaming. Allowing the pitch to settle is vital in optimising tape production. The presence of gases in the pitch can lead to the development of internal flaws such as holes and breakages as a result of gas bubbles in the spun tapes (Bacon 1979).

In the degassing process (figure 40) the pitch pressure vessel is flushed with nitrogen, the taps are then closed and the vessel heated to 315°C at a rate of around 20°C an hour before being held for 1 hour in a flow of nitrogen, the nitrogen is then switched off and the taps to the vessel are closed once again. The temperature is reduced to 295°C and held there for a further 4 hours before the pitch is ready to be spun (Anton-Arulrajah 2006).

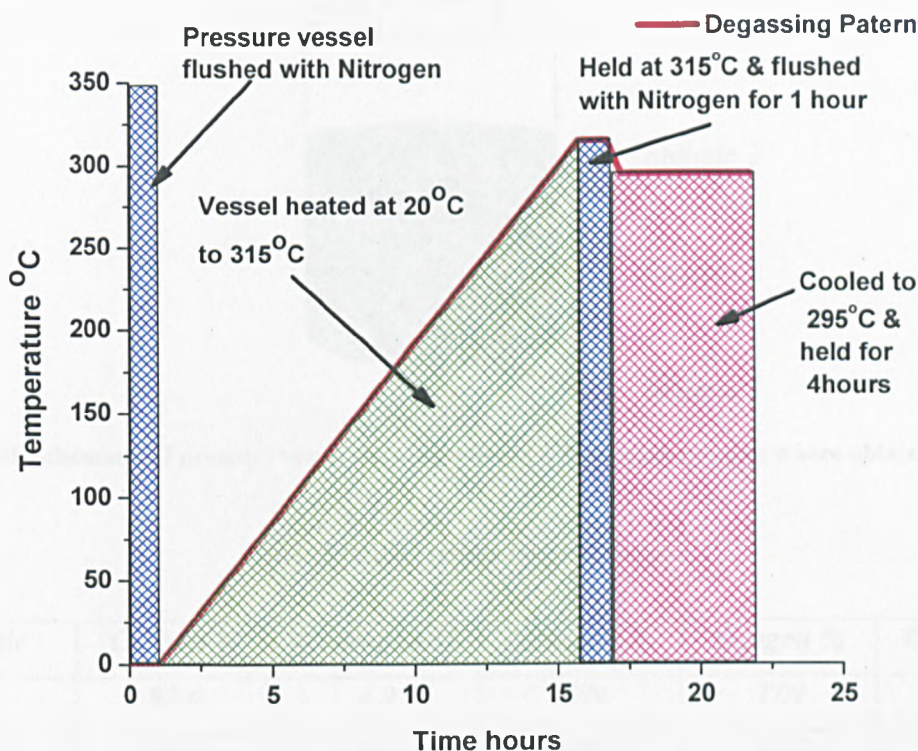


Figure 40 Graphical representation of the de-gassing route

To evaluate the degassing process further samples of pitch were collected at different positions throughout the pressure vessel by siphoning off the degassed pitch at different times during the tape spinning process (figure 41). These samples were then analysed by CHNO chemical analysis. Sample 1 was taken just after the first few centimeters of the mesophase pitch-based carbon tapes had been successfully spun. Sample 2 was obtained in the middle of the spin after about 300g of tapes had been spun from the 600g of pitch. Finally sample 3 was collected as the spin was coming to an end and the tapes could no longer be spun consistently without breakages and holes developing.

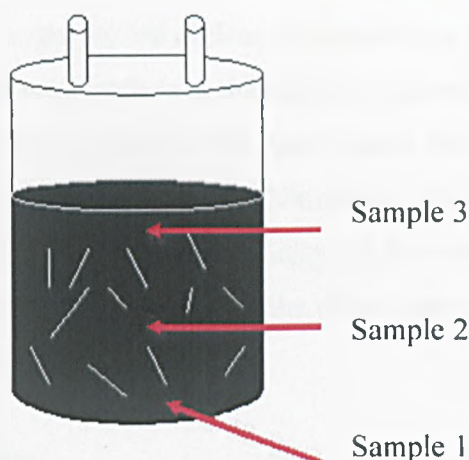


Figure 41 Schematic of pressure vessel showing where CHNO degas samples were obtained from

Table 5 CHNO results for pitch degas

| Sample | Carbon % | Hydrogen % | Nitrogen % | Oxygen % | Difference % |
|--------|----------|------------|------------|----------|--------------|
| 1 | 93.6 | 4.9 | T/N | T/N | 1.5 |
| 2 | 93.8 | 4.9 | T/N | T/N | 1.3 |
| 3 | 94.8 | 4.9 | T/N | T/N | 0.3 |

T/N = trace or nil < (0.3), elemental analysis error is $\pm 0.3\%$ in all cases.

Difference in % chemical analysis which is greater than that of the experimental error can be accounted for by the presence of sulphur

The CHNO results for the degassed pitch (table 5) show that a successful degas was obtained by implementing the degassing program described in (figure 40). Using this route it has been possible to remove the low molecular weight volatiles (exhibited by a slight drop in hydrogen and carbon content when comparing degassed results with those obtained from the as-received material in (table 3) and produce a relatively consistent material that spun well.

Keeping a constant temperature throughout the spinning process is of the utmost importance, The mesophase pitch behaves as a thermoplastic; as the temperature increases so the viscosity decreases and thus the pitch flows more easily. At temperatures below $\sim 280^{\circ}\text{C}$ the pitch will not flow; if the temperature is above $\sim 310^{\circ}\text{C}$ then the pitch

flows much more easily. Both scenarios are useless in the spinning process. Spinning can only take place when the mesophase pitch is at the optimum spinning temperature which in this case is 295°C i.e. when the viscosity of the pitch is such that dimensionally stable tapes can be spun. (Anton-Arulrajah, et al 2006). Nitrogen at 3-bar pressure is used to force the material through the die before the tape is taken up by a drum rotating at 20rpm (figure 42 & 43). It is an advantage to slightly wet the drum with a fine mist of water to allow the tape to stick more easily to it.

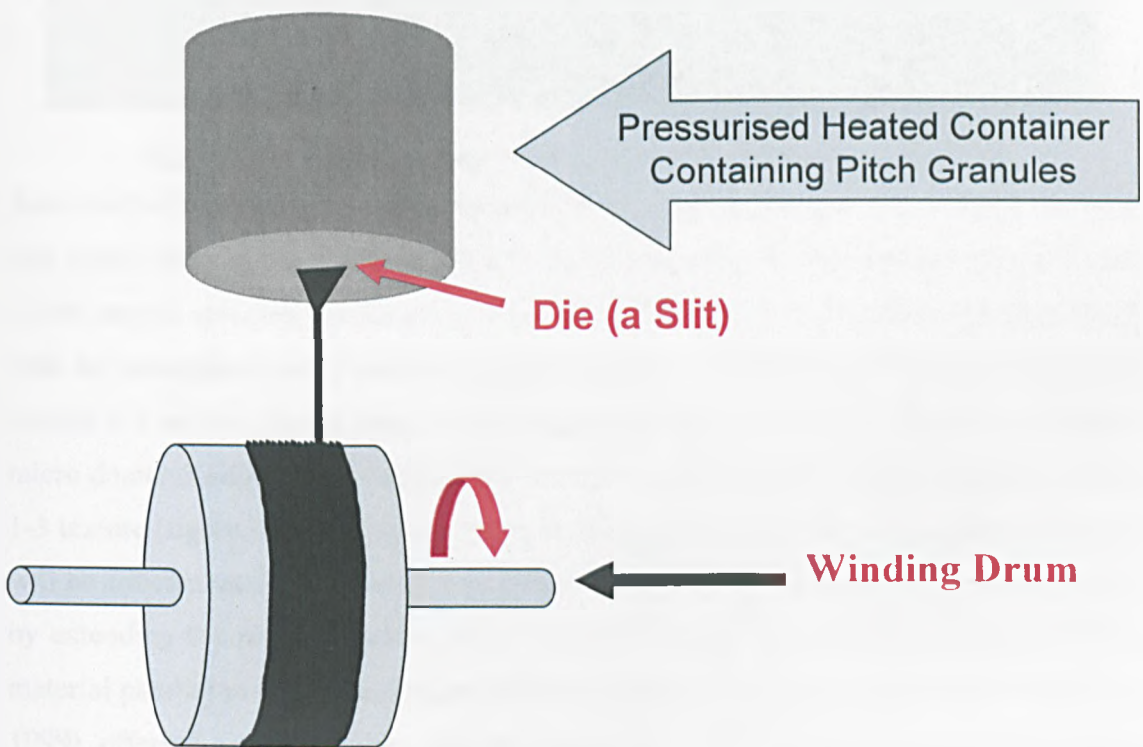


Figure 42 Schematical diagram of spinning operation

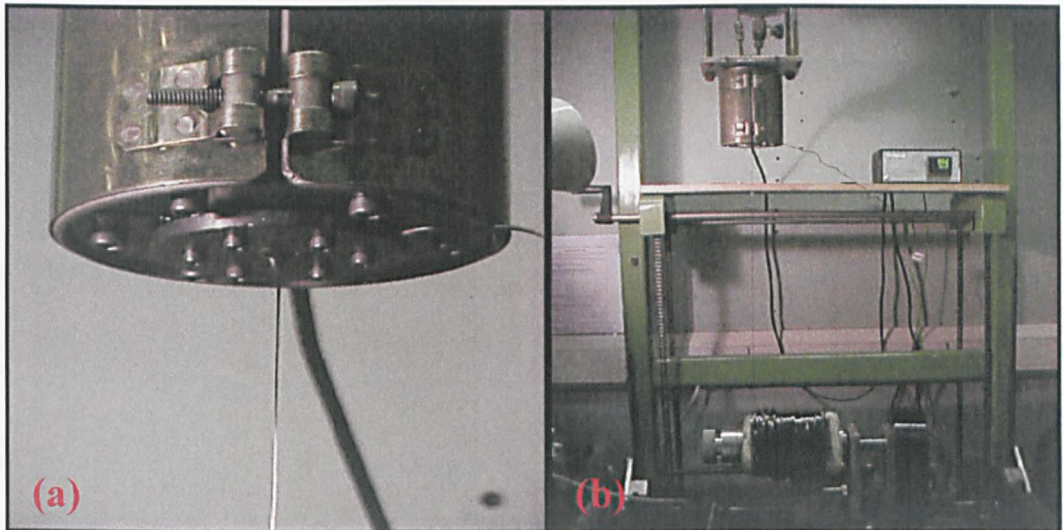


Figure 43 (a) Mesophase tape extruding through die, (b) Spinning apparatus

As a result of controlling the spinning parameters i.e. pitch temperature, nitrogen pressure and drum winding speed it is feasible to control the type of tape that can be produced. Under normal spinning conditions of a moderate shear rate it is possible to produce tapes with the mesophase micro domains aligned parallel to the tapes surface; these have been termed 1-2 texture (figure 44a). By increasing the shear rate, tapes with the mesophase micro domains aligned perpendicular to the tapes surface can be formed these are termed 1-3 texture (figure 44b). For the purpose of this work it will be the 1-2 texture tapes that will be concentrated on. Firstly it has already been proven by Korai and co-workers that by extending the planar structure of a material by orientating the layer structure of the material parallel to the tapes surface graphitisation can be improved (Korai, Hong et al. 1999), offering e.g. exceptional thermal conductivity. Secondly upon manufacturing the tapes via the melt spinning process it proved to be far easier to control the alignment of the mesophase micro-domains and the uniform morphology of the tapes at more moderate shear rates required to produce the 1-2 textured tapes (shear rate 494 s^{-1}). The 1-3 textured tapes are produced at the higher shear rate of 783 s^{-1} . The probability of breakages and defects in the tapes also increases significantly during the spinning process at the increased shear rates required to produce 1-3 orientated tapes. As stabilisation is in part a diffusion controlled process it is more than likely that 1-2 and 1-3 textured tapes will exhibit different stabilisation properties.

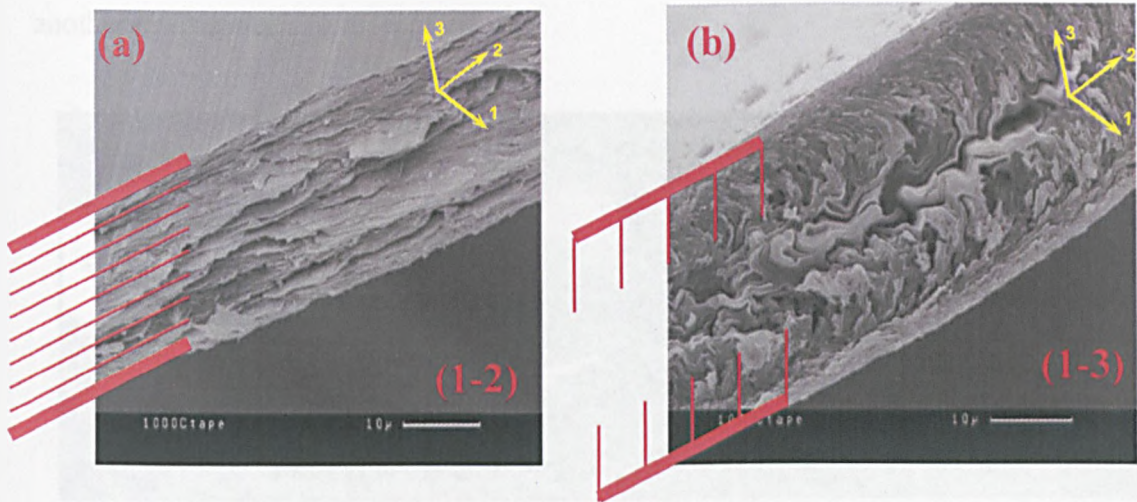


Figure 44 SEM images showing different tape textures available with controlled shear rate 1-2 tape texture produced at a shear rate of 494 s^{-1} , 1-3 tape texture produced at a shear rate of 783 s^{-1}

5.3 Examination of spun tapes

Randomly selected tapes were collected from varying points during the tape spinning procedure. These tapes were then stabilised to reveal their microstructure and carefully examined using a SEM in order to establish if the process had been successful and the tapes were without structural defects. Even when using standard spinning conditions defects can be incorporated into the sample as a result of other factors.

From time to time small holes can be seen to have developed in the centre of the tapes which run throughout their full length (figure 45(a)); if these holes are present the whole batch of spun tapes is scrapped. The occurrence of these holes was found to be dramatically reduced with improvements in the degassing route (figure 45(b)); however there are several other possible factors which may have caused the development of these holes: small solid particles on the die slit, the nitrogen pressure being too high leading to holes being developed as a possible escape route for the gas, uneven molecular orientation and interlayer shrinkage (i.e. the tapes may not have true 1-2 or 1-3 alignment and maybe a mixture of both if the shear rate is not accurately controlled so the parallel aligned layers and the vertical aligned layers have different shrinking directions and thus

holes are pulled open). Evaporation of foreign matter in the tape during stabilisation is another alternative.

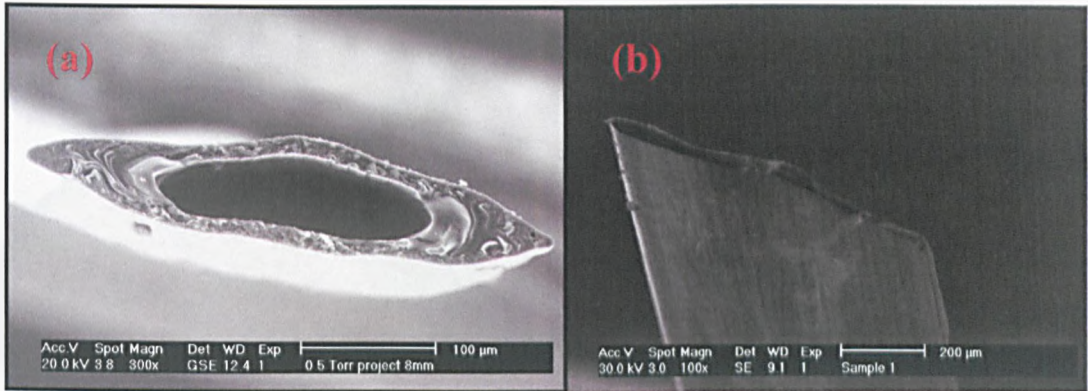


Figure 45 (a) Defected mesophase pitch tape, (b) undefected mesophase pitch tape

Pole figures of the tapes produced are determined to ensure that the alignment of the layer planes in the tape is as perfect as possible. Figure 46 shows a good alignment of the spatial planes within the tape in the 1 direction i.e. along the length of the tape. However more disordered alignment is evident in the 2 direction i.e. along the width of the tape.

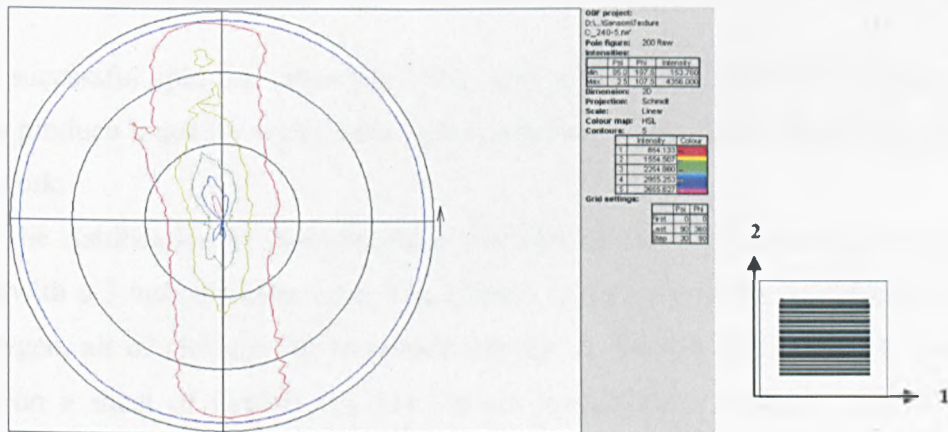


Figure 46 Pole figure of 240°C 5hrs stabilised mesophase pitch carbon tape spun at 1.5bar and 295°C

A 3D representation of a pole figure for a tape which has been stabilised and then carbonised to 1600°C is shown in figure 47. Excellent ordering of the mesophase micro domains along the length of the tape can be seen and with carbonisation the textural

alignment of the planes improves even further. This particular sample has a textural misorientation (FWHM) angle of 21° about 1 axis and 6° about the 2 axis. Upon graphitisation this textural alignment sees an even greater improvement.

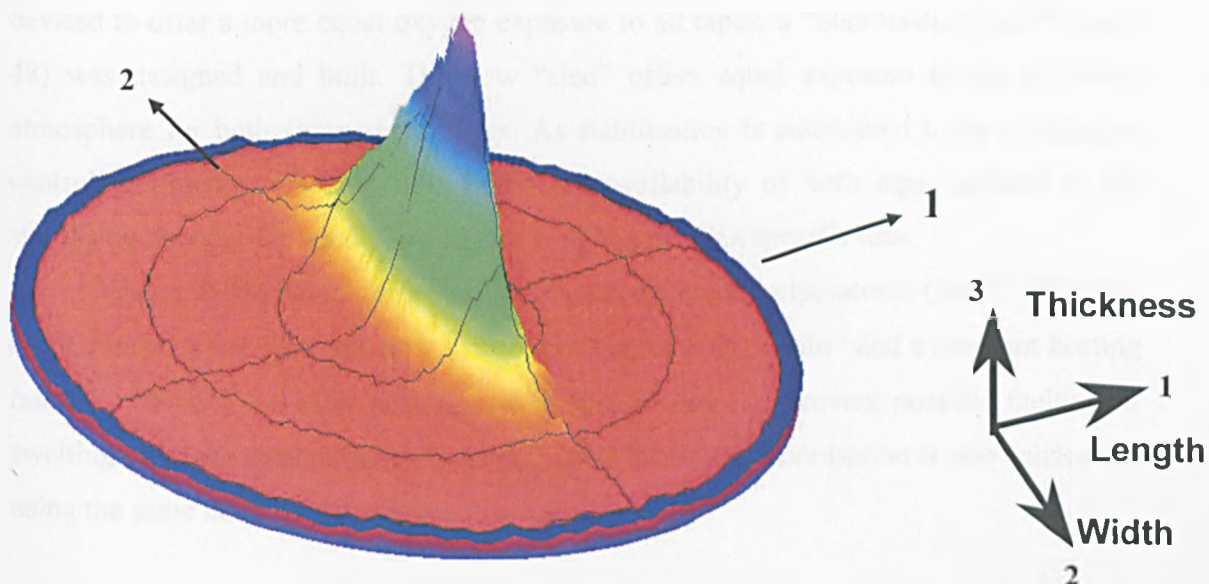


Figure 47 3D representation of a pole figure for a tape which has been carbonised to 1600°C

5.4 Stabilisation of tapes

Once a successful spin has taken place the next, and possibly the most critical step in order to produce a quality mesophase carbon product, is the stabilisation step, the focus of this work.

The stabilisation of the mesophase pitch-based tapes is carried out using a tube furnace with a 3 inch diameter tube. The furnace is set up to allow a controlled flow of gas (oxygen, air or nitrogen) to be passed through it. Initially the tapes were randomly layered on a sheet of Grafoil (UCAR Carbon manufactures produce Grafoil flexible graphite as a rolled sheet. It is a flexible, compressible, resilient, chemically inert, fire safe, heat sink and is stable under load and temperature) (www.grafoilsales.com) before being placed in the furnace. The weight gain which was experienced by the tapes using this technique initially was lower than expected when comparing it with previously reported results on the stabilisation of mesophase tapes (Collins 2005) (Birlson 2004). A

preliminary investigation into this discrepancy pointed to oxygen access issues. Tapes which were in the middle and bottom of the random lay up were not seeing the same abundance of oxygen as those tapes on the top. A new method of arranging the tapes was devised to offer a more equal oxygen exposure to all tapes; a “Stabilisation sled” (figure 48) was designed and built. The new “sled” offers equal exposure to the oxidative atmosphere for both sides of the tapes. As stabilisation is considered to be a diffusion controlled process (Galanopoulos 2003) the availability of both tape surfaces to the stabilising atmosphere results in a higher weight gain for a specific time.

The stabilisation is carried out at several different temperatures (160°C, 240°C & 300°C) under a constant gas flow (oxygen or air) of 100 ml min⁻¹ and a constant heating rate of 2 °C min⁻¹. A slow heating rate is used in order to prevent possible melting or swelling up of the mesophase carbon tapes upon heating. Carbonisation is also carried out using the same heating rate and gas flow rate.

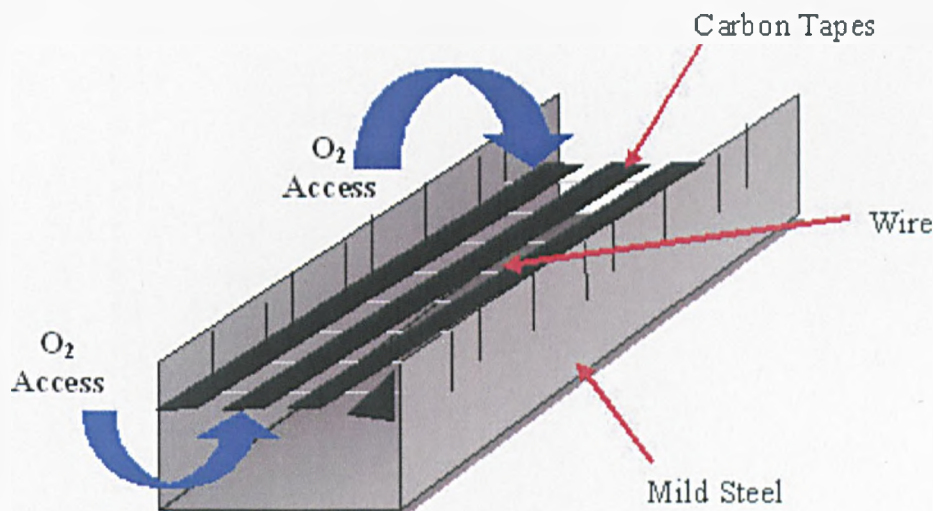


Figure 48 schematical representation of the "stabilisation sled"

Standard practice for the stabilisation method involves oxidative heating of samples in either air or oxygen to between 200-300°C (Fathollahi 2005). Although stabilisation of mesophase specimens have been reported at temperatures as low as 130°C (Fathollahi 2001) where it is believed that lower temperatures of stabilisation may well avoid the effects of over stabilisation. However 160°C was selected as the lowest



temperature of stabilisation as it is believed that the majority of the chemical reactions which occur between oxygen and the mesophase pitch take place above 150°C (Fathollahi 2005). It is for this reason that the temperature range that will be investigated will be between 160°C and 300°C.

6 Stabilisation

6.1 Weight change upon stabilisation of tapes

It is clear that during stabilisation many different competing reactions are occurring and these have a variety of effects on the mesophase pitch-based tapes, the most noticeable of these being the gain in weight that the samples experience when exposed to an oxidising atmosphere. To consider this further, a TGA (thermogravimetric analyser) was employed to simulate the stabilisation conditions the tapes experienced in the tube furnace. The TGA was programmed at a heating rate of $2^{\circ}\text{C min}^{-1}$ to go to a range of temperatures between $160\text{--}300^{\circ}\text{C}$. At the desired temperature the furnace was held isothermally for a period of 25hrs. This experiment was originally carried out twice, first in air and secondly in oxygen; both had a gas flow of 100 ml min^{-1} .

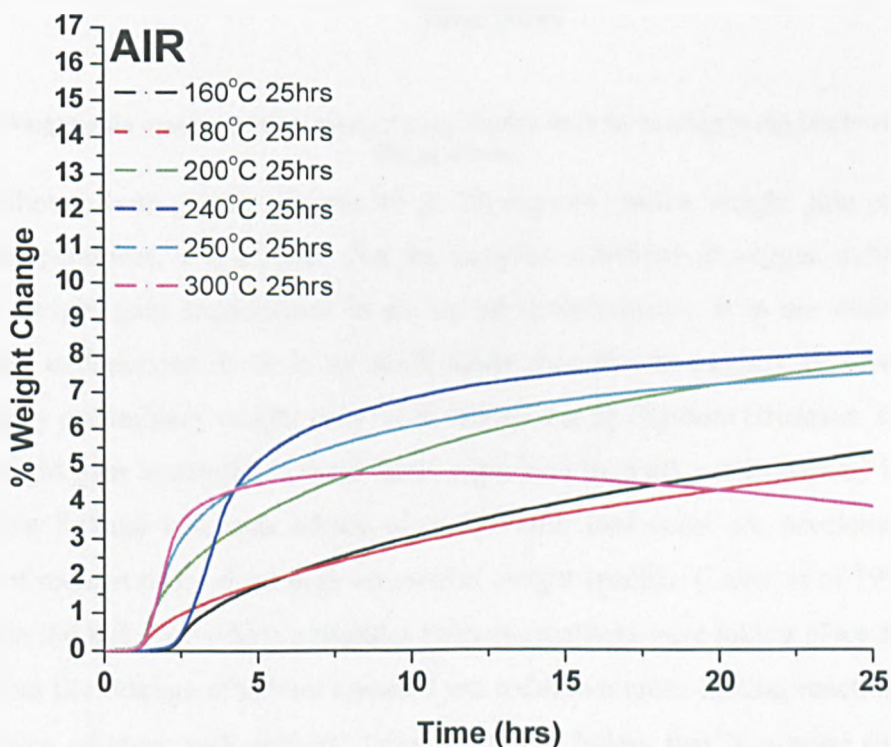


Figure 49 Weight gain experienced by tapes during stabilisation by heating in air to various final temperatures

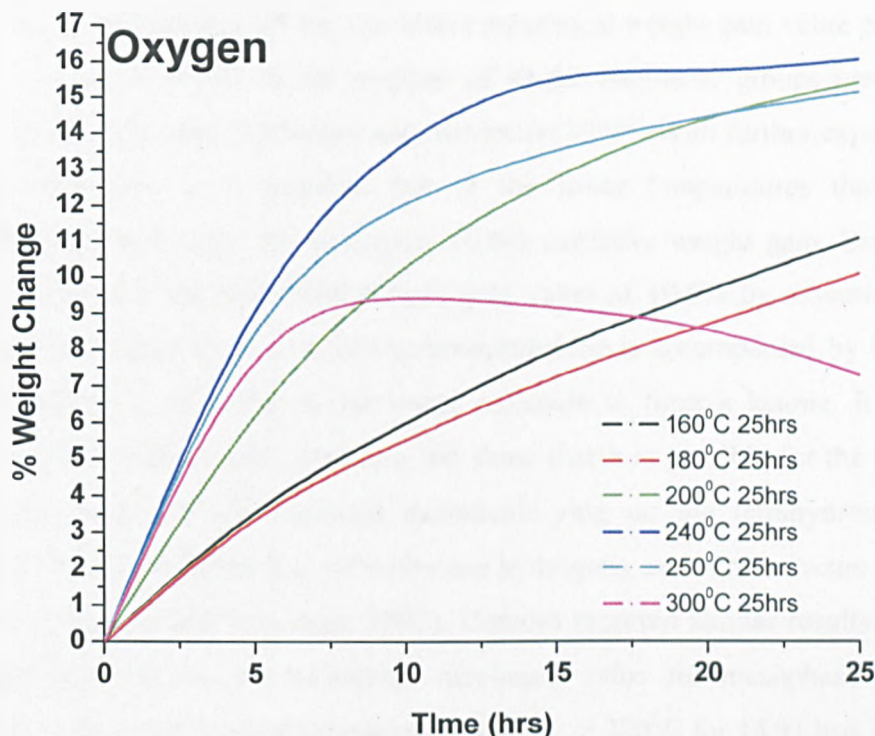


Figure 50 Weight gain experienced by tapes during stabilisation by heating in oxygen to various final temperatures

Although both graphs (figures 49 & 50) express similar weight gain patterns for specific temperatures, it is of note that the samples stabilised in oxygen exhibit nearly twice the weight gain experienced in air (at all temperatures). It is not clear why the weight gain experienced in air is so much lower than that in oxygen. However, this is backed up by preliminary weight gain work carried out by Birleson (Birleson 2004). This greater weight gain in oxygen is most likely explained by work carried out by Lavin who showed that linkage reactions taking place between molecules are accelerated in the presence of oxygen to produce high-molecular weight species, (Lavin et al 1992). In his work Lavin did not state which particular linkage reactions were taking place although it is likely that the linkage reactions reported are oxidative cross-linking reactions such as the formation of ether and carbonyl links. It should follow that in a more oxygen rich environment oxidative reactions are speeded up. In both cases there is enough oxygen supplied to the samples in order to completely convert them into carbon dioxide. The

lower temperatures (160°C, 180 °C, 200°C) for the air weight gain graph (figure 50) appears to be in agreement with the maximum theoretical weight gain value proposed by Drbohlav of around 10.6% for the reaction of all the naphthenic groups present in the structural units of the pitch (Drbohlav and Stevenson 1995). With further exposure to the oxidising atmosphere it is possible that at the lower temperatures the extent of stabilisation may well reach the theoretical 10.6% oxidative weight gain. Drbohlav and Stevenson calculated the theoretical weight gain value of 10.6% by assuming that the addition of one oxygen atom to a tetrahydronaphthalene is accompanied by loss of two hydrogens and the production of one water molecule to form a ketone. It should be pointed out that Drbohlav and Stevenson did show that it is possible for the addition of more oxygen atoms to the saturated naphthenic ring on the tetrahydronaphthalene molecule as a result of further loss of methylene hydrogens, emission of water and ketone production (Drbohlav and Stevenson 1995). Dumont reported similar results for weight gains experienced below the theoretical maximum value for mesophase pitch after oxidative heat treatment in air at atmospheric pressure at 220°C for 13.91 hrs. They stated that stabilisation could be carried out without decomposition reactions and carbon loss by controlling the experimental conditions to limit the oxidative modification that were made to the mesophase during the stabilisation step (Dumont, Dourges et al. 2005).

The graphs (figures 49 & 50) illustrate that the weight gain due to oxidation of the sample during stabilisation is not only temperature dependent but is also atmospherically influenced. In both atmospheres it is evident that as temperature increases so does the weight gain experienced by the mesophase pitch-based tapes. This is clear (tables 6 & 7) up to 240°C. Once above this temperature the weight gain is not as prevalent. In the extreme case of the tape stabilised at 300°C, a loss in weight is evident after a swift initial uptake; this is probably due to the tape burning off as a result of the elevated levels of surface oxidation resulting from the formation of a skin core structure. The rate of weight gain is also influenced by temperature, in both oxygen and air a more rapid initial weight gain over the first 5 – 10 hours can be observed with stabilising temperatures up to 240°C. Above this temperature both the rate and amount of weight gain as a result of oxidation begins to decrease. Lower temperatures (160°C & 180°C) show a steady weight

increase of approximately 2% weight gain for every 5 hours of stabilisation in air. This contrasts with the claims of Drbohlav and Stevenson that weight gain in naphthalene derived mesophase pitch is more widespread at lower temperatures and over shorter periods of time (Drbohlav and Stevenson 1995). However this is only true for mesophase pitches as other pitches behave differently (Lu 2002)

Table 6 % mass gain for samples stabilised at varying degrees of temperature and time in air

| Stabilisation Temperature °C | Mass Gain (%) After Stabilisation Time (hrs) in Air | | | | |
|------------------------------|---|------|------|------|------|
| | 5 | 10 | 15 | 20 | 25 |
| 160 | 1.7% | 3.1% | 4.0% | 4.7% | 5.4% |
| 180 | 1.8% | 2.9% | 3.7% | 4.3% | 5.0% |
| 200 | 3.6% | 5.3% | 6.4% | 7.2% | 7.9% |
| 240 | 5.1% | 6.9% | 7.5% | 7.9% | 8.1% |
| 250 | 4.7% | 6.1% | 6.8% | 7.2% | 7.6% |
| 300 | 4.5% | 4.8% | 4.7% | 4.3% | 3.9% |

Table 7 % mass gain for samples stabilised at varying degrees of temperature and time in oxygen

| Stabilisation Temperature °C | Mass Gain (%) After Stabilisation Time (hrs) in Oxygen | | | | |
|------------------------------|--|-------|-------|-------|-------|
| | 5 | 10 | 15 | 20 | 25 |
| 160 | 3.5% | 5.9% | 7.9% | 9.6% | 11.0% |
| 180 | 3.3% | 5.4% | 7.2% | 8.8% | 10.1% |
| 200 | 6.2% | 10.2% | 12.7% | 14.4% | 15.4% |
| 240 | 9.0% | 13.8% | 15.5% | 15.7% | 16.0% |
| 250 | 8.5% | 12.1% | 13.5% | 14.4% | 15.1% |
| 300 | 7.6% | 9.4% | 9.1% | 8.5% | 7.3% |

Over shorter periods of stabilisation (≤ 25 hours), 240°C initially appears to be the optimum temperature based on the assumption that rate and amount of oxidised weight gain is a clear indicator of stabilising potential. However, examining the trends displayed in the figures 49 & 50 it looks as though lower temperatures of stabilisation may well surpass the maximum oxidising weight achievable for higher temperatures over longer periods of time. The 240°C oxygen stabilised samples appear to have already reaching a plateau at about 15.9% after only 25 hours stabilisation whereas the lower temperatures of 160°C and 180°C showing the steady weight gain increments of roughly 2% for every 5hrs of stabilisation may well be able to surpass this value. This could be as a result of several different factors; first the mechanism driving the stabilisation reaction could differ with temperature. At lower temperatures the reaction could be chemically controlled whereas at elevated temperatures the reaction is likely to be diffusion driven (i.e.

diffusion-controlled). Another factor which could affect the overall weight gain at higher temperatures of stabilisation is the phenomenon of skin-core structure formation (Mochida, Zeng et al. 1990; Mochida, Zeng et al. 1991; Lu, Wu et al. 1998); here a thick skin of stabilised material develops as a crust around the surface of the sample leaving the core unstabilised. As stabilisation is considered to be diffusion-controlled at higher temperatures, the formation of this skin-core structure could inhibit the diffusion of oxygen into the core of the sample preventing greater oxygen uptake and leading to a saturation of the sample's surface regions. It is possible to consider a saturation of the surface rather than a balanced reaction between oxygen diffusion into the sample and the evolution of product gases, Figure 51 shows that the evolution of these gases decreases after a given time of stabilisation in all cases even if at the higher temperature of 300°C this decrease in CO₂ production is prolonged. The greater amounts of evolved gases at elevated temperatures may also contribute to this. As they are emitted in greater volumes they can help decrease the rate of diffusion as a counter diffusion process is set up where the accumulation of the product gases may actually inhibit the forward reaction.

It could be assumed that as the stabilisation temperature increases so the controlling factor of the stabilisation process changes. At 160°C the reaction may be chemically driven so that at this temperature diffusion of oxygen into the tape is not an issue, diffusion is taking place faster than the chemical reaction. The evolved gases during stabilisation are at a minimum, at such a low stabilisation temperature, and if the activation energies of many of the stabilising reactions is high (Fathollahi 2005) then the rapid formation of a skin-core structure is unlikely. At the intermediate temperature of 240°C the stabilisation temperature is high enough to rapidly promote the additional oxidation reactions with the mesophase pitch. However, at this temperature a greater quantity of evolved gas is also being given off which will hinder the access of oxygen to the core of the tape leading to an increased likelihood of reactions taking place on the outer surface of the tape, eventually lead to the formation of a skin-core structure. Both are factors that may limit stabilisation at this temperature. Indeed it may be astute to summarise that at 240°C the tape stabilisation processes are no longer chemically controlled but are now diffusion-controlled, both internally (as a result of increased gas

evolution inhibiting forward oxygen diffusion into the tape) and at the surface (as a result of the increased likelihood of reaction at the tapes' surface due to the higher temperature increasing the likelihood of cross-linking reaction taking place which may result in skin-core formation). At this temperature it is likely that a competition exists between these two diffusion-controlled processes in order to get sufficient oxygen into the mesophase pitch-based tapes (so that cross-linking reactions can take place to maintain the tapes morphology) before the formation of an impenetrable skin. At the highest temperature of stabilisation (300°C), excessive surface reaction can be expected to take place due to the elevated temperature, which also gives rise to a more vigorous evolution of product gases which may prevent the ingress of oxygen to the centre of the sample. At these temperatures the formation of a skin-core structure might take place very rapidly and, once formed, no further oxygen may be able to penetrate the tape to cross-link the structure. This is likely to lead to an over-saturation of the tapes' outer surface resulting in significantly increased CO and CO₂ evolution upon carbonisation of the sample and a reduction in the mesophase pitch-based tapes' carbon yield. These theories will be backed up in later sections which will look at how stabilisation temperature affects oxygen uptake, pitch softening point and optical appearance.

6.2 Evolution of gases during the stabilisation step

Monitoring of the stabilisation process was performed using a TGA-FTIR (thermo-gravimetric analysis-Fourier transform infra-red) instrument with a view to analysing the evolution of gases. The TGA was programmed at a heating rate of 2°C min⁻¹ to go to 160°C, 240°C and 300°C. Once at the required temperature the TGA furnace would be held isothermally for 5 hours before being allowed to cool to room temperature. Throughout this heating the evolved gases were analysed by FTIR. This simulation was carried out in both oxygen and in air. Unfortunately as a result of a limitation of the system it was only possible to monitor the stabilisation over the first 5 hours.

In figure 51 the weight gain patterns are again evident showing how increased temperature and oxygen concentration influence weight gain; the evolution of CO₂ and H₂O taking place during stabilisation is also visible in the FTIR data however, no CO

evolution was observed during the isothermal stabilisation simulation. In all cases, the evolution of CO₂ appears to commence between 63 - 92 minutes of the oxidative stabilisation heat treatment. It should be noted that the onset of the CO₂ evolution time is increased in those samples which show a significant H₂O evolution regardless of atmosphere. The intensity of these evolved gases is noticeably influenced by stabilisation temperature and atmosphere, at a given temperature of stabilisation the intensity and abundance CO₂ is greater in an oxygen atmosphere compared to that of air (table 8). The air-stabilised samples exhibit a much lower intensity of evolved gases, as a result of this it is logical to conclude that after the initial stabilisation, samples which have undergone the heat treatment in air will have a higher carbon content, (carbon content before carbonisation, not carbon yield). This is confirmed by calculations of the evolved CO₂ peak area (table 8) showing that for all temperatures stabilisation in air evolved less CO₂ than in oxygen and CHNO chemical analysis of the samples (table 9). These results cast doubt on the claim of Dumont and co-workers that they were able to successfully stabilise mesophase pitch without decomposition reactions or carbon loss taking place during the stabilisation step of mesophase pitch.(Dumont, Chollon et al. 2002) Again the influence of temperature on stabilisation is evident, the CO₂ evolution peak maximum time can be seen increase with stabilisation temperature (table 8) Figure 51 also agrees with the CHNO Data in table 9 showing the evolution of water for the oxygen system at both 240°C and 300°C where a significant drop in hydrogen content can be observed. No H₂O evolution is observed in the samples stabilised at 160°C and 240°C in air. However, at 300°C in air a small amount of evolved water is detected; this is reflected in CHNO data (table 9) by a more significant loss in hydrogen content at this temperature. It is likely however that H₂O is indeed being evolved at these lower temperatures and it is as a result of the limitations of the experimental apparatus that it is not being detected. When the FTIR gas cell analyser is first switched on in the morning it has an increased baseline, even though the cell is heated to 300°C and allowed an hour to normalise it is likely that a small amount of H₂O are still present in the gas cell. As experiments are carried out throughout the day the levels of H₂O present in the gas cell decrease thus reducing the

baseline allowing greater levels of evolved H₂O to be detected in those experiments ran towards the end of the day.

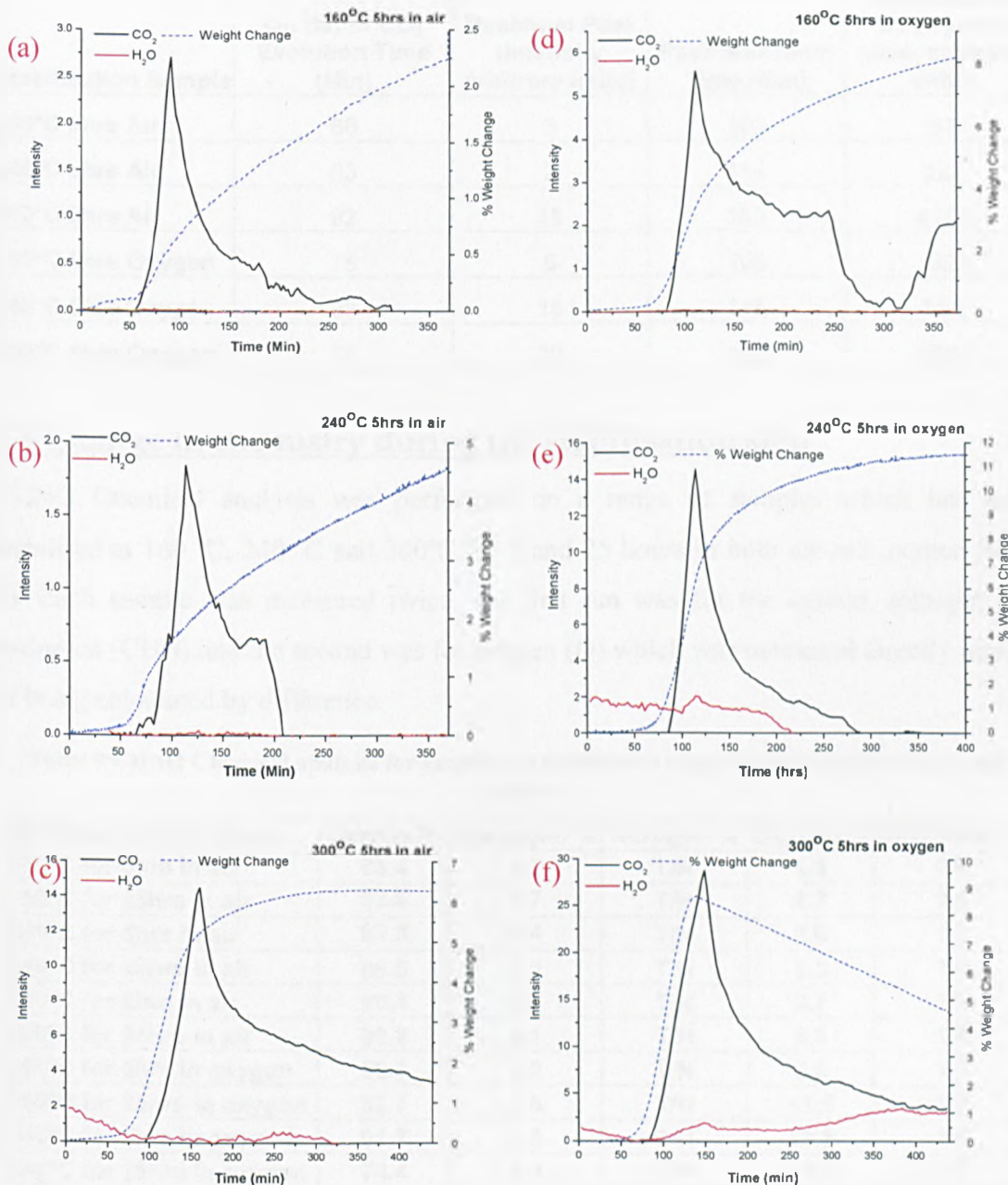


Figure S1 Evolution of evolved gases during stabilisation (a) 160°C 5hrs in air (b) 240°C 5hrs in air (c) 300°C 5hrs in air (d) 160°C 5hrs in oxygen (e) 240°C 5hrs in oxygen (f) 300°C 5hrs in oxygen, all samples heated at 2°C min⁻¹. Data acquired using TGA-FTIR, wavenumber range used for CO₂ analysis 2250-2350 cm⁻¹

Table 8 Table of evolved gas data for isothermally stabilised tapes in both air and oxygen

| Stabilisation Sample | On Set of CO ₂ Evolution Time (Min) | Maximum Peak (Intensity arbitrary units) | Peak Maximum Time (Min) | Peak Area (evolution of CO ₂ against time, arbitrary units) |
|----------------------|--|--|-------------------------|--|
| 160°C 5hrs Air | 66 | 3 | 102 | 57 |
| 240°C 5hrs Air | 63 | 2 | 114 | 222 |
| 300°C 5hrs Air | 92 | 15 | 163 | 4151 |
| 160°C 5hrs Oxygen | 75 | 6 | 108 | 1323 |
| 240°C 5hrs Oxygen | 83 | 15 | 115 | 551 |
| 300°C 5hrs Oxygen | 76 | 29 | 150 | 6667 |

6.3 Change in chemistry during the stabilisation step

CHNO Chemical analysis was performed on a range of samples which had been stabilised at 160 °C, 240 °C and 300°C for 5 and 25 hours in both air and oxygen (table 9). Each sample was measured twice, the first run was for the carbon, nitrogen and hydrogen (CHN) and the second was for oxygen (O) which was measured directly instead of being calculated by difference.

Table 9 CHNO Chemical analysis for samples stabilised over a range of temperatures in air and oxygen

| Stabilisation Conditions | Carbon % | Hydrogen % | Nitrogen % | Oxygen % | Difference % |
|---------------------------|----------|------------|------------|----------|--------------|
| 160°C for 5hrs in air | 93.4 | 4.7 | T/N | 1.3 | 0.6 |
| 160°C for 25hrs in air | 92.6 | 4.7 | T/N | 2.3 | 0.4 |
| 240°C for 5hrs in air | 92.3 | 4.4 | T/N | 2.8 | 1.0 |
| 240°C for 25hrs in air | 89.5 | 4.2 | T/N | 5.3 | 1.0 |
| 300°C for 5hrs in air | 90.4 | 4.3 | T/N | 3.7 | 1.6 |
| 300°C for 25hrs in air | 89.2 | 4.1 | T/N | 5.6 | 1.2 |
| 160°C for 5hrs in oxygen | 90.0 | 4.2 | T/N | 5.6 | 0.2 |
| 160°C for 25hrs in oxygen | 82.7 | 3.5 | T/N | 12.5 | 1.3 |
| 240°C for 5hrs in oxygen | 81.7 | 3.5 | T/N | 13.6 | 1.2 |
| 240°C for 25hrs in oxygen | 74.4 | 2.4 | T/N | 21.5 | 1.7 |
| 300°C for 5hrs in oxygen | 75.6 | 2.2 | T/N | 22.1 | 2.1 |
| 300°C for 25hrs in oxygen | 71.2 | 1.8 | T/N | 26.7 | 0.3 |

T/N = trace or nil < (0.3), elemental analysis error is $\pm 0.3\%$ in all cases.

Difference in % chemical analysis which is greater than that of the experimental error can be accounted for by the presence of sulphur

Table 9 confirms that those samples which have been stabilised in oxygen exhibit a larger compositional uptake in oxygen albeit at the expense of the carbon and hydrogen content. As the incorporation of oxygen into the samples is considered to be key in the stabilisation step for the purpose of this work oxygen will be the primary atmosphere of choice used for the stabilisation of the mesophase pitch-based carbon tapes for the remainder of this project. Another key indicator in the decision to concentrate on oxygen as the stabilisation atmosphere of choice was a Van Krevelen plot comparing air-stabilised samples with oxygen-stabilised samples. The Van Krevelen method of elemental analysis of hydrocarbons is usually associated with coal science to analyse chemical changes occurring during coal processing. (Van Krevelen 1957) The directional arrows in the master Van Krevelen plot (figure 52) indicate the development of different gaseous products of pyrolysis.

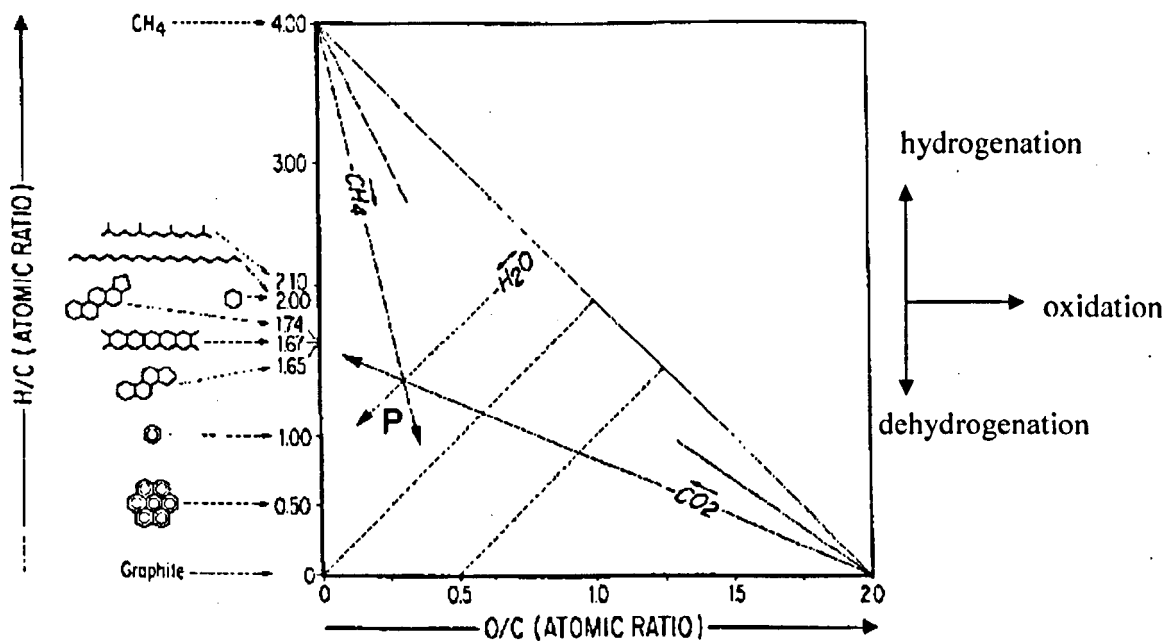


Figure 52 Master Van Krevelen Plot (Van Krevelen 1957)

Upon plotting the CHNO data from table 9 in the Van Krevelen format, (figure 53), the samples stabilised in the oxygen atmosphere it is clearly apparent that a far greater oxidation is occurring accompanied by significant dehydrogenation. It should however be pointed out that this increase in the O/C atomic ratio is not solely as a result of increased

oxygen levels as the loss in carbon content as a result of CO₂ emission is also a contributing factor, again no CO evolution was observed during the stabilisation process. Concentrating on the samples stabilised in the oxygen atmosphere (figure 54) it is of interest that the data for different temperatures of stabilisation and for additional times all follow the same line with the exception of those samples which have been stabilised at 300°C for greater than 10hrs in oxygen. Here, the graph suggests that a greater oxidation of the sample has occurred but when looking more closely at the CHNO data it become apparent that the shift in trend is as a result of not only a greater oxygen uptake but a greater loss in carbon pointing to a possible “over stabilisation” (where gasification occurs more readily), as already seen in figure 49 and 50. Only increasing time and temperature of stabilisation dictate lower H/C and higher O/C atomic ratios for samples stabilised in oxygen (figure 54).

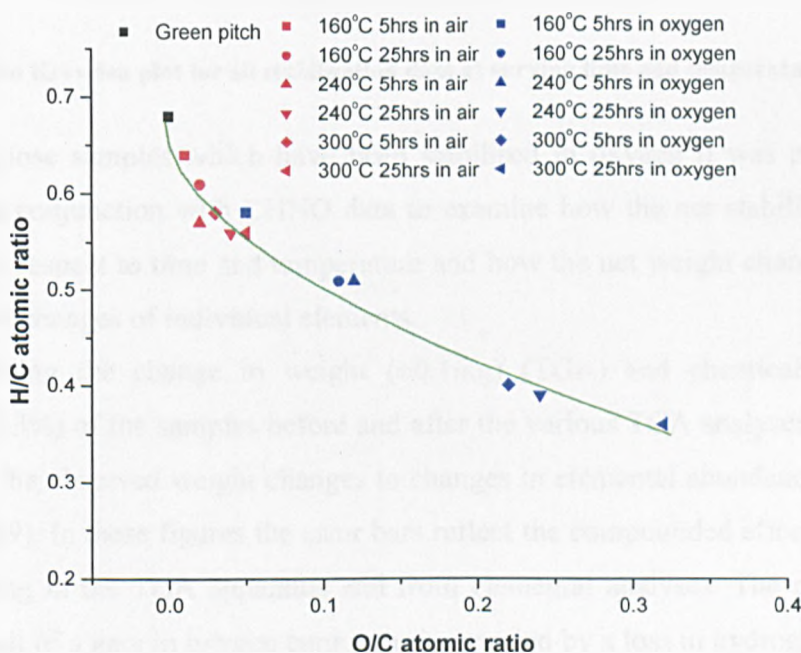


Figure 53 Van Krevelen plot for samples stabilised over a range of time and temperatures in air and oxygen

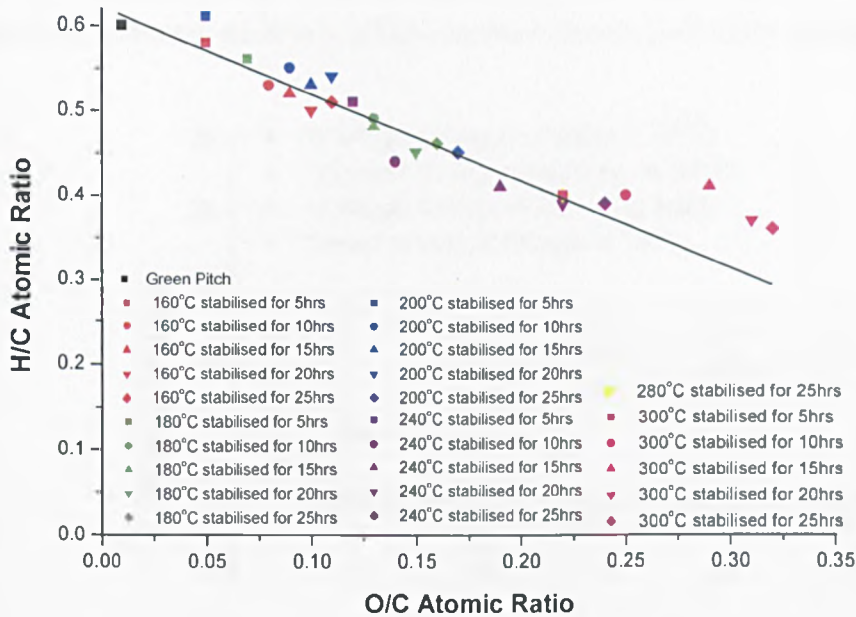


Figure 54 Van Krevelen plot for all stabilisation data at varying time and temperatures in oxygen

For those samples which have been stabilised in oxygen it was possible using TGA data in conjunction with CHNO data to examine how the net stabilisation weight changes with respect to time and temperature and how the net weight change is affected by the weight changes of individual elements.

By using the change in weight ($\pm 0.1\text{mg}$) (TGA) and chemical composition (CHNO) ($\pm 0.3\%$) of the samples before and after the various TGA analyses it is possible to attribute the observed weight changes to changes in elemental abundance in the tapes (figures 55-59). In these figures the error bars reflect the compounded effect of the errors from weighing in the TGA apparatus and from elemental analyses. The overall weight gain is a result of a gain in oxygen content accompanied by a loss in hydrogen and carbon which is in agreement with the Van Krevelen plot data. As the temperature and time of stabilisation increases so does the net weight gain up to 240°C where (figure 58) it appears to reach a plateau after 25hrs, at 300°C (figure 59) a decrease takes place after only the first 5hrs, this coincides with an increase in the total amount of carbon lost in the

form of CO₂ (figure 51). Although the increase in oxygen content aids the stabilisation process it ultimately adversely affects the final carbon yield of the stabilised product.

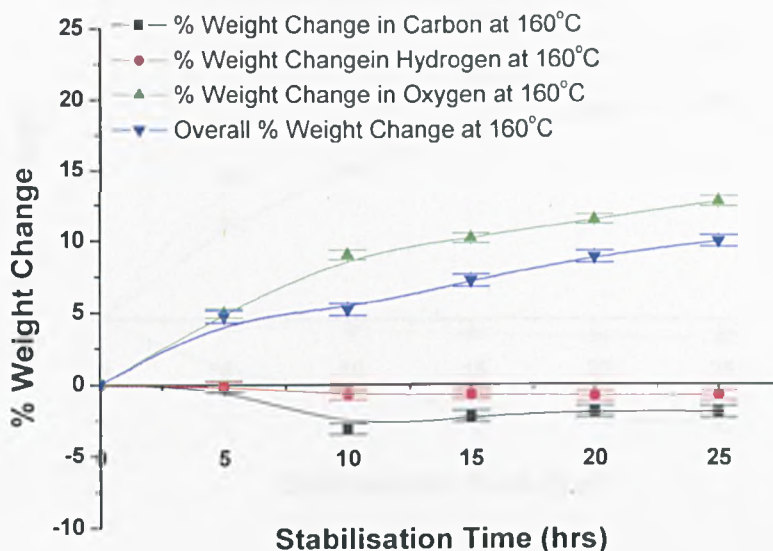


Figure 55 CHO elemental weight change with stabilisation at 160°C with respect to time for oxygen stabilised samples

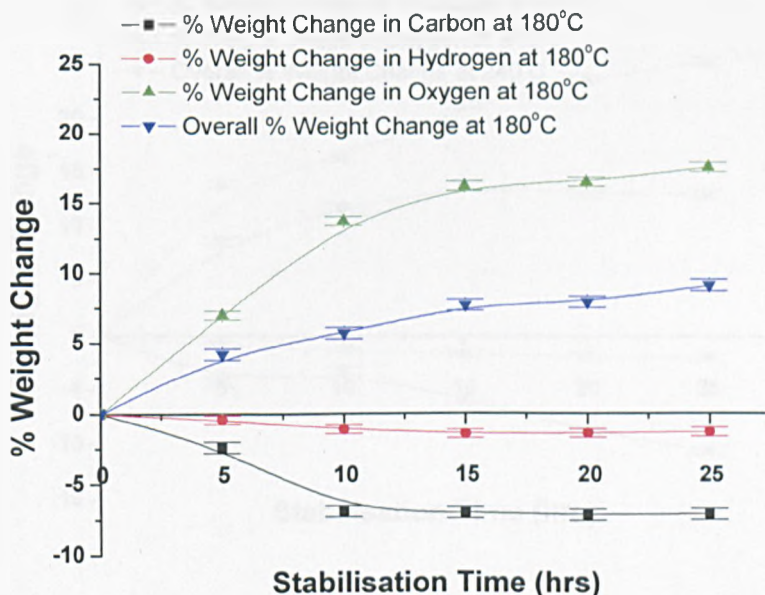


Figure 56 CHO elemental weight change with stabilisation at 180°C with respect to time for oxygen stabilised samples

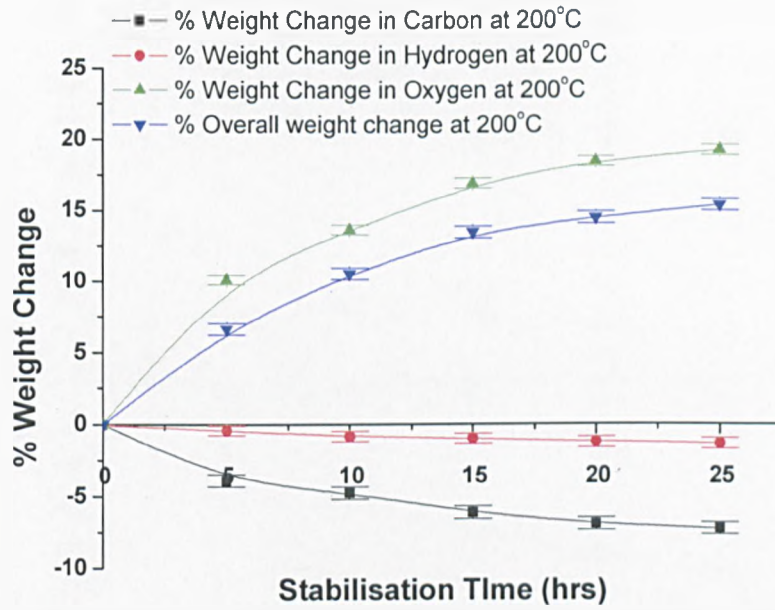


Figure 57 % CHO weight change for stabilisation at 200°C with respect to time for oxygen stabilised samples

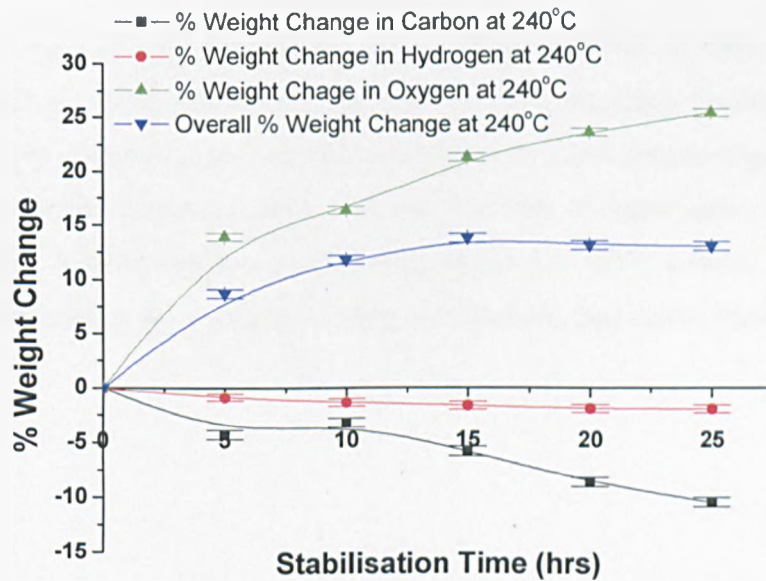


Figure 58 % CHO weight change for stabilisation at 240°C with respect to time for oxygen stabilised samples

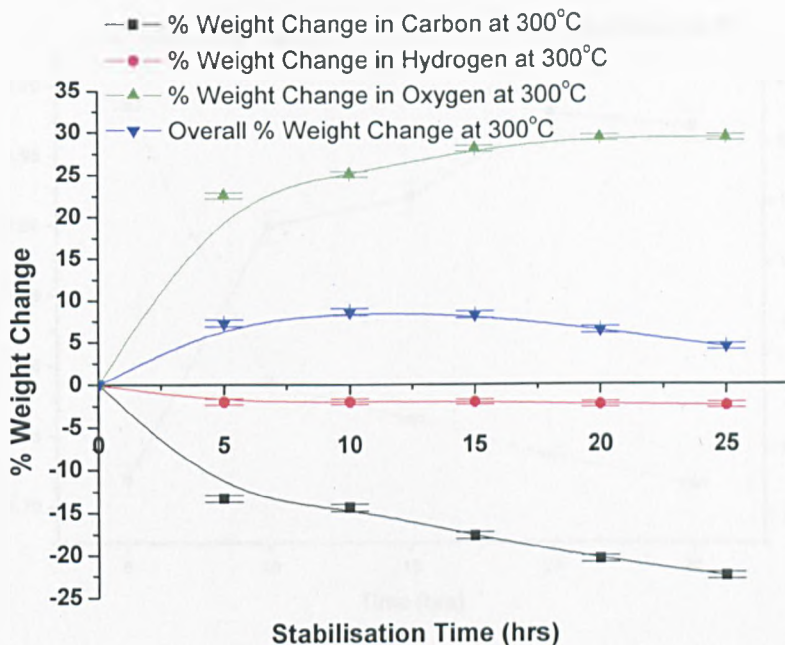


Figure 59 % CHO weight change for stabilisation at 300°C with respect to time for oxygen stabilised samples

Upon plotting the C/H and C/O atomic ratios (figures 60-64 & table 10) it can be observed that as the stabilisation advances the C/O ratio decreases exhibiting the uptake of oxygen and its incorporation. For all the samples the most noteworthy changes in the C/H and C/O atomic ratios take place over the first 5hrs of stabilisation from the green pitch at t = 0 hrs, with the greatest change occurring in the 300°C sample. No green pitch 0 point has been used in these graphs in order to obtain the best scale possible for viewing the data.

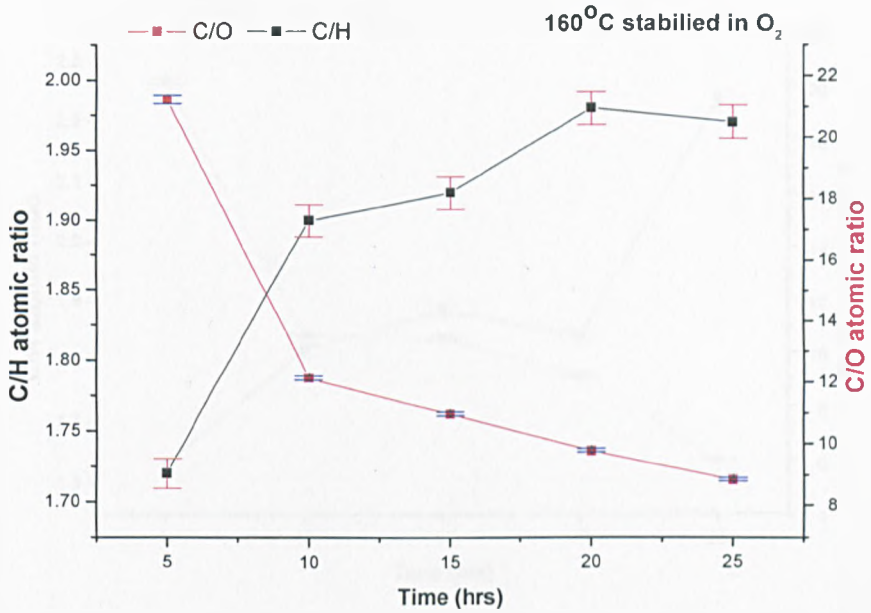


Figure 60 Effect of stabilisation at 160°C in oxygen on C/H and C/O atomic ratio

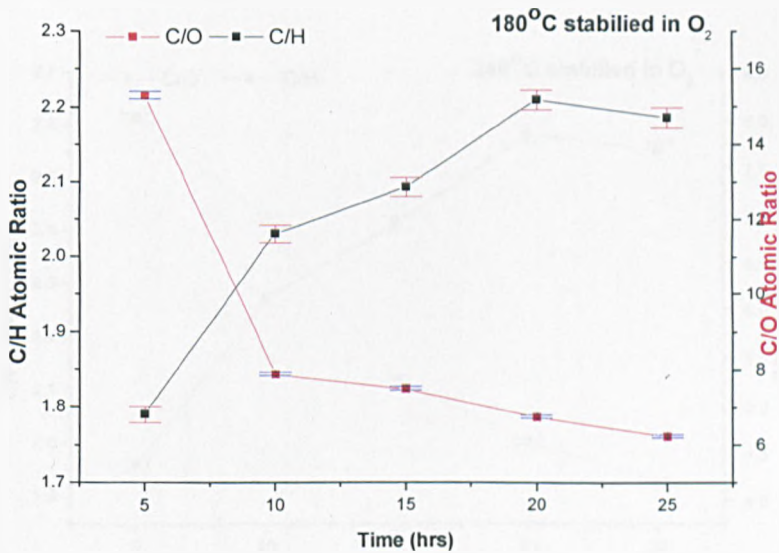


Figure 61 Effect of stabilisation at 180°C in oxygen on C/H and C/O atomic ratio

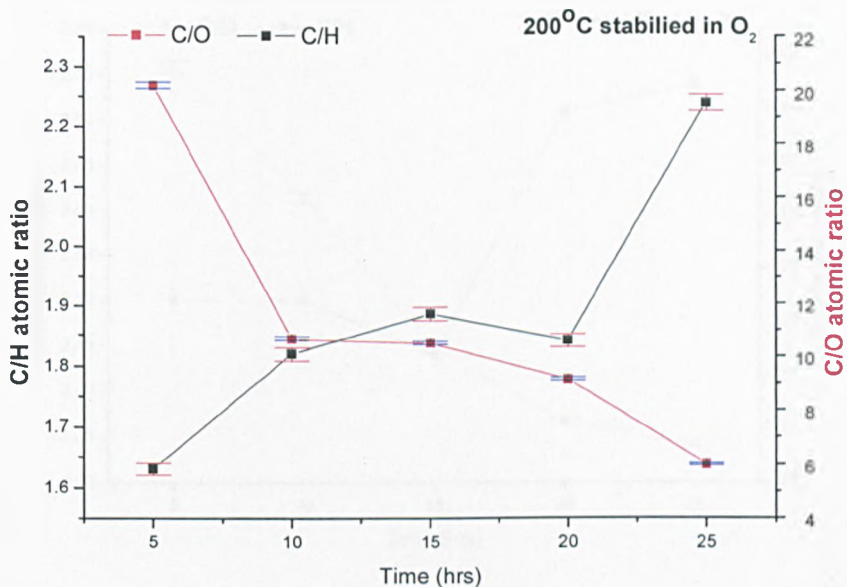


Figure 62 Effect of stabilisation at 200°C in oxygen on C/H and C/O atomic ratio

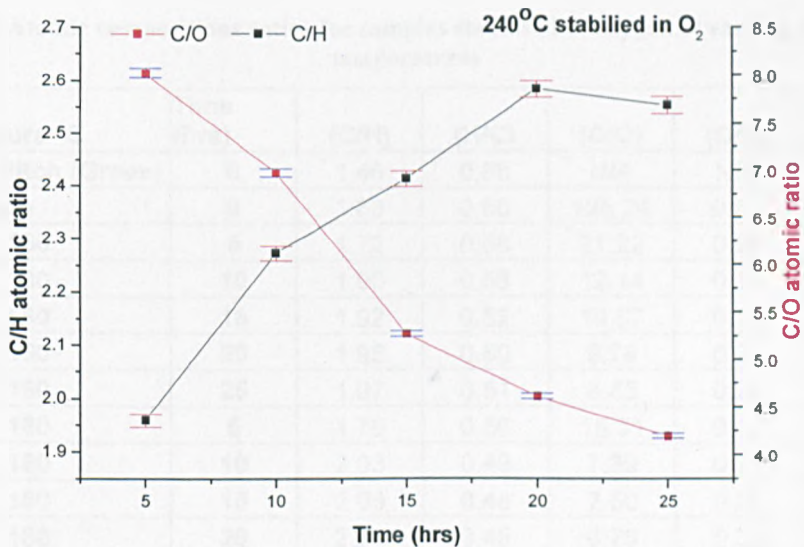


Figure 63 Effect of stabilisation at 240°C in oxygen on C/H and C/O atomic ratio

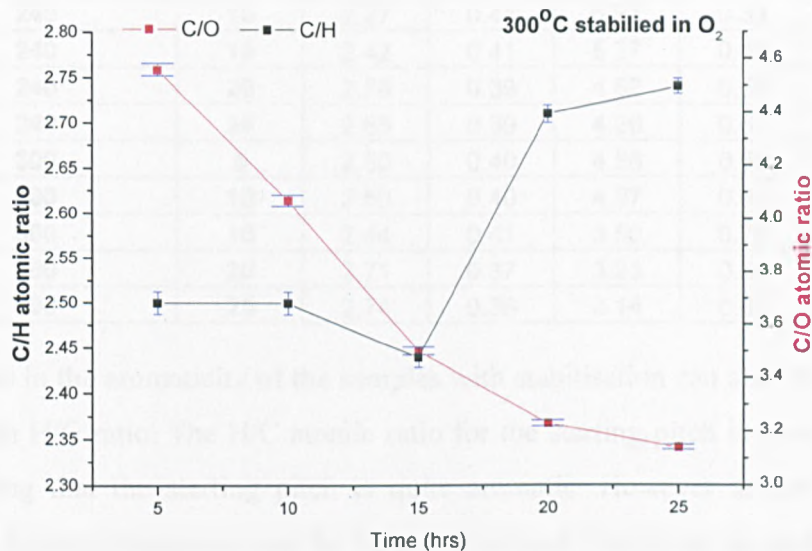


Figure 64 Effect of stabilisation at 300°C in oxygen on C/H and C/O atomic ratio

Table 10 Atomic compositions ratios for samples stabilised in oxygen at varying times and temperatures

| Temperature °C | Time (hrs) | (C/H) | (H/C) | (C/O) | (O/H) | (O/C) |
|---------------------|------------|-------|-------|--------|-------|-------|
| ARMPH Pitch (Green) | 0 | 1.46 | 0.68 | N/A | N/A | N/A |
| Green Tape | 0 | 1.68 | 0.60 | 128.24 | 0.01 | 0.01 |
| 160 | 5 | 1.72 | 0.58 | 21.22 | 0.08 | 0.05 |
| 160 | 10 | 1.90 | 0.53 | 12.14 | 0.16 | 0.08 |
| 160 | 15 | 1.92 | 0.52 | 10.97 | 0.18 | 0.09 |
| 160 | 20 | 1.98 | 0.50 | 9.78 | 0.20 | 0.10 |
| 160 | 25 | 1.97 | 0.51 | 8.85 | 0.22 | 0.11 |
| 180 | 5 | 1.79 | 0.56 | 15.31 | 0.12 | 0.07 |
| 180 | 10 | 2.03 | 0.49 | 7.89 | 0.26 | 0.13 |
| 180 | 15 | 2.09 | 0.48 | 7.50 | 0.28 | 0.13 |
| 180 | 20 | 2.21 | 0.45 | 6.75 | 0.33 | 0.15 |
| 180 | 25 | 2.19 | 0.46 | 6.24 | 0.35 | 0.16 |
| 200 | 5 | 1.63 | 0.61 | 20.19 | 0.08 | 0.05 |
| 200 | 10 | 1.82 | 0.55 | 10.63 | 0.17 | 0.09 |
| 200 | 15 | 1.89 | 0.53 | 10.48 | 0.18 | 0.10 |
| 200 | 20 | 1.84 | 0.54 | 9.12 | 0.20 | 0.11 |
| 200 | 25 | 2.24 | 0.45 | 5.99 | 0.37 | 0.17 |

| | | | | | | |
|-----|----|------|------|------|------|------|
| 240 | 5 | 1.96 | 0.51 | 8.02 | 0.24 | 0.12 |
| 240 | 10 | 2.27 | 0.44 | 6.97 | 0.33 | 0.14 |
| 240 | 15 | 2.42 | 0.41 | 5.27 | 0.46 | 0.19 |
| 240 | 20 | 2.58 | 0.39 | 4.62 | 0.56 | 0.22 |
| 240 | 25 | 2.55 | 0.39 | 4.20 | 0.61 | 0.24 |
| 300 | 5 | 2.50 | 0.40 | 4.56 | 0.55 | 0.22 |
| 300 | 10 | 2.50 | 0.40 | 4.07 | 0.61 | 0.25 |
| 300 | 15 | 2.44 | 0.41 | 3.50 | 0.70 | 0.29 |
| 300 | 20 | 2.71 | 0.37 | 3.23 | 0.84 | 0.31 |
| 300 | 25 | 2.74 | 0.36 | 3.14 | 0.87 | 0.32 |

The increase in the aromaticity of the samples with stabilisation can also be observed by the change in H/C ratio. The H/C atomic ratio for the starting pitch is already relatively low indicating that the starting pitch is quite aromatic. However as the samples are stabilised at higher temperature and for longer periods of time it can be seen that the H/C atomic ratio drops, pointing to an increase in the aromatic content. Considering that graphite is the final stage in the evolution of the pitch, it is expected that the aromaticity and condensation of the aromatics will increase during the stabilisation process, especially at higher temperatures which are closer to carbonisation temperatures.

6.4 FTIR characterisation of stabilised mesophase pitch-based tapes

This increase in the aromaticity can also be observed in Fourier transform infrared (FTIR) spectra of samples which have seen successively more aggressive oxidative stabilisation environments. FTIR examination of the chemical changes occurring in the tape during the stabilisation process was performed on a Burker Vortex 70 DRIFTS spectrometer fitted with a mid-IR source; the experiments were carried out in reflection mode as described in the experimental methodology chapter.

The green tape spectrum seen in Figures 65-71. Line (a) shows aromatic C-H stretching around the 3040 cm^{-1} , aliphatic C-H stretching bands around $2850\text{-}3000\text{ cm}^{-1}$, aromatic C-C stretching around 1600 cm^{-1} and methylene C-H in-plane bending around 1440 cm^{-1} which are both of relatively weak intensity. This is accompanied by aromatic C-H deformation between $700\text{-}900\text{ cm}^{-1}$ band. Figures 65 & 66 show the development of FTIR spectra from a green tape with increasing stabilisation time up to 5hrs at $160\text{ }^{\circ}\text{C}$ and

240°C respectively. The same pattern is evident in the spectra for both temperatures with the 240°C sample showing a more rapid progression. A decrease in the hydrogen content is clearly evident at both temperatures with increasing stabilisation time seen by the disappearance of the aliphatic C-H stretching bands in the 2850-3000 cm^{-1} assigned to the methyl and methylene hydrogen (Fanjul, Granda et al. 2002). The consumption of hydrogen is also confirmed by a decrease in the intensity of the bands representing the aromatic C-H out of plane vibration between 700-900 cm^{-1} with increasing stabilisation time and temperature. At the higher temperature of stabilisation the hydrogen consumption is mainly aliphatic as after only 1hr of heat treatment at the elevated 240°C temperature virtually no aromatic hydrogen remains indicated by the disappearance of the bands between 2850 and 3000 cm^{-1} . Fanjul observed a similar result for coal tar pitch (Fanjul, Granda et al. 2002) yet stated that this effect was less exaggerated in naphthalene based mesopahse. In these results it is temperature which affects the hydrogen loss taking place, as was shown by the TGA-FTIR results (figure 51). As stabilisation progresses an increase in the functionalisation of the pitch is evident with a significant increase in the C-O-C and O-C-O asymmetric stretching band around 1100 cm^{-1} , carbonyl stretching bands around 1650 – 1850 cm^{-1} (figure 67) and the development of bands between 3400 – 3600 cm^{-1} associated with the stretching mode of free hydroxyl groups and hydrogen bonded hydrogen groups similar to those results reported by Fanjul (Fanjul, Granda et al. 2002). The intensity of these bands increases with increasing stabilisation time and temperature. Table 11 shows how the aromatic indices (as defined in 4.4 equation 4) change with increasing stabilisation time at both 160°C and 240°C, calculated by the equation outlined by Fanjul in 2002, as discussed in the FTIR experimental methodology 4.4 (Fanjul, Granda et al. 2002). very little shift in the aromatic index can be seen at 160°C after the first hour of stabilisation, however at 240°C a more distinct shift the aromatic index can be observed from 0.34 to a maximum of 0.67, showing a greater increase in the aromaticity for those tapes which have been stabilised at higher temperatures and longer periods of time.

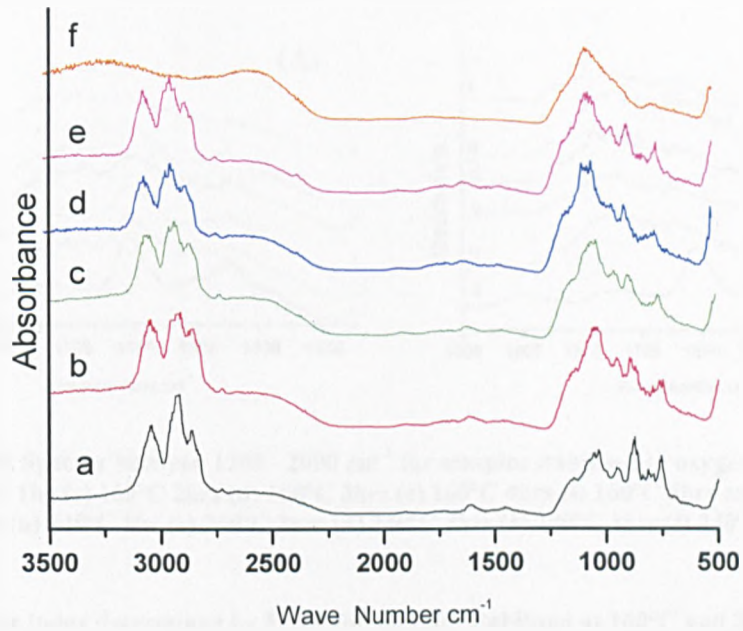


Figure 65 FTIR Spectra for 160°C stabilised tape in oxygen (a) Green (b) 160°C 1hr (c) 160°C 2hrs (d) 160°C 3hrs (e) 160°C 4hrs (f) 160°C 5hrs

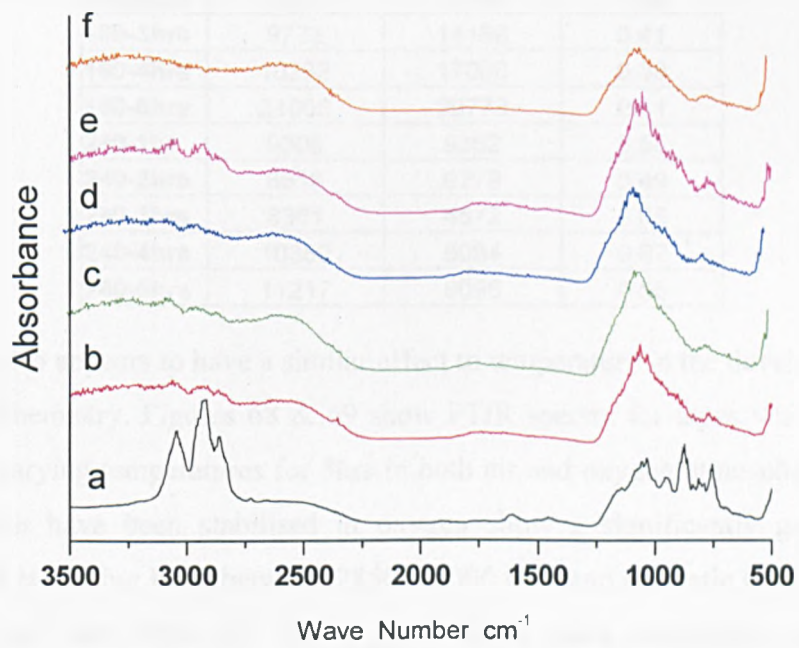


Figure 66 FTIR spectra for 240°C stabilised tapes in oxygen (a) Green (b) 240°C 1hr (c) 240°C 2hrs (d) 240°C 3hrs (e) 240°C 4hrs (f) 240°C 5hrs

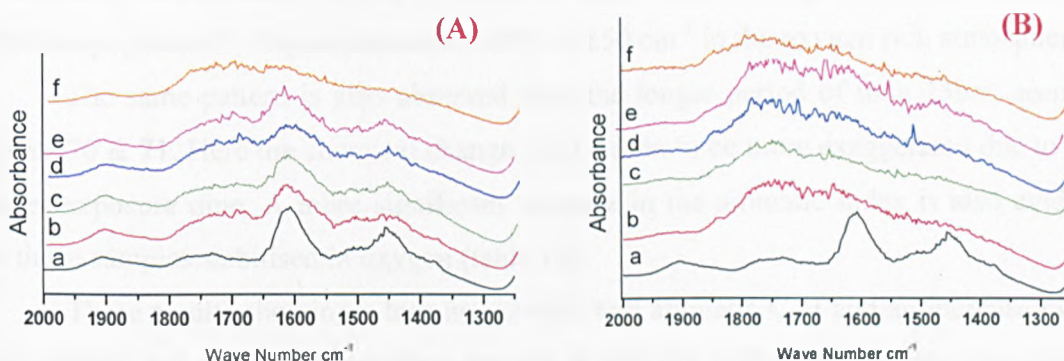


Figure 67 FTIR Spectra between 1200 - 2000 cm⁻¹ for samples stabilised in oxygen (Graph A) (a) Green (b) 160°C 1hr (c) 160°C 2hrs (d) 160°C 3hrs (e) 160°C 4hrs (f) 160°C 5hrs and (Graph B) (a) Green (b) 240°C 1hr (c) 240°C 2hrs (d) 240°C 3hrs (e) 240°C 4hrs (f) 240°C 5hrs

Table 11 Aromatic index determined by FTIR for samples stabilised at 160°C and 240°C between 1-5 hrs in oxygen

| Sample | Ar 3150-2900 | Ar 2900-2800 | <i>I-Ar</i> |
|----------|--------------|--------------|-------------|
| Green | 10988 | 21078 | 0.34 |
| 160-1hr | 9693 | 14913 | 0.39 |
| 160-2hrs | 7303 | 11318 | 0.39 |
| 160-3hrs | 9773 | 14168 | 0.41 |
| 160-4hrs | 10832 | 17060 | 0.39 |
| 160-5hrs | 21008 | 29773 | 0.41 |
| 240-1hr | 9308 | 9362 | 0.50 |
| 240-2hrs | 6618 | 6779 | 0.49 |
| 240-3hrs | 8361 | 4572 | 0.65 |
| 240-4hrs | 10359 | 5064 | 0.67 |
| 240-5hrs | 11217 | 9096 | 0.55 |

Atmosphere also appears to have a similar affect to temperature in the development of the stabilisation chemistry. Figures 68 & 69 show FTIR spectra for tapes which have been stabilised at varying temperatures for 5hrs in both air and oxygen atmospheres. The tape samples which have been stabilised in oxygen show a significantly greater loss in aliphatic C-H stretching band between 2850 – 3000 cm⁻¹ and aromatic C-H loss between 700 – 900 cm⁻¹ and 3050 cm⁻¹ for a given for a given temperature over the 5hr stabilisation period than in air. This is also true for the aliphatic hydrogen band around 3050 cm⁻¹, this concurs with CHNO results which show a more significant loss of carbon

and hydrogen for samples stabilised in oxygen. The development of C-O-C and O-C-O asymmetric band around 1100 cm^{-1} is also more pronounced along with the development of carbonyl groups C=O groups around $1650 - 1850\text{ cm}^{-1}$ in the oxygen rich atmosphere.

The same pattern is also observed over the longer period of time 25hrs, seen in figures 70 & 71. Here the chemical change can be seen to be more exaggerated due to the longer exposure time. A more significant increase in the aromatic index is also evident for those samples stabilised in oxygen (table 12).

These results showing a loss in aromatic and aliphatic C-H and an increase in C-O-C, O-C-O and C=O functionalities also tie in with the CHNO results for tapes which have seen the same stabilising conditions. With increasing time and temperature of stabilisation carbon content and hydrogen content decrease with an increase in oxygen content, this is observed to be more exaggerated in oxygen.

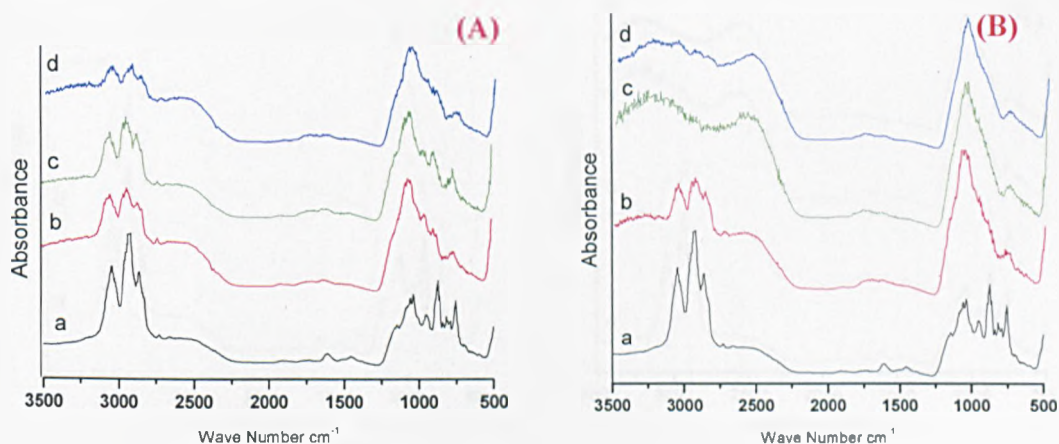


Figure 68 (Graph A) FTIR spectra for tapes stabilised in air for 5 hrs over a range of temperatures, line; (a) Green (b) 160°C 5hrs in air (c) 240°C 5hrs in air (d) 300°C 5hrs in air. **(Graph B)** FTIR spectra for tapes stabilised in oxygen for 5 hrs over a range of temperatures, line; (a) Green (b) 160°C 5hrs in oxygen (c) 240°C 5hrs in oxygen (d) 300°C 5hrs in oxygen.

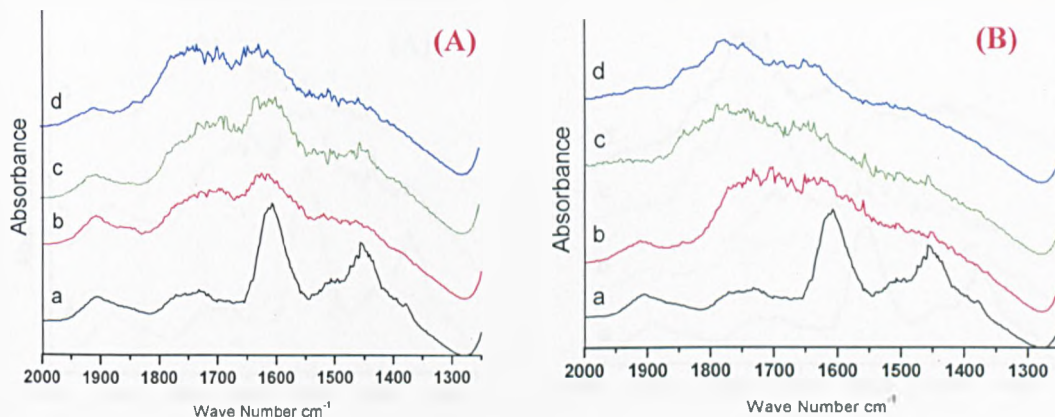


Figure 69 FTIR Spectra between 1200 - 2000 cm^{-1} for samples stabilised in oxygen (Graph A) (a) Green (b) 160°C 5hr in air (c) 240°C 5hrs in air (d) 300°C 5hrs air. (Graph B) (a) Green (b) 160°C 5hrs in oxygen (c) 240°C 5hrs in oxygen (d) 300°C 5hrs in oxygen.

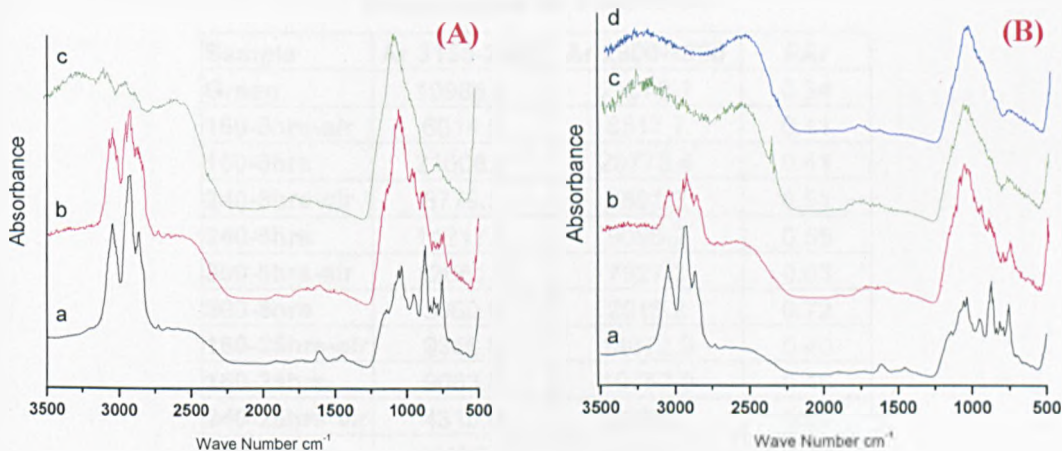


Figure 70 (Graph A) FTIR spectra for tapes stabilised in air for 25 hrs over a range of temperatures, line; (a) Green (b) 160°C 25hrs in air (c) 240°C 25hrs in air. (Graph B) FTIR spectra for tapes stabilised in oxygen for 5 hrs over a range of temperatures, line; (a) Green (b) 160°C 25hrs in oxygen (c) 240°C 25hrs in oxygen (d) 300°C 25hrs in oxygen

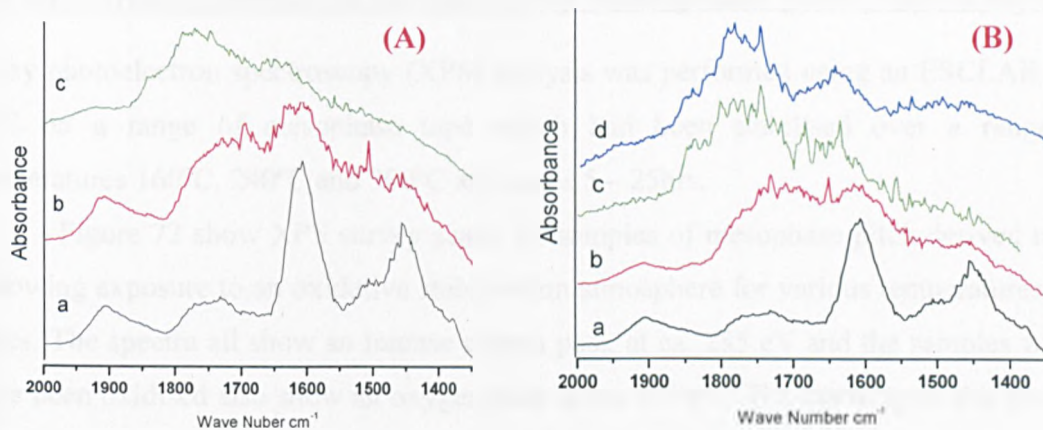


Figure 71 FTIR Spectra between 1200 - 2000 cm⁻¹ for samples stabilised in oxygen (Graph A) (a) Green (b) 160°C 25hr in air (c) 240°C 25hrs in air (. (Graph B) (a) Green (b) 160°C 25hrs in oxygen (c) 240°C 25hrs in oxygen (d) 300°C 25hrs in oxygen.

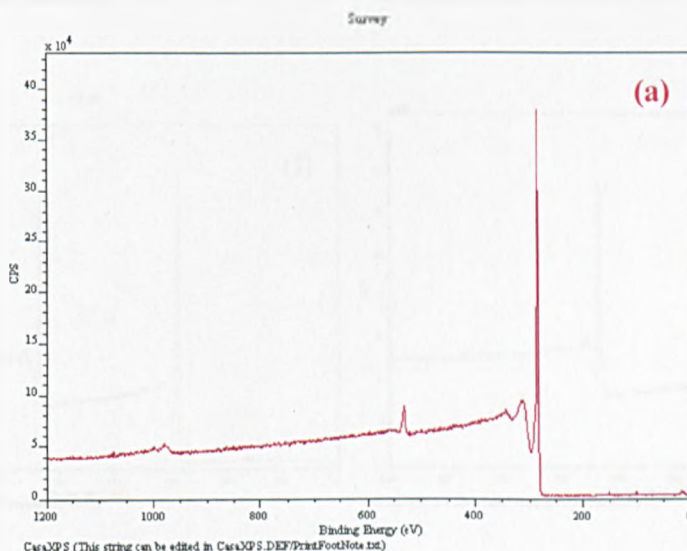
Table 12 Aromatic index determined by FTIR for samples stabilised at 160°C, 240°C and 300°C in air and oxygen for 5 and 25 hrs

| Sample | Ar 3150-2990 | Ar 2900-2800 | <i>I-Ar</i> |
|---------------|--------------|--------------|-------------|
| Green | 10988.4 | 21078.1 | 0.34 |
| 160-5hrs-air | 6014.5 | 8517.7 | 0.41 |
| 160-5hrs | 21008.4 | 29773.4 | 0.41 |
| 240-5hrs-air | 8779.5 | 8591.3 | 0.51 |
| 240-5hrs | 11217.0 | 9096.2 | 0.55 |
| 300-5hrs-air | 12661.0 | 7327.3 | 0.63 |
| 300-5hrs | 5090.0 | 2019.2 | 0.72 |
| 160-25hrs-air | 9356.6 | 14072.9 | 0.40 |
| 160-25hrs | 9053.5 | 10757.0 | 0.46 |
| 240-25hrs-air | 4315.0 | 2986.0 | 0.59 |
| 240-25hrs | 14121.7 | 4576.1 | 0.76 |
| 300-25hrs | 9811.9 | 2499.1 | 0.80 |

6.5 XPS characterisation of stabilised mesophase pitch based tapes

X-ray photoelectron spectroscopy (XPS) analysis was performed using an ESCLAB 250 XPS on a range of mesophase tape which had been stabilised over a range of temperatures 160°C, 240°C and 300°C and times 5 – 25hrs.

Figure 72 show XPS survey scans for samples of mesophase pitch-derived tapes following exposure to an oxidative stabilisation atmosphere for various temperatures and times. The spectra all show an intense carbon peak at ca. 285 eV and the samples which have been oxidised also show an oxygen peak at ca. 533 eV. The intensity of this peak is observed to correlate with oxidation time and temperature. In the case of the spectra in figures 72 (b) & (g) the two extremes of the oxidative stabilisation conditions can be observed, a much greater oxygen uptake is observed in figure 72(g) owing to the greater oxidation time and temperature. This increased oxygen content is confirmed by CHNO chemical analyses as shown in (table 9). The green sample (figure 72(a)) exhibits the lowest intensity oxygen signals in its spectra. It is likely the low-intensity signal is as a result of surface oxidation via chemisorption of oxygen. It should also be noted that no nitrogen signals are detected in the spectra for any of the tapes spun from the Mitsubishi ARMP 2004 mesophase pitch regardless of any treatment they have undergone.



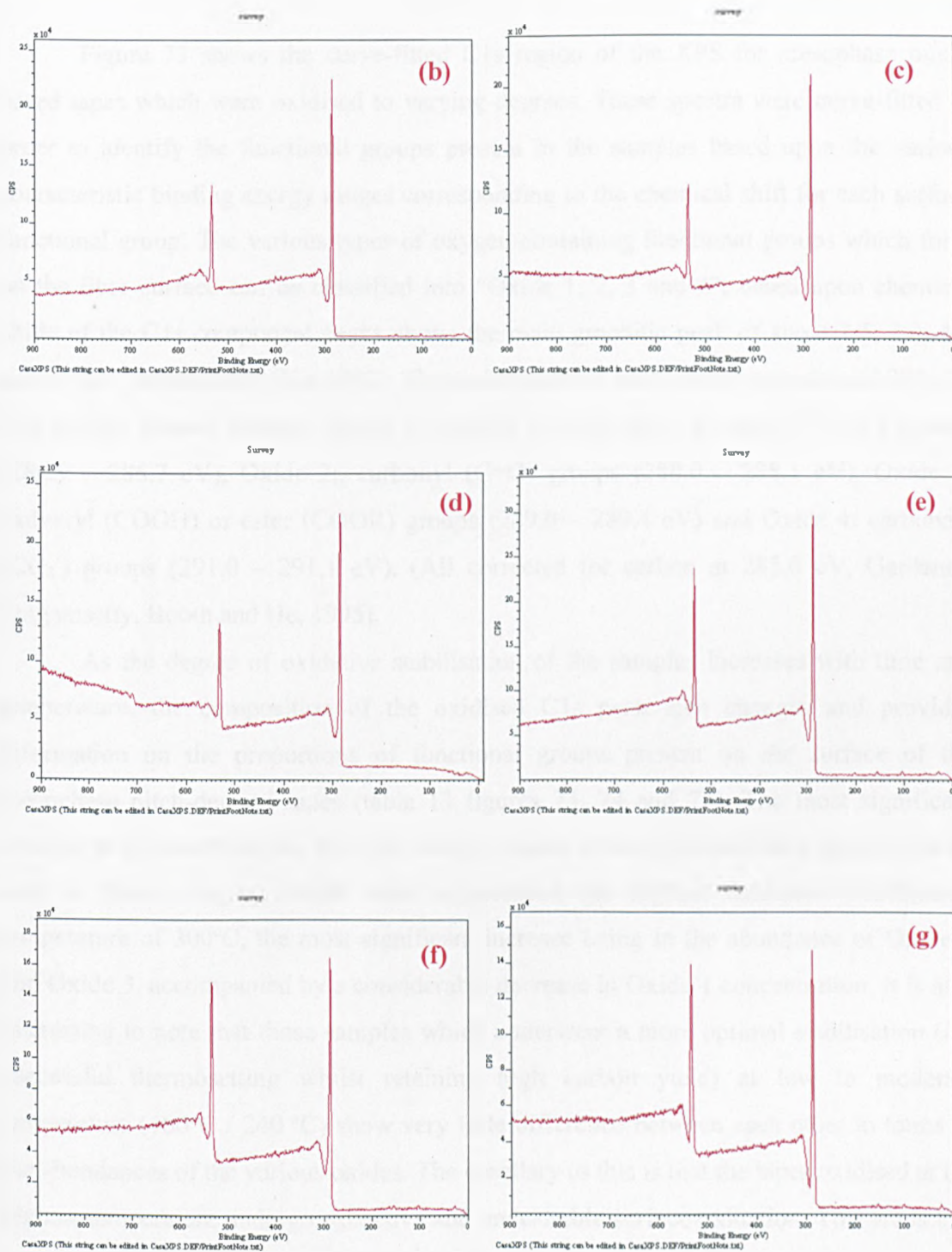
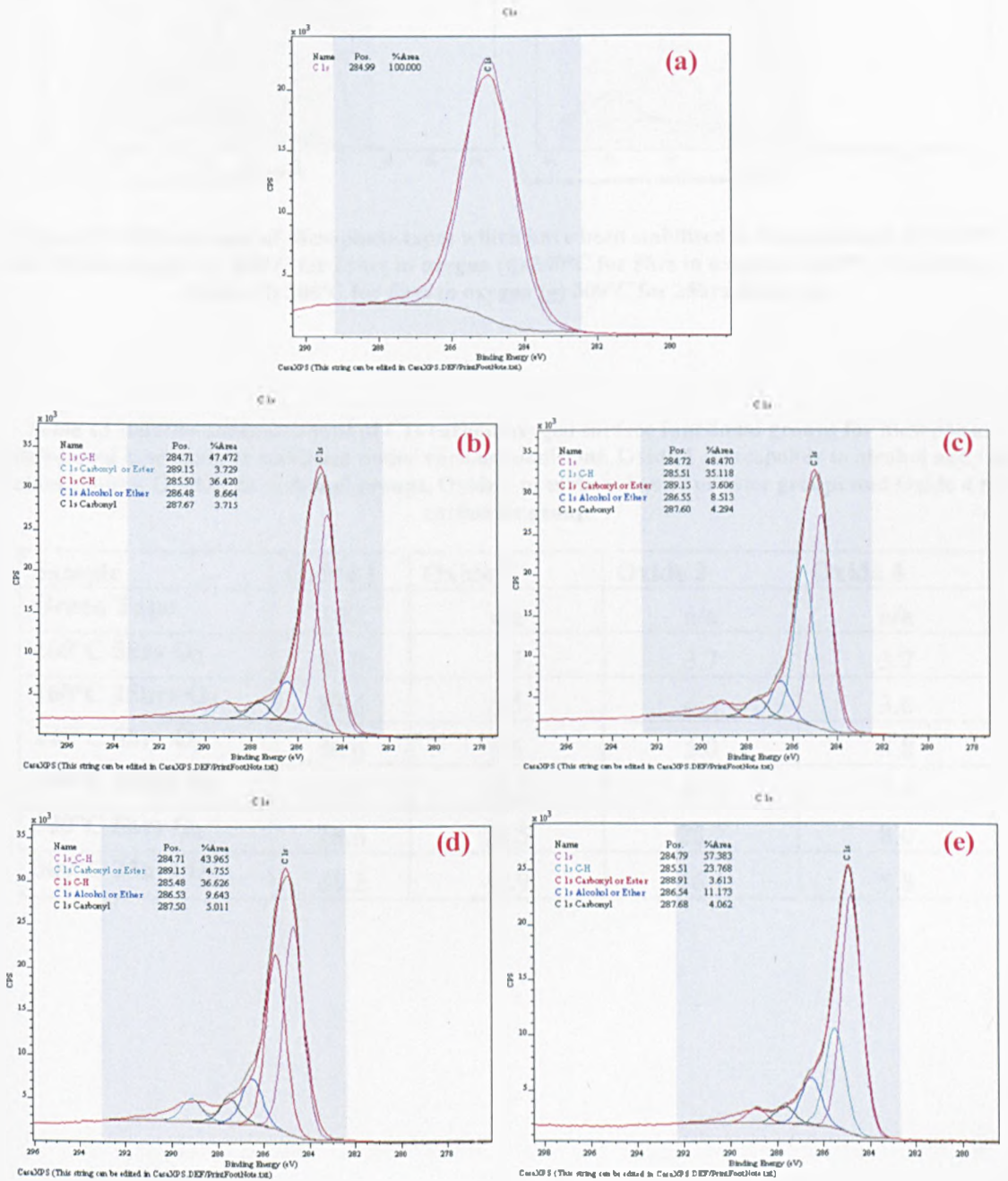


Figure 72 XPS survey scan of Mesophase tapes which have been stabilised to (a) green tape (b) 160°C for 5hrs in oxygen (c) 160°C for 25hrs in oxygen (d) 240°C for 5hrs in oxygen (e) 240°C for 25hrs in oxygen (f) 300°C for 5hrs in oxygen (g) 300°C for 25hrs in oxygen. note small sulphur peaks can be observed at approximately 163.3eV in some survey scans.

Figure 73 shows the curve-fitted C1s region of the XPS for mesophase pitch-based tapes which were oxidised to varying degrees. These spectra were curve-fitted in order to identify the functional groups present in the samples based upon the various characteristic binding energy ranges corresponding to the chemical shift for each surface functional group. The various types of oxygen-containing functional groups which form on the fibre surface can be classified into "Oxide 1, 2, 3 and 4", based upon chemical shifts of the C1s component peaks above the main graphitic peak of about 1.5, 3.0, 4.5 and 6.1 eV, respectively (Xie 1992). The main graphitic peak can be seen around 285 eV. The oxides present include: Oxide 1: alcohol (C-OH) and / or ether (C-O-C) groups (286.9 – 286.7 eV), Oxide 2: carbonyl (C=O) groups (288.0 – 288.1 eV), Oxide 3: carboxyl (COOH) or ester (COOR) groups (289.0 – 289.4 eV) and Oxide 4: carbonate (CO₃) groups (291.0 – 291.1 eV). (All corrected for carbon at 285.0 eV, Gardener, Singamsetty, Booth and He, 1995).

As the degree of oxidative stabilisation of the samples increases with time and temperature, the composition of the oxidised C1s peak area changes and provides information on the proportions of functional groups present on the surface of the mesophase pitch-derived tapes (table 13 figures 73, 74 and 75). The most significant changes in the contributions from the various classes of oxygen-containing species can be seen in those samples which have experienced the highest oxidative stabilisation temperature of 300°C, the most significant increase being in the abundance of Oxide 2 and Oxide 3, accompanied by a considerable decrease in Oxide 1 concentration. It is also interesting to note that those samples which underwent a more optimal stabilisation (i.e. successful thermosetting whilst retaining high carbon yield) at low to moderate temperature (160°C / 240 °C) show very little difference between each other in terms of the abundances of the various oxides. The corollary to this is that the tapes oxidised at the highest temperature undergo excessive and undesirable surface oxidation. This leads to a reduced carbon yield upon carbonisation owing to increased CO₂ production, as was observed using TGA-FTIR (figure 51). Another example of undesirable excessive surface oxidation can be seen in the formation of "skin-core" structure. At elevated oxidation temperatures the tapes are successfully stabilised only to a depth of about 2-3µm from the

surface, leaving the tape core unstabilised and thermally softenable. Formation of skin-core structure was confirmed using AFM micro-thermal analysis profiling to investigate sample softening point vs. probe position across a cross section of the tape (section 7.2) and optical microscopy (section 9.0).



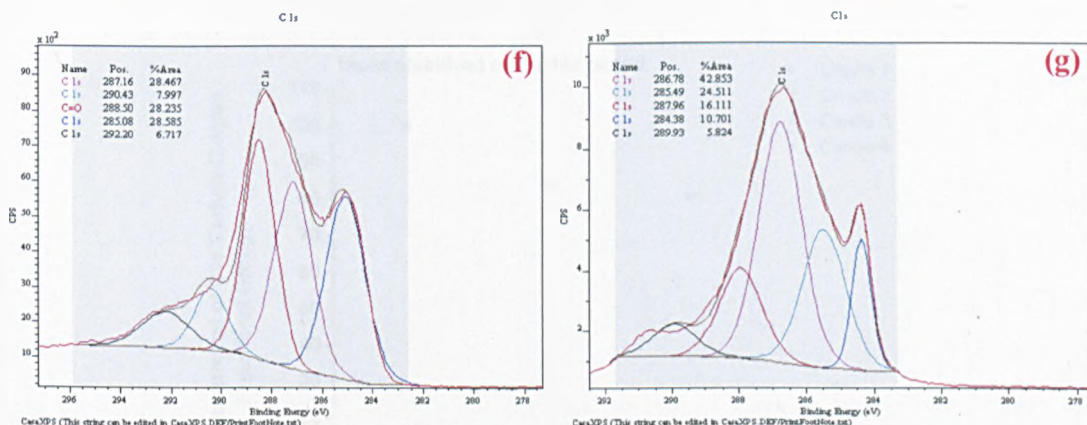


Figure 73 XPS C1s scan of Mesophase tapes which have been stabilised to (a) green tape (b) 160°C for 5hrs in oxygen (c) 160°C for 25hrs in oxygen (d) 240°C for 5hrs in oxygen (e) 240°C for 25hrs in oxygen (f) 300°C for 5hrs in oxygen (g) 300°C for 25hrs in oxygen

Table 13 Relative concentrations of C1s carbon-oxygen surface functional groups for mesophase pitch-based tape samples stabilised under various conditions. Oxide 1 corresponds to alcohol and / or ether groups, Oxide 2 to carbonyl groups, Oxide 3 to carboxyl and / or ester groups and Oxide 4 to carbonate group

| Sample | Oxide 1 | Oxide 2 | Oxide 3 | Oxide 4 |
|----------------------------|---------|---------|---------|---------|
| Green Tape | 100 | n/a | n/a | n/a |
| 160°C 5hrs O ₂ | 83.9 | 8.7 | 3.7 | 3.7 |
| 160°C 25hrs O ₂ | 83.6 | 8.5 | 4.3 | 3.6 |
| 240°C 5hrs O ₂ | 80.6 | 9.6 | 5.0 | 4.8 |
| 240°C 25hrs O ₂ | 81.2 | 11.2 | 4.1 | 3.6 |
| 300°C 5hrs O ₂ | 28.6 | 28.5 | 28.2 | 8.0 |
| 300°C 25hrs O ₂ | 35.2 | 42.9 | 16.1 | 5.8 |

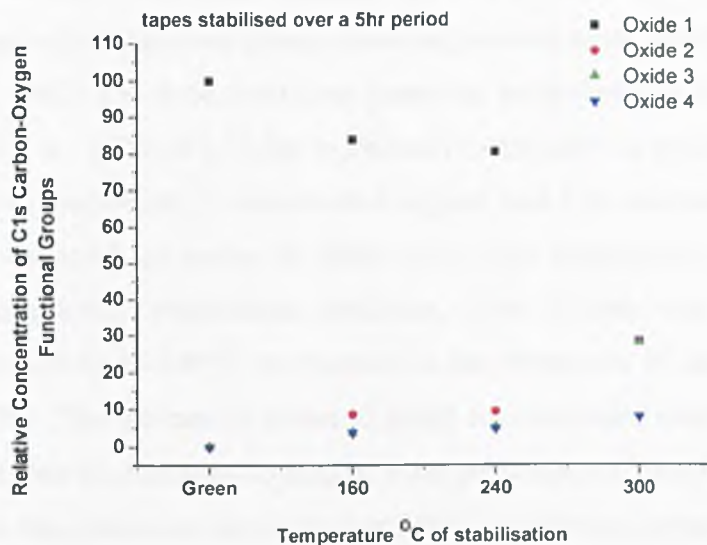


Figure 74 change in relative concentrations of C1s carbon-oxygen surface functional groups for mesophase pitch-based tape samples stabilised under various conditions for 5hrs. Oxide 1 corresponds to alcohol and / or ether groups, Oxide 2 to carbonyl groups, Oxide 3 to carboxyl and / or ester groups and Oxide 4 to carbonate groups

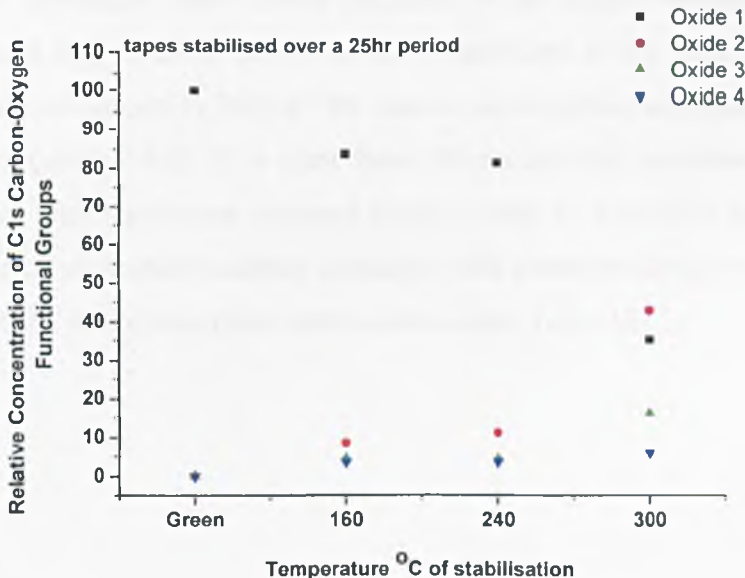


Figure 75 change in relative concentrations of C1s carbon-oxygen surface functional groups for mesophase pitch-based tape samples stabilised under various conditions for 25hrs. Oxide 1 corresponds to alcohol and / or ether groups, Oxide 2 to carbonyl groups, Oxide 3 to carboxyl and / or ester groups and Oxide 4 to carbonate groups

In the same way as for the C1s peaks, the O1s spectral region can be separated into three corresponding functional groups based on previous work carried out by Xie and co-workers (Xie 1992). The three constituent peaks can be attributed to Oxide 1; carbonyl (C=O) groups (531.6 - 532.0 eV), Oxide 2; alcohol (C-OH) and / or ether (C-O-C) groups (533.2 - 533.5 eV) and Oxide 3: chemisorbed oxygen and / or adsorbed water (535.8 - 536.2 eV) (All corrected for carbon at 285.0 eV). Upon examination of how the O1s functionality changes with stabilisation condition, it can be seen that, with increasing time and temperature up to 240°C, an increase in the proportion of carbonyl content is evident (figure 76). This increase in carbonyl group concentration, which emerges in the XPS O1s region, can be attributed to ketone, ester and carboxyl groups (Gardner et al., 1995). For those tapes which were oxidised at 300°C, a different pattern can be seen. In this case, no carbonyl groups are detected and the majority of the surface functionality remains in the form of alcohols and / or esters. However traces of chemisorbed oxygen and / or adsorbed water can be detected and, again, the intensity of this signal increases with oxidation time. This increase can also be seen in the weight loss patterns of tapes when they are carbonised since those oxidised at the higher temperatures show a significant weight loss at about 100°C which is attributed to the removal of adsorbed water and this is also evident in TGA-FTIR data for carbonisation of samples stabilised to varying degrees (section 8.2). It is clear from the results that stabilisation at elevated temperatures not only suppresses carbonyl group (Oxide 1) formation but also leads to increased levels of undesirable surface oxidation with correspondingly reduced ultimate carbon yield for the mesophase pitch-based carbon tape (Table 14).

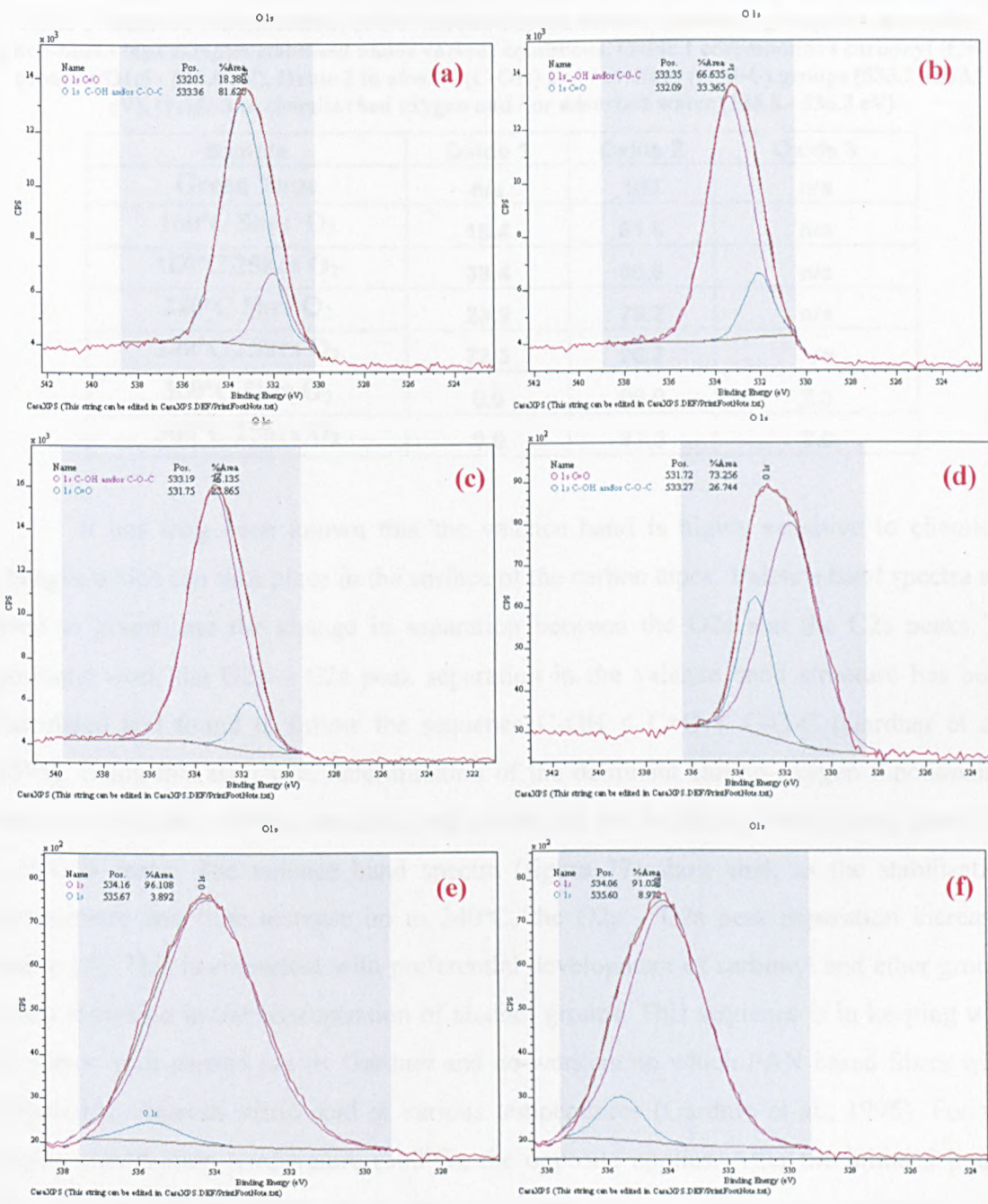
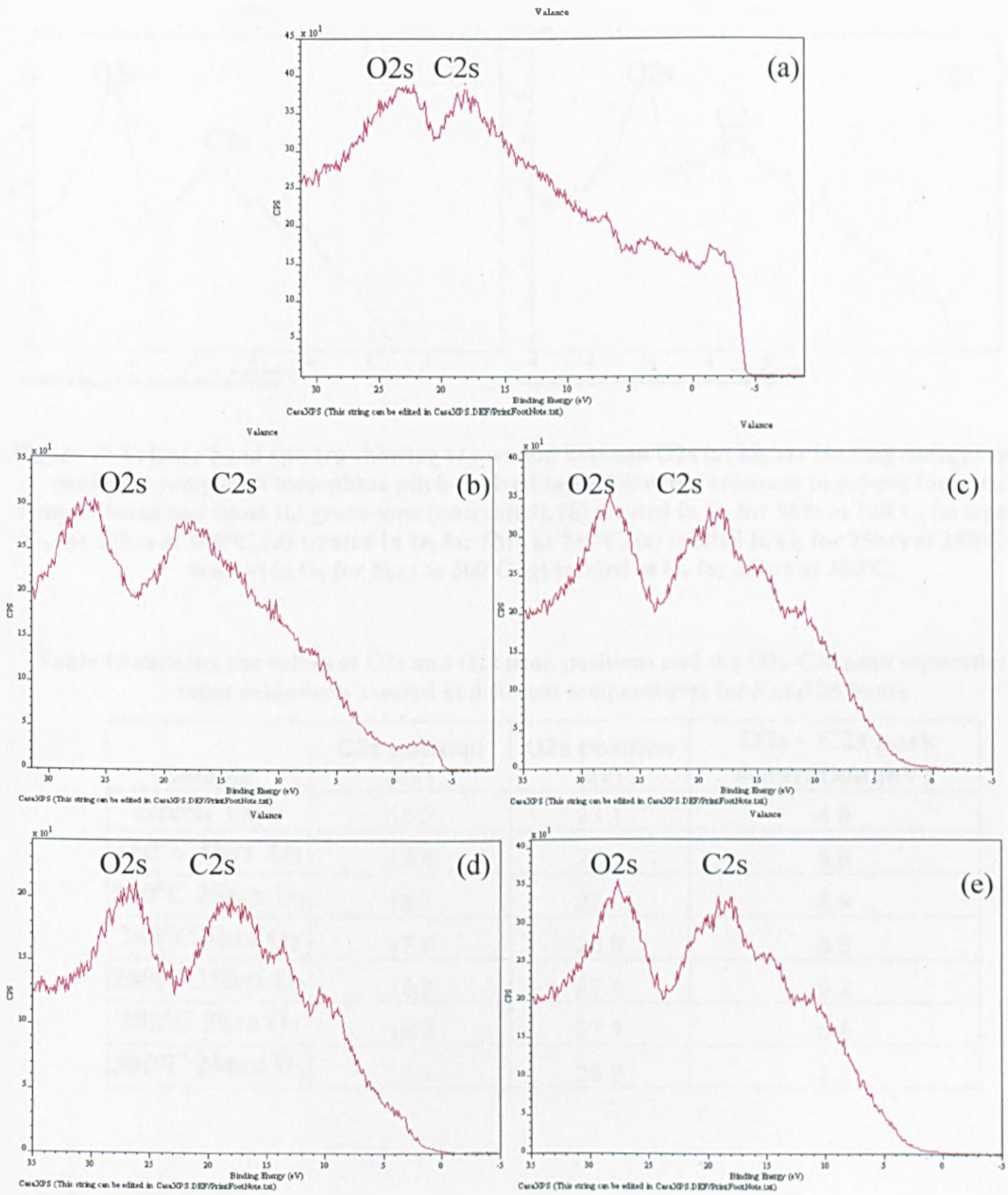


Figure 76 XPS O1s scan of Mesophase tapes which have been stabilised to (a) 160°C for 5hrs in oxygen (b) 160°C for 25hrs in oxygen (c) 240°C for 5hrs in oxygen (d) 240°C for 25hrs in oxygen (e) 300°C for 5hrs in oxygen (f) 300°C for 25hrs in oxygen

Table 14 Relative concentrations of O1s carbon-oxygen surface functional groups for mesophase pitch-based tape samples stabilised under various conditions. Oxide 1 corresponds to carbonyl (C=O) groups (531.6 - 532.0 eV), Oxide 2 to alcohol (C-OH) and / or ether (C-O-C) groups (533.2 - 533.5 eV), Oxide 3 to chemisorbed oxygen and / or adsorbed water (535.8 - 536.2 eV)

| Sample | Oxide 1 | Oxide 2 | Oxide 3 |
|----------------------------|---------|---------|---------|
| Green Tape | n/a | 100 | n/a |
| 160°C 5hrs O ₂ | 18.4 | 81.6 | n/a |
| 160°C 25hrs O ₂ | 33.4 | 66.6 | n/a |
| 240°C 5hrs O ₂ | 23.9 | 76.2 | n/a |
| 240°C 25hrs O ₂ | 73.3 | 26.7 | n/a |
| 300°C 5hrs O ₂ | 0.0 | 98.0 | 2.0 |
| 300°C 25hrs O ₂ | 0.0 | 91.0 | 9.0 |

It has long been known that the valence band is highly sensitive to chemical changes which can take place in the surface of the carbon tapes. Valence band spectra are used to investigate the change in separation between the O2s and the C2s peaks. In previous work the O2s – C2s peak separation in the valence band structure has been calculated and found to follow the sequence C-OH < C=O < C-O-C (Gardner et al., 1995). Using this sequence, determination of the dominant carbon-oxygen functionality becomes possible, whereas alcohols and ethers can not be distinguished using their C1s and O1s peaks. The valence band spectra (figure 77) show that, as the stabilisation temperature and time increase up to 240°C, the O2s – C2s peak separation increases (table 15). This is consistent with preferential development of carbonyl and ether groups and a reduction in the concentration of alcohol groups. This sequence is in keeping with previous work carried out by Gardner and co-workers, in which PAN-based fibres were exposed to aqueous nitric acid at various temperatures (Gardner et al., 1995). For the higher stabilisation temperature (300°C), the opposite applies. After the initial 5 hours, the valence peak separation can be seen to increase (table 15) indicating the formation of ether groups but after longer periods this separation reduces, pointing to a predominance of alcohol groups and suggesting no carbonyl formation.



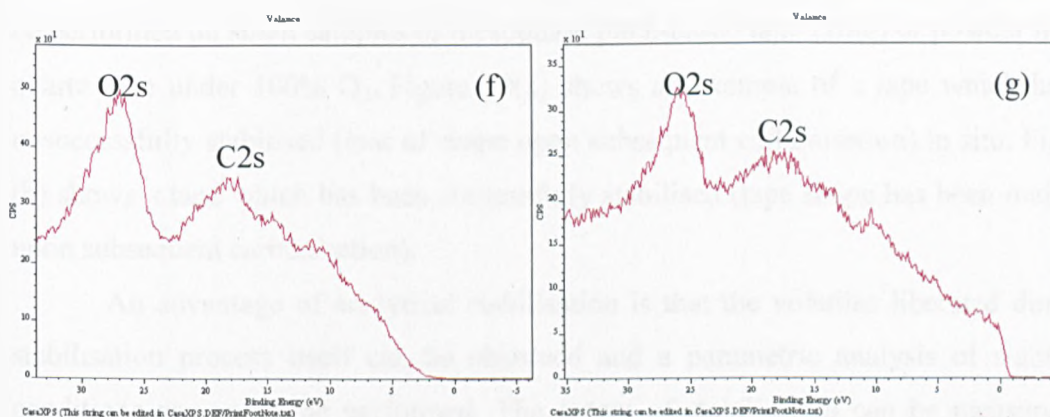


Figure 77 Valence band spectra showing separation between O2s (at higher binding energy) and C2s peaks for samples of mesophase pitch-derived tapes following exposure to oxygen for various temperatures and times (a) green tape (untreated), (b) treated in O₂ for 5hrs at 160°C, (c) treated in O₂ for 25hrs at 160°C, (d) treated in O₂ for 5hrs at 240°C, (e) treated in O₂ for 25hrs at 240°C & (f) treated in O₂ for 5hrs at 300°C (g) treated in O₂ for 25hrs at 300°C.

Table 15 showing the values of C2s and O2s peak positions and the O2s-C2s peak separation for tapes oxidatively treated at different temperatures for 5 and 25 hours

| Sample | C2s position (eV) | O2s position (eV) | O2s – C2s peak separation (eV) |
|----------------------------|-------------------|-------------------|--------------------------------|
| Green Tape | 18.2 | 23.1 | 4.9 |
| 160°C 5hrs O ₂ | 18.5 | 27.1 | 8.6 |
| 160°C 25hrs O ₂ | 18.1 | 27.0 | 8.9 |
| 240°C 5hrs O ₂ | 17.9 | 26.5 | 8.6 |
| 240°C 25hrs O ₂ | 18.2 | 27.4 | 9.2 |
| 300°C 5hrs O ₂ | 18.3 | 27.1 | 8.8 |
| 300°C 25hrs O ₂ | 18.1 | 25.8 | 7.7 |

6.6 Py-GC-MS characterisation of mesophase pitch-based carbon tapes

Analytical pyrolysis methods such as pyrolysis-gas chromatography-mass spectrometry (Py-GC-MS) are ideal for investigating the structure of macromolecular polymeric materials (Jones 2006). Operation of Py-GC-MS in reactive gas mode allows a simulated oxidative treatment to be carried out on an analytical scale. The oxidative treatment can

be performed on small samples of mesophase pitch-based tape (2mg) or powder held in a quartz tube under 100% O₂. Figure 78(a) shows an example of a tape which has been unsuccessfully stabilised (loss of shape upon subsequent carbonisation) in situ. Figure 78 (b) shows a tape which has been successfully stabilised (tape shape has been maintained upon subsequent carbonisation).

An advantage of analytical stabilisation is that the volatiles liberated during the stabilisation process itself can be observed and a parametric analysis of stabilisation conditions can easily be performed. The extent of stabilisation can be measured by a number of methods; firstly by the appearance of oxygenated volatile fragments desorbed from the Tenax trap at the end of the oxidative treatment, secondly by the carbon yield of the tape upon further pyrolysis at 1000°C and thirdly by the appearance of the stabilised carbon tape upon subsequent pyrolysis at 1000°C (figure 78) (i.e. whether its shape is retained). Figures 79, 80 and 81 show the volatile products from analytical scale oxidative stabilisation of a green tape over 5 hours at 160°C, 240°C and 300°C respectively.



Figure 78 (a) Sample unsuccessfully stabilised in situ has softened and flowed (b) Sample successfully stabilised in situ retains original shape

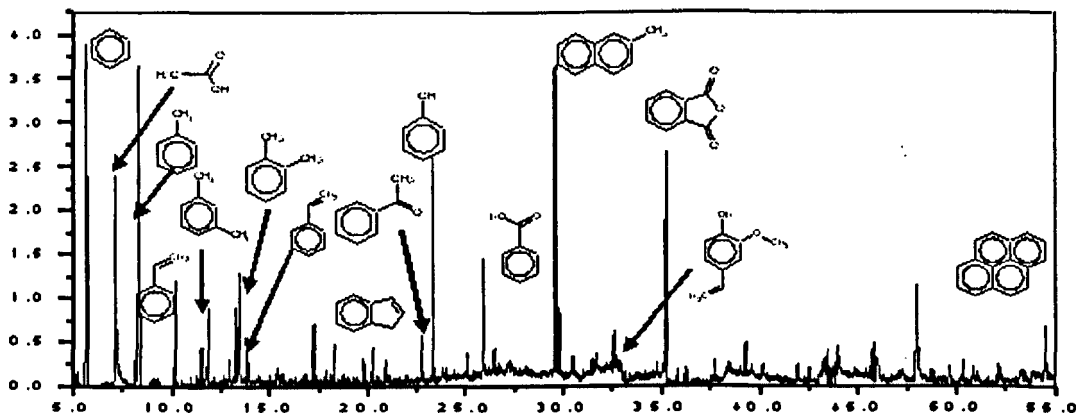


Figure 79 Fragment retention time (x-axis) vs. abundance (y-axis) results from Py-GC-MS of green tape in reactive mode at 160 °C for 5 hours in 100% O₂

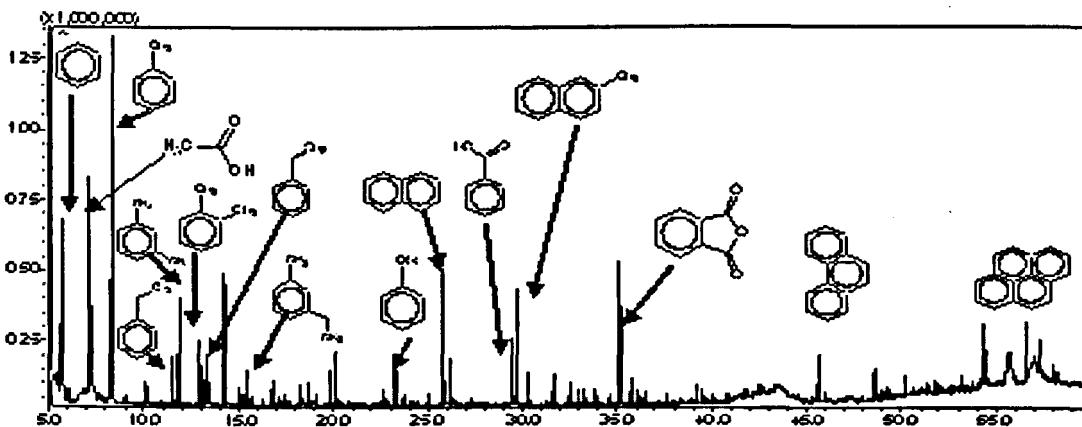


Figure 80 Fragment retention time (x-axis) vs. abundance (y-axis) results from Py-GC-MS of a green tape in reactive mode at 240 °C for 5 hours in 100% O₂

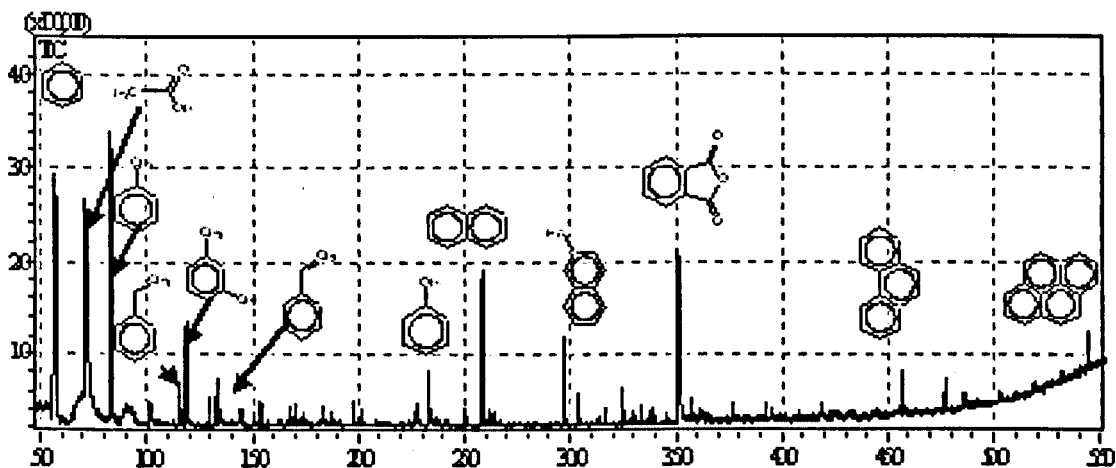


Figure 81 Fragment retention time (x-axis) vs. abundance (y-axis) results from Py-GC-MS of a green tape in reactive mode at 300 °C for 5 hours in 100% O₂

Consideration of the combination of observed oxygenated species evolved during analytical stabilisation of the green pitch provides insight into the functionality of oxygen incorporation during oxidative stabilisation and possible mechanistic routes. Firstly, it is clear that significant quantities of alkyl substituted polycyclic aromatic hydrocarbons (Alkyl-PAH) are present in the green pitch. These alkyl sites are thought to be oxidised first, forming aldehyde and carboxylic acid groups. Both of these analogues are observed for benzene. Secondly, it is proposed that these groups form anhydride linkages which can either link larger polycyclic aromatic hydrocarbon (PAH) moieties or form smaller fragments such as phthalic anhydride and its naphthalene analogue (both observed). These smaller anhydride-containing fragments may form linkages via reaction with phenolic fragments to form esters. The observation of phthalic anhydride is significant and this may form via oxidation of butene or benzene, although normally this reaction occurs catalytically, alternatively it may be formed via pyrolytic degradation of acid anhydrides. It is likely that anhydride linkage formation is key to the stabilisation process, this holds true with the work reported by Drbohlav et al (Drbohlav and Stevenson 1995).

6.7 Raman characterisation of stabilised mesophase pitch-based tapes

Raman scattering has been used as a successful technique for studying lattice modes in graphite and various other carbons (Angell and Lewis 1978) (Dresselhaus, Fung et al. 1992; Lu, Blanco et al. 2002). It is known that increasing crystalline disorder in different carbon materials induces the appearance of two broad features around 1350 cm^{-1} (D band) and ca. 1600 cm^{-1} (G band) in Raman spectra. The intensity of these peaks $D(D_{(i)})$ and $G(G_{(i)})$ can also be used to give an indication of the material's in-plane structural order with the $D_{(i)}/G_{(i)}$ ratio being used to quantify the material's structural order. A lower $D_{(i)}/G_{(i)}$ ratio corresponds to more highly ordered structure.

The sharp G peak and the broad D band features in the Raman spectrum of mesophase pitch are in keeping with those usually observed in disordered carbon materials (Angell and Lewis 1978; Rogovoi and Amerik 1993; Dumont, Chollon et al. 2002; Montes-Moran, Crespo et al. 2002). This can be explained by the structure of the mesophase, which is a mixture of molecules that have developed as a result of polycondensation of naphthalene based oligomers only. Therefore the variety of molecules present in the naphthalene-based pitch is limited much more than in naturally occurring carbonaceous pitches (Dumont, Chollon et al. 2002). The G band at around 1600 cm^{-1} for the naphthalene-derived mesophase shows a greater relative intensity and a narrower width than those G bands typically observed in other carbon materials such as carbonaceous pitches and disordered carbons (Dumont, Chollon et al. 2002). The structure of the molecules present in the mesophase pitch differs significantly from the graphene layers in disordered carbon, as the former can be characterised by the presence of aryl-aryl C-C bonds, naphthenic rings and alkyl groups on the periphery of these molecules.

Figure 82 illustrates the region of the mesophase pitch-based tapes which the Raman microscope was focused on in order to obtain the Raman spectra of the stabilised tapes.

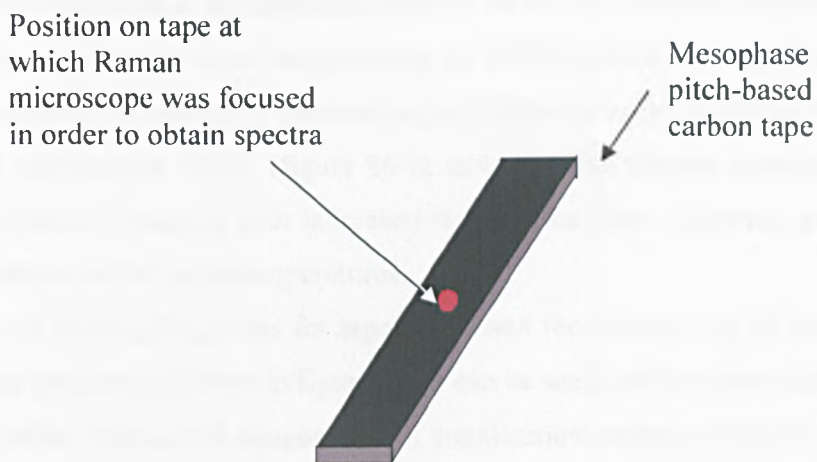


Figure 82 Position which Raman microscope was focused on mesophase pitch-based tape in order to obtain Raman Spectra

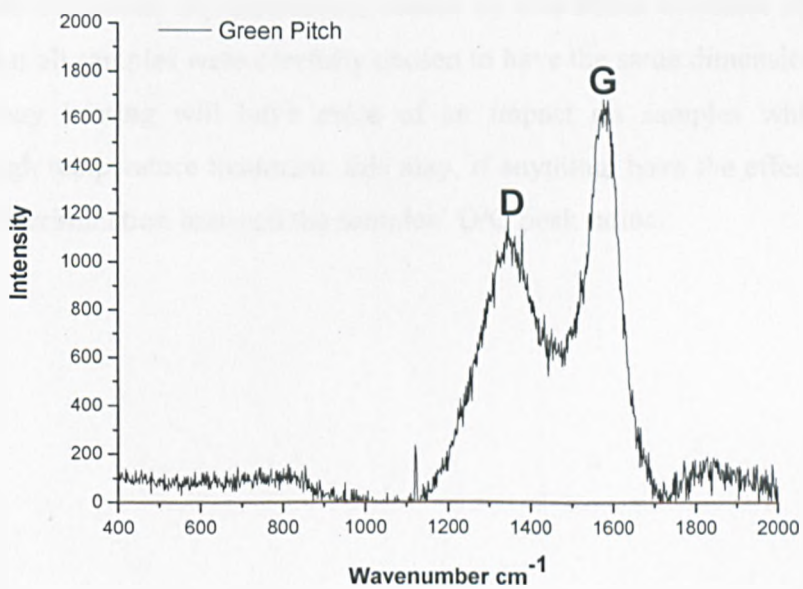


Figure 83 Raman Spectrum of green mesophase pitch

When comparing the $D_{(i)}/G_{(i)}$ ratios of Raman spectra for tapes of uniform dimension which have been stabilised at the same temperature for the two different lengths of time it became apparent that at the lower temperatures of 160°C and 240°C longer stabilisation time display a greater reduction in the ordering as illustrated in figures 84 & 85 and table 16. The tapes stabilised at 300°C (figure 86 & table 16) still display a reduction in the ordering of the tapes' structure with increased stabilisation time. However, this effect is not as prominent as at the lower temperatures.

A plot of the $D_{(i)}/G_{(i)}$ ratios for tapes stabilised for 5 hours and 25 hours against stabilisation temperature is shown in figure 87. It can be seen, for the tapes stabilised over the 5hr time period, that as the temperature of stabilisation increases, the $D_{(i)}/G_{(i)}$ ratios increases. Samples stabilised for 25 hours display a similar increase as stabilisation temperature increases from 160°C to 240°C. However, the tape stabilised at 300°C for 25hr break this trend by then showing a decrease in the $D_{(i)}/G_{(i)}$ ratio.

It should also be noted that during this experiment there may have been a heating effect on the sample as a result of the Raman laser beam (25mW) which could have led to an increase in the G peak as this heating may tend to increase the ordering in the tapes' microstructure. However, any differences caused by this effect will have been mitigated by the fact that all samples were carefully chosen to have the same dimensions (1.1mm in width). As any heating will have more of an impact on samples which have not undergone high temperature treatment, this may, if anything, have the effect of reducing the level of discrimination between the samples' D/G peak ratios.

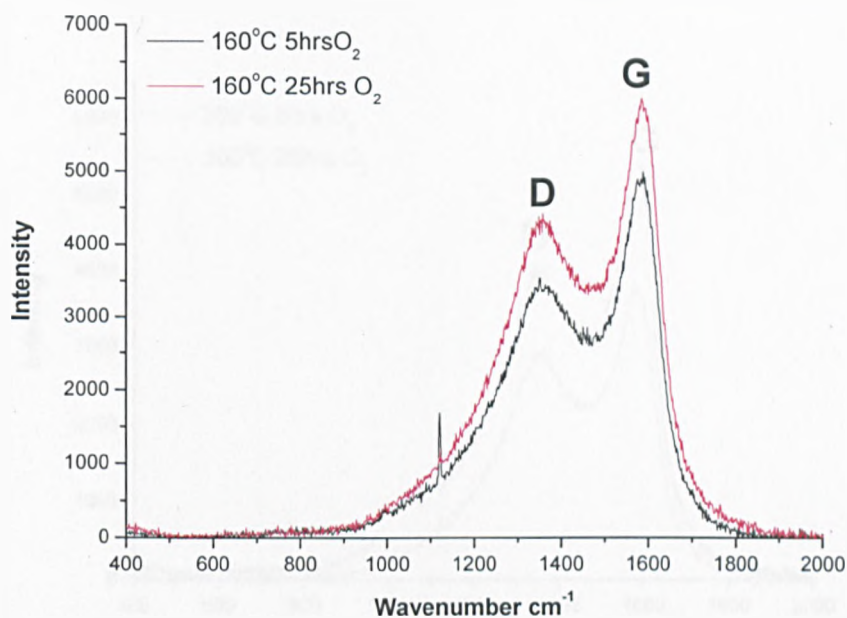


Figure 84 Raman spectra for tapes stabilised at 160°C for 5 and 25hrs

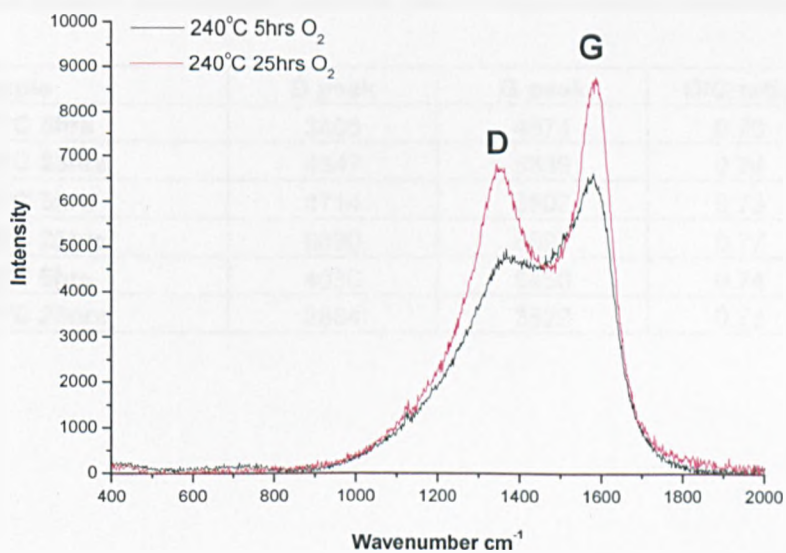


Figure 85 Raman spectra for tapes stabilised at 240°C for 5 and 25hrs

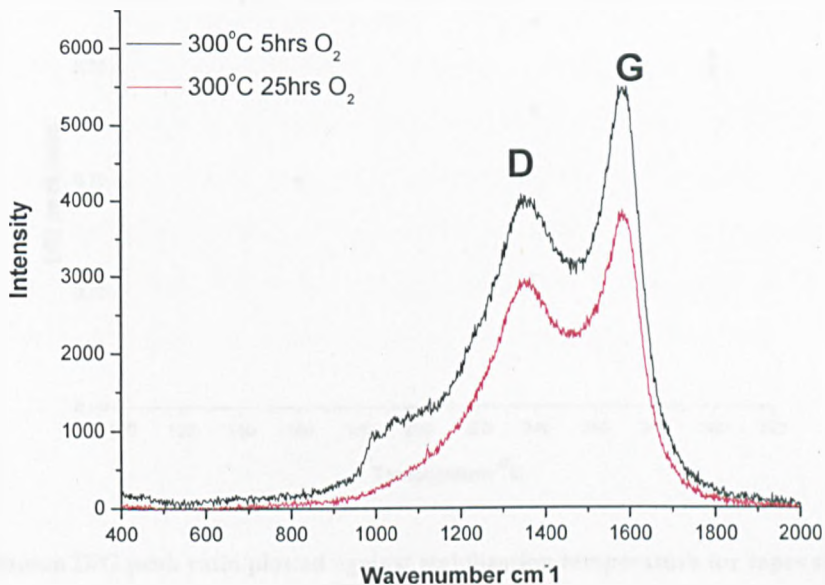


Figure 86 Raman spectra for tapes stabilised at 300°C for 5 and 25hrs

Table 16 Raman D and G peak intensity and D/G ratio for tapes stabilised under various conditions

| Sample | D peak | G peak | D/G ratio |
|-------------|--------|--------|-----------|
| 160°C 5hrs | 3406 | 4874 | 0.70 |
| 160°C 25hrs | 4347 | 5836 | 0.74 |
| 240°C 5hrs | 4714 | 6502 | 0.73 |
| 240°C 25hrs | 6690 | 8697 | 0.77 |
| 300°C 5hrs | 4036 | 5450 | 0.74 |
| 300°C 25hrs | 2884 | 3822 | 0.75 |

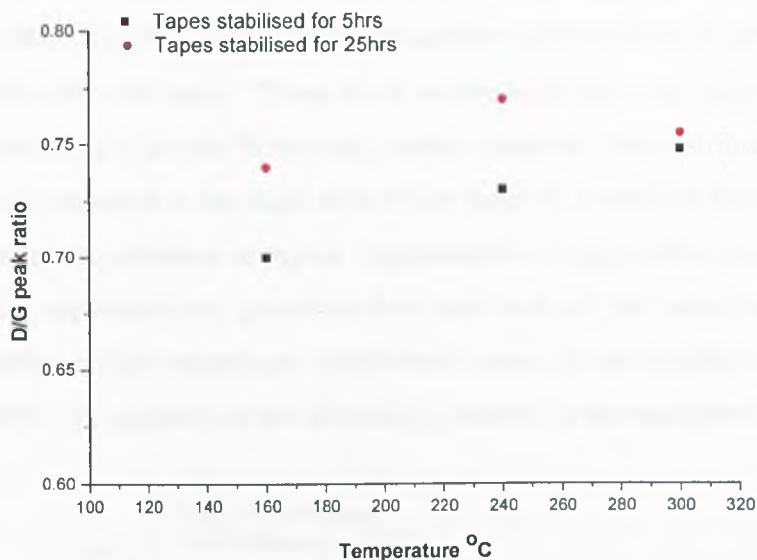


Figure 87 Raman D/G peak ratio plotted against stabilisation temperature for tapes stabilised for 5hrs and 25hrs

This increased disorder evident at longer stabilisation time at 160°C and 240°C may well be as a result of the oxygen incorporated into the mesophase pitch-based tapes inducing the structural disorder. Figure 88 shows a plot of the % oxygen content of the tapes obtained by CHNO analysis against the D/G peak ratio for the tapes stabilised to varying conditions. It can be seen that at the lower temperatures of stabilisation (160°C and 240°C) as the % oxygen content rises in tapes so does the disorder. At 300°C disorder of the tapes structure is still observed by the higher D/G peak ratios however the samples do not exhibit the same amount of structural disorder as the tapes stabilised at lower temperature for a comparable % oxygen contents (240°C 25hrs oxygen and 300°C 5hrs oxygen). This is likely to be as a result of how the oxygen has distributed itself throughout the tapes structure at the different temperatures of stabilisation. At the lower temperatures of 160°C and 240°C the oxygen can be seen to diffuse deeper into the tapes, the tapes stabilised at the higher temperature of 300°C exhibit the majority of the oxygen uptake on the surface of the tape (these results are discussed in more detail in the EPMA section 7.3 figures 106 & 107). It is this variation in oxygen distribution throughout the cross-section of the mesophase pitch-based tapes with stabilisation temperature and time

that gives rise to the variation in molecular disorder. At 160°C and 240°C oxygen is permitted to diffuse into the centre of the tapes thus incorporating a greater degree of structural defects into the tapes. Those tapes which have seen the 300°C stabilisation temperature do exhibit a higher % oxygen content however, the distribution of oxygen uptake is heavily weighted to the outer-skin of the tapes as a result of the tapes tendency to develop a skin core structure at higher temperatures of stabilisation. Here the oxygen has not had an opportunity to penetrate into the core of the tapes and disturb the molecular ordering of the mesophase pitch-based tapes. In the samples that have been stabilised to 300°C the majority of the disorder is detected at the tapes surface.

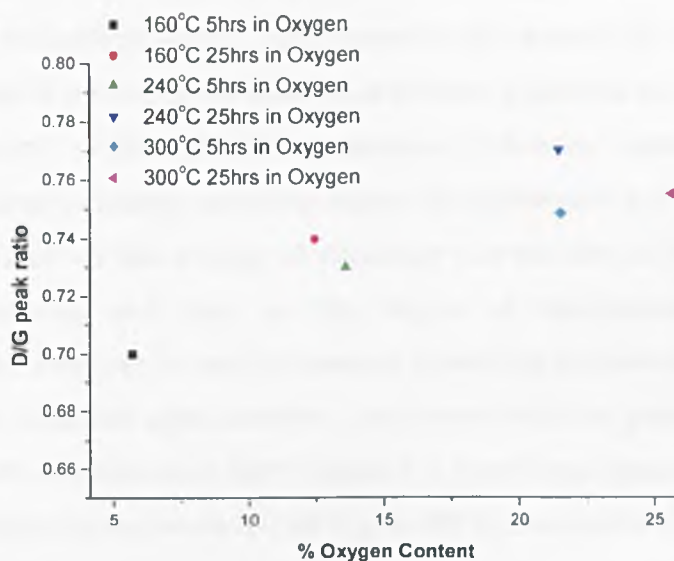


Figure 88 Raman D/G peak ratio plotted against % Oxygen content for tapes stabilised for 5hrs and 25hrs

6.8 Stabilisation of mesophase pitch-based tapes weight change and chemistry conclusion.

During the stabilisation step the mesophase pitch-based tapes experience a weight gain, the extent of which is determined not only by the stabilisation atmosphere but also the temperature. It is of note that those tapes stabilised to the higher temperature of 300°C actually experience a weight loss after an initial rapid weight gain. The atmosphere and temperature at which stabilisation is carried out also dictates the spectral peaks intensity

of the evolved gases (CO_2 & H_2O) during the stabilisation step. This accompanied by the uptake of oxygen during the stabilisation step lead to a change in the chemistry of the mesophase pitch-based tapes. The changing chemistry of the mesophase pitch-based tapes is better illustrated by CHNO data (table 9) and Van Krevelen plots (figure 53 & 54). Here the greater oxygen content of those tapes stabilised in the oxygen atmosphere is evident and conversely it can be seen that the tapes which have been stabilised in air have a higher carbon content after the stabilisation step, suggesting that air stabilisation may well be the key to an increased carbon yield. In breaking down the weight change experienced by the pitch-based tapes (figures 55-59), it is clear that the overall weight change in the tapes is as a direct result of an increased oxygen content accompanied by a loss in hydrogen and carbon content. An increase in the aromaticity of the tapes can be seen to be a feature of prolonged stabilisation at elevated temperatures.

FTIR spectra of the stabilised mesophase pitch-based carbon tapes samples clearly show a chemical change occurring during the stabilisation process (figures 65-67 & 68-71). The extent of this change of chemistry can be seen to be dictated by the stabilisation conditions and time, as the degree of stabilisation progresses the functionality of the tapes can be seen to increase. Increasing aromaticity can also be seen to develop in the stabilised tapes between 1 to 5 hours with the greatest change taking place at the higher temperature of 240°C (table 11). Over longer periods of stabilisation up to 25hrs the higher temperatures of 240°C and 300°C also exhibit the highest levels of aromaticity (table 12).

The atmosphere of stabilisation can also be seen to have a significant affect on the chemistry of the mesophase pitch-based tapes, because those samples which have been stabilised in an oxygen atmosphere display a greater loss in aliphatic C-H and aromatic C-H for a given temperature than those samples which have been stabilised in air. These results are corroborated by CHNO chemical analysis data for the stabilised mesophase pitch-based tapes, likely to be as a result of the significant loss of hydrogen and carbon which can be observed during the stabilisation step as illustrated in figure 48. This is accompanied by a greater increase in the functionalisation of the tapes for those stabilised in the oxygen atmosphere. Mesophase pitch based tapes stabilised in oxygen also

experience a much larger increase in aromaticity with increasing temperature and time of stabilisation than those tapes stabilised in the air atmosphere.

The XPS results for the mesophase pitch-based carbon tapes which had been subjected to varying degrees of stabilisation helped to shed some light on the functional groups which are present on the tapes surface. As the degree of stabilisation of the samples increased with time and temperature changes the oxygenated species which were present in the C1s peak were seen to alter. At 300°C of stabilisation a decrease in Oxide 1: (alcohol (C-OH) and / or ether (C-O-C) groups (286.9 – 286.7 eV)) and increase abundance of Oxide 2: (carbonyl (C=O) groups (288.0 – 288.1 eV)) and Oxide 3: (carboxyl (COOH) or ester (COOR) groups (289.0 – 289.4 eV)) was observed whilst at the lower temperatures of 160°C and 240°C show much less variation between the oxygenated functional species on the tapes surface with the majority of the functional groups being Oxide 1: (alcohol (C-OH) and / or ether (C-O-C) groups (286.9 – 286.7 eV) (Table 13). Upon examination of the O1s peak for the stabilised mesophase pitch based tapes change in the tapes functionality is again observed with increasing time and temperature the proportion of carbonyl content increases in the ketone ester and carboxyl group region. When treated at 300°C the bulk of the surface functionality is detected as alcohols and/or esters, also traces of chemisorbed oxygen / and or adsorbed oxygen can be seen to show increased intensities with increasing time of oxidative stabilisation.

XPS valance bands spectra for the stabilised mesophase pitch-based tapes indicate how the varying conditions affect the separation between the O2s and C2s peaks. The valence band spectra (figure 73) illustrate that, as the stabilisation temperature and time increase up to 240°C, the O2s – C2s peak separation increases consistent with preferential development of carbonyl and ether groups and a reduction in the concentration of alcohol groups. At 300°C, the opposite is observed, over the initial first 5 hours, the valence peak separation can be seen to increase indicating the formation of ether groups. However with longer periods of stabilisation this separation reduces, pointing to a predominance of alcohol groups and suggesting no carbonyl formation.

Py-GC-MS proved to be a useful technique for studying the nature of oxidative treatment of mesophase pitch and identifies a range of oxygenated fragments which can

be attributed to the reaction pathways during stabilisation. A correlation was observed between the evolution of oxygenated fragments and the degree of stabilisation potential in the pitch (as defined by softening point behaviour). This may represent an important, and possibly commercial, diagnostic application of the Py-GC-MS pitch characterisation technique. Py-GC-MS in reactive mode in oxygen enables stabilisation to be performed on an analytical scale, producing further evidence for the proposed stabilisation mechanism. The methods which have been developed in this work are capable of screening pitch samples, investigating stabilisation reaction pathways and optimising the conditions for oxidative treatment.

In all of the Raman spectra disorder within the mesophase is a noticeable feature as shown by the D peak around 1350 cm^{-1} . The C-C antisymmetric stretching vibration is also still a prominent feature of the spectra as shown by the G peak around 1600 cm^{-1} . At lower temperatures 160°C & 240°C the ordering of the mesophase pitch-based tapes decreases significantly with increasing time as a result of the disruptive effect of oxygen incorporation in the tapes (figures 84 & 85) (table 16). This however, is not observed in the 300°C tapes since only a very marginal decrease in ordering is observed at this temperature with increasing stabilisation time (figure 86) (table 16). This pattern is also evident when plotting % oxygen content against D/G peak ratio (figure 88). This could well be as a result of over stabilisation at higher temperatures leading to oxygen-induced defects being so rapidly incorporated into the tapes' structure that stabilisation time has less effect (Blanco, Lu et al. 2003). Similar arguments regarding the structurally disruptive effect of oxygen incorporation can be made when considering the effect that increasing stabilisation temperature has on reducing the $D_{(i)}/G_{(i)}$ ratio. The exception is that $D_{(i)}/G_{(i)}$ ratio slightly decreases when the 25 hour stabilisation temperature is increased from 240°C to 300°C and this may be due to the fact that the 300°C is high enough and 25 hours is long enough for some thermally induced structural ordering to start to compete with the oxygen-induced disordering.

Examining the change in weight and chemistry as a result of the varying stabilisation conditions has gone some way to explaining some of the effects of the stabilisation process on the mesophase pitch based tapes. Oxygen has been proven to be

the key element in ensuring the stabilisation of the tapes. To investigate this further an investigation into the transport of oxygen into the mesophase pitch based carbon tapes will be considered

It is apparent that the stabilisation process is extremely complicated and there are still many questions left unanswered, such as: how the final carbon yield and chemistry of the mesophase pitch based tapes is affected by stabilising conditions? Why different functionalities are observed at varying stabilisation conditions and how do they affect the resultant tapes? In order to explore this further, characterisations of stabilised mesophase pitch based tapes will be considered in the hope that it will shed more light on the complexities of the stabilisation reaction taking place in the mesophase pitch based tapes.

7 Oxygen transport study

7.1 The effect of stabilisation on molecular ordering of mesophase pitch-based tapes

Mesophase pitch-based tapes which had been stabilised to varying degrees were mounted end-on using the same method adopted for optical, ThAFM and EPMA characterisations in order that the cross-section of the tapes could be revealed. The samples were then scanned at tape edge and middle sites (figure 89) using the Raman microscope to investigate how the extent of stabilisation experienced by the samples affected their Raman spectral signature.

Position at which Raman microscope was focused on in order to obtain a Raman Spectra for the middle of the stabilised mesophase pitch-based tape transverse cross section

Position at which Raman microscope was focused on in order to obtain a Raman Spectra for the edge of the stabilised mesophase pitch-based tape transverse cross section

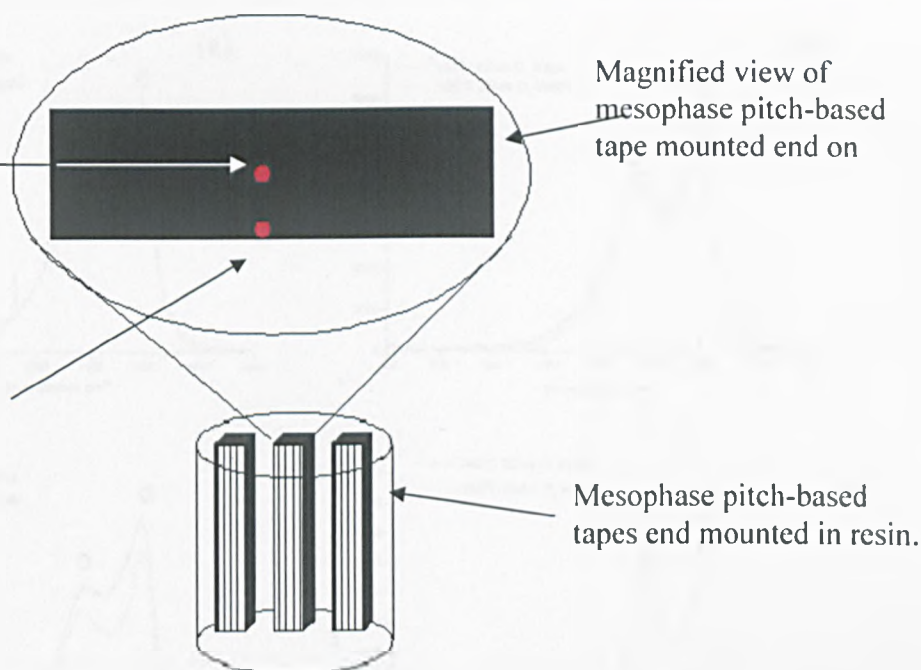


Figure 89 Illustration of positions Raman microscope was focused on in order to obtain a Raman spectra for both the edge and middle of the stabilised mesophase pitch-based carbon tapes

Figure 90 and table 17 illustrates that the Raman signatures at the edge and middle of the tapes is not only affected by time but also the temperature of stabilisation. After stabilisation at 160°C for 5 hours it is evident that the tapes see a slightly higher $D_{(i)}/G_{(i)}$ ratio in their middle compared with that at their edges, pointing to a greater degree of ordering at the edge of the tapes compared with their centre. Increasing time of stabilisation can be seen to lead to an increase in the difference between the middle to edge $D_{(i)}/G_{(i)}$ ratios for the 160°C stabilised tape.

For the samples stabilised at 240°C and 300°C the changes that can be observed between the $D_{(i)}/G_{(i)}$ ratio at the edge and middle of the samples are almost the same within experimental error and thus difficult to draw any firm conclusions from.

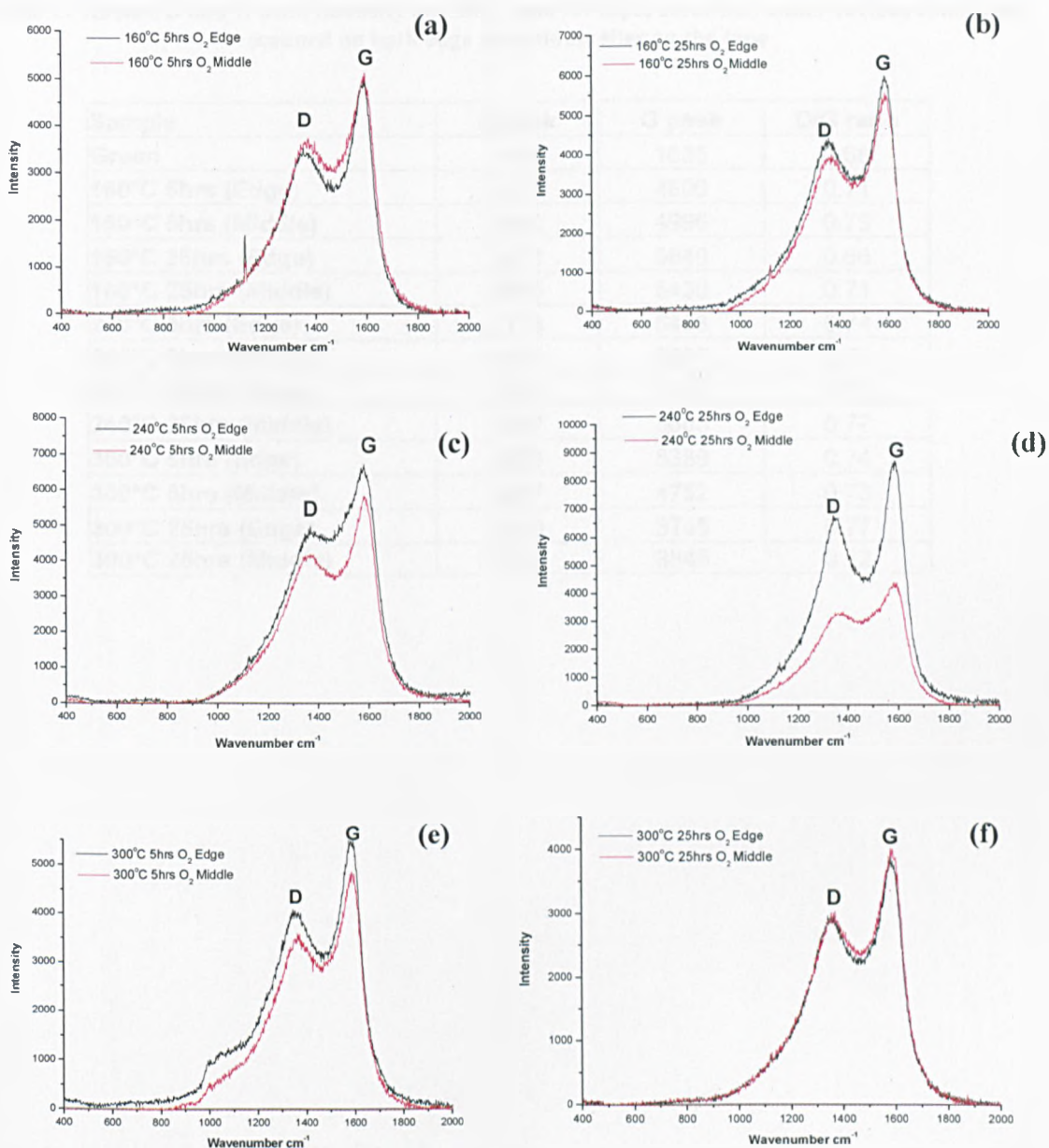


Figure 90 Raman Spectra of scans made through the cross-section of mesophase pitch-based tapes which have been stabilised to varying degrees in oxygen; (a) 160°C for 5hrs, (b) 160°C for 25hrs (c) 240°C for 5hrs, (d) 240°C for 25hrs, (e) 300°C for 5hrs, (f) 300°C for 25hrs

Table 17 Raman D and G peak intensity and D/G ratio for tapes stabilised under various conditions, scanned on both edge and middle sites on the tape

| Sample | D peak | G peak | D/G ratio |
|----------------------|--------|--------|-----------|
| Green | 1104 | 1635 | 0.68 |
| 160°C 5hrs (Edge) | 3414 | 4806 | 0.71 |
| 160°C 5hrs (Middle) | 3640 | 4996 | 0.73 |
| 160°C 25hrs (Edge) | 3871 | 5848 | 0.66 |
| 160°C 25hrs (Middle) | 3849 | 5430 | 0.71 |
| 240°C 5hrs (Edge) | 4778 | 6483 | 0.74 |
| 240°C 5hrs (Middle) | 4151 | 5807 | 0.71 |
| 240°C 25hrs (Edge) | 3304 | 4243 | 0.78 |
| 240°C 25hrs (Middle) | 6597 | 8603 | 0.77 |
| 300°C 5hrs (Edge) | 3993 | 5389 | 0.74 |
| 300°C 5hrs (Middle) | 3457 | 4752 | 0.73 |
| 300°C 25hrs (Edge) | 2870 | 3745 | 0.77 |
| 300°C 25hrs (Middle) | 2750 | 3845 | 0.72 |

7.2 Characterisation of stabilised mesophase pitch-based tapes using Micro-thermal Analysis Atomic Force Microscope

Figure 91 shows a local micro thermal plot of sensor vertical displacement against temperature for a green tape. The tape can be seen to soften at approximately 322°C, this is very close the 325°C softening point reported by Blanco for unstabilised ARA24 (Blanco, Lu et al. 2003) a ARMP prototype.

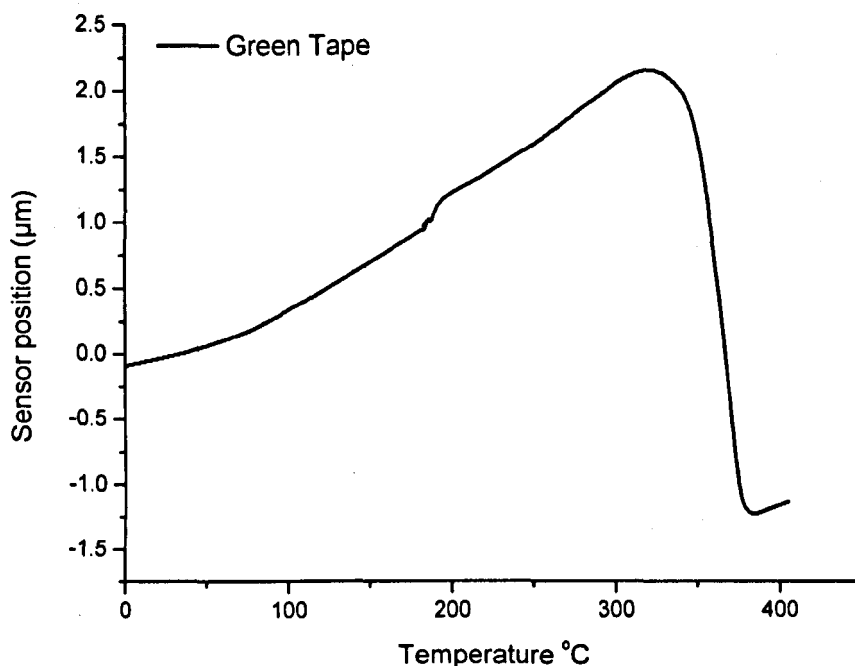


Figure 91 Micro-thermal analysis of a green tape

Figure 92 shows a thermal image of a tape which has been stabilised for 5hrs at 160°C, the lighter contrast in the image indicates areas of greater heat dissipation from the probe tip. The tape has a darker contrast than the resin due to it having a lower thermal conductivity only having undergone the stabilisation process; if it had then been subsequently carbonised the opposite would be true. It should be noted that the qualitative nature of the information obtained from the thermal images is significantly

limited but is still a useful tool for studying the thermal properties of the mesophase carbon tapes.

Local thermal analysis was performed on tapes which had been stabilised for 5hrs at 160°C, 240°C and 300°C (figures 93, 95 & 97) and was repeated for samples which had been stabilised for 25hrs at 160°C, 240°C and 300°C (figures 99, 101 & 103). The samples were analysed at varying positions throughout the tapes cross-section (polished longitudinal section), marked with a red circle and numbered on the thermal images. The tapes which were examined during this experiment had a cross-sectional width which ranged between 25-30 μm in the 3 direction.

Figure 93 shows the local thermal softening plots which correspond to the locations 1-5 marked on the thermal image in figure 92. No softening has occurred at position 1 implying that stabilisation has successfully taken place. As the local softening point positions move deeper into the tape 2-5 the softening temperature of the pitch decreases to 337.6, 330.8, 322.6 and 317.3°C respectively. When the tape has been treated to the higher temperature of 240°C for the 5hr period the first two positions from the tape surface show no softening, pointing to a deeper stabilisation penetration. As with the 160°C sample, the further from the edge of the tape the test position is taken (Positions 3-5) the greater the decrease in softening point from 372.8°C to 344.1°C to 338.8°C. In the 240°C sample the softening points have all increased in temperature above that of the green pitch, as a result of a deeper oxygen penetration taking place at the higher temperature and the beginning of cross-linking. The highest heat treatment temperature of 300°C over the 5hrs shows a similar pattern to that of the 160°C tape. The tape exhibits stabilisation at the edge of the sample whilst showing softening behaviour from positions 2-5 at 320.5, 317.3, 315.2 and 320.5°C respectively. At these locations the softening point of the pitch is the same as that of the green pitch indicating that no cross-linking has taken place. This corroborates the theory of a skin-core structure forming at higher temperatures of stabilisation. It can be seen that even at the lower temperature of 160°C an increase in pitch softening temperatures can be observed at those locations which have not fully stabilised suggesting some oxygen content and the early development of partial cross-linking.

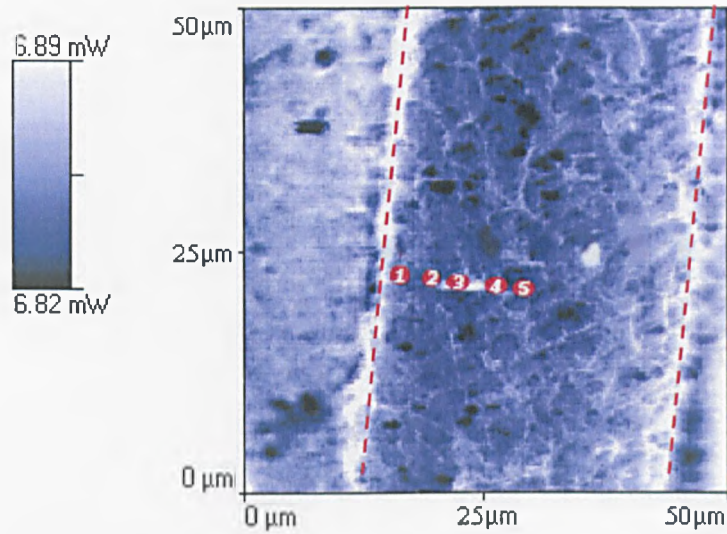


Figure 92 Thermal image of a tape stabilised at 160°C for 5hrs showing micro-thermal analysis sample position (edge of the tape indicated by the red dashed line)

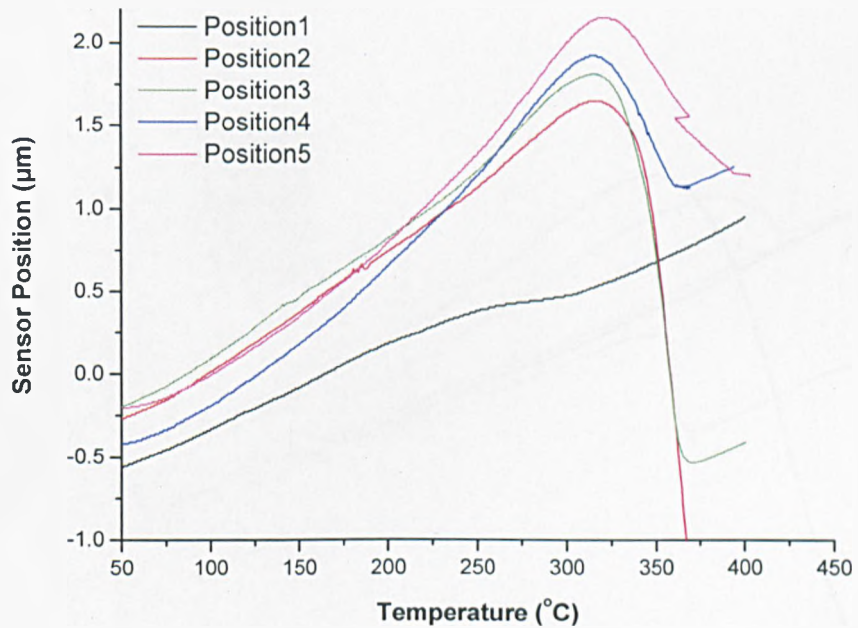


Figure 93 Micro-thermal analysis of tape stabilised at 160°C for 5hrs at varying positions throughout its cross-section

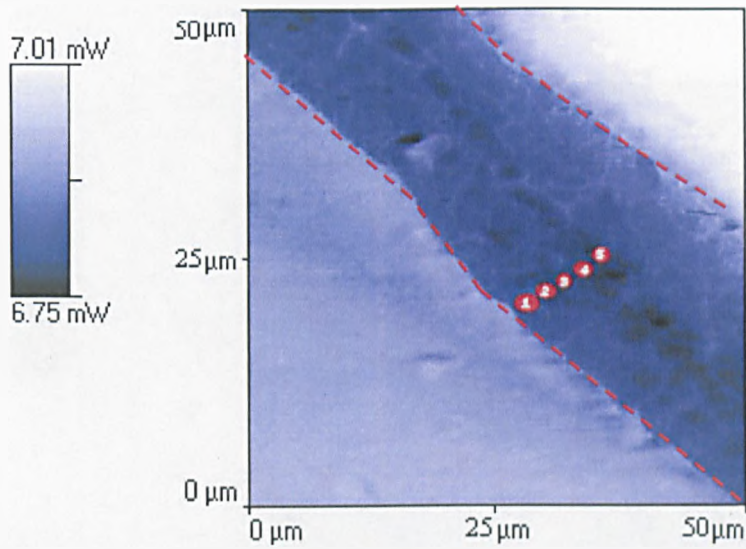


Figure 94 Thermal image of a tape stabilised at 240°C for 5hrs showing micro-thermal analysis sample position (edge of the tape indicated by the red dashed line)

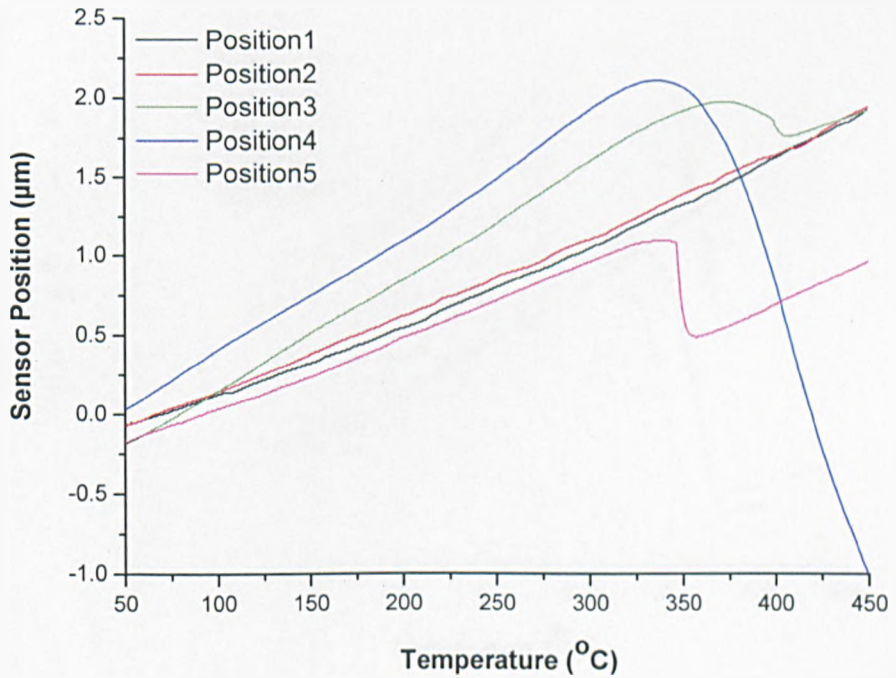


Figure 95 Micro-thermal analysis of tape stabilised at 240°C for 5hrs at varying positions throughout its cross-section

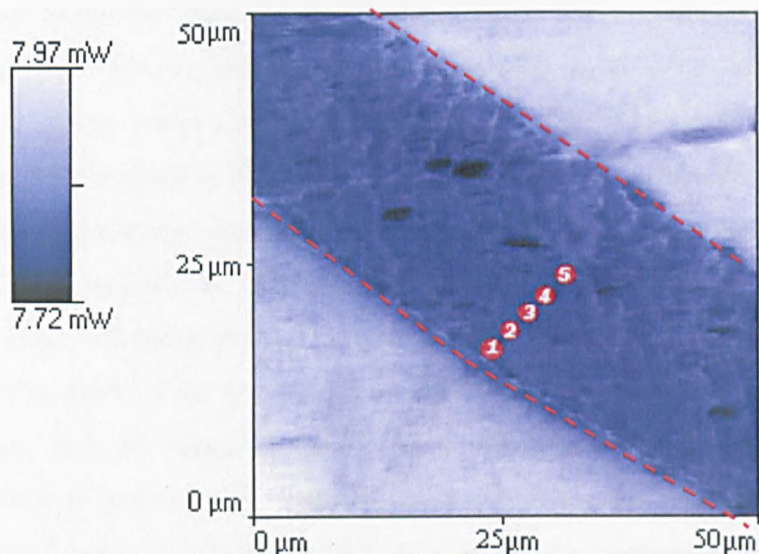


Figure 96 Thermal image of a tape stabilised at 300°C for 5hrs showing micro-thermal analysis sample position (edge of the tape indicated by the red dashed line)

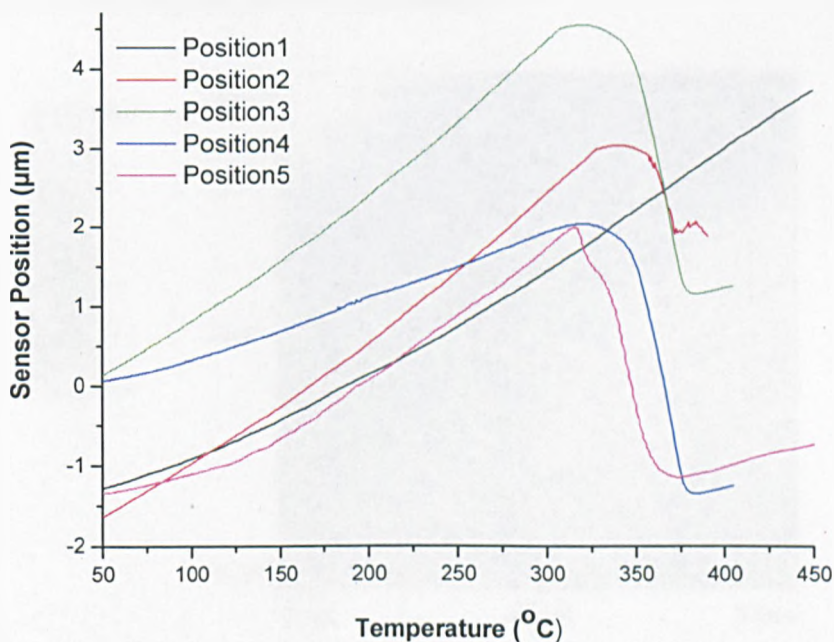


Figure 97 Micro-thermal analysis of tape stabilised at 300°C for 5hrs at varying positions throughout its cross-section

Similar trends can be observed in the tapes which have undergone the longer 25hrs period of thermal heat treatment. After 25hrs the stabilisation can be seen to have penetrated deeper as a result of the extended stabilisation time. The 160°C 25hr sample can now be seen to have a region which can be considered to be stabilised up to 5 μm where the softening point of the pitch is 395.1°C, in keeping with the trends observed in the 5hr samples as the test positions move further from the edge of the tape the softening points decrease to 334.5°C at position 4 and 318.59°C at position 5 (figures 98 & 99). The 240°C sample only shows softening at position 5 of 433.5°C (7 μm from the tape edge) (figures 100 & 101). The 300°C 25hr tape continues the same trend observed in the 300°C 5hrs stabilised tapes, here the sample is stabilised at positions 1 and 2. The tape begins to soften (331.3°C) at position 3 a distance of 4 μm from the tapes surface the other positions 4 and 5 soften at 322.7 and 321.7°C respectively, temperatures which are very similar to that of the green pitch (figure 102 & 103). This behaviour is again a clue to the formation of an impenetrable barrier at higher temperatures of stabilisation which restricts the diffusion of oxygen into the sample (EPMA figures 106 & 107 Section 7.3 page 153) and thus the promotion of cross-linking.

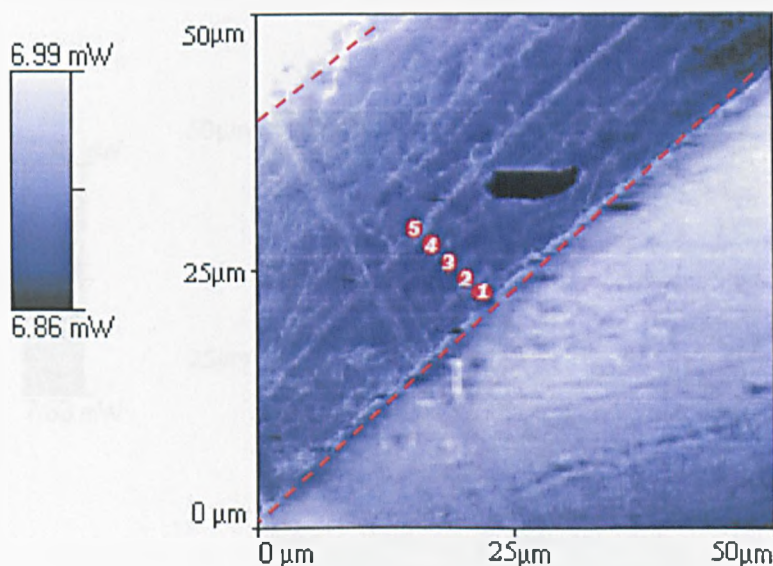


Figure 98 Thermal image of a tape stabilised at 160°C for 25hrs showing micro-thermal analysis sample position (edge of the tape indicated by the red dashed line)

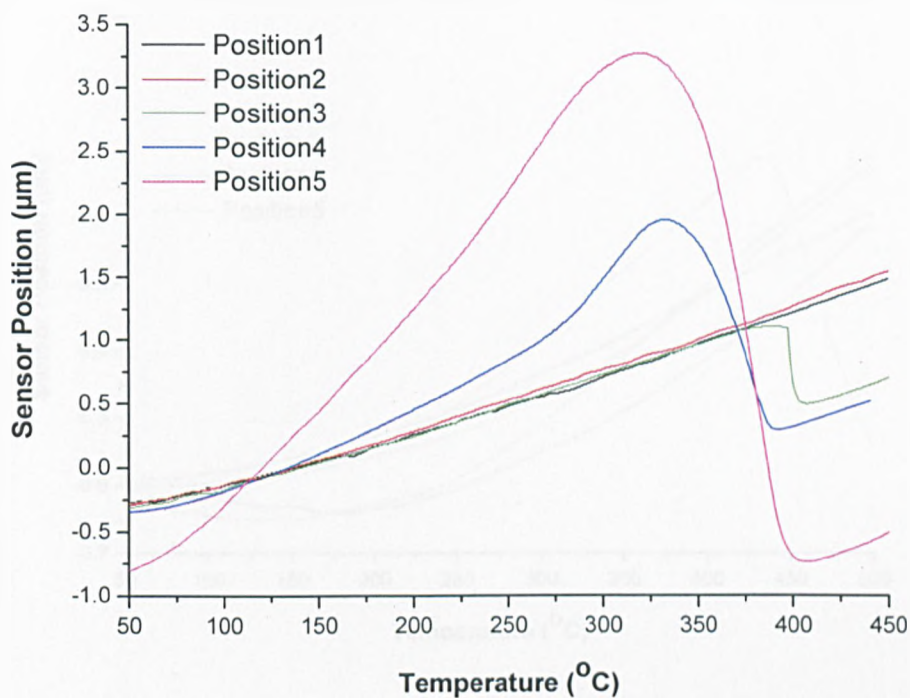


Figure 99 Micro-thermal analysis of tape stabilised at 160°C for 25hrs at varying positions throughout its cross-section

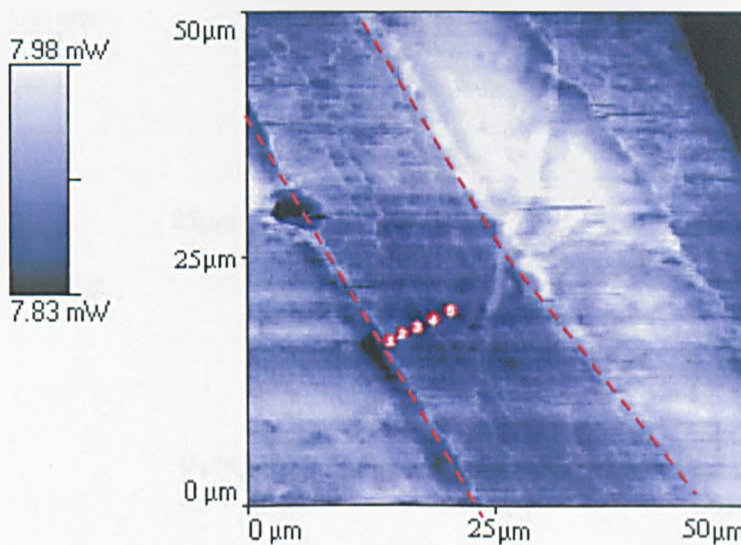


Figure 100 Thermal image of a tape stabilised at 240°C for 25hrs showing micro-thermal analysis sample position (edge of the tape indicated by the red dashed line)

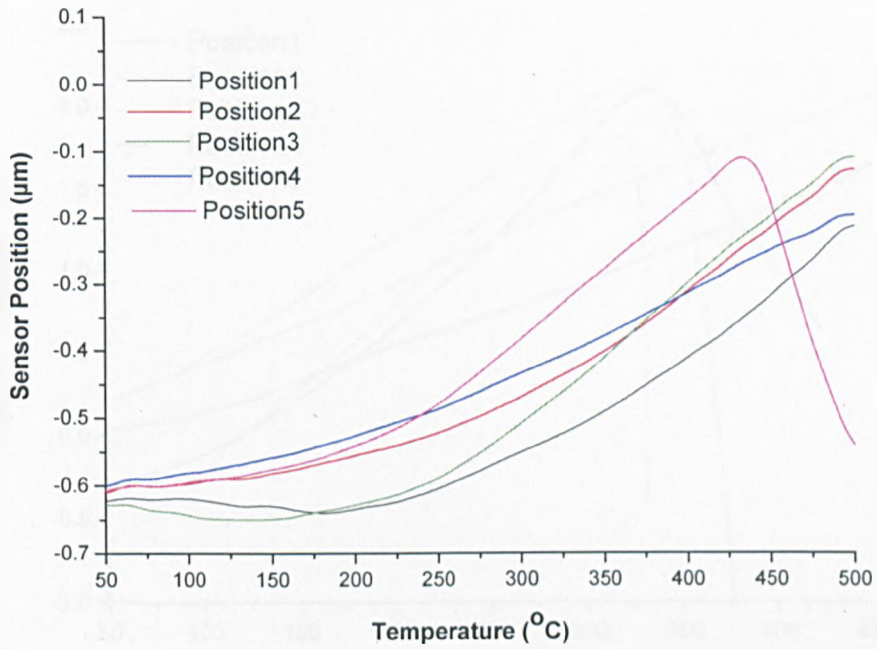


Figure 101 Micro-thermal analysis of tape stabilised at 240°C for 25hrs at varying positions throughout its cross-section

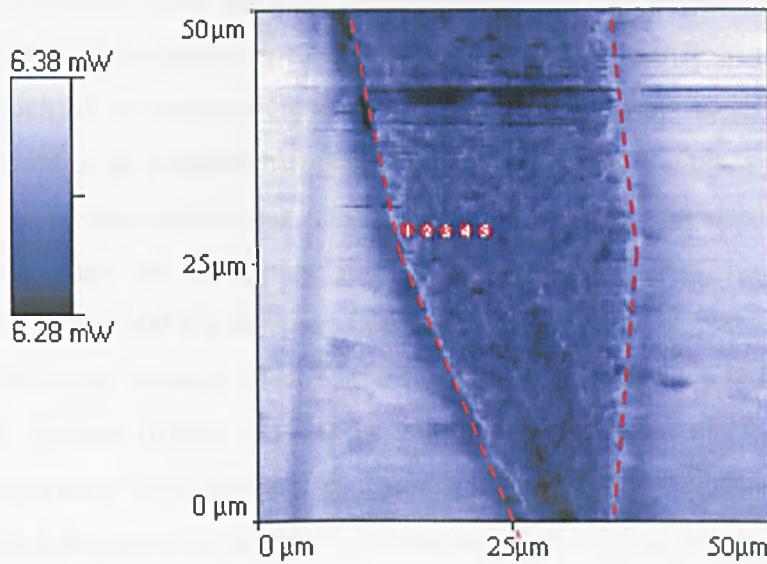


Figure 102 Thermal image of a tape stabilised at 300°C for 25hrs showing micro-thermal analysis sample position (edge of the tape indicated by the red dashed line)

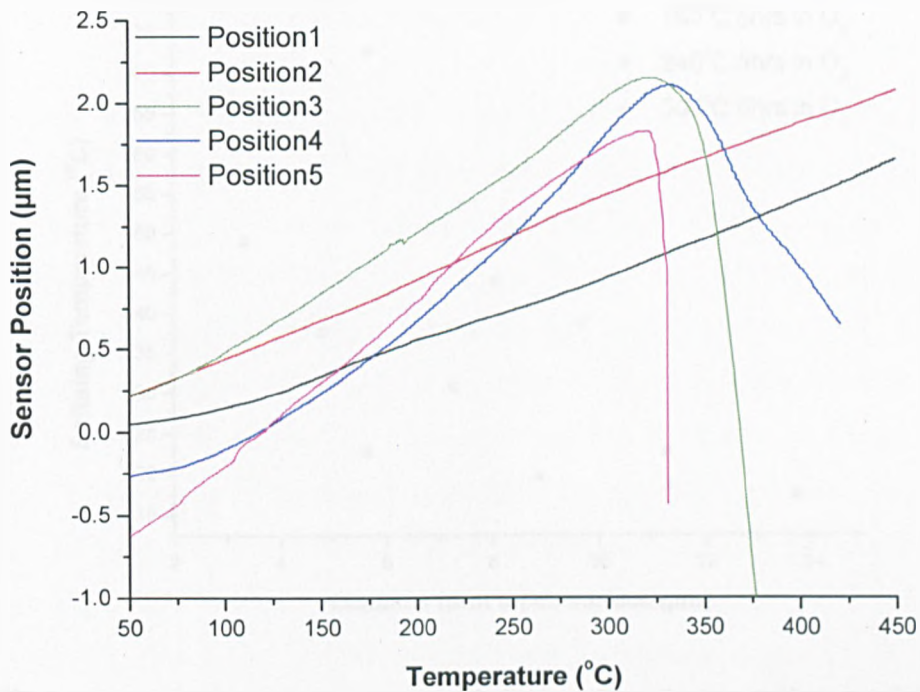


Figure 103 Micro-thermal analysis of tape stabilised at 300°C for 25hrs at varying positions throughout its cross-section

Using the data obtained from the local thermal analysis it was possible to build a set of graphs which show how softening temperature varies with distance from the surface of the tape for each of the temperatures at the 5 and 25hr exposure times (figures 104 & 105). It is evident at all temperatures that as the distance from the tapes surface increase the softening point temperatures can be seen to decrease. At shorter stabilisation time the softening temperature can be seen to reach a maximum at 240°C, however when the sample is stabilised at 300°C a decrease in the softening temperature is evident, this most probably is due to the adverse affect of the formation of a skin-core structure inhibiting the cross-link process (figure 104). Over 25hrs of stabilisation the same decrease in softening temperature with increase in distance from the tapes surface the maximum softening point is attributed to the 240°C is observed again (figure 104 & 105).

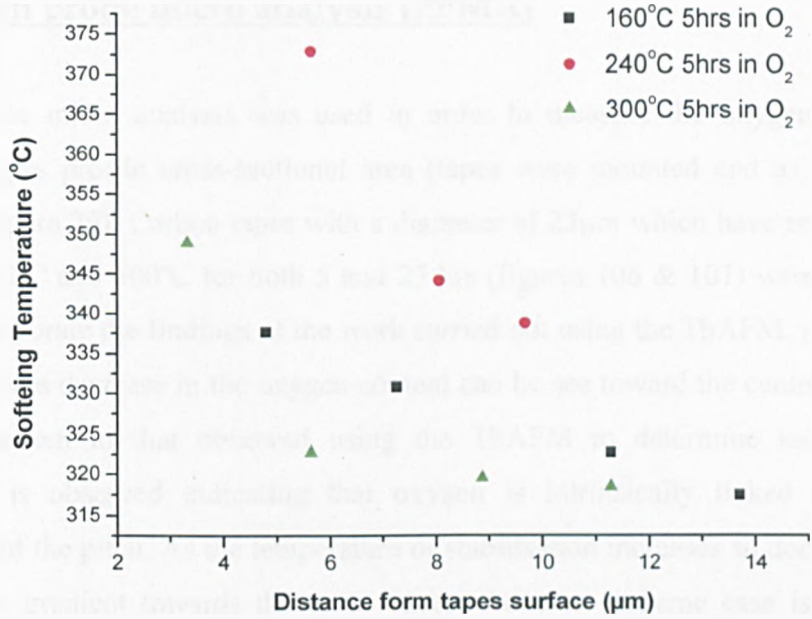


Figure 104 Variation of softening temperature with distance from the tape surface as a function of stabilisation temperature after 5hrs

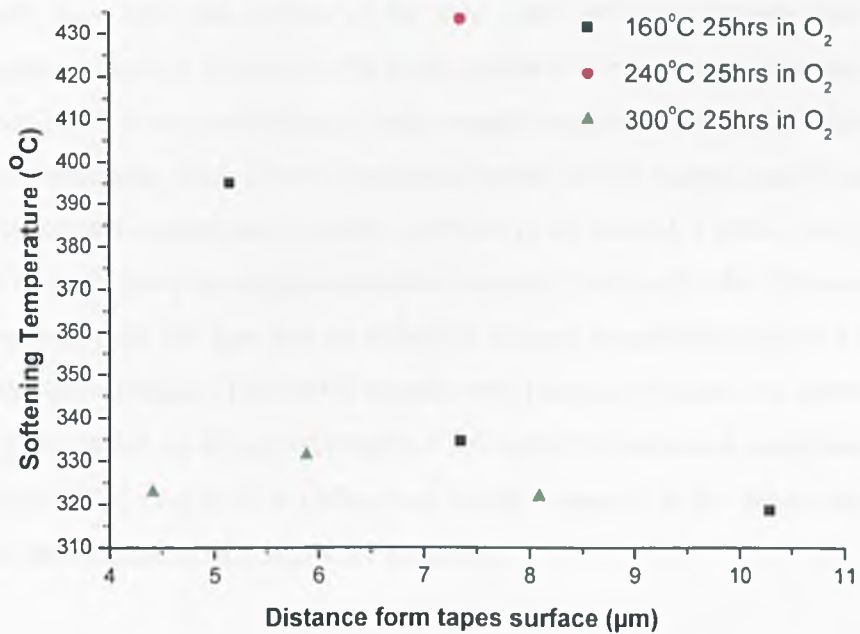


Figure 105 Variation of softening temperature with distance from the tape surface as a function of stabilisation temperature after 25hrs

7.3 Electron probe micro analysis (EPMA)

Electron probe micro analysis was used in order to measure the oxygen distribution across the tapes profile cross-sectional area (tapes were mounted end as described in section 4.7 figure 29). Carbon tapes with a diameter of $23\mu\text{m}$ which have been stabilised at 160°C , 240°C and 300°C for both 5 and 25 hrs (figures 106 & 107) were analysed in order to corroborate the findings of the work carried out using the ThAFM. At both times of stabilisation a decrease in the oxygen content can be seen toward the centre of the tape. A similar pattern to that observed using the ThAFM to determine local softening temperature is observed indicating that oxygen is intrinsically linked to softening temperature of the pitch. As the temperature of stabilisation increases so does the oxygen concentration gradient towards the tapes edges, the most extreme case is observed at 300°C . Figure 106 shows that in both the 160°C and 300°C samples towards the center of the tapes the oxygen content is close to 0 wt%. The 160°C 5hrs sample shows oxygen penetration up to approximately $5\mu\text{m}$ and the 300°C 5hr sample showing it up to approximately $4\mu\text{m}$ from the surface of the tape. The 240°C 5hr sample can be seen to have an oxygen content of around 2 wt% at the centre of the tape, this presence of oxygen confirms that 240°C is not a sufficiently high enough temperature to initiate the formation of a skin-core structure. After 25hrs of stabilisation the 160°C sample can be seen to have an increased oxygen content at the center of the tape of around 2 wt%. The 240°C tape can be seen to again have an oxygen content of around 2 wt% after the 25hrs stabilisation period. However, now the tape has an effective oxygen penetration above 5 wt% up to $9\mu\text{m}$ from the tapes surface. The 300°C sample only marginally shows an improvement in the oxygen penetration up to approximately $6\mu\text{m}$ with the increased stabilisation time of 25 hrs (Figure 107); this with the abundant oxygen present at the tapes edge is again indicative of the formation of a skin core structure

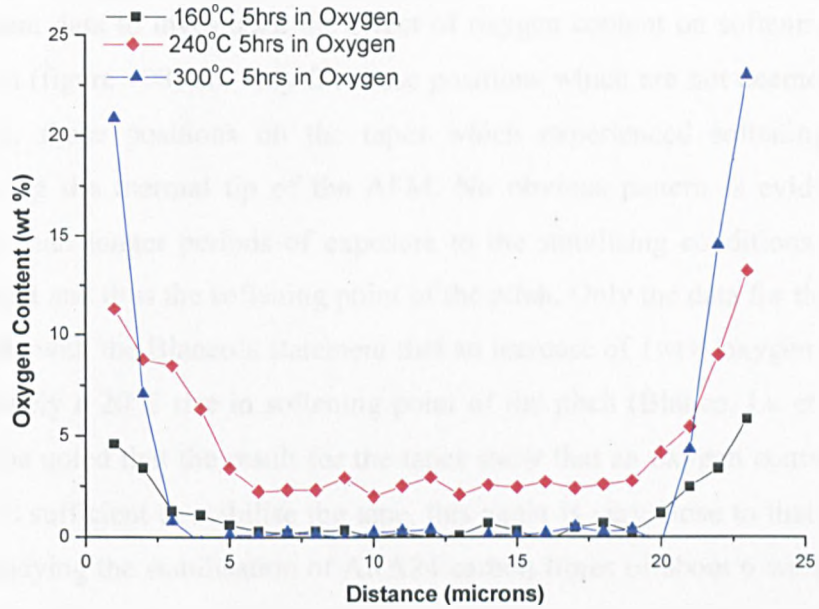


Figure 106 Semi-quantitative analysis of tape oxygen content carried out using an EPMA for 160, 240 and 300°C over 5hrs

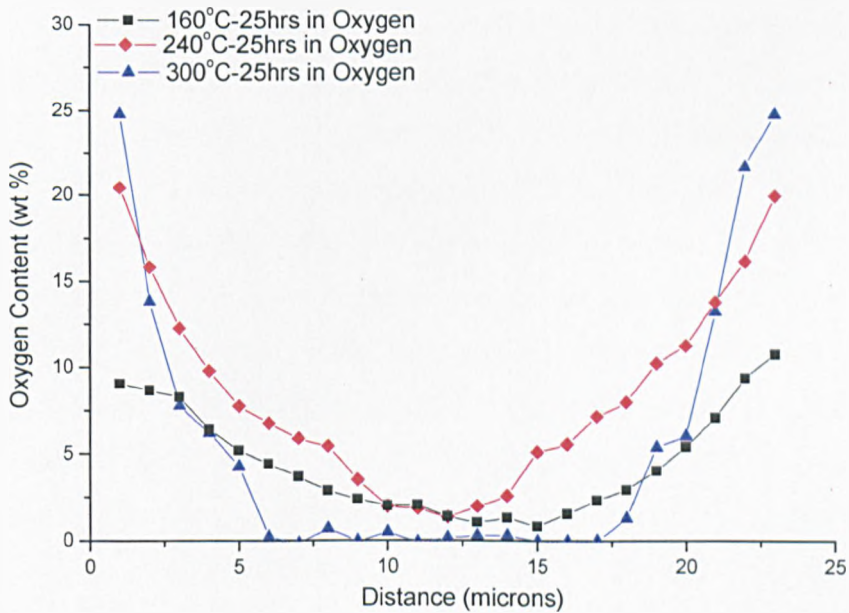


Figure 107 Semi-quantitative analysis of tape oxygen content carried out using an EPMA for 160, 240 and 300°C over 25hrs

The softening point data obtained from using the ThAFM was combined with the EPMA oxygen content data to investigate the effect of oxygen content on softening point. The results shown (figure 108) are only for those positions which are not deemed to be fully stabilised i.e. those positions on the tapes which experienced softening upon heat treatment using the thermal tip of the AFM. No obvious pattern is evident from the results other than longer periods of exposure to the stabilising conditions increase the oxygen content and thus the softening point of the pitch. Only the data for the 160°C tape does conclude with the Blanco's statement that an increase of 1wt% oxygen would result in approximately a 20°C rise in softening point of the pitch (Blanco, Lu et al. 2003). It should also be noted that the result for the tapes show that an oxygen content of greater than 5 wt% is sufficient to stabilise the tape, this again is very close to that observed by Blanco in studying the stabilisation of ARA24 carbon fibres of about 6 wt%. Figure 108 also shows that there is a relationship between stabilisation temperature, oxygen content and softening point, as those tapes which are stabilised at the higher temperatures 240°C and 300°C can be seen to have a significantly higher softening point at a much lower oxygen content, this trend however must be discounted when considering the 300°C 25hr sample.

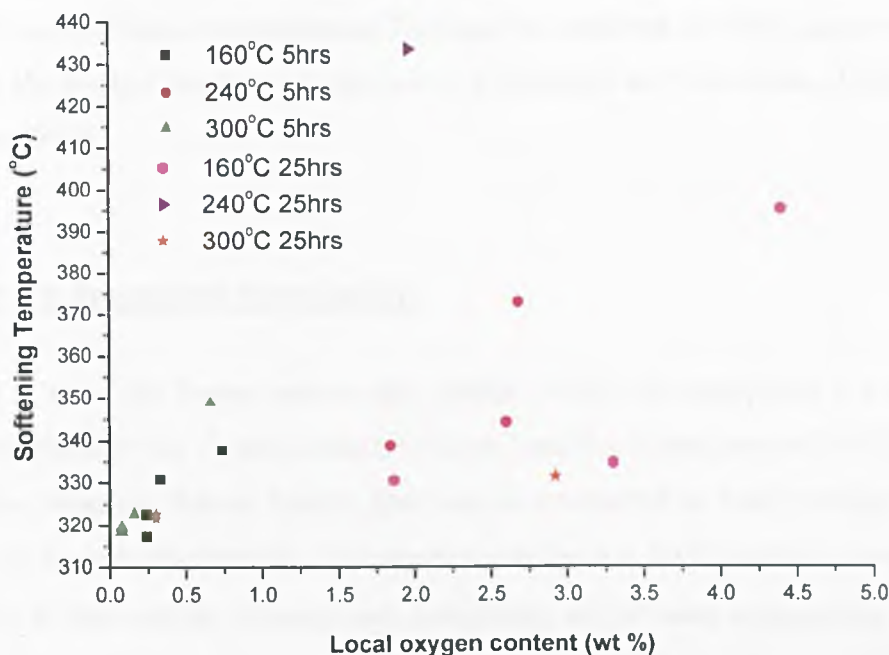


Figure 108 Variation of the softening temperature with oxygen content

It is not clear why this occurs but it is possible that this is an effect of how higher temperatures alter the mechanism of stabilisation. At higher temperatures there is a clear gain in the oxygen content is greatly increased especially at the surface of the tape. However, it is likely that this over-oxidation will be ultimately detrimental to the final properties of the tape leading to a reduced final carbon yield and the possible development of defects in the tapes upon carbonisation (Blanco, Lu et al. 2003). The competition reaction between the weight gain and weight loss reaction which takes place during the stabilisation process is well documented both in this study and the literature (Drbohlav and Stevenson 1995) showing that the stabilising weight gain is accompanied by the production of H_2O , CO and CO_2 (Drbohlav and Stevenson 1995). However, in this study of mesophase tapes no CO production was detected only CO_2 upon stabilisation and only small quantities of H_2O were detected at higher temperatures of stabilisation. This project also shows differing results to that of the work of Drbohlav and Stevenson who reported a weight loss after only 240 min at 240°C and a maximum weight gain of 10% (Drbohlav and Stevenson 1995). Tape samples in this study stabilised to 240°C in

oxygen exhibited a far higher weight gain in the region of 15% and did not record any weight loss up to 25hrs of stabilisation. The samples stabilised at 300°C appear to behave more like the pitches described in the work of Drbohlav and Stevenson (Drbohlav and Stevenson 1995).

7.4 Oxygen transport conclusion

It is clear in all of the Raman spectra that disorder within the mesophase is a noticeable feature illustrated by the D peak around 1350 cm^{-1} and the G peak around 1600 cm^{-1} . It is also evident from the Raman Spectra that there is a variation in their ordering from the edges of the tapes to their middle. The samples stabilised at 160°C exhibit a lower degree of ordering at their middle, although only marginally. At the lower temperature of 160°C, oxygen diffuses slowly into the tape's core and the stabilisation temperature is low enough so that only a minimum number of reactions take place at the surface (edge). This in turn allows better oxygen access to the centre of the tapes for a longer period of time and as a result the textural ordering is reduced at the centre of the tapes due to oxygen disrupting the structure. When stabilised at higher temperatures of 240°C and 300°C, the results for the edge and middle of the tapes were almost the same within experimental error and thus difficult to draw any firm conclusions from.

It is evident from the results that EPMA and ThAFM are both complimentary characterisation techniques which can be used in the study of stabilisation of mesophase carbon tapes. A clear correlation between softening point and oxygen content is evident with increased oxygen content leading to higher softening points. Exposure time and temperature of stabilisation can also be seen to have a significant effect on the depth and extent of oxygen penetration into the tapes. The results seem to indicate that for longer periods of stabilisation oxygen penetrates deeper into the tapes at lower temperatures (160°C & 240°C) with the 240°C tapes experiencing the greater oxygen uptake throughout its cross-section. With increasing time at the higher temperature of stabilisation (300°C) oxygen uptake is only detected towards the edges of the tape. This

exaggerated oxygen uptake on the surface of the tape could well be as a result of the formation of a diffusion barrier having been created at the rapid initial higher oxidation temperature (Lin 1991).

It should be pointed out that the EPMA results obtained for the tapes in this study differ from the observations made by Blanco for carbon fibres, Blanco stated that oxygen content towards the centre of the fiber decreases with increasing temperature of stabilisation (Blanco, Lu et al. 2003). However, the tape study does agree with the fiber study regarding the observation of high oxygen contents on the outer region of the fiber. One reason for this discrepancy in results maybe down to the difference in textural orientation between the radial textured fibres and the 1-2 textured tapes affecting the oxygen diffusion routs into the centre of the tape/fiber. Another could be as a result of the differing scales of the tape diameter $\sim 25\mu\text{m}$ and the fiber diameter $\sim 100\mu\text{m}$. To confirm this theory a future study could be undertaken to compare and contrast oxygen uptake and local thermal softening points for samples of mesophase tapes of different texture (1-2 and 1-3) and mesophase fibres of different textures such as radian, onion skin and random which have all been stabilised under identical conditions. This experiment should help in understanding further the effect mesophase texture has on the stabilisation process.

8 Carbonisation of stabilised tapes

8.1 Weight change upon carbonisation

Tapes which experience the higher temperature of stabilisation over 25hrs can be seen to experience the greatest weight loss upon carbonisation (figure 109). The results suggest that tapes which have experienced a higher stabilisation temperature are ultimately going to exhibit a lower final carbon yield (carbon yield being the percentage weight of carbonaceous residue after heat treatment to a given temperature in an inert atmosphere) than those tapes which have been stabilised at lower temperatures. It is of note that the tape stabilised at 160°C for 25 hours displays a weight loss less than that experienced by the green tape upon carbonisation. This will be considered below.

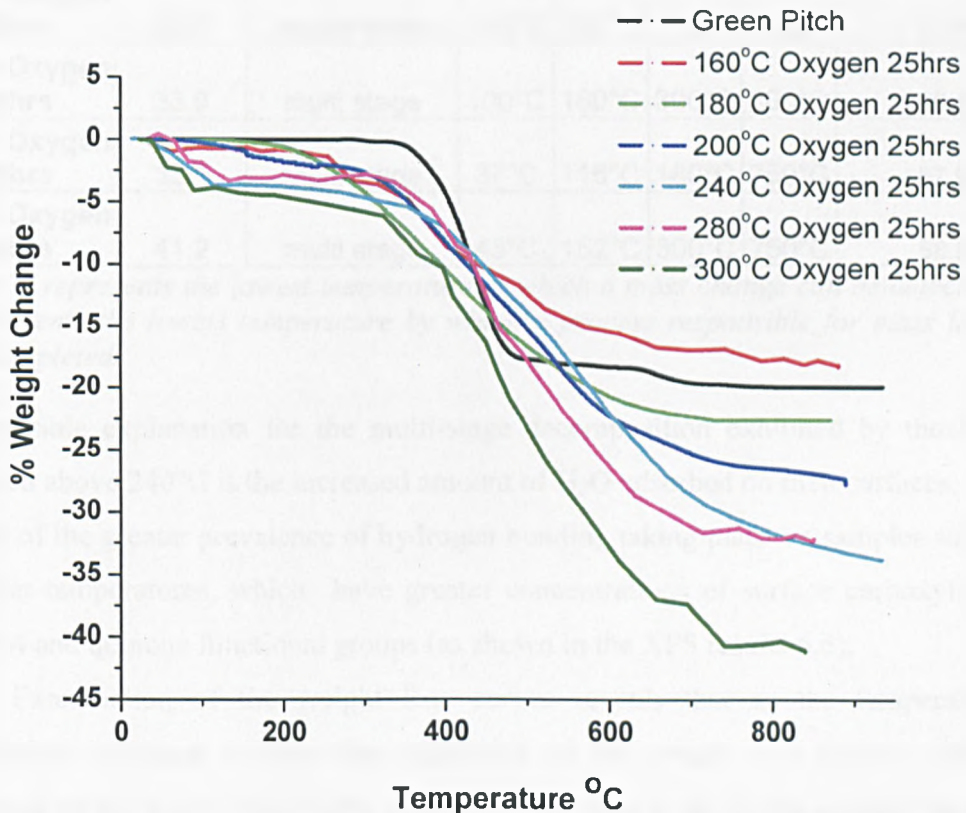


Figure 109 Change in weight of sample tapes which have undergone varying temperatures of stabilisation over a 25hr period upon subsequent carbonisation

Figure 109 shows that there are two clear different types of TG curves taking place during the carbonisation of the stabilised samples. They can be classified into samples those which have undergone a stabilisation temperature below 200°C which can be characterised by single stage decomposition and those samples which have been stabilised above 200°C which show multi stage decompositions (table 18)

Table 18 Carbonisation TG curve information for tapes stabilised at varying temperatures for 25hrs

| Stabilisation Condition | % Weight Change | Decomposition Type | Ti | Tf | Ti(2) | Tf(2) | Carbon Yield from stabilised weight = 100% |
|-------------------------|-----------------|--------------------|-------|-------|-------|-------|--|
| Green Pitch | 21.1 | single stage | 350°C | 500°C | Na | Na | 78.3 |
| 160°C Oxygen 25hs | 18.2 | single stage | 200°C | 791°C | Na | Na | 81.9 |
| 180°C Oxygen 25hrs | 22.6 | single stage | 180°C | 620°C | Na | Na | 77.3 |
| 200°C Oxygen 25hrs | 28.5 | single stage | 180°C | 750°C | Na | Na | 71.6 |
| 240°C Oxygen 25hrs | 33.9 | multi stage | 100°C | 160°C | 300°C | 800°C | 66.1 |
| 280°C Oxygen 25hrs | 32.1 | multi stage | 37°C | 116°C | 180°C | 750°C | 67.9 |
| 300°C Oxygen 25hrs | 41.2 | multi stage | 45°C | 152°C | 300°C | 750°C | 58.8 |

Where Ti represents the lowest temperature at which a mass change can be detected and Tf represents the lowest temperature by which a process responsible for mass loss has been completed.

One possible explanation for the multi-stage decomposition exhibited by those tapes stabilised above 240°C is the increased amount of H₂O adsorbed on their surfaces. This is a result of the greater prevalence of hydrogen bonding taking place on samples stabilised at higher temperatures, which have greater concentrations of surface carboxylic acid, carbonyl and quinone functional groups (as shown in the XPS results 6.5).

Examination of the weight loss curves reveals that as the temperature of stabilisation increases so does the magnitude of the weight loss (figure 109). The magnitude of the weight loss is also affected by the time at which the samples have been exposed to the stabilisation conditions (figure 110). The onset temperature of the weight loss reaction decreases with stabilisation temperature.

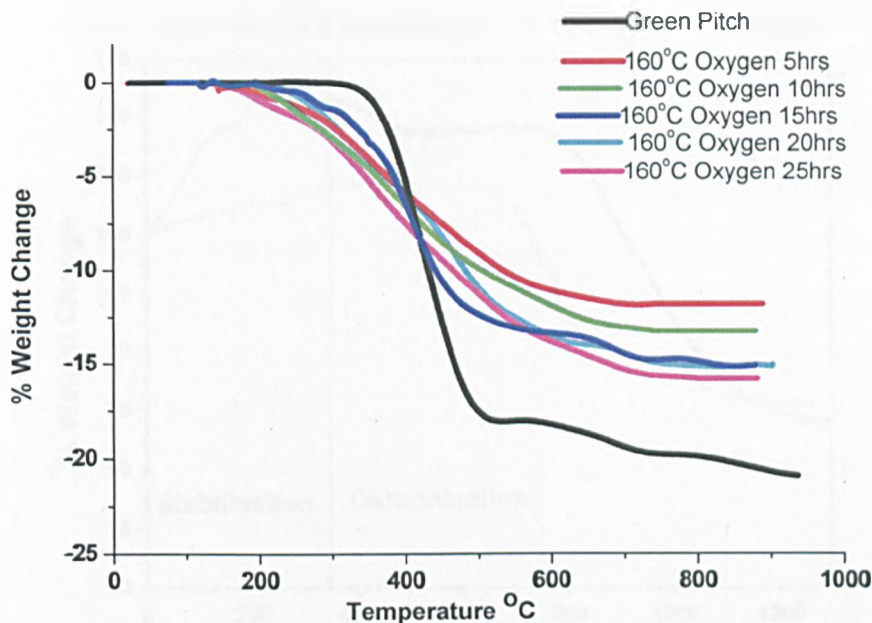


Figure 110 Graph showing how stabilisation time at 160°C can affect the weight loss

When examining the change in weight which takes place over both the stabilisation and carbonisation of the mesophase pitch-based tapes the true final carbon yield of the tapes can be more clearly observed i.e. the final weight of carbon as a percentage of the initial weight of unstabilised tape. Figures 111 & 112 exhibit a similar pattern. Those tapes which have been stabilised at the higher temperature, 240°C, display a greater weight gain during the stabilisation step as a result of increased oxygen uptake. Both the 240°C samples display a multistage decomposition which is markedly greater than that of the 160°C tapes during the carbonisation step. In figures 111 & 112 the 160°C samples can be seen to have the higher final carbon yield even though they experience the lowest weight gain during the stabilisation step. In the case of the 5hr samples both the 160°C and 240°C tapes show an increase in the final carbon yield of the tape from that of the green tape (78.3%); this is also true for the 160°C 25hrs tape. Moreover it is important to recognise that the 160°C 25hr tape shows an improved final carbon yield of ~ 87.5%, increased compared to that of the 5 hrs sample (~85%), once again indicating the effective use of incorporated oxygen in initiating cross-linking.

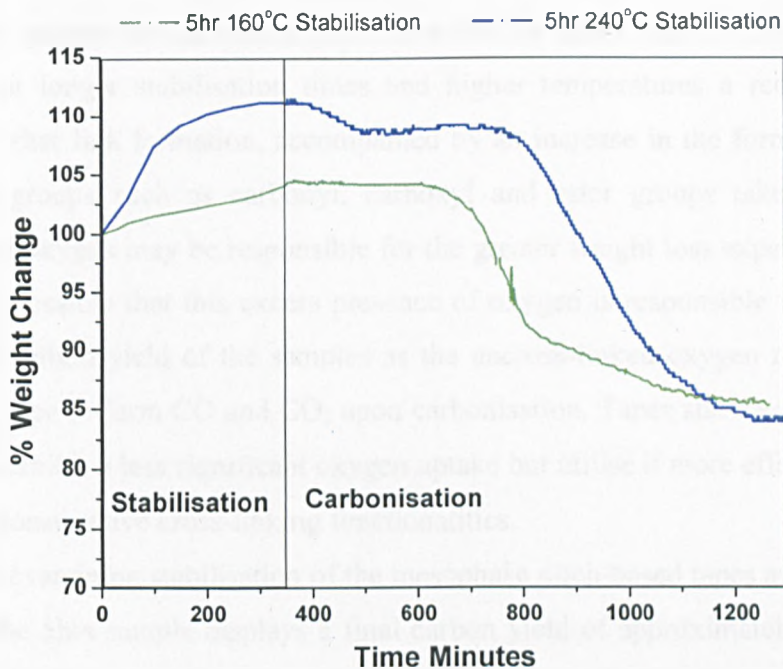


Figure 111 Weight gain/loss and final carbon yield for samples stabilised in O₂ for 5hrs at 160 and 240°C

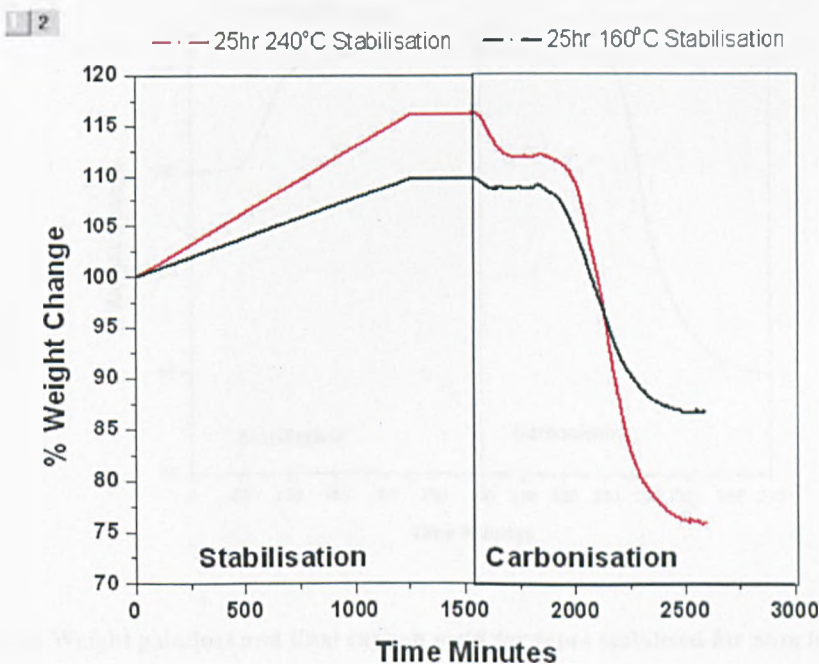


Figure 112 Weight gain/loss and final carbon yield for samples stabilised in O₂ for 25hrs in O₂ at 160 and 240°C

The opposite is observed in the 240°C tapes; the longer, 25hr stabilisation (~74%) shows a significantly greater loss in carbon yield than the 5hr 240°C tape (~83%). This could suggest that at longer stabilisation times and higher temperatures a reduction in the regularity of ether link formation, accompanied by an increase in the formation of non-cross-linking groups such as carbonyl, carboxyl and ester groups takes place. This uncross-linked oxygen may be responsible for the greater weight loss experienced by the samples. It is possible that this excess presence of oxygen is responsible for the greatly reduced final carbon yield of the samples as the uncross-linked oxygen reacts with the carbon in the tape to form CO and CO₂ upon carbonisation. Tapes stabilised at the lower temperatures exhibit a less significant oxygen uptake but utilise it more effectively by the formation of constructive cross-linking functionalities.

When examining stabilisation of the mesophase pitch-based tapes at 300°C it is of interest that the 5hrs sample displays a final carbon yield of approximately 90% (figure 113). The 300°C 25hrs sample shows a final carbon yield of approximately 66% (figure 114).

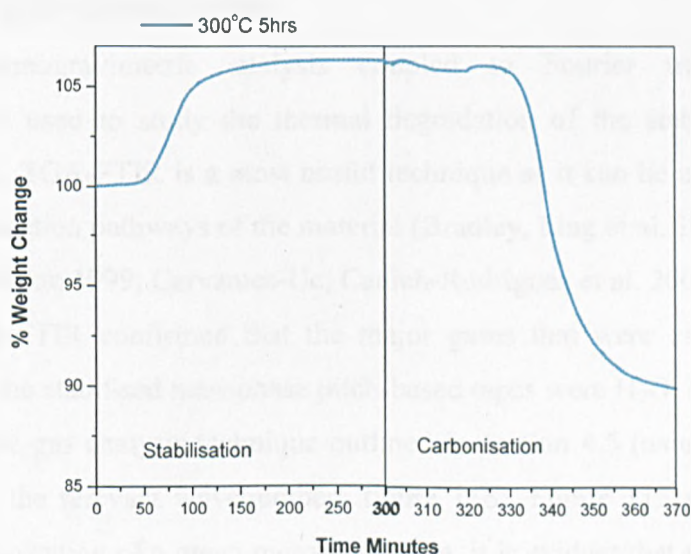


Figure 113 Weight gain/loss and final carbon yield for tapes stabilised for 5hrs in O₂ at 300°C

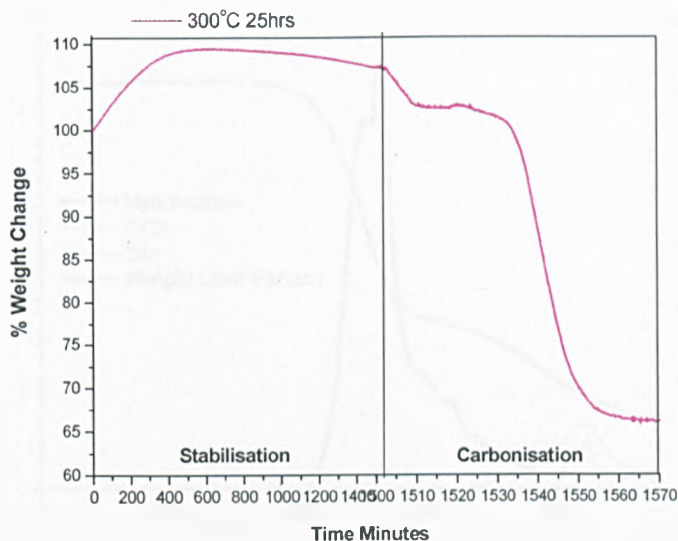


Figure 114 Weight gain/loss and final carbon yield for tapes stabilised for 25hrs in O₂ at 300°C

8.2 Evolution of gases during carbonisation of stabilised mesophase pitch-based tapes.

TGA-FTIR, thermogravimetric analysis coupled to Fourier transform infrared spectroscopy was used to study the thermal degradation of the stabilised mesophase pitch-based tapes. TGA-FTIR is a most useful technique as it can be used to understand the thermal degradation pathways of the material (Bradley, Ling et al. 1993; de la Puente, Pis et al. 1997; Wilkie 1999; Cervantes-Uc, Cauch-Rodriguez et al. 2006).

The TGA-FTIR confirmed that the major gases that were evolved during the carbonisation of the stabilised mesophase pitch-based tapes were H₂O, hydrocarbons, CO and CO₂ using the gas analysis technique outlined in section 4.5 (using the software IR library to assign the relevant wavenumbers figure 116). Figure 115 shows TGA-FTIR data for the carbonisation of a green mesophase tape, it is evident that the majority of the weight loss experienced by the green tape upon carbonisation is as a result of hydrocarbon evolution beginning at approximately 400°C. At the higher temperature of ~850°C it is also possible to see small quantities of evolved CO and CO₂, this is likely as a result of some surface oxidation on the tape as it was not dried before the test.

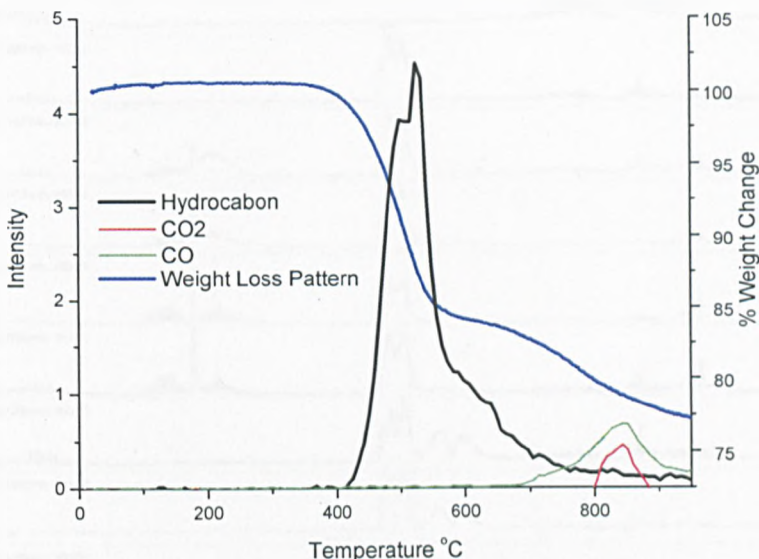


Figure 115 TGA-FITR results for the carbonisation of a green tape

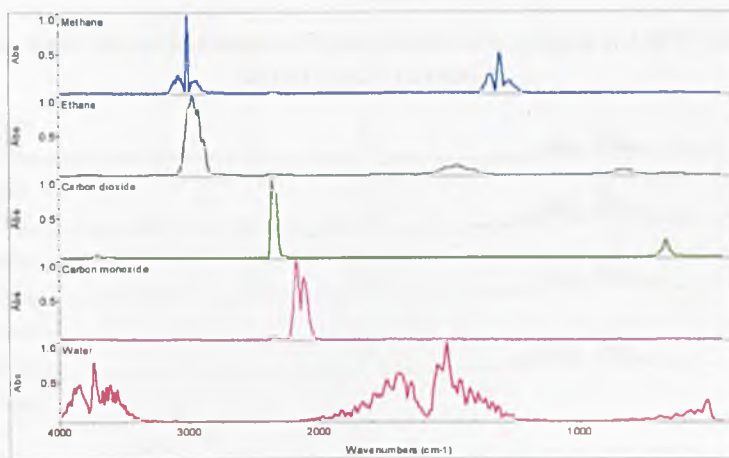


Figure 116 Library IR spectra of specific molecules

Although water was detected during the carbonisation of the stabilised mesophase tapes the signal was erratic and difficult to analyse in the same way as the other evolved gases. The IR time stacks of a tapes stabilised at 160°C for 5hrs and 240°C for 25hrs in both air and oxygen (Figures 117-120 represent FTIR readings of the gases present at intervals different temperature intervals throughout the carbonisation process, this information can only be used as a rough guide) shown in figures 117, 118, 119 & 120 confirm the presence of water upon carbonisation of mesophase tapes stabilised in both oxygen and air, with the air stabilised samples showing a greater intensity.

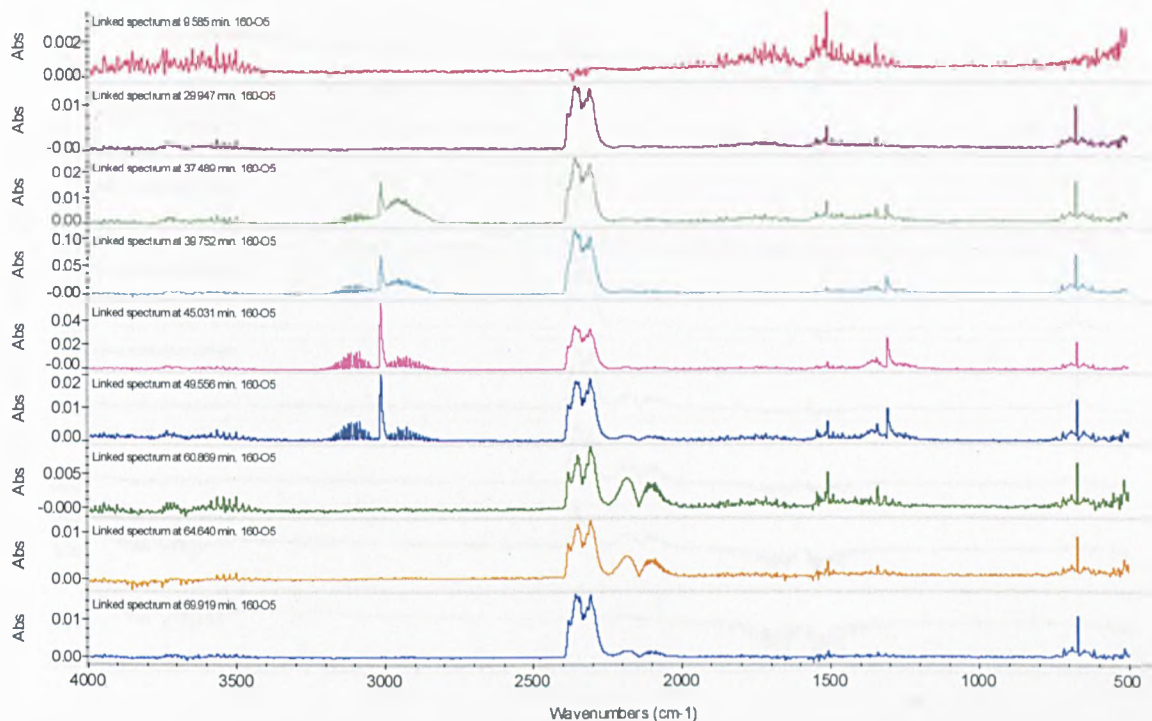


Figure 117 IR time stack for carbonisation of tape stabilised in oxygen at 160°C for 5hrs, heating rate of 15°C min⁻¹ to 1000°C

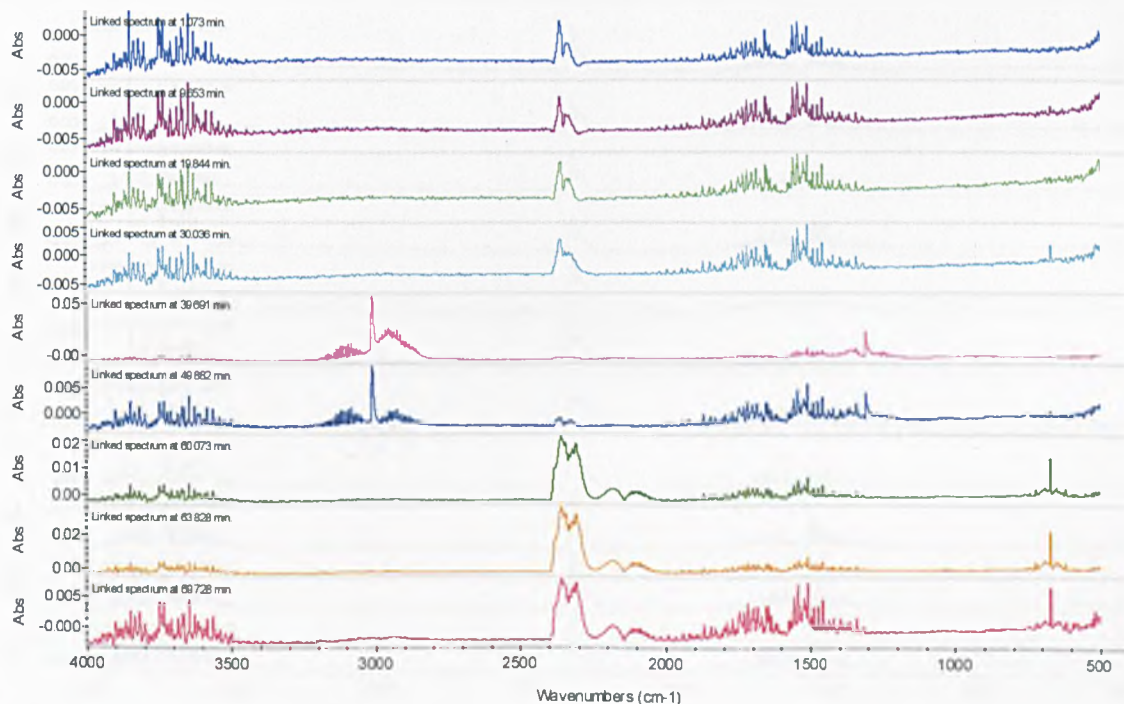


Figure 118 IR time stack for carbonisation of tape stabilised in air at 160°C for 5hrs, heating rate of 15°C min⁻¹ to 1000°C

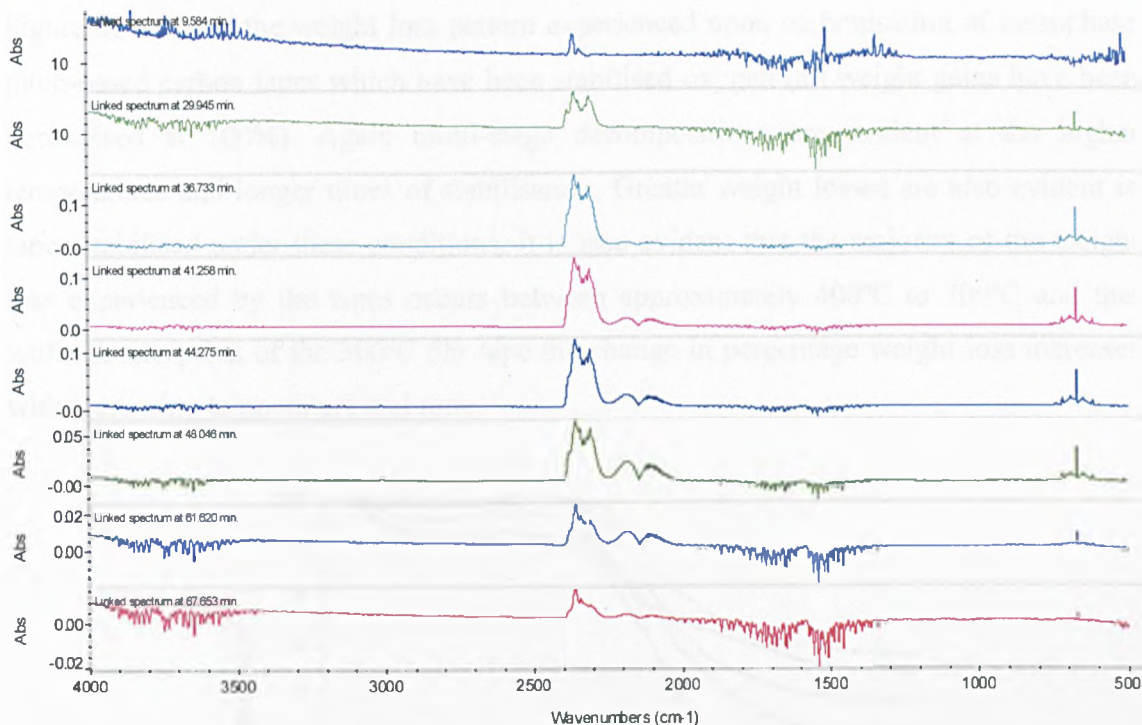


Figure 119 IR time stack for carbonisation of tape stabilised in oxygen at 240°C for 25hrs, heating rate of 15°C min⁻¹ to 1000 °C

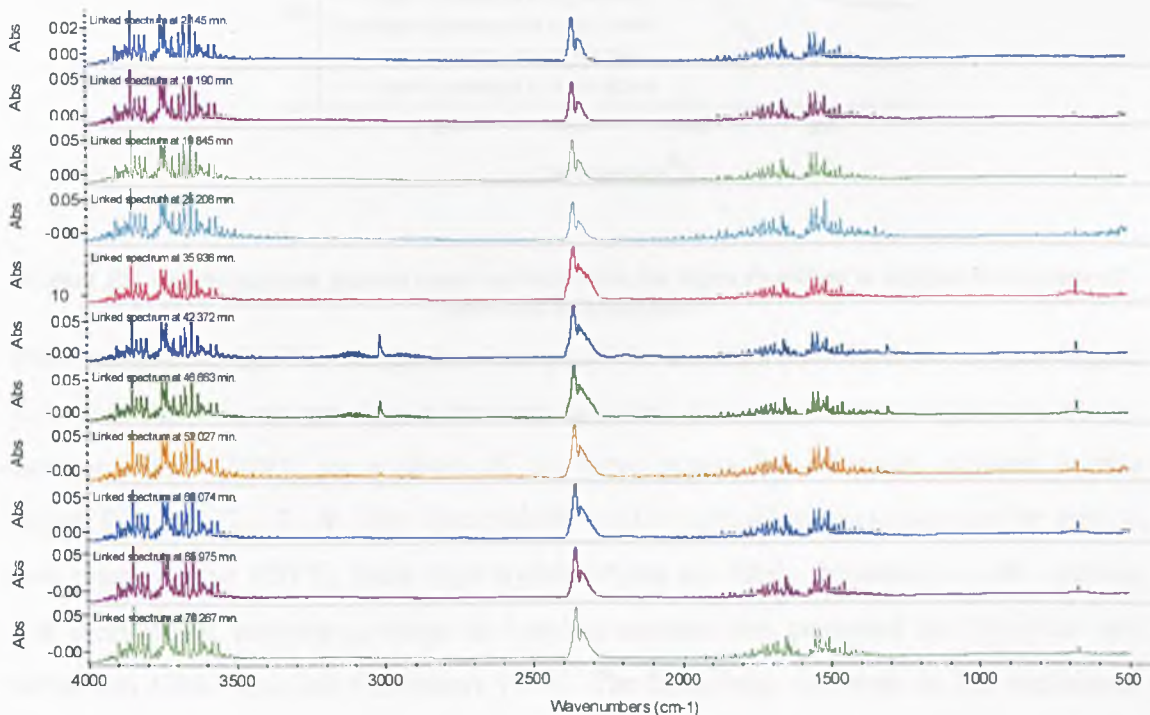


Figure 120 IR time stack for carbonisation of tape stabilised in air at 240°C for 25hrs, heating rate of 15°C min⁻¹ to 1000 °C

Figure 121 shows the weight loss pattern experienced upon carbonisation of mesophase pitch-based carbon tapes which have been stabilised oxygen (all weight gains have been normalised at 100%). Again multi-stage decompositions are evident at the higher temperatures and longer times of stabilisation, Greater weight losses are also evident in tapes stabilised under these conditions. It is also evident that the majority of the weight loss experienced by the tapes occurs between approximately 400°C to 700°C and that with the exception of the 300°C 5hr tape the change in percentage weight loss increases with increasing temperature and time.

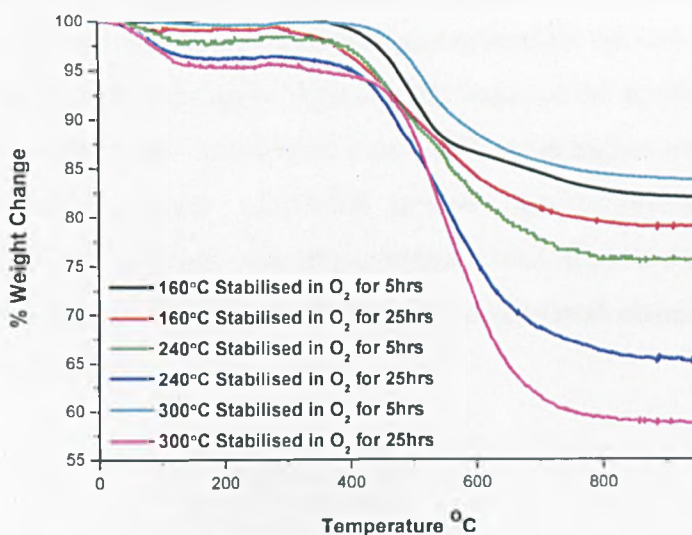


Figure 121 weight changes pattern upon carbonisation for tapes stabilised in oxygen for a range of times and temperatures

When comparing the TG weight loss curves of the samples stabilised in oxygen (figure 121) with the evolved gas data it becomes apparent that the greatest weight loss occurs between 400 – 700°C as a result of the large proportion of gases evolved in this region (figures 122, 123 & 124). The majority of the light alkane emission can be seen to take place around 600°C, these light hydrocarbons are likely generated by the opening and cleavage of naphthenic rings in keeping mechanisms proposed by Drhoblav and Stevenson (Drhoblav and Stevenson 1995). The homolytic cleavage of the naphthenic rings leads to the formation of radicals, which subsequently recombine to form a more condensed structure, after the elimination of alkanes such as methane, ethane and propane

(Dumont, Chollon et al. 2002). The shape of the hydrocarbon evolution curve is seen to be different for each stabilisation condition, this is again similar to observation made in work carried out by Dumont and co-workers (Dumont, Dourges et al. 2005). The intensity of hydrocarbon evolution can be seen to reduce with increasing temperatures and time of stabilisation. Only a trace amount is detected in the tape which has been stabilised at 240°C for 25hrs, no hydrocarbon evolution was detected in the tapes which had been stabilised at 300°C (figure 122 & table 19). It is probable that this decrease in hydrocarbon evolution is as a result of the multi-stage decomposition seen in those tapes which have been treated to a higher temperature, with hydrogen being lost in the form of water. It is likely that the majority of the hydrogen molecules are lost during this period and do not survive to see the higher temperatures required for hydrocarbon evolution. Another possibility is that tapes which have been stabilised at higher temperatures display more readily oxidised surface functional groups, this oxidation changing their functionality reducing the amount of hydrocarbons evolved. It should also be considered that at higher temperatures the chemical reactivity of the basal planes is being reduced (Bradley, Ling et al. 1993).

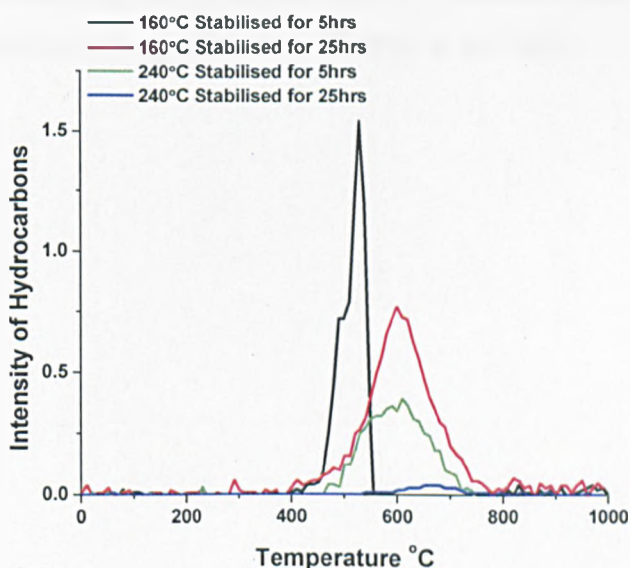


Figure 122 Evolution of hydrocarbons with increasing stabilisation time and temperature in oxygen upon carbonisation

The evolution of CO and CO₂ can be seen to increase with temperature and time of oxidative stabilisation upon carbonisation, (figure 123 & 124) in contrast to the hydrocarbon evolution. For both CO and CO₂ the 25hrs 240°C and 300°C tapes display the greatest intensities of gas evolution (table 19), this excess evolution of CO and CO₂ is reflected by the in the reduced final carbon yield (figure 121). Figure 123 show that the majority of the CO evolution takes place between the ~450°C to ~900°C and figure 124 show that the bulk of the CO₂ is evolved between ~300°C to ~700°C regardless of the stabilisation conditions, which is reflected again in the weight loss curves (figure 121).

It can also be seen that with the exception of the 160°C 5hr tape where the CO peak reaches a maximum around 820°C all the other stabilisation conditions saw CO production upon carbonisation reach a peak maximum at approximately 600°C (figure 123 & table 19). The peak maximum for evolution of CO₂ upon carbonisation of stabilised tapes (oxygen treated) is around approximately 500°C (figure 124 & table 19). This difference between the evolution of CO, CO₂ and hydrocarbons can be explained by the breaking of bonds different within the mesophase pitch-based carbon tapes. It has been proposed by Dumont and co-workers that the mechanism involved here may correspond to the breaking of methyl groups present in certain aromatic rings and require a higher thermal activation energy (Dumont, Chollon et al. 2002).

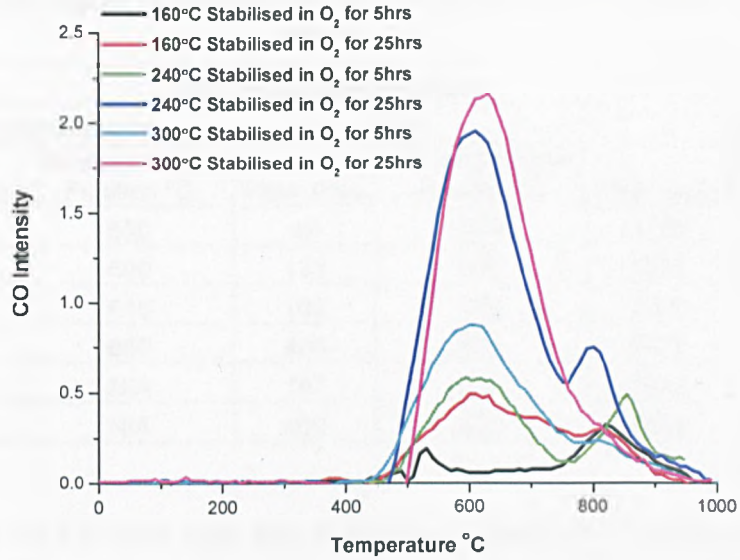


Figure 123 Evolution of CO with increasing stabilisation time and temperature in oxygen upon carbonisation

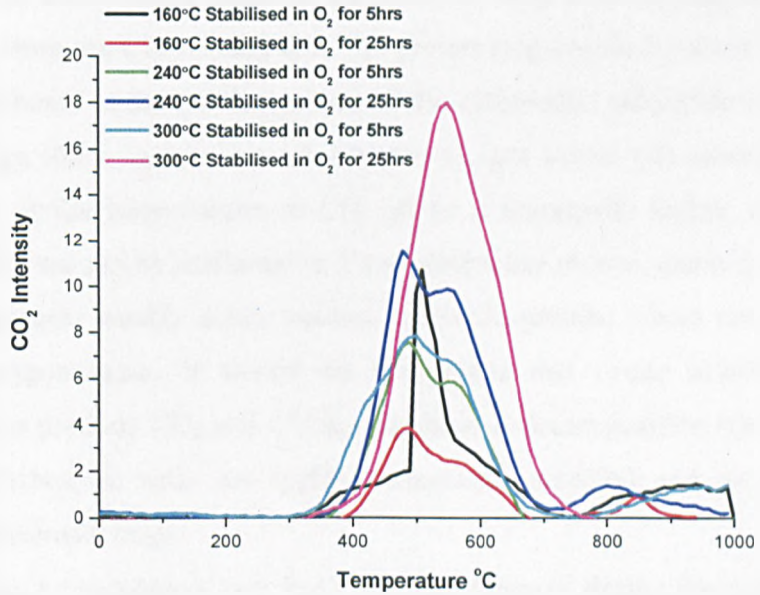


Figure 124 Evolution of CO₂ with increasing stabilisation time and temperature in oxygen upon carbonisation

Table 19 Peak areas and maximum peak positions for evolved gases during carbonisation of tapes which have seen varying degrees of stabilisation in oxygen (all experiments carried out using 95mg of sample)

| Oxygen Stabilised Tapes | | | | | | |
|-------------------------|--------------|--------------------------|-----------|--------------------------|-----------------|--------------------------|
| Gas | Hydrocarbons | | CO | | CO ₂ | |
| | Peak Area | Maximum Peak Position °C | Peak Area | Maximum Peak Position °C | Peak Area | Maximum Peak Position °C |
| 160°C 5hrs | 104 | 530 | 42 | 820 | 1186 | 510 |
| 160°C 25hrs | 95 | 600 | 133 | 600 | 1585 | 500 |
| 240°C 5hrs | 65 | 610 | 102 | 594 | 1585 | 490 |
| 240°C 25hrs | 5 | 660 | 406 | 610 | 2102 | 480 |
| 300°C 5hrs | N/A | N/A | 197 | 610 | 1642 | 500 |
| 300°C 25hrs | N/A | N/A | 460 | 630 | 2818 | 550 |

For the evolution of CO and CO₂ the evolved gas analysis illustrates that as the stabilisation temperature and time increase so does the intensity of the evolved CO and CO₂. The intensity of the CO₂ is far greater than that of the CO. As a result of this it can be surmised that higher stabilisation temperatures and longer times ultimately have an adverse affect on the final carbon yield of the product. This is in keeping with earlier conclusions drawn from the CHNO data 6.3. The groups responsible for the evolution of CO₂ have been attributed to the decomposition of the carboxylic, anhydride and lactone groups: acidic groups where carbon is bonded to two oxygen atoms. CO desorption takes place at a roughly similar temperatures to CO₂ all be it marginally higher, the surface oxygen groups which are can be attributed to it's evolution are phenol, carbonyl, quinone, ether and pyrene groups: weakly acidic neutral and basic groups, where one carbon is bonded to one oxygen atom. It should be recognized that cyclic anhydrides and carboxylic acids also produce CO₂ and CO during thermal decomposition (de la Puente, Pis et al. 1997) Carboxylic acids are highly temperature sensitive and can be found locally on the polyaromatic rings.

It should also be recognised that H₂O was also released during the carbonisation however the evolved levels were to low to study independently but it can be reasonable surmised that the it originates from hydrogen bonded H₂O associated with acidic oxygen complexes and from the condensation of any adjacent phenolic and carboxylic acids groups present in the samples.

In order to compare how the stabilising atmosphere affected the mesophase pitch-based tape upon carbonisation, the test was repeated in air. As with the oxygen carbonisation weight loss patterns those sample tapes which experienced the longest times and highest temperatures of stabilisation also experience the greatest weight loss and display multi-stages decomposition. However, unlike the oxygen carbonisation weight loss patterns the weight loss experienced by those samples stabilised at a lower temperature were all significantly lower (figure 125). It is also not clear why the 300°C 5hrs tape again as with the oxygen samples experiences the lowest weight loss upon carbonisation.

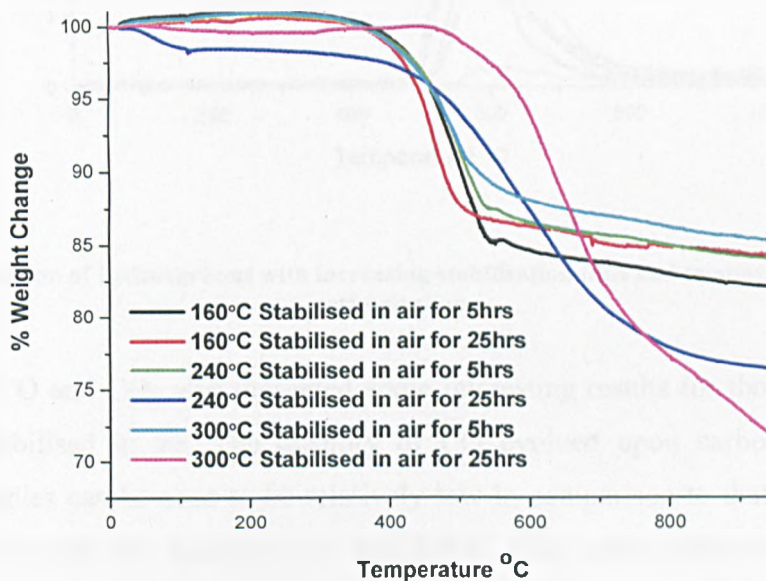


Figure 125 TGA weight changes pattern upon carbonisation for tapes stabilised in air for a range of times and temperature

Unlike the oxygen stabilised tapes no defined pattern can be observed in the intensity of hydrocarbon evolution although it is notable that no hydrocarbons were detected for the 240°C 25hr tape and only a relatively small quantity was detected after 300°C 25hrs. The intensity of the hydrocarbons evolved during the carbonisation of the air stabilised tapes was far greater than that observed under the same conditions in oxygen (figure 126 & table 20).

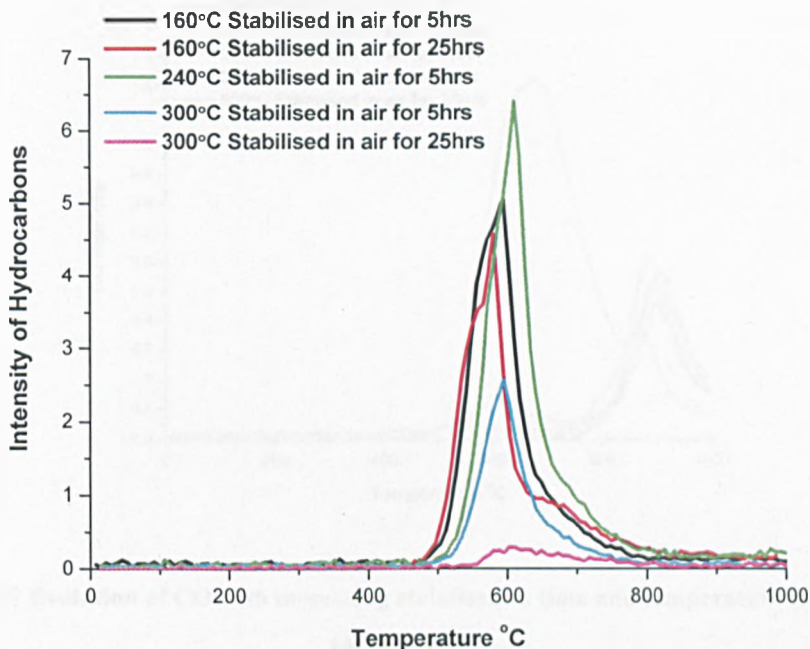


Figure 126 Evolution of hydrocarbons with increasing stabilisation time and temperature in air upon carbonisation

The evolved CO and CO₂ also presented some interesting results for those tapes which have been stabilised in air. The quantity of CO evolved upon carbonisation of air stabilised samples can be seen to be relatively low in comparison to that of the oxygen stabilised tapes with the exception of the 300°C 25hr tapes. Interestingly the peak maximum position for the lower temperatures of stabilisation is much higher than that shown for the oxygen stabilised tapes of around 600°C (table 20). The air CO evolution peak maximum is observed at approximately 900°C with the exception of the 300°C 25hrs, tape where its maximum is recorded at 679°C (figure 127 & table 20).

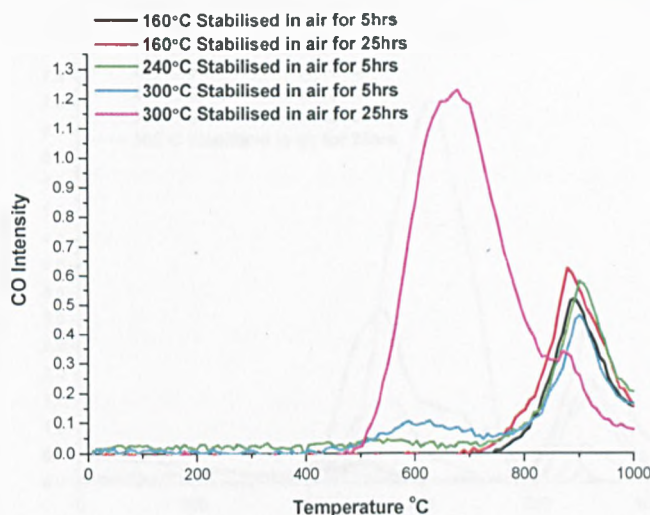


Figure 127 Evolution of CO with increasing stabilisation time and temperature in air upon carbonisation

More significant quantity of CO_2 were observed for the air treated tapes but as with the CO evolution the peak maximums for the lower temperatures and times of stabilisation were observed at a much higher temperature (approximately 900°C). As with the evolved CO those samples which display the greater weight loss after higher temperatures of stabilisation also displayed a more significant quantity of evolved CO_2 with a peak maximum around the lower temperature of 600°C (figure 128 & table 20).

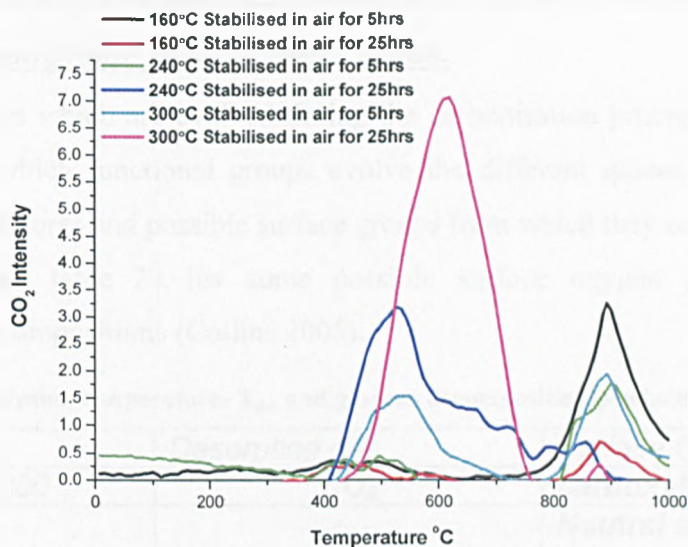


Figure 128 Evolution of CO₂ with increasing stabilisation time and temperature in air upon Carbonisation

Table 20 Peak areas and maximum peak positions for evolved gases during carbonisation of tapes which have seen varying degrees of stabilisation in air (all experiments carried out using 95mg of sample)

| Air Stabilised Tapes | | | | | | |
|----------------------|--------------|--------------------------|-----------|--------------------------|-----------------|--------------------------|
| Gas | Hydrocarbons | | CO | | CO ₂ | |
| | Peak Area | Maximum Peak Position °C | Peak Area | Maximum Peak Position °C | Peak Area | Maximum Peak Position °C |
| 160°C 5hrs | 474 | 595 | 43 | 893 | 276 | 893 |
| 160°C 25hrs | 423 | 581 | 55 | 879 | 48 | 879 |
| 240°C 5hrs | 528 | 610 | 33 | 900 | 262 | 900 |
| 240°C 25hrs | Na | 660 | Na | Na | 684 | 526 |
| 300°C 5hrs | 217 | 595 | 39 | 900 | 394 | 893 |
| 300°C 25hrs | 48 | 603 | 259 | 679 | 1215 | 618 |

8.3 Examination of the gases evolved during carbonisation of stabilised mesophase pitch-based tapes.

Knowing the gases which are evolved during the carbonisation process it is possible to determine from which functional groups evolve the different gasses. Table 21 shows desorption temperatures and possible surface groups from which they could potentially be evolved from and table 22 list some possible surface oxygen groups and their corresponding decompositions (Collins 2005).

Table 21 Desorption temperatures T_{des} and gaseous decomposition products (Collins 2005)

| T_{des} (°C) | Desorption gas | Surface Groups |
|----------------|----------------|--|
| 180-200,300 | CO_2 | carboxylic groups |
| 250-600 | CO_2 | Neutral and weakly acidic groups carrying two oxygen atoms (i.e. different types of lactone groups) |
| 500-600 | CO_2 | Neutral and peroxide groups |
| 400-900 | CO | Hydroxylic and hydroquinone groups |
| 500-900 | CO, CO_2 | Carbonylic and quinonic groups |
| 900, 1200 | CO, CO_2 | Pyrone or chromene structures |

Table 22 Some oxygen surface groups and corresponding decomposition products (Collins 2005)

| Functional Groups | Products |
|----------------------|--------------|
| Carbonyl | CO |
| Quinone | CO |
| Ether | CO |
| Carboxylic Anhydride | CO, CO_2 |
| Lactone | CO_2 |
| Carboxylic Acid | CO_2, H_2O |
| Phenol | CO, H_2O |

The TGA-FTIR data can be used to help determine which surface groups are evolving the product gases during the carbonisation of stabilised samples using a Gaussian fit to deconvolute the peaks. For CO and CO₂ evolved during carbonisation a typical example will be investigated and deconvoluted for tapes stabilised in oxygen and air.

Upon examination of a typical CO gas spectra for oxygen and air stabilised samples it is apparent that the evolved CO is a product of the desorption of a wide range of functional groups. In the oxygen treated samples the bulk of the CO is evolved from neutral and weakly acidic groups carrying two or more oxygen atoms closely followed by carbonylic and quinonic groups (figure 129) where as the air stabilised sample shows that the majority of the CO is evolved from carbonylic and quinonic groups and pyrone or chromene structures (figure 130). However, it should be noted that the majority of samples that were stabilised in air only produced CO from pyrone or chromene structures as shown in table 20 by the higher temperatures of CO evolution. Only in the 300°C 25hrs sample were more significant quantity of CO evolved (table 20) was a reasonable amount of carbonylic and quinonic groups detected (figure 130).

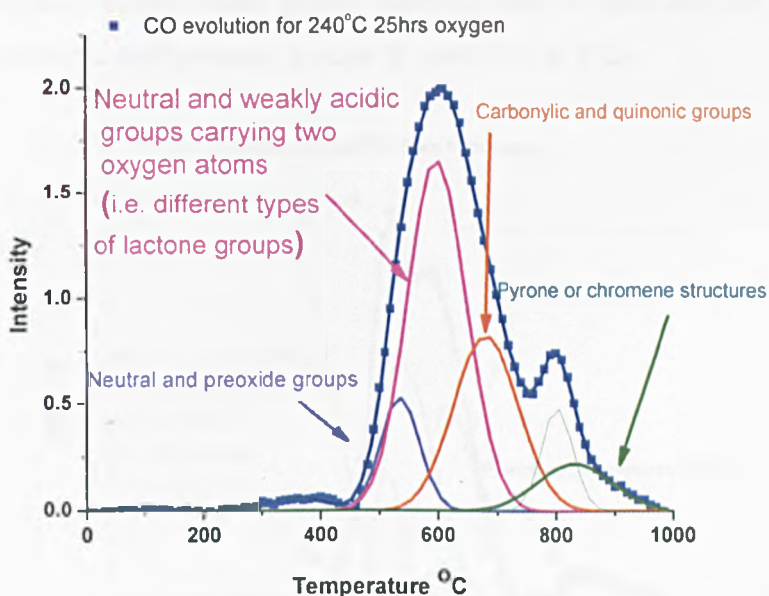


Figure 129 Deconvolution of CO evolution peak for samples stabilised at 240°C in O₂ for 25hrs

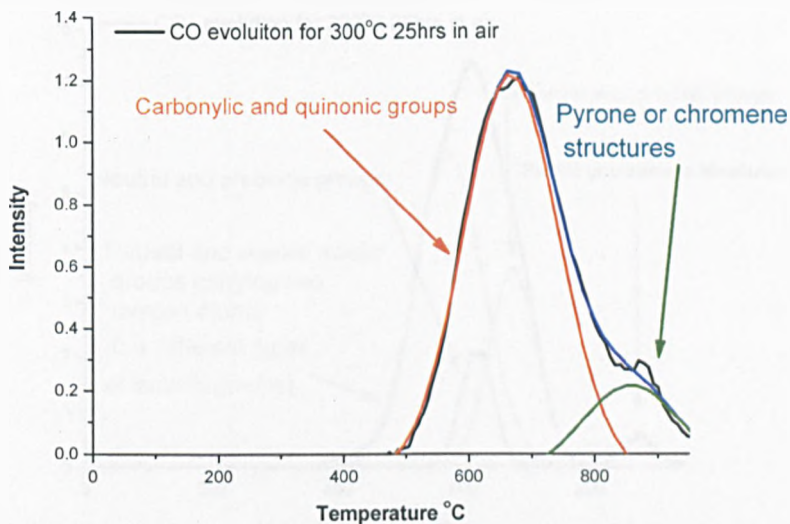


Figure 130 Deconvolution of CO evolution peak for samples stabilised at 300°C in air for 25hrs
 As with the evolved CO, the CO₂ which is evolved during the carbonisation of tapes stabilised in oxygen and air is as the result of the desorption of several functional groups. Again the functional groups which are responsible for the majority of the production of CO₂ are neutral and weakly acidic groups carrying two or more oxygen atoms closely followed by carbonylic and quinonic groups (figures 131 & 132).

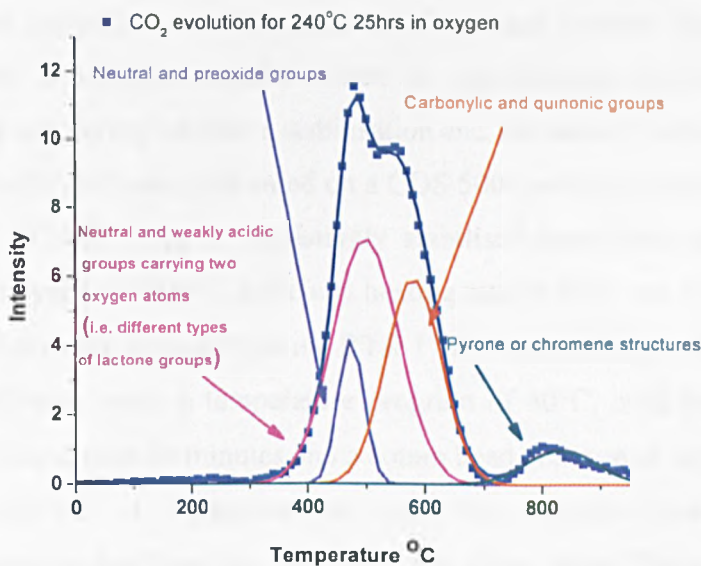


Figure 131 Deconvolution of CO₂ evolution peak for a sample stabilised at 240°C in O₂ for 25hrs

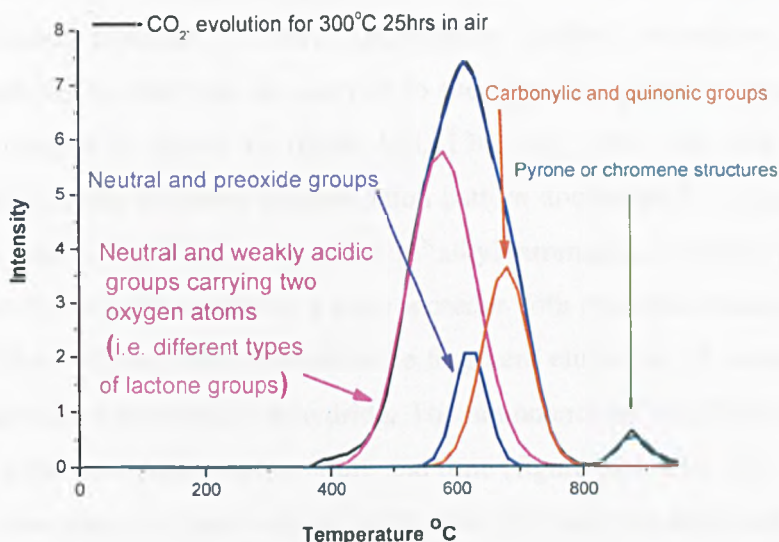


Figure 132 Deconvolution of CO₂ evolution peak for a sample stabilised at 300°C in air for 25hrs

8.4 Pyrolysis-gas chromatography-mass spectrometry characterisation of carbonised mesophase pitch-based tapes

Strong inferences regarding pitch structure and composition can be drawn from the identification and quantification of hydrocarbon fragments evolved during pyrolysis of pitch. Py-GC-MS is therefore ideally suited to identification of structural changes occurring in the pitch during oxidative stabilisation and subsequent carbonisation (figures 133-139). The Py-GC-MS was performed on a CDS 5000 series pyrolyser connected to a Shimadzu 2010 GC-MS. 2mg of oxidatively stabilised mesophase pitch-based tapes samples were pyrolysed at 1000°C in He at a heating rate of 20°C /ms with a hold time of 20 sec. The products were separated on a n RTX 1701 60m capillary column, 0.25mm id, 0.25µm film thickness, using a temperature program of 40°C, hold time of 2 minutes, ramped to 250°C, hold time 30 minutes and a column head pressure of 30 psi at 40° C.

The Py-GC-MS of oxygen-treated mesophase pitches show a significantly different fingerprint to that from the “as spun”, i.e. green, pitch. The products from the “flash” pyrolysis of the green pitch at 1000°C are shown in figure 133. The products

include aromatic fragments consisting of between one and four fused rings, as expected, with a significant presence of alkyl (principally methyl) substituted content. No oxygenated species are evolved. In contrast to the pyrolysis products from an oxygen-treated pitch sample is shown in figure 133, 134, 135, 136, 137, 138 & 139. This indicates a significantly different fragmentation pattern dominated by oxygen-containing hydrocarbons and a significant reduction in alkyl aromatics. Carbon yields can be estimated from Py-GC-MS and show a clear increase with oxidative treatment compared to the green pitch. Of particular interest is the fragment eluting at 35 minutes, identified by mass spectrometry as phthalic anhydride. The abundance of this fragment appears to increase with both stabilisation temperature and time (figure 133, 134, 135, 136, 137, 138 & 139). This correlates not only with an increase in O/C ratio but also with the degree of stabilisation potential in the various oxygen-treated pitches (as established by softening point behaviour, ThAFM, section 7.3). The naphthalene analogue of phthalic anhydride is also present. Additional oxygenated analogues include benzoic acid and phenol as well as a number of ether containing fragments. Generation of acetic acid implies the presence of acetyl groups in the stabilised matrix.

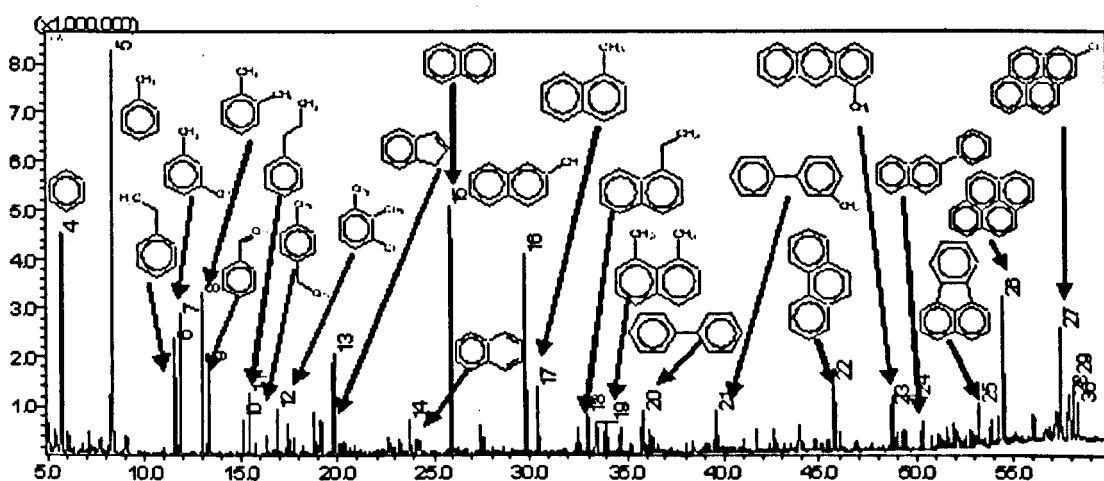


Figure 133 Fragment retention time (x-axis) vs. abundance (y-axis) results from Py-GC-MS at 1000°C of a green mesophase pitch tape;

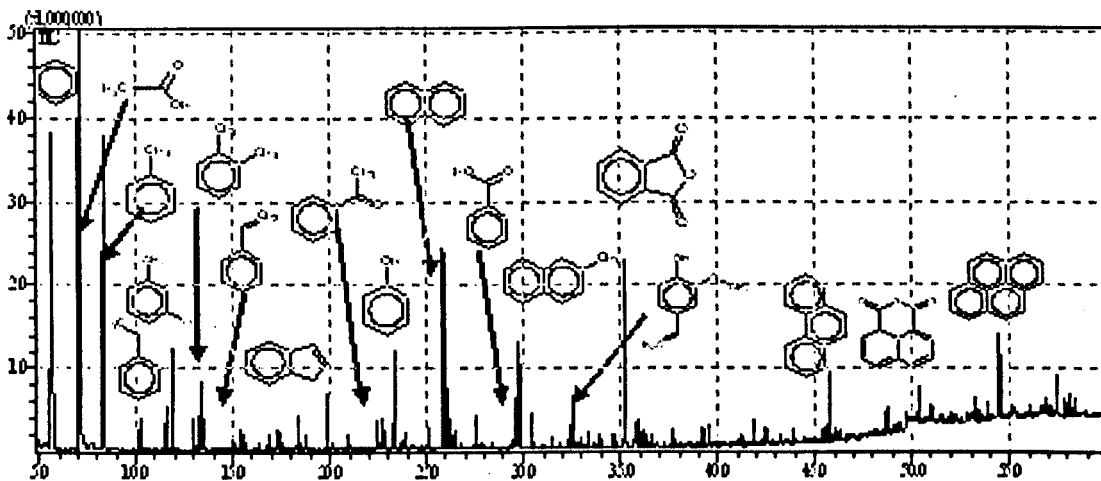


Figure 134 Fragment retention time (x-axis) vs. abundance (y-axis) results from Py-GC-MS at 1000°C of mesophase pitch tape; stabilised at 160°C for 5hrs

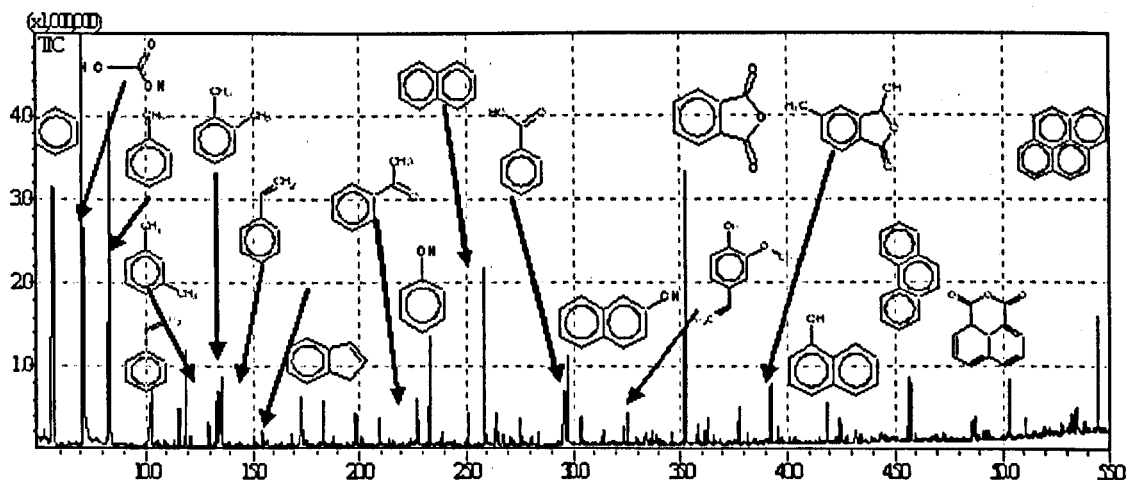


Figure 135 Fragment retention time (x-axis) vs. abundance (y-axis) results from Py-GC-MS at 1000°C of mesophase pitch tape; stabilised at 160°C for 25hrs

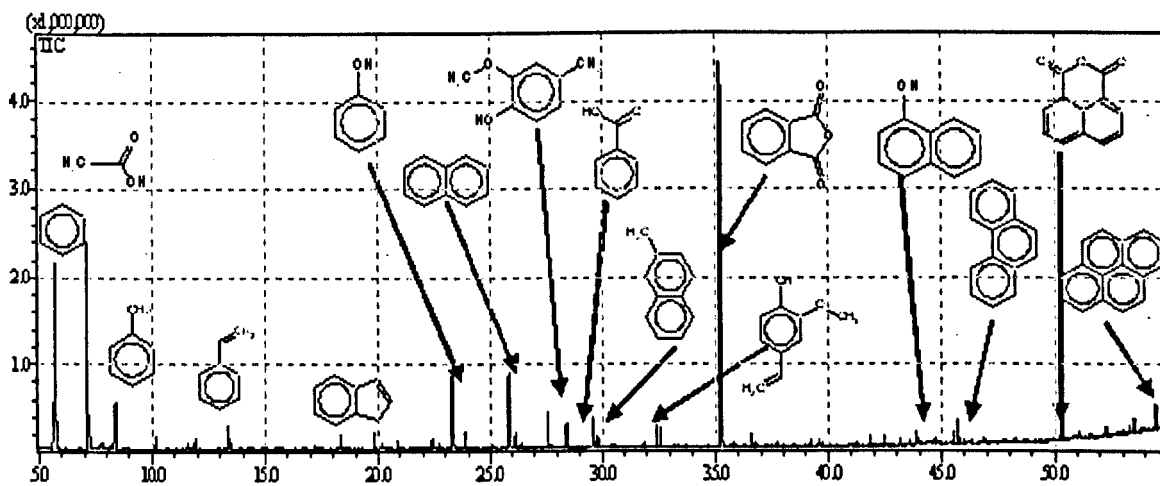


Figure 136 Fragment retention time (x-axis) vs. abundance (y-axis) results from Py-GC-MS at 1000°C of mesophase pitch tape; stabilised at 240°C for 5hrs

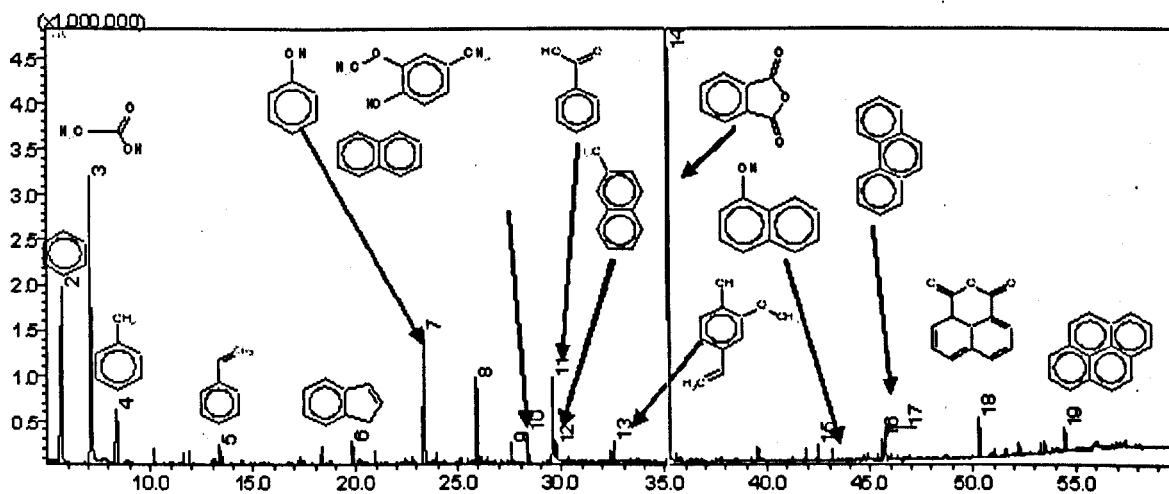


Figure 137 Fragment retention time (x-axis) vs. abundance (y-axis) results from Py-GC-MS at 1000°C of mesophase pitch tape; stabilised at 240°C for 25hrs

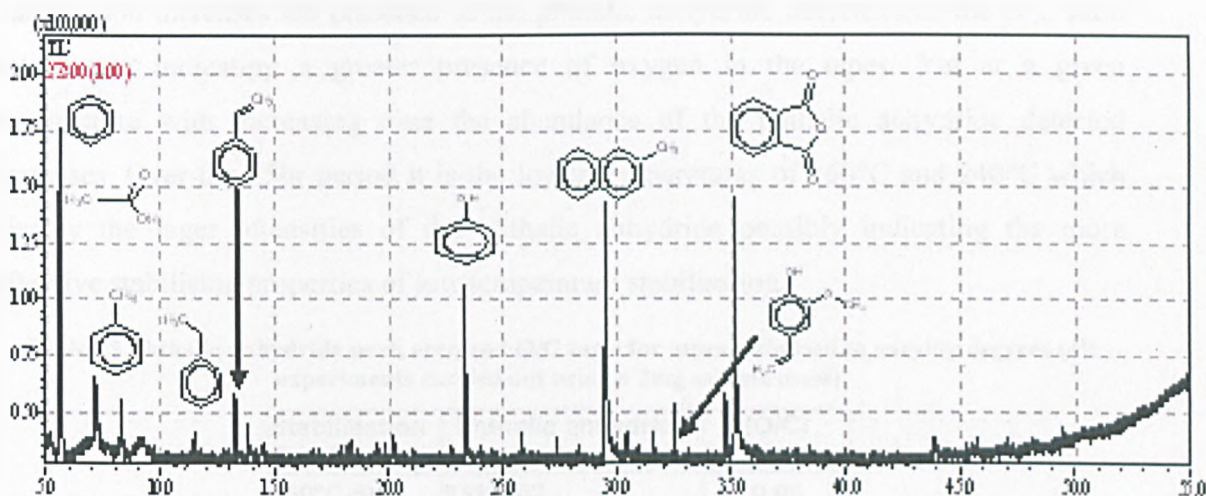


Figure 138 Fragment retention time (x-axis) vs. abundance (y-axis) results from Py-GC-MS at 1000°C of mesophase pitch tape; stabilised at 300°C for 5hrs

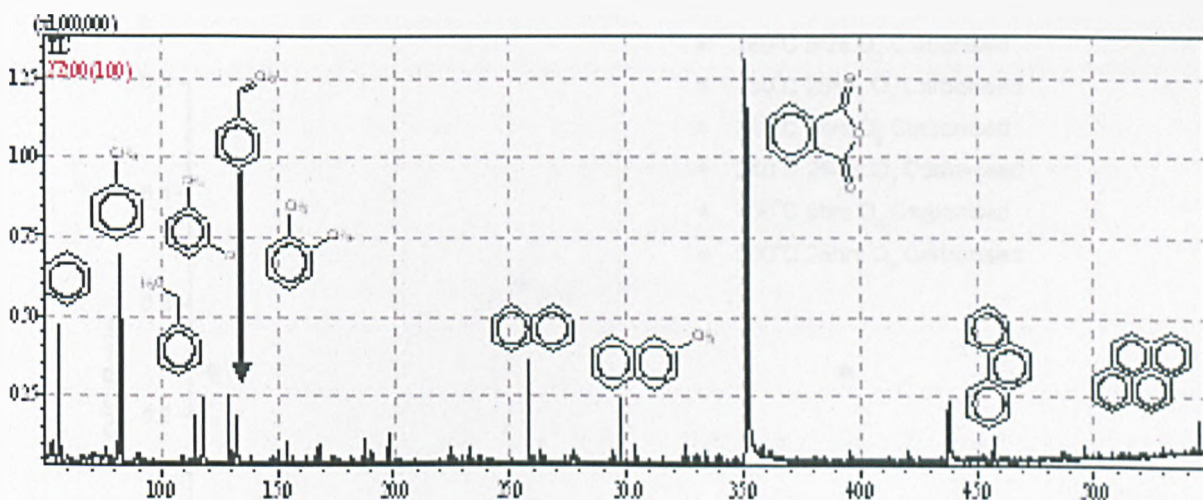


Figure 139 Fragment retention time (x-axis) vs. abundance (y-axis) results from Py-GC-MS at 1000°C of mesophase pitch tape; stabilised at 300°C for 25hrs

In order to assess further the significance of the phthalic anhydride fragment eluting at 35 minutes, the area of the phthalic anhydride was calculated using integration and then plotted against the O/C ratios recorded for tape samples which had experienced the same stabilising conditions. It can be seen in figure 140 and table 23 that as temperature of

stabilisation increases the presence of the phthalic anhydride decreases as the O/C ratio gets larger indicating a greater presence of oxygen in the tapes. Yet at a given temperature with increasing time the abundance of the phthalic anhydride detected increases. Over the 25hr period it is the lower temperatures of 160°C and 240°C which display the larger intensities of the phthalic anhydride possibly indicating the more effective stabilising properties of low temperature stabilisation.

Table 23 Phthalic anhydride peak area and O/C ratio for tapes stabilised to varying degrees (all experiments carried out using a 2mg sample mass)

| Stabilisation Condition | Phthalic anhydride peak area | (O/C) Ratio |
|-------------------------|------------------------------|-------------|
| 160°C-5hrs | 6533402 | 0.05 |
| 160°C -25hrs | 13367890 | 0.11 |
| 240°C -5hrs | 1386649 | 0.12 |
| 240°C -25hrs | 13599329 | 0.24 |
| 300°C -5hrs | 431494 | 0.24 |
| 300°C -25hrs | 6795668 | 0.32 |

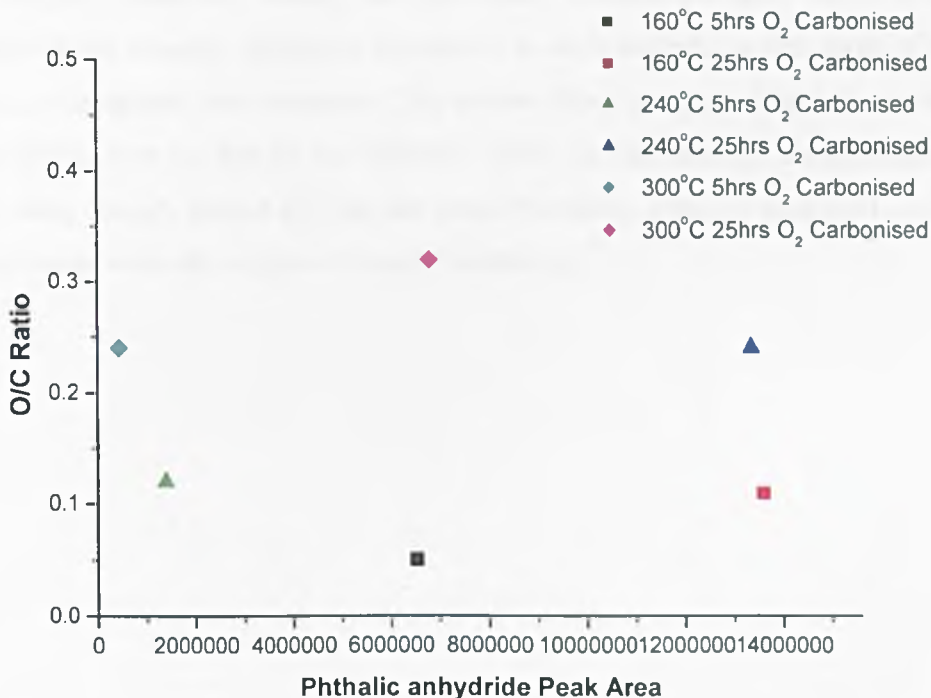


Figure 140 O/C ratio for samples stabilised to various conditions vs. the phthalic anhydride (peak area) signals produced upon carbonisation



8.5 Raman characterisation of carbonised mesophase pitch-based carbon tapes

When the samples have undergone a subsequent 450°C heat treatment (partial carbonisation) there is a decrease in the intensity of both the D peak around 1350 cm⁻¹ and the G peak around 1600 cm⁻¹.

Partial carbonisation heat treatment to 450°C can be seen to increase the ordering of the mesophase pitch-based tapes stabilised at 160°C and 240°C (figure 141 & 142) displayed by the lower $D_{(i)}/G_{(i)}$ ratio at these temperatures. (This ordering of the micro domains within the tapes upon heat treatment is also evident in the optical characterisation section 9). The 300°C samples do not exhibit the same pattern, (figure 143) as there is a slight increase in the $D_{(i)}/G_{(i)}$ ratio of the tapes suggesting, if anything, slightly more molecular disorder. This has most likely arisen as a direct result of the excess oxygen observed locally on the tapes surface (EPMA, XPS & Optical Characterisation) causing molecular disruption as it is evolved in the form of CO and CO₂ upon subsequent heat treatment. The reason there is only a slight decrease in the order at 300°C may be due to the fact that 300°C is high enough temperature and 25 hours is long enough period of time for some thermally induced structural ordering to start to compete with the oxygen-induced disordering.

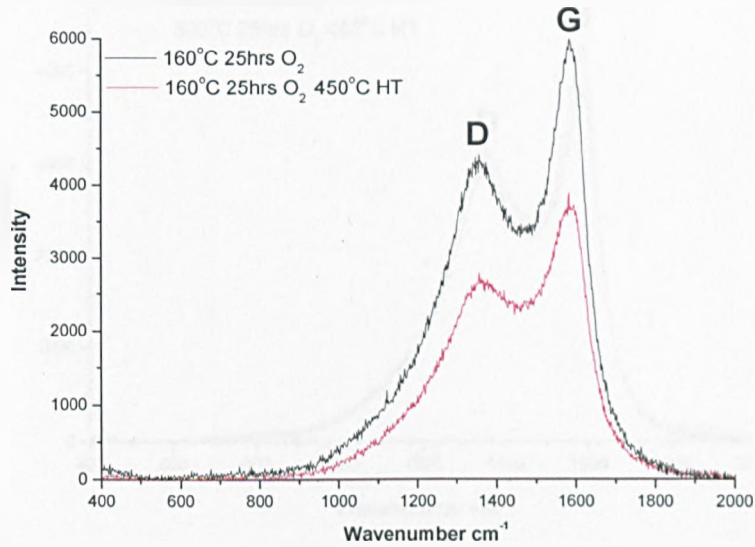


Figure 141 Raman spectra of tape stabilised at 160°C for 25hrs and tape stabilised at 160°C for 25hrs and subsequently heat treated to 450°C

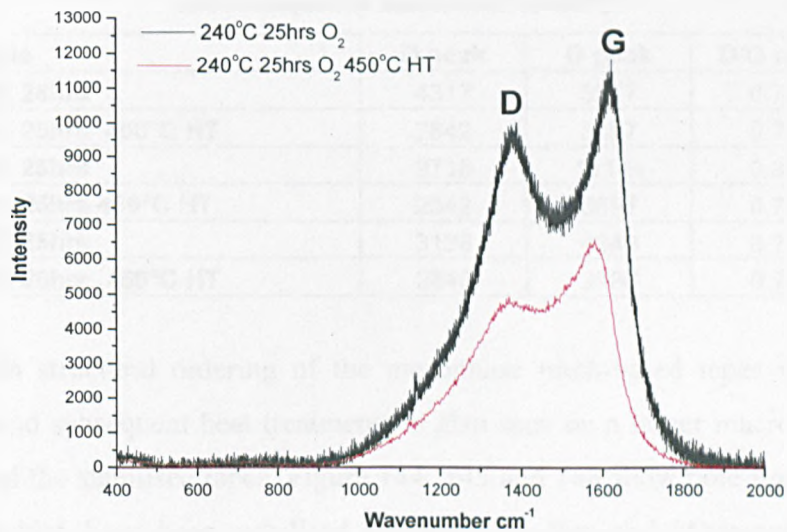


Figure 142 Raman spectra of tape stabilised at 240°C for 25hrs and tape stabilised at 240°C for 25hrs and subsequently heat treated to 450°C

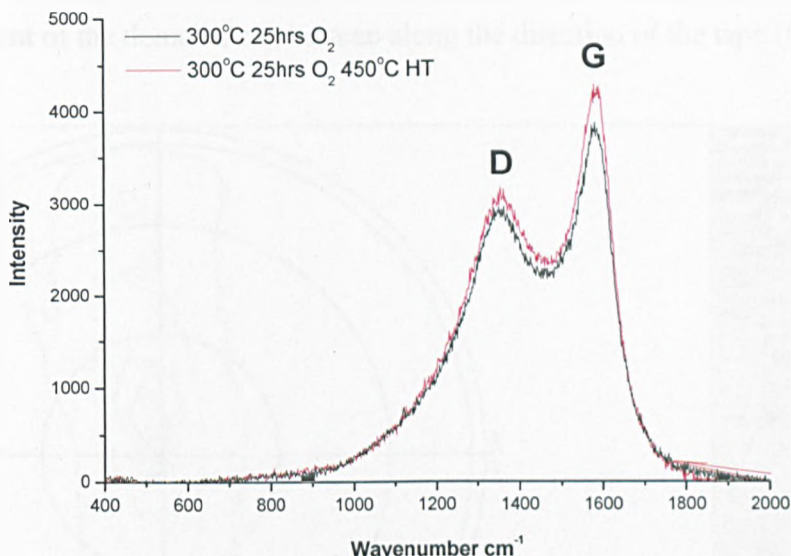


Figure 143 Raman spectra of tape stabilised at 300°C for 25hrs and tape stabilised at 300°C for 25hrs and subsequently heat treated to 450°C

Table 24 Raman D and G peak intensity and D/G ratio for tapes stabilised under various condition and subsequently heat treated to 450°C

| Sample | D peak | G peak | D/G ratio |
|----------------------|--------|--------|-----------|
| 160°C 25hrs | 4317 | 5917 | 0.73 |
| 160°C 25hrs 450°C HT | 2642 | 3697 | 0.71 |
| 240°C 25hrs | 9718 | 11144 | 0.87 |
| 240°C 25hrs 450°C HT | 2642 | 3697 | 0.71 |
| 300°C 25hrs | 3128 | 4249 | 0.74 |
| 300°C 25hrs 450°C HT | 2845 | 3786 | 0.75 |

The change in structural ordering of the mesophase pitch-based tapes with oxidative stabilisation and subsequent heat treatments is also seen on a larger macro scale in pole figure taken of the stabilised tapes. Figure 144, 145 and 146 show pole figures for pitch-based tapes which have been stabilised at 240°C for 5hrs and 25hrs and stabilised at 240°C for 25hrs then heat treated to 450°C respectively. The pole figures clearly show that as the time of exposure to the oxidative atmosphere increases (figure 144 & 145) the disorder in the alignment of the tapes micro-domains also increases, however upon

further heat treatment to 450°C of the tape stabilised to 25hrs a significant improvement in the alignment of the domains can be seen along the direction of the tape (figure 146).

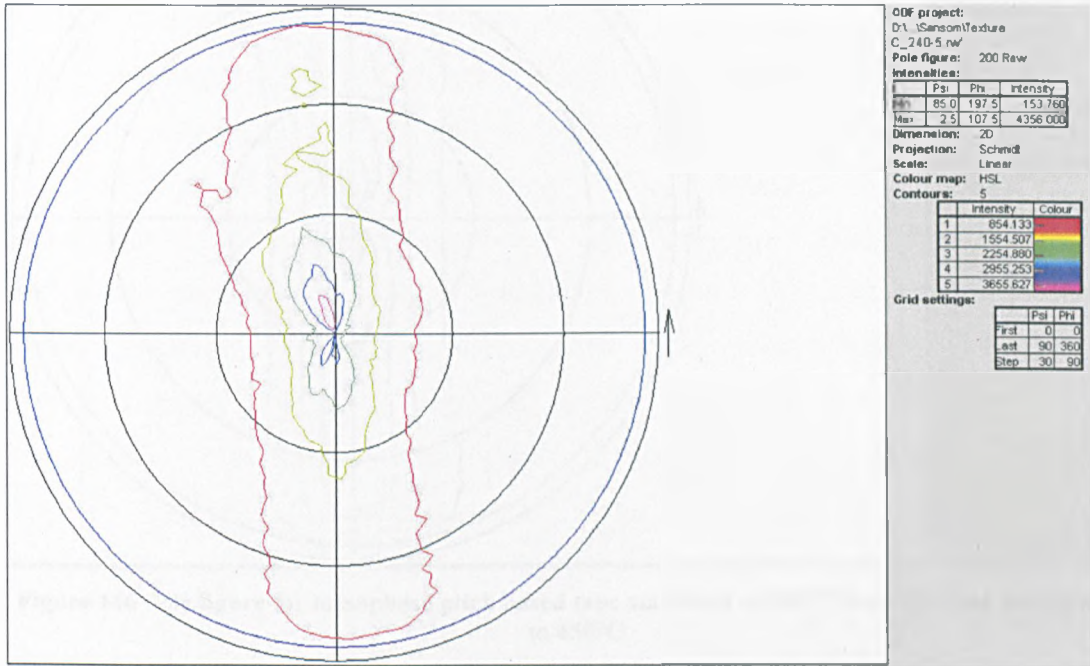


Figure 144 Pole figure for mesophase pitch based tape stabilised at 240°C for 5hrs

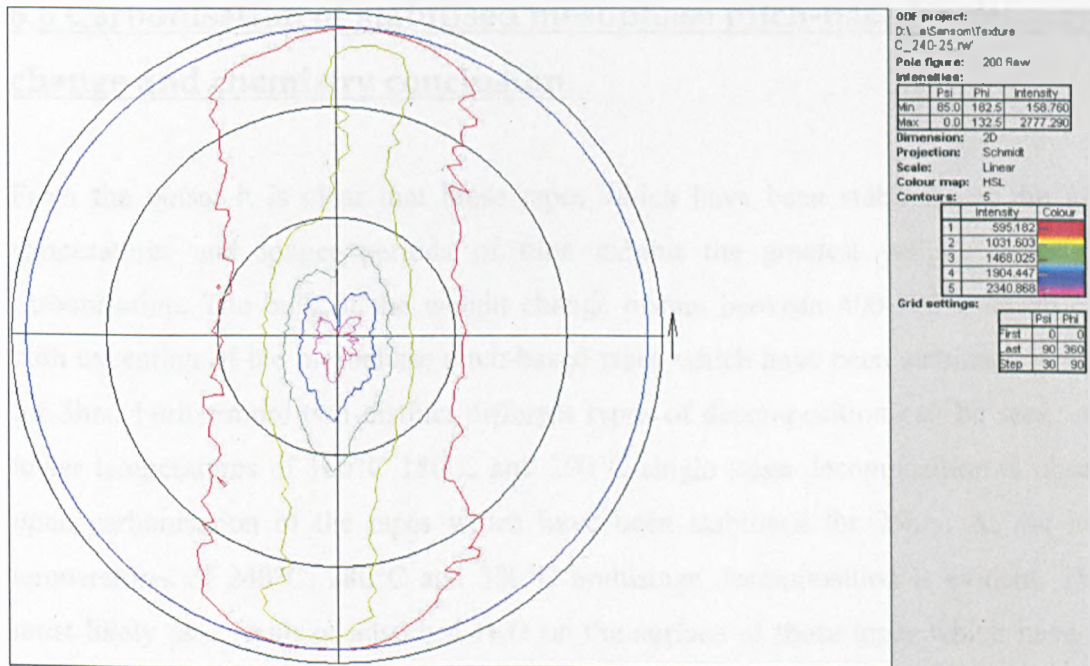


Figure 145 Pole figure for mesophase pitch based tape stabilised at 240°C for 25hrs

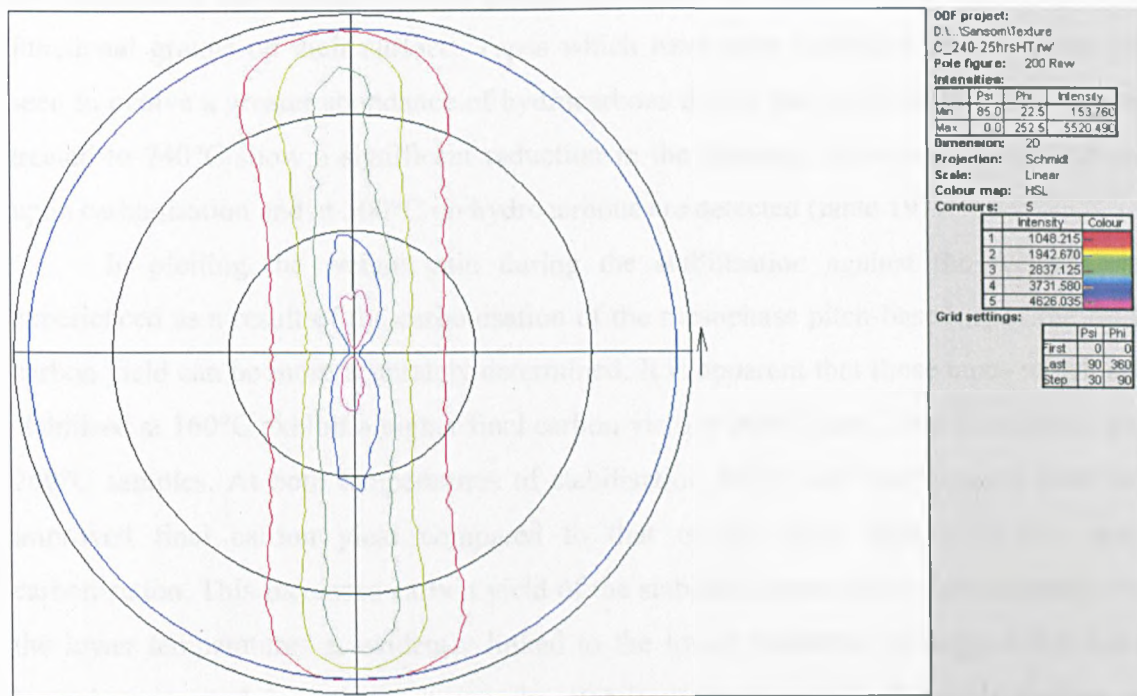


Figure 146 Pole figure for mesophase pitch based tape stabilised at 240°C for 25hrs and heat treated to 450°C

8.6 Carbonisation of stabilised mesophase pitch-based tapes weight change and chemistry conclusion

From the outset it is clear that those tapes which have been stabilised at the higher temperatures and longer periods of time exhibit the greatest weight losses upon carbonisation. The bulk of the weight change occurs between 400-700°C in all cases, with exception of the mesophase pitch-based tapes which have been stabilised to 300°C for 5hrs. Furthermore two distinct different types of decomposition can be seen; at the lower temperatures of 160°C 180°C and 200°C single stage decomposition is observed upon carbonisation of the tapes which have been stabilised for 25hrs. At the higher temperatures of 240°C, 280°C and 300°C multistage decomposition is evident. This is most likely as a result of adsorbed H₂O on the surface of those tapes which have been stabilised at higher temperatures (above 200°C) and that tapes treated at a higher

temperatures of stabilisation have a greater abundance of carbonyl and carboxylic acid functional groups on their surface. Tapes which have been stabilised at 160°C can be seen to evolve a greater abundance of hydrocarbons during the carbonisation step. Tapes treated to 240°C show a significant reduction in the intensity of evolved hydrocarbons upon carbonisation and at 300°C no hydrocarbons are detected (table 19).

In plotting the weight gain during the stabilisation against the weight loss experienced as a result of the carbonisation of the mesophase pitch-based tapes the final carbon yield can be more accurately determined. It is apparent that those tapes which are stabilised at 160°C exhibit a higher final carbon yield at both 5 and 25hrs than that of the 240°C samples. At both temperatures of stabilisation 160°C and 240°C tapes show an improved final carbon yield compared to that of the green tape (~78.3%) upon carbonisation. This increased carbon yield of the stabilised tapes which have experienced the lower temperatures is evidently linked to the lower quantities of oxygen that have been incorporated into them during the stabilisation step (table 9). This finding is corroborated further by the lower intensities of CO and CO₂ which were evolved during their subsequent carbonisation (table 19). Tapes which have been stabilised to 300°C display the highest final carbon yield for the 5hrs (~90%) tape yet the lowest for the 25hr tape (~66%).

When examining the gases evolved during the carbonisation of oxygen stabilised tapes the largest proportion of the gases are emitted between 400-700°C, the same temperatures that the majority of the weight change is observed. There are notably three main gases evolved during the carbonisation; hydrocarbons, CO and CO₂. As the temperature and time of stabilisation increased a decrease in the intensity of the evolved hydrocarbons takes place. Furthermore it was observed that as the temperature and time of the stabilisation increases so does the intensity of the evolved CO and CO₂. Again, this is likely to be as a result of the increased oxygen uptake which is experienced at the higher temperatures of stabilisation and the increased carbonyl, carboxyl and ester functionality observed at the higher temperatures in the XPS.

When considering air as the stabilising atmosphere it is apparent that similar weight loss patterns can be seen as in oxygen TG curves. However, upon examination of

the evolved gases emitted during carbonisation of the stabilised mesophase pitch-based tapes hydrocarbons can be seen to be in both the 240°C 5hr tape and the 300°C 5 & 25hr tapes. Unlike the oxygen treated samples there was very little variation in the intensities of evolved of the CO with the exception of the 300°C 25hrs samples and notably for these tapes the maximum peak position is at 679°C differing from the 900°C of the other tapes (table 20). For the evolved CO₂ the pattern of evolution again differs, a decrease in evolved intensity can be seen with increasing time of stabilisation for the 160°C tapes. An increase in the intensity is observed for those tapes which have been to 240°C and 300°C with increasing time. As with the CO production the CO₂ maximum peak position can be seen to alter as stabilisation time and temperature increase. The tapes stabilised at 160°C for 5 and 25hrs and 240°C and 300°C for 5hr show a higher maximum peak position temperature for the evolved CO₂ at approximately 900°C (table 20). The tapes stabilised to 240°C and 300°C for 25hrs show a much lower temperature for the maximum peak position for the evolution of CO₂ (table 20). This suggest that the tapes which have the higher peak maximum will have the oxygen more strongly bound into its structure, these results tie in nicely with the weight loss pattern and final carbon yields for the air stabilised tapes (figure 125). Those tapes which have the lower maximum peak position for both CO and CO₂ also display lower final carbon yields. The tapes which display the lower maximum peak position temperature for CO and CO₂ evolution may well have been over stabilised, possibly as a result of the increase oxygenated functionalities detected on the tapes surface with increasing stabilisation time and temperature, as illustrated in XPS and EPMA results. This could be investigated further in future work by altering the partial pressure of the stabilising gases and observing how the chemistry of the tapes changes at incremental stages throughout the carbonisation process.

Py-GC-MS was used to evaluate the products for the pyrolysis of the stabilised tapes. Mesophase pitch-based tape samples which have been stabilised exhibited significantly different finger prints to that of the green pitch. A wide range of fragments was found in the results, with notably a significant presence of oxygen-containing hydrocarbons fragments. Of particular interest was the fragment eluting at 35 minutes,

phthalic anhydride. The abundance of this fragment appeared to increase with stabilisation time at a given temperature, correlating with an increase in O/C (table 23 & figure 140) and the stabilisation potential of the various oxygenated pitch as set out in ThAFM results. As the oxygen content of the pitch increases for a given temperature the abundance of phthalic anhydride detected in the tapes can be seen to increase, however as the temperature of stabilisation increases the amount of phthalic anhydride present in the scans was detected to decrease. It is not clear what is the significance of this phthalic anhydride fragment but if it is an indicator of the stabilising potential of the mesophase pitch-based tapes then perhaps it is suggesting that the lower temperatures of stabilisation are more favourable.

After the partial carbonisation of the tapes which had been stabilised at 160°C, 240°C and 300°C for 25hrs to 450°C (partial carbonisation to was 450°C was used as it was found to be the optimum heat treatment temperature for imparting the maximum strain to failure of the tapes (Sansom et al 2004) Raman was used to determine whether the ordering of the samples had changed as a result. It was observed that the greatest increase in ordering of the tapes occurred in the 240°C stabilised mesophase pitch-based tapes after heat treatment, indicated by the decrease in $D_{(i)}/G_{(i)}$ ratio (table 24). A slight increase in the disorder of the tapes was seen in those samples stabilised to 300°C. This is believed to be as a result of the high carbonyl, carboxyl and ester functionality detected on the surface of the tapes treated to this temperature and the structural damage which the tapes undergo as a result of the higher intensities of CO and CO₂ evolution taking place during heat treatment (figure 123 & 124).

This improved ordering of the tapes upon heat treatment is also seen on a macro scale in Pole figure scans (figure 144, 145 & 146), they illustrate how increasing exposure to oxygen leads to greater disorder in the structure of the tapes. However upon further heat treatment to higher temperatures these defects in the micro-domains of the tapes structure can be seen to be annealed out thus improving the tapes ordering. These findings only reiterate how an optical study (section 9) of the tapes microstructure is an important key in determining the effects of stabilising conditions on the tapes and the subsequent carbonisations.

9 Optical characterisation of stabilised tapes

Optical microscopy is an important method of characterisation for a wide range of carbon materials as a lot can be learned from their microstructure. In order to carry out the optical characterisation of the tapes a Nikon optical microscope was used in reflectance mode linked to a Zeiss Axiocam MRc5 digital camera. The digital camera was connected to a computer using AxioVision software for image processing. Polarised light and a half λ plate was used to observe the interference colours generated by the different orientations present in the carbon lamellae layers of the tapes, blue, yellow and purple are used in order to interpret the optical texture.

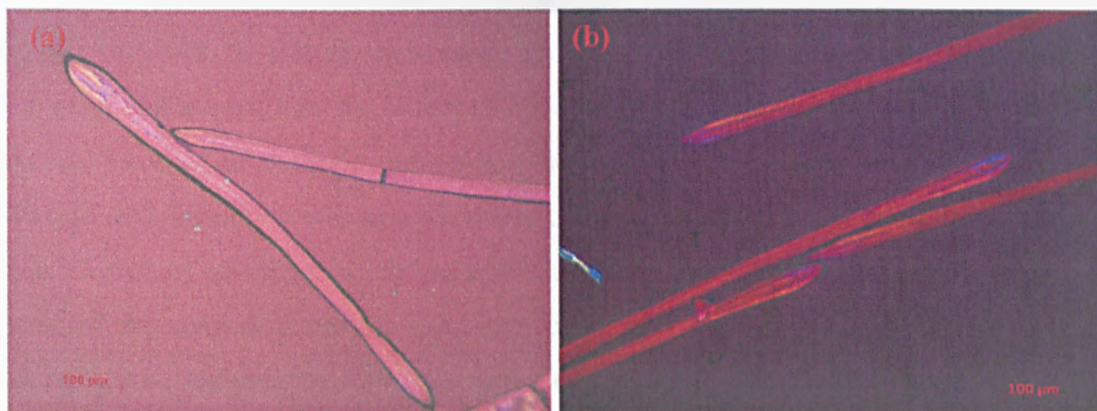


Figure 147 Optical image of tape (a) stabilised at 160°C for 5hrs in O₂ (b) stabilised at 160°C for 25hrs in O



Figure 148 Optical image of tape (a) stabilised at 240°C for 5hrs in O₂ (b) stabilised at 240°C for 25hrs in O₂

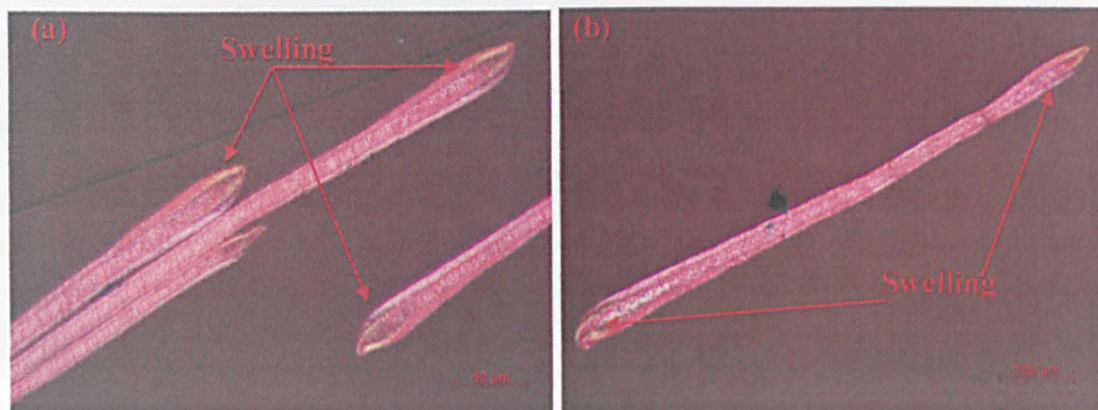


Figure 149 Optical image of tape (a) stabilised at 300°C for 5hrs in O₂ (b) stabilised at 300°C for 25hrs in O₂

Figures 147, 148, & 149 all show tapes which have been stabilised to varying degrees. Not much difference can be observed between the images except for some swelling towards the ends of the tapes which had been stabilised at higher temperatures (figure 149 (a)&(b)). Initially it was suspected that this swell towards the ends of the tapes could be as a result of an effect which has come to be termed “dumb-bell shaped”; this is as a result of the extrusion rate of the tapes being too high when spinning the tapes at relatively low temperatures and pressures (Anton-Arulrajah 2006). This however was quickly dispelled as a possible reason upon examination of the green tapes which shows no sign of the “dumb-bell” effect. There are a couple of possibilities for this, such as decreased pitch viscosity due to stabilisation above the softening point of the pitch or as a result of increased oxygen uptake at the tape edges which becomes more noticeable at higher temperatures. However it is not certain which of these possibilities apply. Once these samples have been carbonised more information can be deduced about the extent and success of the varying stabilisation conditions.

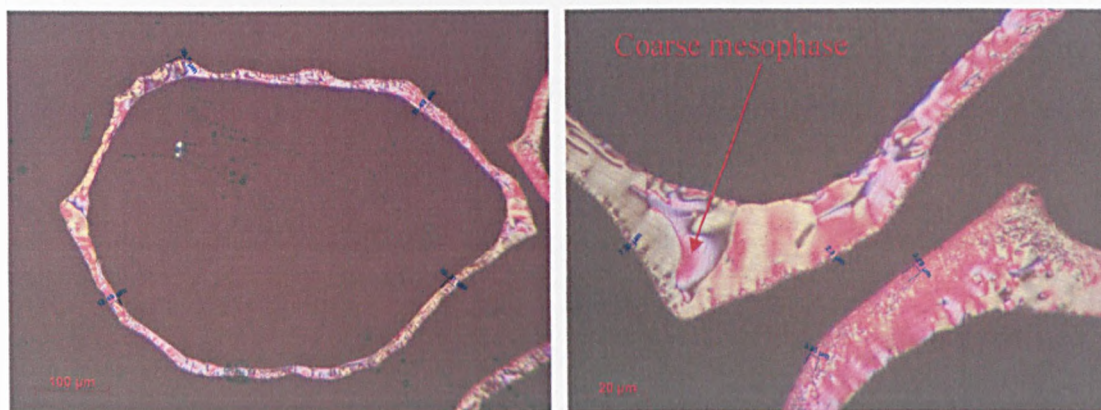


Figure 150 Optical images of samples stabilised at 160°C for 5hrs and carbonised to 1000°C

Figure 150 shows an image of a mesophase carbon tape which has been stabilised to 160°C for 5hrs in oxygen and then carbonised to 1000°C, here a small degree of stabilisation on the surface of the sample is evident accompanied by a coarsening of this mesophase, this is similar to the results reported on carbon-carbon composites by Chioujones and co workers (Chioujones, Ho et al. 2006). However upon carbonisation it is clear that not enough stabilisation has taken place to preserve the dimensional stability of the tape, the tape surface has been stabilised enough to preserve the tape from completely melting. Upon carbonisation the bulk of the tape has melted away only leaving a thinly stabilised shell approximately 2.5µm thick, which remained in tact. The unstabilised material has melted away upon carbonisation as a result of the lower viscosity of the unstabilised regions. The tape has been forced open into an almost circular “shark jaw” shape leaving a small amount of unstabilised mesophase material around the outer shell approximately 15µm thick which has appeared to have coarsened . It is likely that this material did have a small amount of oxygen incorporated into it during the stabilisation step which has gone on to form ether links preventing it from fully melting away. The presence of this is confirmed by work carried out using XPS as an analytical surface technique examining both the C1s, O1s and valance bands and confirming that at lower temperatures of stabilisation an abundance of ether links are present on the tape surface (section 6.5). The formation of these ether links could be responsible for the plastic behaviour of the stabilised outer layer of the tapes.



Figure 151 Optical images of samples stabilised at 160°C for 25hrs and carbonised to 1000°C

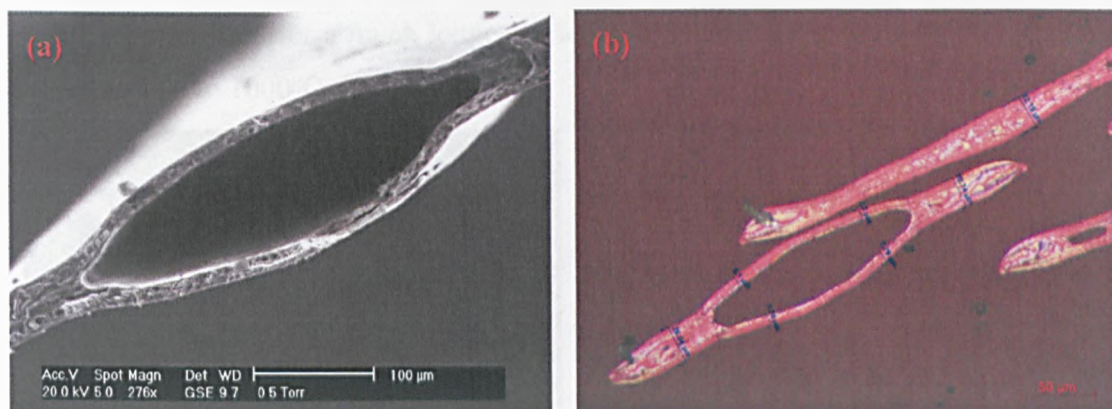


Figure 152 (a) SEM image (b) optical images, of a tape stabilised to 160°C for 25hrs and carbonised to 1000°C

Samples which have been stabilised at 160°C for 25hrs and carbonised (figures 151 & 152) show a similar pattern to the 160°C 5hrs tape only more developed. A thicker stabilised region can be seen on the surface of the tape, thick enough to impart sufficient dimensional stability to prevent the tape being fully forced open during the carbonisation process, The more substantial stabilised shell still however appears to exhibit enough plasticity in order to prevent cracking and splitting taking place upon carbonisation, again most likely as a result of the abundance of ether links present on the tape surface at lower temperatures of stabilisation. As with the 160°C 5hrs tapes some coarsening of the mesophase is present towards the ends of the tapes. The rough shape of the tapes is starting to be preserved although again some of the mesophase pitch from the centre of

the tape has melted away upon carbonisation. Pitch from the centre of the tape that has not melted away can be seen to have none of the orientation imparted to the tapes during the spinning process. This is likely to be as a result of the viscosity of the unstabilised mesophase at some point during the carbonisation becoming sufficiently low and flowing, structurally rearranging the mesophase into larger domains (Chioujones, Ho et al. 2006). Figure 151 & 152 (a) & (b) confirm that this is a consistent occurrence for tapes which have been stabilised under these conditions. It is likely that with careful control of the stabilisation conditions of mesophase tapes it may well be possible to constantly produce hollow tapes. It should be noted that the hollow tapes shown in figure 151 and 152 are different from the hollow tapes shown in figure 45 (a) as these tapes have been stabilised for a much longer period of time and have undergone a subsequent heat treatment to 1000°C

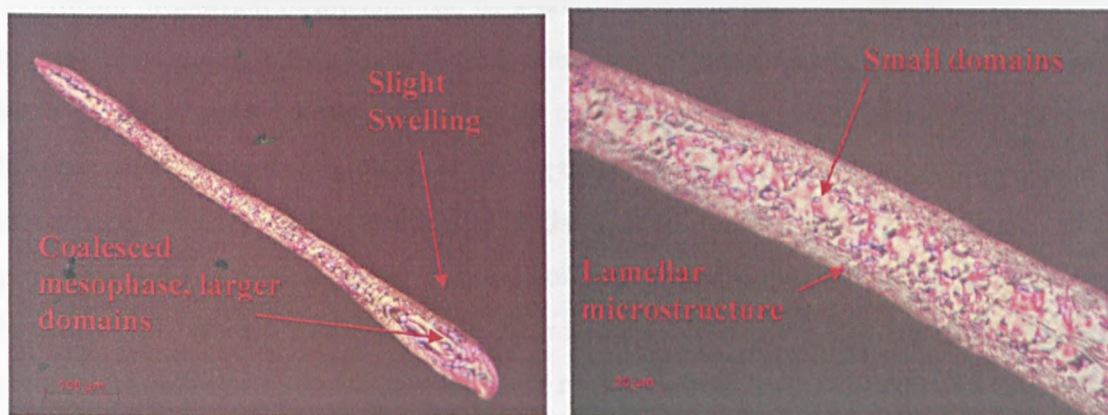


Figure 153 Optical images of samples stabilised at 240°C for 5hrs and carbonised to 1000°C

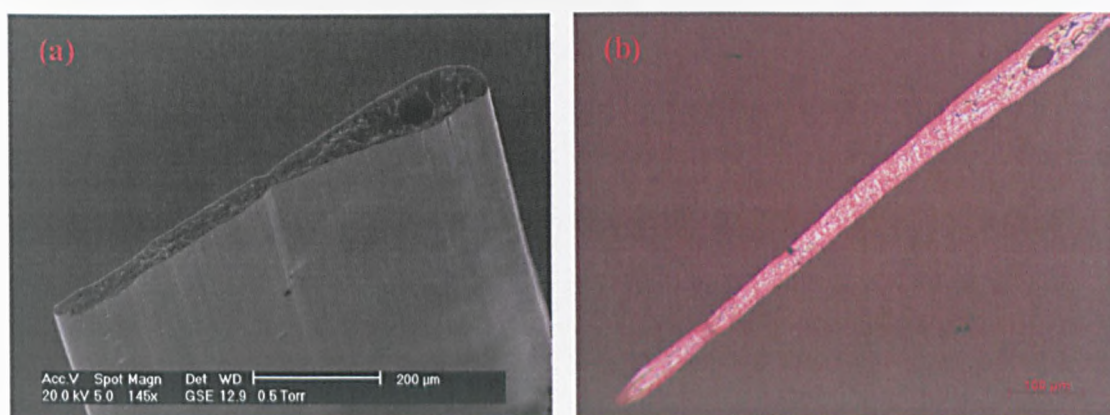


Figure 154 (a) SEM image (b) optical image of a tape stabilised at 240°C for 5hrs and carbonised to 1000°C

At 240°C the stabilisation reaction is accelerated over the shorter 5 hr periods, here a significant proportion of the tape can be seen to have maintained its dimensional stability and morphology. A much thicker outer crust of stabilised material can be observed in these samples, upon closer inspection of the original images the controlled lamellae microstructure imparted to the tapes during the controlled spinning process is evident in this region. Only a slight swelling towards one end of the tape can be seen, this is generally consistent throughout tapes stabilised under these conditions as shown in (figure 153 (a) & (b)). The mesophase pitch in the middle of the tape which has not been completely stabilised can be seen to have more controlled orientation than that of the 160°C sample in the respect that the mesophase domains are present are smaller and that the larger coalesced domains present in the lower temperature stabilised samples. This is almost certainly linked to the abundance of oxygen present through out the sample as shown by EPMA data on the cross-sections of tapes stabilised to varying degrees (section 7.3). However after only 5hrs at 240°C the tapes are by no means fully stabilised, evident in Figure 154 (a) & (b)) by the small amount of unstabilised mesophase pitch towards one end of the tape has melted away during the carbonisation.

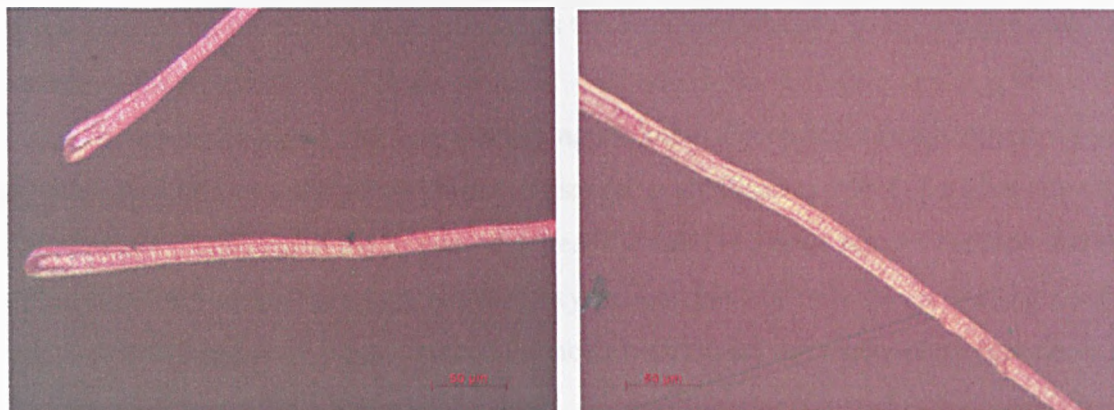


Figure 155 Optical images of samples stabilised at 240°C for 25hrs and carbonised to 1000°C



Figure 156 Optical image of a tape stabilised at 240°C for 25hrs and carbonised to 1000°C showing the alignment of the mesophase micro domains

Once carbonised the tape which have seen a stabilisation at 240°C for 25hrs in oxygen appear to have undergone a sufficient amount of stabilisation to fully maintain both the dimensional stability of the tapes and its morphology (figure 155). Examining figure 156 the stabilised crust is still evident; as stabilisation at elevated temperatures is a diffusion controlled reaction the surface of the tapes will always experience the highest degree of stabilisation. However lamellar microstructure is also evident through out the full width

of the tape all be it not as closely packed as the lamellar domains in the oxygen rich out surface of the tapes.

It should be noted that when polishing the tapes for optical microscopy it proved difficult to obtain an even polish across the samples stabilised at 240°C for 25hrs due the difference in toughness of the oxygen rich heavily stabilised crust around the tape and the softer stabilised core. This suggests that oxygen content not only has a bearing on the extent of stabilisation a sample has experienced but also on the mechanical properties of the final mesophase pitch based tape.

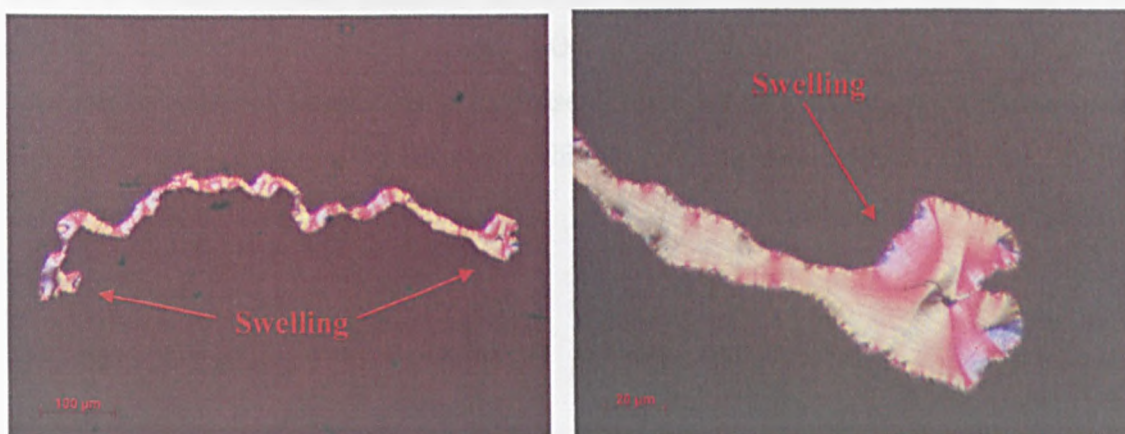


Figure 157 Optical images of samples stabilised at 300°C for 5hrs and carbonised to 1000°C

Figure 157 shows a tape which has been stabilised to 300°C for 5hrs and then carbonised. A thin stabilised crust can be seen around the surface of the tape. However, it is clear that during the carbonisation step a severe shrinkage of the tape has taken place. EPMA Data shows that those samples which have experienced higher temperatures of stabilisation have a greater abundance of oxygen present at their surfaces. The small layer of stabilised material may well have been thicker before carbonisation but may have burnt off as a result of the oxygen rich skin layer that forms at higher temperature of stabilisation. As in the un-carbonised sample stabilised at 300°C for 5hrs swelling of the tape is still evident towards the tape edges (figure 149 (a)).

There are two possible explanations for edge swelling; it could be as a result of a change in orientation of the tapes from 1-2 to 1-3 orientation, this would result in the tapes contraction in a different direction during carbonisation. The 1-2 orientation would

shrink across the thickness of the tape i.e. in the 3 direction, where the 1-3 orientated lamellae would contract across the width of the tape i.e. in the 2 direction. However this hypothesis was made redundant upon closer inspection of Figure 157 (b), clear 1-2 lamellar microstructure is evident running parallel to the tapes major surface even at the edges. Therefore as a sound alternative it maybe that as the tapes are carbonised the centre of the tapes becomes less viscous allowing it to flow. (This remains unstabilised due to the formation of the skin core structure at the higher temperature of stabilisation, as reported in ThAFM data) However at higher temperatures the stabilised outer crust does not exhibit as much plasticity as in the samples stabilised at 160°C due to its chemical makeup i.e. more C=O and C-OH groups present. Therefore in the 300°C stabilised sample the unstabilised mesophase is forced to flow to the edges illustrated in Figure 157 upon carbonisation since the stabilised outer regions contract together.

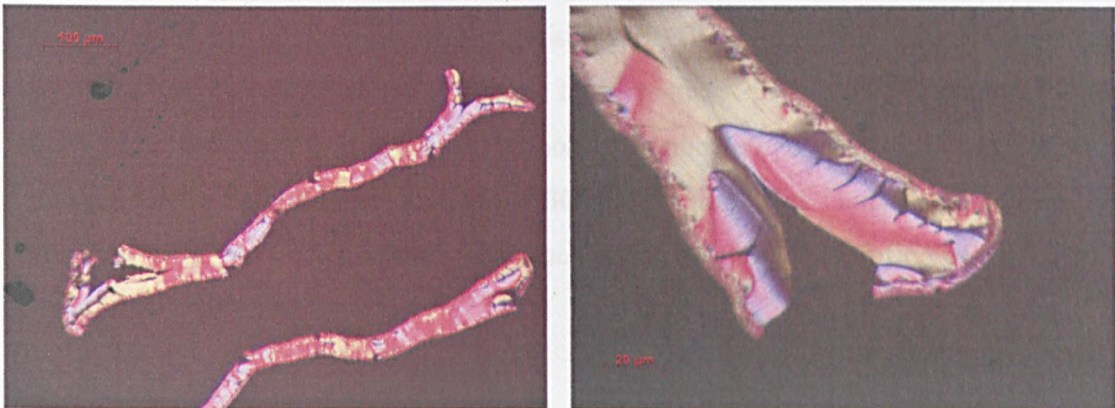


Figure 158 Optical images of samples stabilised at 300°C for 25hrs and carbonised to 1000°C

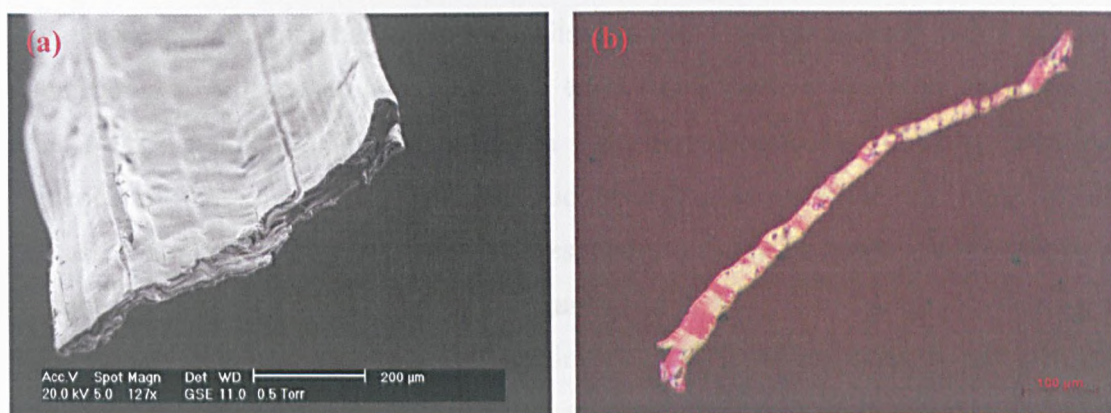


Figure 159 (a) SEM image (b) optical image of a tape stabilised at 300°C for 25hrs and carbonised to 1000°C

Figure 158 shows a tape which has undergone stabilisation at 300°C for 25hrs and subsequent carbonisation to 1000°C, a thick crust is evident around the outer layer of the tape, similar to that seen in the samples stabilised at 300°C for 5hrs but much thicker. In the case of the sample stabilised for 25hrs the thicker skin structure results in greater shape preservation and rigidity in the sample upon carbonisation. By the same mechanism as described above for the tape stabilised at 300°C for 5hrs. This leads to the viscous core being very strongly forced towards the tape edges resulting in splitting of the edges as seen in Figure 158 & 159.

9.1 Optical conclusion

Very little can be determined optically about the extent of the stabilisation which has taken place in the mesophase pitch-based carbon tapes after the stabilisation step apart from some slight swellings which can be observed towards the ends in those tapes which have been stabilised at 300°C. After subsequent carbonisation to 1000°C the effect of the varying stabilisation conditions in imparting dimensional stability and maintaining the molecular alignment during the spinning process becomes more apparent.

At the lower temperature of 160°C over both times of 5 and 25hrs it is clear that insufficient stabilisation has taken place although in both cases coarsening of the mesophase is evident as well as an outer shell of stabilised material, which appears to still exhibit some plasticity (figures 150, 151 & 152).

Mesophase pitch based tapes stabilised at 240°C shows a much higher degree of dimensional stability when compared with tapes stabilised over the same time period at both 160°C and 300°C. The tapes which have been treated at 240°C for 5hrs show evidence of the aligned 1-2 lamellar microstructure imparted to the tapes in their processes, a mixture of larger and small mesophase domains and only a slight swelling is evident towards the ends of the tapes (figures 153 & 154). This increased dimensional stability and maintained morphology points to 240°C being close to the optimum temperature of stabilisation. After 25hrs at 240°C the mesophase pitch-based carbon tapes have undergone sufficient stabilisation to fully maintain both their dimensional stability and morphology (figures 155 & 156).

The mesophase pitch-based tapes which were stabilised at 300°C at both 5hrs and 25hrs and subsequently carbonised to 1000°C show a very different behaviour. Here after the carbonisation step severe shrinkage can be observed with swelling evident towards the ends of the tapes and in the cases of the 300°C, 25hr tapes splitting at the edges is evident (figures 158 & 159). This effect is believed to be as a result of the over stabilisation of the outer skin of the tape and this leads to the formation of a skin-core structure which inhibits the access of oxygen into the centre of the tape and thus the stabilisation process, as discussed earlier in EPMA and ThAFM results.

All of the optical results presented tie in with the data from both the EPMA and ThAFM. Not only is there a correlation between the softening points of the mesophase across the tapes transverse cross-section and the local oxygen content prior to carbonisation but also a correlation between the local oxygen distribution across the tapes and the extent of maintained dimensional stability and morphology post carbonisation. The tapes which show the most even distribution of oxygen (figures 106 & 107) i.e. the 240°C tapes exhibit a much greater success of maintained morphology.

As a result of the effects of the different microstructure which are realised as a consequence of the varying stabilising conditions it would be of interest to investigate how the mechanical properties of the mesophase pitch-based carbon tapes are affected by the different conditions.

10 Mechanical properties

10.1 Strength and engineering Young's modulus of mesophase pitch - based carbon tapes

Previous work carried out by Sansom as part of an undergraduate project on tapes stabilised at 240°C for 5hrs then and heat treated to a range of temperatures below 1000°C illustrated how heat treatment temperature affected the mechanical properties of the mesophase pitch-based tapes (Sansom et al 2004). It is evident from the typical example of a load displacement curve produced by the mesophase pitch-based tapes (figure 160) that displacement increases with load in a linear manner. The load increases to the maximum before the tape experiences a catastrophic failure, which is indicative of a brittle material.

The optimum heat treatment temperature for the tapes in terms of maximised strain to failure is 450°C; at this temperature the tape can withstand stresses up to 2.74N and a displacement of as much as 0.4mm before failure (table 25).

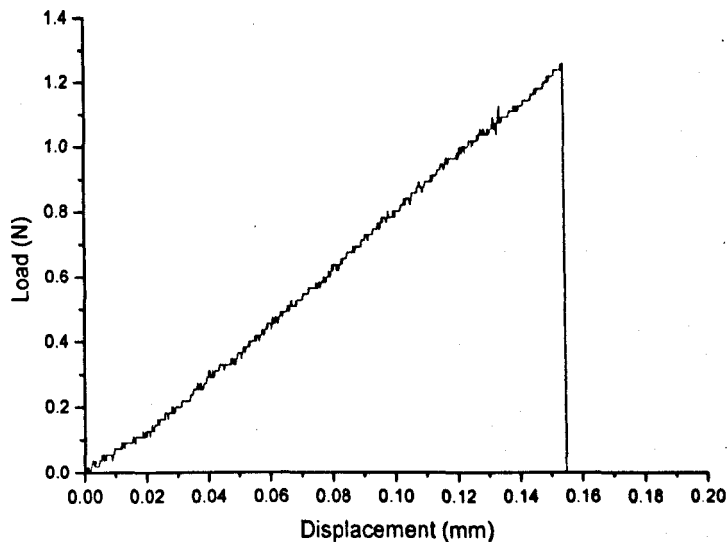


Figure 160 Typical example of an original load displacement curve produced when mechanically testing mesophase pitch based tapes which have undergone stabilisation at 240°C for 5hrs in Oxygen and subsequently been heat treated to 400°C (Sansom 2004).



Table 25 Average load displacement table for tapes heat treated to different temperatures after stabilisation at 240°C for 5hrs (Sansom 2004) average results are an average of 10 samples.

| Sample | Average Load (N) | Average Displacement (mm) |
|--------|------------------|---------------------------|
| Green | 0.27 | 0.06 |
| 250°C | 0.62 | 0.12 |
| 350°C | 0.81 | 0.15 |
| 400°C | 1.25 | 0.16 |
| 450°C | 2.74 | 0.40 |
| 500°C | 3.59 | 0.24 |
| 600°C | 4.22 | 0.14 |
| 700°C | 5.80 | 0.10 |

Table 26 illustrates the stress-strain results for tapes stabilised in oxygen at 240°C for 5hrs and then heat treatment at a range of temperatures. Linear fracture behaviour is apparent, implying that no relaxation of the stresses on these mesophase pitch-based carbon tapes takes place before the tape fails in a brittle and catastrophic manor (figure 161). The maximum tensile strength of the tape increases with increasing heat treatment temperature (table 26).

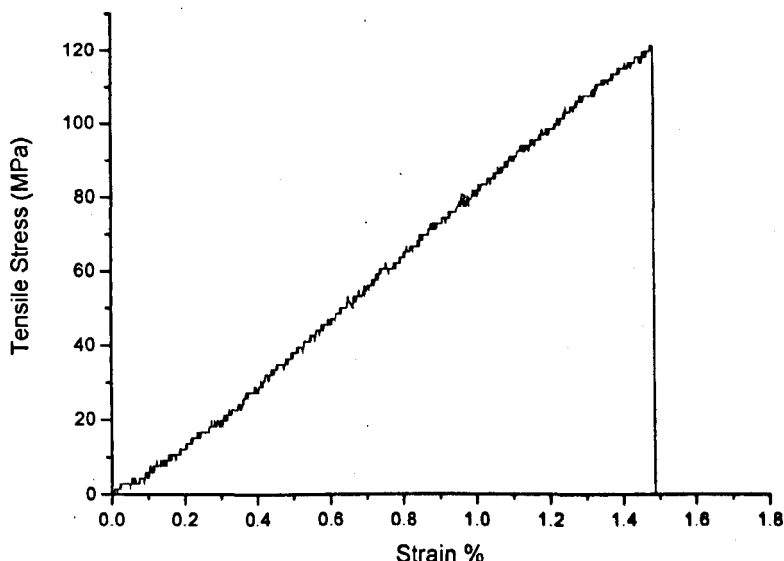


Figure 161 Typical example of an original stress-strain curve produced when mechanically testing mesophase pitch based tapes which have under gone stabilisation at 240°C for 5hrs in Oxygen and subsequently been heat treated to 450°C (Sansom 2004).

Table 26 Stress strain table for tapes stabilised at 240°C for 5hrs and subsequently heat treated to a variety of temperatures (Sansom 2004)

| Sample | Average Strain (%) | Average Tensile Strength (MPa) | Strength standard deviation (MPa) | Average Engineering Young's Modulus (MPa) | Engineering Young's Modulus standard deviation (MPa) |
|--------|--------------------|--------------------------------|-----------------------------------|---|--|
| Green | 0.3 | 12 | ±7 | 41 | ±12 |
| 250°C | 0.5 | 27 | ±5 | 57 | ±6 |
| 350°C | 0.6 | 39 | ±6 | 65 | ±7 |
| 400°C | 0.7 | 45 | ±5 | 67 | ±11 |
| 450°C | 1.5 | 119 | ±12 | 79 | ±7 |
| 500°C | 1.0 | 135 | ±10 | 132 | ±9 |
| 600°C | 0.7 | 158 | ±10 | 225 | ±12 |
| 700°C | 0.5 | 263 | ±13 | 527 | ±25 |

This is a logical pattern of events, as the heat treatment temperature increases to 1000°C (carbonisation temperature) the number of ether links present in the tapes will be reduced as heteroatoms are eliminated and replaced by even more carbon-carbon bonds. Subsequently condensation of polyaromatic species imparts a lower strain to failure in the tapes but also significantly increased tensile strength (figure 162). The elimination of heteroatoms through out the carbonisation of the stabilised mesophase pitch-based tapes is illustrated in the Py-GCMS section 8.4, figures 134-139.

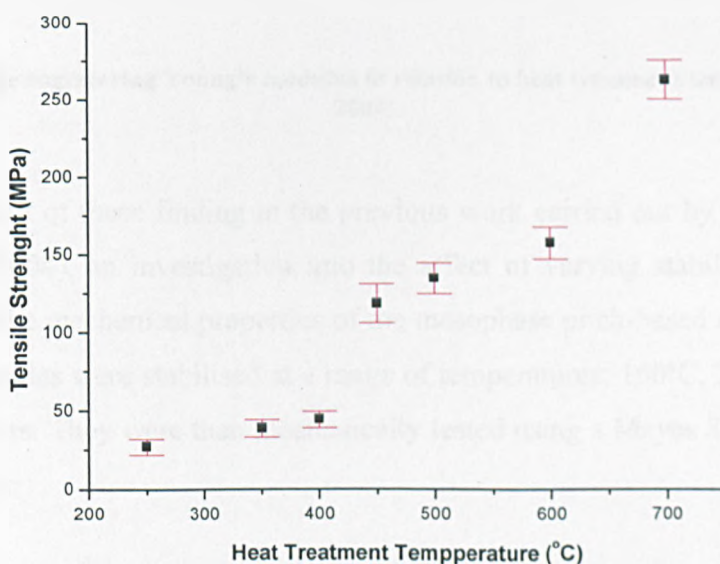


Figure 162 Tensile strength of the tape in relation to heat treatment temperature (Sansom 2004)

The engineering Young's modulus of the tapes can also be seen to increase with increasing heat treatment temperature (HTT). The "modulus" is observed to be ~ 41 MPa for the green tapes and the "modulus" value of the stabilised tape is seen at ~ 60 MPa increasing to a value of ~ 526 MPa at a maximum HTT of 700°C (table 26 & figure 163).

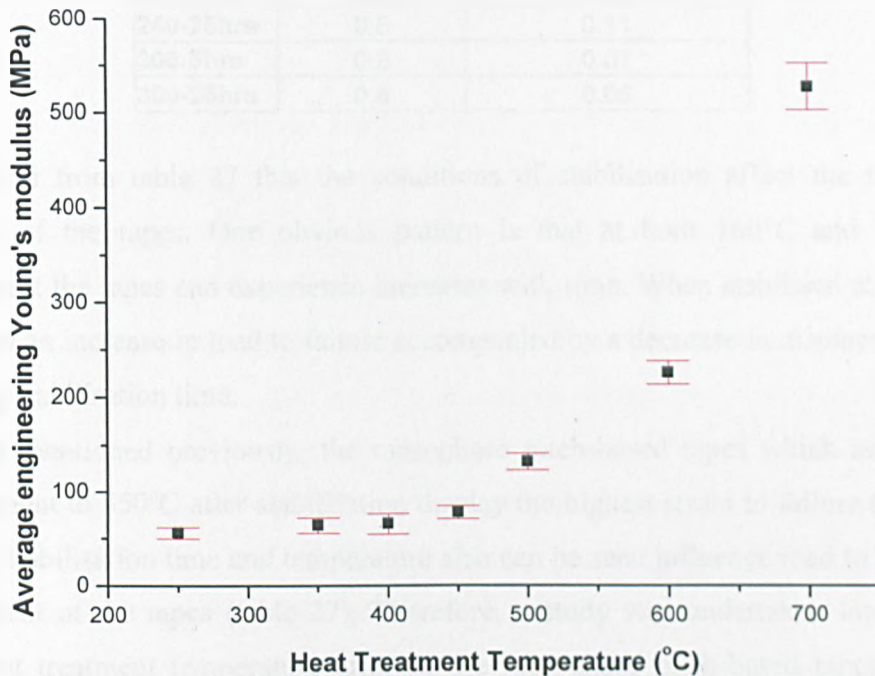


Figure 163 Average engineering Young's modulus in relation to heat treatment temperature (Sansom 2004)

As a result of these findings in the previous work carried out by Sansom in 2004 (Sansom et al 2004), an investigation into the effect of varying stabilisation time and temperature on the mechanical properties of the mesophase pitch-based carbon tapes was undertaken. Samples were stabilised at a range of temperatures; 160°C, 240°C and 300°C for 5hrs and 25hrs. They were then mechanically tested using a Mayes SM50 mechanical testing apparatus.



Table 27 Average load-displacement table for mesophase tapes which have experienced a variety of stabilisation conditions

| Sample | Average Load (N) | Average Displacement (mm) |
|-----------|------------------|---------------------------|
| Green | 0.3 | 0.06 |
| 160-5hrs | 0.3 | 0.07 |
| 160-25hrs | 0.4 | 0.08 |
| 240-5hrs | 0.5 | 0.08 |
| 240-25hrs | 0.6 | 0.11 |
| 300-5hrs | 0.8 | 0.07 |
| 300-25hrs | 0.8 | 0.06 |

It is evident from table 27 that the conditions of stabilisation affect the mechanical properties of the tapes. One obvious pattern is that at both 160°C and 240°C the displacement the tapes can experience increases with time. When stabilised at 300°C the tapes show an increase in load to failure accompanied by a decrease in displacement with increasing stabilisation time.

As mentioned previously, the mesophase pitch-based tapes which underwent a heat treatment to 450°C after stabilisation display the highest strain to failure (Sansom et al 2004). Stabilisation time and temperature also can be seen influence load to failure and displacement of the tapes (table 27). Therefore, a study was undertaken into how this 450°C heat treatment temperature affected the mesophase pitch-based tapes stabilised under different conditions.

Tape samples were again stabilised over the same range of conditions and heat treated to 450°C. Table 28 shows that tapes which have been stabilised at 160°C and 240°C for 25hrs exhibit a marginally higher tensile strength and strain to failure than the tapes stabilised for 5hrs. In contrast, the tape stabilised at 300°C shows a greater strain to failure after stabilisation for 5 hrs than after 25hrs (table 28). However, in all cases, upon subsequent heat treatment of these samples to 450°C, the tapes experiencing the 25hr stabilising period now exhibit higher tensile strength but a lower strain to failure than those stabilised for 5hrs.

It is important to recognise the significant increase that the 450°C heat treatment imparts both to the tensile strength and to the strain to failure for all of the samples. One possible explanation for this is that during the stabilisation period, oxygen infiltration into

the sample takes place (EPMA 7.3, CHNO chemical analysis Table 9, XPS 6.5, FTIR 6.4) but only partial cross-linking occurs. When the tapes are heat treated to 450°C the number of cross-linking reaction is significantly accelerated between the mesophase pitch and incorporated oxygen. Table 28 also show that the maximum strain to failure occurs for the 240°C tapes, both after stabilisation and after the 450°C heat treatment (table 28). The maximum tensile strength also appears to be achieved for tapes stabilised at 240°C, both before and after heat treatment (table 28).

It is clear from previous work (FTIR 6.4, EPMA 7.3, and XPS 6.5) that, as stabilisation proceeds and oxygen enters the tapes, the presence of C-O-C (ether) linkages increases, representing cross-linking within the tapes. This correlates with an increased strain to failure at a later stage of production (i.e. after 450°C heat treatment), this relationship was also noticed in the work of Kaushik (Kaushik and Bhardwaj 1994)

It is possible that the ether links impart the increased mechanical strain to failure to the tapes with the ether linkages acting as springs when loaded under tension. The idea of the C-O-C ether linkages within the tapes being more flexible than C-C bonds leads to one possible explanation why the tapes stabilised for longer periods of time exhibit increased tensile strength but reduced strain to failure after the subsequent heat treatment step. The presence of oxygen gives rise to the subsequent formation of ether links upon heat treatment. It is fair to assume that the greater the oxygen content, the greater the probability of ether link formation. Using the analogy of an ether link acting as a spring (greater flexibility than C-C bonds) within the tape to impart greater strength and strain to failure (table 28) it can be hypothesised that the greater the number of ether links present, the higher the tensile strength of the material will become. However, although the addition of small quantities of ether links may have little effect on engineering Young's modulus (or even reduce it somewhat), with increasing numbers of ether links comes the increased likelihood of them becoming entangled as a result of the disorder the oxygen imparts to the tapes structure, causing the material to become stiffer. In essence the inclusion the ether links into the mesophase carbon structure caused the basal planes to become hyperfunctionalised and act as hyperbranched polymer. (Kwak, Ahn et al. 2004). Trollsas and co-workers reported in there work on hyperbranched polymers that highly

branched architecture produces materials with inevitable brittleness (Trollsas et al 1998). This factor, accompanied by a greater number of C-C bonds forming at higher temperatures of stabilisation and heat treatment as the mesophase pitch tends towards carbonisation, could well be responsible for the decrease in the strain to failure of the tapes.

The combination of high mechanical strength and high strain to failure displayed by the samples stabilised at 240°C (table 28) may well result from the achievement of a suitable balance of ether linkages and C-C bonds after the 450°C heat treatment. (The 240°C-stabilised tape shows a good proportion of Oxide I in the XPS results (table 13) which can be linked to a greater presence of ether links). Those tapes which have undergone stabilisation at only 160°C followed by the 450°C heat treatment may not have developed as many C-C bonds, and this is manifested in the low tensile strengths displayed by these tapes. The tape stabilised at 300°C can be seen via XPS (table 13) to have an under-developed proportion of ether links prior to being heat treated at 450°C, which may well be accompanied by a correspondingly greater proportion of C-C bonds as a result of the higher stabilisation temperature. These tapes therefore display a high tensile strength but low strain to failure.

Table 28 Table displaying the Stress strain and engineering Young's modulus data for tape samples stabilised at 160°C, 240 °C and 300 °C for 5 and 25 hrs and then subsequent heat treatment to 450°C

| Stabilisation Condition | Average Strain % | Average Tensile Strength (MPa) | Strength standard deviation (MPa) | Average Engineering Young's Modulus (MPa) | Engineering Young's Modulus standard deviation (MPa) |
|-------------------------|------------------|--------------------------------|-----------------------------------|---|--|
| Green | 0.3 | 12 | 6 | 41 | 12 |
| 160°C 5hrs | 0.3 | 14 | 3 | 51 | 14 |
| 160°C 25hrs | 0.3 | 15 | 2 | 50 | 11 |
| 240°C 5hrs | 0.3 | 22 | 3 | 70 | 11 |
| 240°C 25hrs | 0.4 | 24 | 3 | 53 | 7 |
| 300°C 5hrs | 0.3 | 30 | 3 | 101 | 10 |
| 300°C 25hrs | 0.3 | 32 | 3 | 129 | 9 |
| 160°C 5hrs (450°C) | 1.0 | 63 | 12 | 64 | 8 |
| 160°C 25hrs (450°C) | 0.8 | 76 | 8 | 100 | 9 |
| 240°C 5hrs (450°C) | 1.6 | 119 | 10 | 74 | 13 |
| 240°C 25hrs (450°C) | 1.1 | 145 | 14 | 129 | 7 |
| 300°C 5hrs (450°C) | 0.6 | 104 | 10 | 170 | 10 |
| 300°C 25hrs (450°C) | 0.4 | 138 | 15 | 374 | 16 |

Tensile strength of the tapes increases with increasing stabilisation time and temperature both at 5 and 25hrs of stabilisation. After the 450°C heat treatment a dramatic improvement in the tensile strength of the tapes can be observed with the maximum values being recorded after stabilisation at 240°C both for tapes stabilised for 5hr and 25hr (figure 164). For the tapes stabilised at 300°C and heat treated a slight decrease in the tensile strength from the 240°C heat treated tapes is observed. This decrease in the tensile strength of the 300°C sample is likely to be as a result of the higher oxygen content on the surface of the tape as shown in the EPMA results (figure 106 & 107). In other words, over oxidation has led to the development of structural defects (as seen in the optical characterisation section 9) in the tapes as a result of the large quantities of evolved CO, CO₂ during the carbonisation process (as shown in TGA-FTIR results in the carbonisation section 8.2 figures 123,124 & table 19).

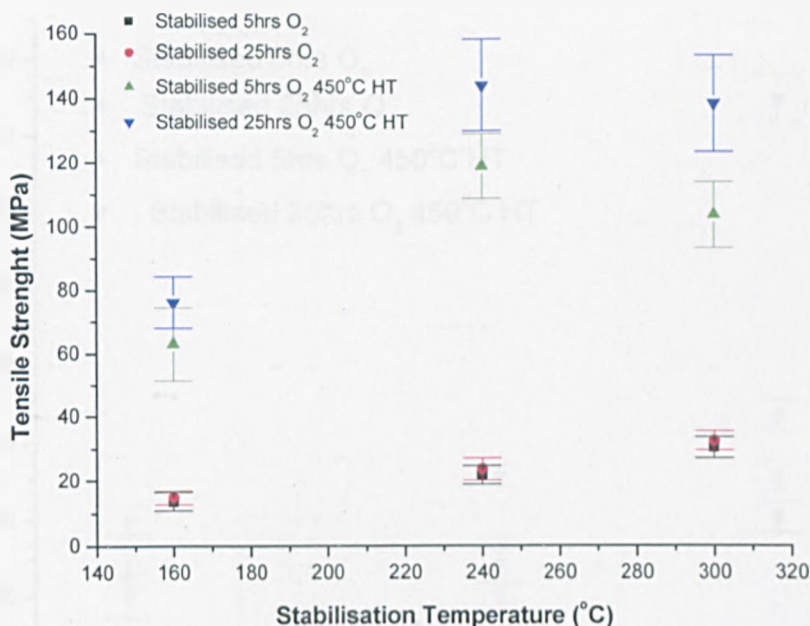


Figure 164 Change in tensile strength with stabilisation conditions, time, temperature and 450°C heat treatment temperature

The engineering Young's modulus of the majority of the mesophase pitch based tapes can be seen to increase both with stabilisation temperature and time (figure 165). However, this trend is broken for the mesophase pitch based tape which has been stabilised at 240°C for 25hrs, here the tapes displays a lower engineering Young's modulus that the other tapes. This could be as a result of the formation of the more flexible C-O-C during the stabilising step. The most significant increase in engineering Young's modulus can be observed in those samples which have undergone the 25hr stabilisation period at the 300°C and then subsequently heat treated to 450°C. This increase in engineering Young's modulus with stabilisation is likely to be as a result of an increased number of stronger stiffer C-C bonds which develop as a result of the tapes tending towards a more graphitic structure as carbonisation progresses (XPS, table 13). The formation of a mechanically tough skin-core structure on the periphery of the tapes (as demonstrated in ThAFM 7.2, EPMA 7.3 and optical characterisation 9.0 sections) could also be a contributing factor to an increase in engineering Young's modulus.

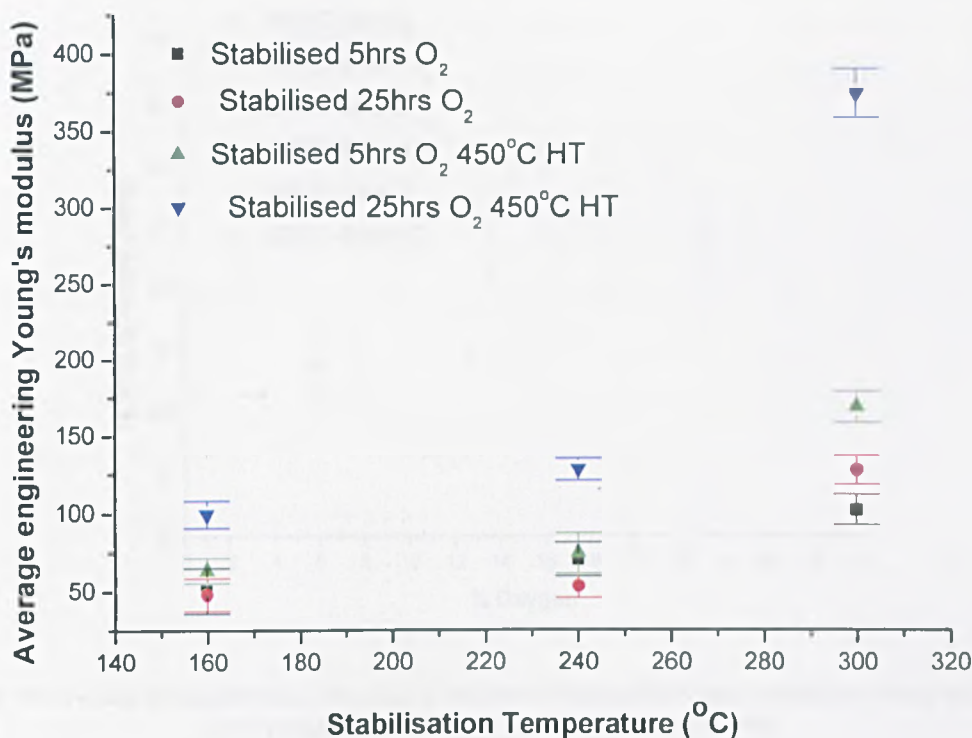


Figure 165 Change in average engineering Young's modulus with stabilisation conditions, time, temperature and 450°C heat treatment temperature

As stabilisation is evidently reliant on the incorporation of oxygen into the mesophase pitch-based tapes and stabilisation time and temperature clearly have an effect on the mechanical properties of the resultant carbon tapes, it was of interest to compare how oxygen content affected the tapes' mechanical properties. Figure 166 shows how increasing oxygen content increases the tensile strength of the tapes. Figure 167 illustrated how the subsequent 450°C heat treatment significantly increases the tensile strength of the tapes even with a reduction in % oxygen content (notable all the tapes with the exception of the 300°C 25hr sample sees approximately a 50% reduction in % oxygen content after heat treatment to 450°C) as a result of the evolution of CO and CO₂ during heat treatment (TGA-FTIR results in the carbonisation section 8.2 figures 123,124 & table 19).

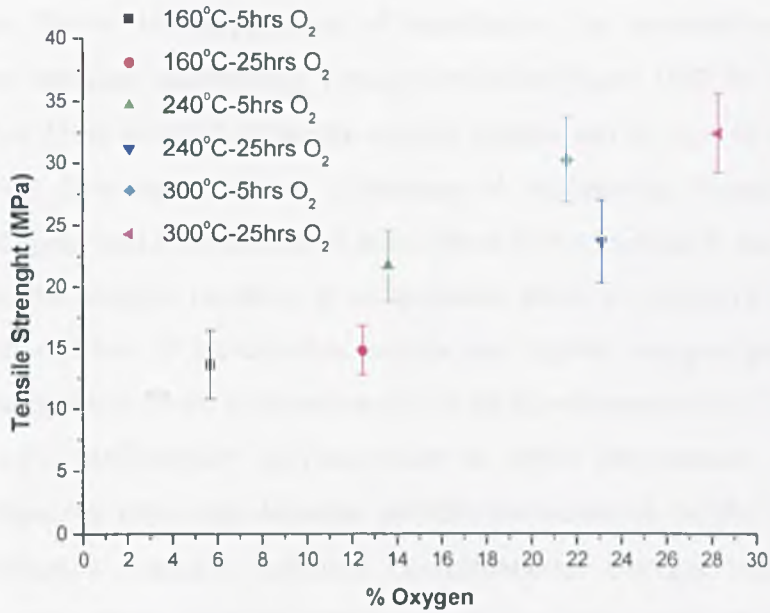


Figure 166 Tensile strength versus % oxygen content of mesophase tapes which have been stabilised over range of stabilisation times and temperatures

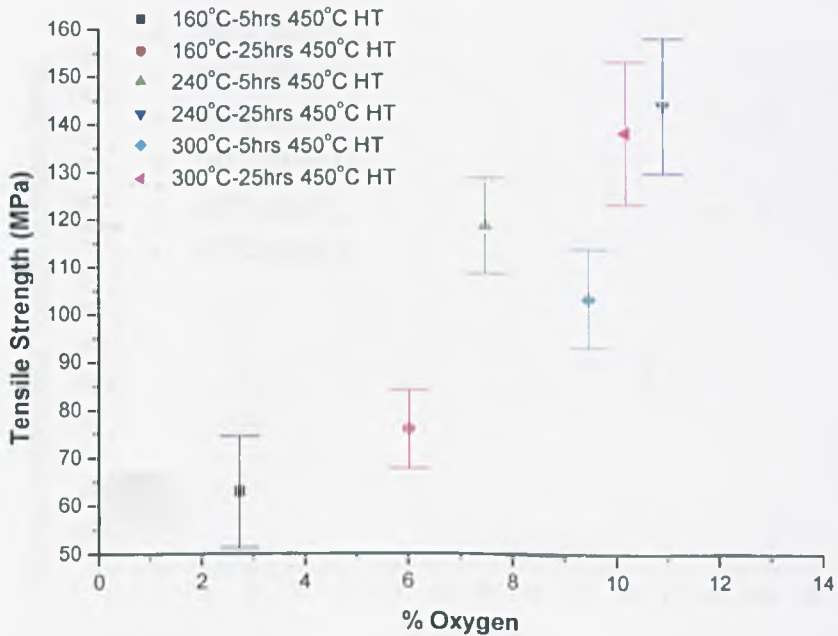


Figure 167 Tensile strength versus % oxygen content of mesophase tapes which have been stabilised over range of stabilisation times and temperatures and subsequently heat treated to 450°C



When comparing oxygen content of the tapes against engineering Young’s modulus it is clear that after 5hrs at all temperatures of stabilisation the increased oxygen content translates to an increased engineering Young’s modulus (figure 168). In the case of the 240°C tape after 25hrs of stabilisation the oxygen content can be seen to have increased from that of the 5hrs tape, however a decrease in engineering Young’s modulus is observed. This again could be considered as evidence for an increase in the number of C-O-C present in the samples resulting in an increased strain to failure of the tapes. The 300°C tape after 25hrs of stabilisation exhibit the highest oxygen and engineering Young’s modulus, this is likely to be as a result of the development of C-C bonds and the development of a mechanically stiff skin-core at higher temperatures (ThAFM 7.2, EPMA 7.3). However there may be other possible explanations for the increase in the engineering Young’s modulus including conformational changes which affect the viscoelasticity of the pitch. For those samples which have been stabilised and heat treated to 450°C, the engineering Young’s modulus increases with stabilisation temperature and time, despite a reduction in oxygen content (figure 169).

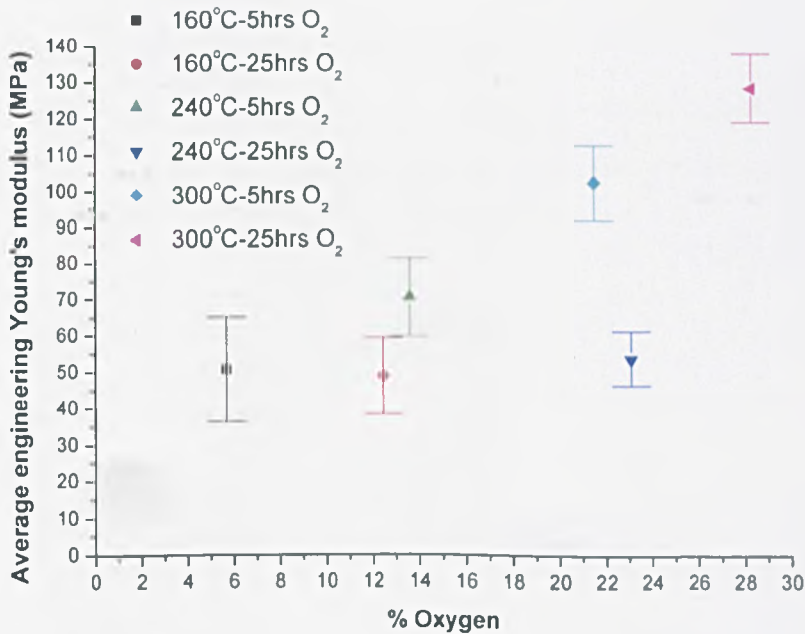


Figure 168 Average engineering Young’s modulus versus % oxygen content of mesophase tapes which have been stabilised over range of stabilisation times and temperatures

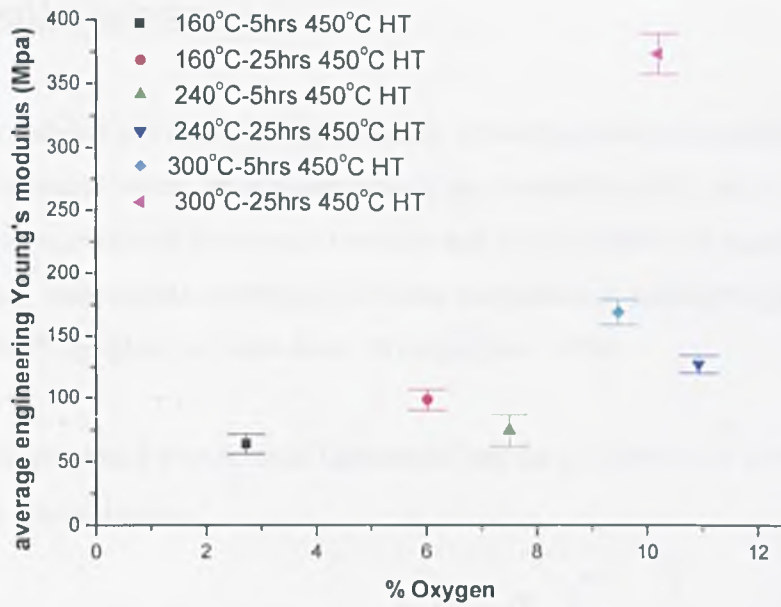


Figure 169 Average engineering Young's modulus versus % oxygen content of mesophase tapes which have been stabilised over range of stabilisation times and temperatures and subsequently heat treated to 450°

10.2 Weibull Analysis

The Weibull modulus is a material characteristic of mechanical homogeneity; it indicates the spread of strength values, m is a measure of the variability of the set. A larger m (30-40) indicates a material that is not very variable and thus "reliable". A smaller value (3-4) indicates a very wide spread of strengths. Some comparisons; soda-lime glass: 2-3, SiC: 4-10, Si₃N₄: 6-15, graphite: 12, cast iron: 38 (Jayatilaka 1979).

Weibull (1936) proposed an empirical formula to link the probability of survival (P_s) to a given stress σ shown below:

$$P_s = 1 - \exp \left[- \int_v \left(\frac{\sigma - \sigma_u}{\sigma_o} \right)^m dv \right]$$

Equation 8 Weibull Equation

Where;

V is the Volume of the specimen under uniaxial stress

σ_u is the minimum strength possible within the sample set (often taken as 0 in practice),

σ_o is a characteristic strength normalising parameter (often for convenience replaced with 1) m the Weibull modulus.

Denoting σ_f as the fracture strength of the specimen,

$$p_f = 1 - \exp \left[-v_c \left(\frac{\sigma_f - \sigma_u}{\sigma_o} \right)^m \right]$$

Equation 9 Weibull modulus equation



Where V_c is the effective volume of the test specimen which can expressed as

$$V_c = \int_v \left(\frac{\sigma - \sigma_u}{\sigma_f - \sigma_u} \right)^m dv$$

Equation 10 Weibull modulus equation

For specimens tested in uniaxial tension, σ is equal to σ_f Equation 10 gives $V_c = V$ thus equation 9 can be simplified as.

$$P_s = 1 - \exp \left[- \left(\frac{\sigma_f - \sigma_u}{MOR_o} \right)^m \right]$$

Equation 11 Weibull modulus equation

Where $MOR_o = \sigma_o V_c^{-1/m}$ is constant thus Equation 11 can be rearranged.

$$\ln \left[\ln \left(\frac{1}{1 - P_f} \right) \right] = m \ln (\sigma_f - \sigma_u) - m \ln MOR_o$$

Equation 12 Weibull modulus equation in form suitable for plotting

The Weibull modulus m is given by the gradient of a linear graph when plotting $\ln\{\ln[1/(1-P_f)]\}$ against $\ln(\sigma_f - \sigma_u)$

The method for finding the Weibull modulus can be explained best by calculating an example. Nine tensile strength values of Green tapes are used to calculate the probability of survival P_s , using the equation;

$$P_f = 1 - i / (N+1)$$

Equation 13 Probability of tape survival

i is the sample rank ($i=2$ for second sample),

N is the total number of samples ($N=9$).

The tensile strengths should be ranked in increasing order.

Table 29 X-Y Co-ordinate parameters of Weibull plot

| Green | | X axis data | Y axis data |
|---------------|------------------|---------------------|-------------------------|
| Sample Number | Tensile Strength | ln Tensile Strength | $\ln\{\ln[1/(1-P_f)]\}$ |
| 1 | 3598455 | 15.10 | -2.25 |
| 2 | 7196911 | 15.79 | -1.50 |
| 3 | 7898538 | 15.88 | -1.03 |
| 4 | 8096524 | 15.91 | -0.67 |
| 5 | 8996138 | 16.01 | -0.37 |
| 6 | 10584531 | 16.17 | -0.09 |
| 7 | 17298978 | 16.67 | 0.19 |
| 8 | 19809335 | 16.80 | 0.48 |
| 9 | 23389959 | 16.97 | 0.83 |

This data is then plotted in figure 170.

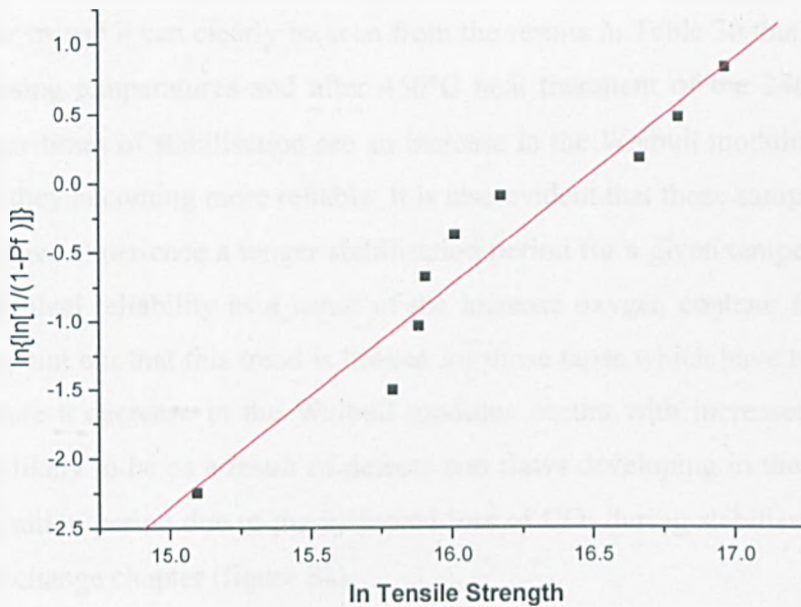


Figure 170 Weibull plot of tensile strength of Green mesophase pitch based carbon tapes

Weibull modulus $m = 1.6$.

Table 30 Average mechanical test values for tapes stabilised under a variety of conditions and tapes which have been stabilised and heat treated to 450°C

| Stabilisation Condition | Load (N) | Displacement (mm) | Strain % | Average Tensile Strength (MPa) | engineering Young's modulus (MPa) | Weibull Modulus |
|-------------------------|----------|-------------------|----------|--------------------------------|-----------------------------------|-----------------|
| Green | 0.3 | 0.06 | 0.3 | 12 | 41 | 1.6 |
| 160°C 5hrs | 0.3 | 0.07 | 0.3 | 14 | 51 | 4.5 |
| 160°C 25hrs | 0.4 | 0.08 | 0.3 | 15 | 50 | 7.6 |
| 240°C 5hrs | 0.5 | 0.08 | 0.3 | 22 | 70 | 7.4 |
| 240°C 25hrs | 0.6 | 0.11 | 0.4 | 24 | 53 | 6.7 |
| 300°C 5hrs | 0.8 | 0.07 | 0.3 | 30 | 101 | 8.8 |
| 300°C 25hrs | 0.8 | 0.06 | 0.3 | 32 | 129 | 10.0 |
| 160°C 5hrs (450°C) | 1.5 | 0.25 | 1.0 | 63 | 64 | 5.8 |
| 160°C 25hrs (450°C) | 1.8 | 0.19 | 0.7 | 76 | 100 | 9.9 |
| 240°C 5hrs (450°C) | 2.8 | 0.40 | 1.6 | 119 | 74 | 12.0 |
| 240°C 25hrs (450°C) | 3.4 | 0.28 | 1.1 | 145 | 129 | 10.8 |
| 300°C 5hrs (450°C) | 3.3 | 0.18 | 0.6 | 104 | 170 | 10.4 |
| 300°C 25hrs (450°C) | 4.2 | 0.13 | 0.3 | 138 | 374 | 9.9 |

Those samples which have a larger Weibull modulus (m) are more reliable than those with a smaller m and it can clearly be seen from the results in Table 30 that at 160°C and 240°C stabilising temperatures and after 450°C heat treatment of the 240°C stabilised samples longer times of stabilisation see an increase in the Weibull modulus of the tapes as a result of them becoming more reliable. It is also evident that those samples (stabilised only) which have experienced a longer stabilisation period for a given temperature exhibit greater mechanical reliability as a result of the increased oxygen content. However, it is important to point out that this trend is broken for those tapes which have been stabilised to 300°C where a decrease in the Weibull modulus occurs with increased stabilisation time. This is likely to be as a result of defects and flaws developing in the tape over the longer stabilisation period due to the increased loss of CO₂ during stabilisation as shown in the weight change chapter (figure 51).

10.3 Mechanical properties: conclusion

The strength of the mesophase pitch-based carbon tapes has been shown to be affected by a number of factors such as oxygen content, stabilisation conditions, heat treatment temperature.

Higher temperatures of stabilisation impart a greater tensile strength to the mesophase pitch-based tapes (table 26), however this is accompanied with a reduction in the maximum % strain. This is likely to be as a result of the formation of the heavily cross-linked mechanically stiff skin-core structure on the surface of the higher temperature stabilised tapes, as characterised in the ThAFM section 7.2, EPMA section 7.3 and optical characterisation section 9.0. The maximum strain to failure for tapes which have not undergone heat treatment to 450°C is achieved by tapes stabilised at 240°C for 25hrs (table 28). In the case of the 160°C and 240°C tape samples increasing time of stabilisation results in an increase in the tensile strength and strain to failure of the tapes (table 28). At 300°C after 25hrs, an increase in tensile strength is still observed accompanied by a decrease in the maximum strain the tapes can sustain before fracture. One possible explanation for this is that at the increased time of stabilisation at

300°C excessive cross linking leads to the development of flaws during the oxidative stabilisation process that act as nucleation sites for cracks to develop in the tapes.

The higher the temperatures of heat treatment the tapes are exposed to the greater the maximum tensile strength of the tapes, shown in table 26. The optimum temperature for the tapes to be heat treated to is 450°C as this offers the largest strain to failure for the tapes making them more durable. When considering how stabilisation conditions affect this optimum heat treatment temperature, it is evident that stabilisation at 240°C over 25hrs gives the best results, not only offers a superior strain to failure for the tapes but also the greatest tensile strength (table 28).

When comparing the oxygen content of tapes to their mechanical properties it is evident after stabilisation and subsequent 450°C heat treatment that the tapes with higher oxygen content exhibit higher tensile strength. However, when considering the engineering Young's modulus of the tapes, the temperature of stabilisation plays a key role. Samples stabilised at lower temperatures show little change or even a slight decrease in their engineering Young's modulus with increasing time of treatment, possibly due to the introduction of some ether or peroxide groups. The 300°C tapes show an increase in the engineering Young's modulus with time of stabilisation, pointing to a stiffening of the material (figure 165). Upon subsequent heat treatment to 450°C, tapes stabilised at each temperature experience a reduction in oxygen content and an increase in their engineering Young's modulus with increasing time and temperature, now perhaps due to a degradation in ether and/or peroxide bonding accompanied by the development of more C-C bonds (figure 165).

It is also evident that those mesophase pitch-based tapes which experienced the longer periods of stabilisation also exhibited the greater mechanical reliability. However, again the 300C stabilised tapes slightly different behaviour by showing a slight decrease in their Weibull modulus. A feasible explanation for this may be as a result of the development of defects and flaws in the tapes over longer periods of stabilisation at the higher 300C as a

11 Overall conclusion

Stabilisation is a complex sequence of competing reactions. Oxygen is clearly key to the stabilisation of the mesophase pitch-based tapes, the extent of the oxygen uptake experienced by the tapes is greatly influenced by temperature, time and atmosphere of the stabilisation, these parameters also dictate the intensity of the gases evolved during the stabilisation step (CO_2 & H_2O).

As oxygen is incorporated into the mesophase-pitch based tapes their chemistry can be seen to change (table 9) at the higher temperatures of stabilisation a greater oxygen content is evident accompanied by a decrease in carbon content. The reduction in carbon content is as a result of the increased intensities of CO_2 evolved at elevated temperatures of stabilisation. The change in chemistry of the mesophase pitch based tapes is also observed in the functional groups present on the surface of the tapes as a result of the different stabilising conditions. This is shown by FTIR and XPS data where increasing aromaticity of the tapes can also be seen in those tapes which display the highest stabilising potential, the greatest of these changes can be observed in those mesophase pitch-based tapes which have been stabilised at 240°C . The incorporation of oxygen into the tapes upon stabilisation not only alters the chemistry of the tapes but also the ordering of the mesophase pitch-based tapes as the oxygen induces structural defects in to them.

A clear correlation between the softening point and oxygen content is evident in the mesophase pitch-based tapes, as oxygen content increases so does the softening point of the tapes. This can be seen to be greatly influenced by the distribution of the oxygen through out the mesophase pitch based tapes which is determined by both temperature and time of stabilisation. At the lower temperatures and extended times of stabilisation greater oxygen penetration is observed, at the higher temperature of 300°C oxygen can only be seen to be incorporated into the tapes at their edges as a result of the development of a skin core structure.

From the outset it was apparent that those mesophase pitch-based tapes which had been stabilised at the higher temperatures and longer periods exhibited the greatest weight losses upon carbonisation and thus offered the lowest final carbon yield. However, in all cases the mesophase pitch-based tapes which have undergone a stabilisation treatment show an improved carbon yield over the unstabilised green tape after carbonisation. The bulk of the weight loss that took place in the tapes during carbonisation occurred between 400-700°C where the bulk of the weight loss occurred due to the loss of carbon and oxygen in the form CO and CO₂, hydrocarbon evolution was also detected but only at the lower temperatures of stabilisation.

Upon partial carbonisation of the mesophase pitch based tapes improvement in structural ordering was observed on both a micro and macro level illustrated by Raman spectra and Pole figures. The greatest improvement in the ordering of the tapes was displayed by the tapes which had seen a 240°C stabilisation temperature. Improved properties can also be observed in the stabilised mesophase pitch based tapes, again tapes which have been stabilised at 240°C for the longer periods of time show a much higher degree of maintained dimensional stability and morphology after carbonisation when examined optically. The mesophase pitch-based tapes which have been stabilised to 160°C show bloating and swelling as the unstabilised mesophase melts during the carbonisation process. At 300°C the tapes display a severe shrinkage with swelling taking place towards the edges causing the tapes to split. This effect is believed to be as the result of the formation of a skin-core structure at the higher stabilising temperatures.

Stabilisation conditions also play a key role in determining the final mechanical properties of the mesophase pitch-based tapes. Higher temperatures of stabilisation can be seen to greatly improve the tensile strength of the tapes, however this comes with a reduction in the maximum strain the tape can withstand. The maximum values of strain to failure were recorded for those tapes which had been stabilised to 240°C for 25hrs. This was also true once the tapes had undergone a heat treatment of 450°C where the 240°C 25hr tapes also displayed the greatest tensile strength. Notably the most mechanically reliable tapes were also the 240°C tapes which had been stabilised for 25hrs.

12 Future work

Stabilisation of mesophase pitch based products is clearly a complex tangled web of competing reactions all of which appear to have an effect on the final properties both chemically and physically of the resultant tapes. As a result of the industrial importance of carbon fibres/tapes and the potential to reduce the processing costs and manipulate the final properties of mesophase products by having a complete understanding of the process, much work can still be done.

Considering the stabilisation step, work could be carried out to assess how the textures induced as a result of different shear rates during the spinning process (Anton-Arulrajah et al 2002) (1-2 or 1-3 textures as discussed in section 5.2) of the mesophase pitch-based tapes effect the extent of the oxygen uptake experience by the tapes for a given temperature and time. This work would help discover how critical the textural orientation of the tapes is in aiding the transport of oxygen into the centre of a mesophase product and may lead to future products being designed with a particular induced texture in order to improve stabilisation.

Again along the theme of the stabilisation step, future work could be carried out on a variety of partial pressures of oxygen with the aim of finding one which offers the best uptake of oxygen into the tape at a given temperature without over oxidising the outer surface of the tapes as a result of an excess presence of oxygen. Understanding this step may also help control the functional groups which form on the outer surface of the mesophase pitch-based tapes.

Other characterisation work which could be carried out in order to understand the effects of stabilisation on the mesophase pitch-based tapes include: A study of how varying stabilisation conditions affect the thermal and electrical properties of the resultant tapes, exploring what affect the inclusion of oxygen atoms into the carbon structure.



Worked could be carried out on how the different surface functionalities which arise as a result of the varying stabilisation conditions affect the inter tape bonding and mechanical strength of laminates produced from the mesophase pitch-based tapes.

Other interesting studies which could be carried out in future work include; some modeling of the microstructure of the mesophase pitch-based tapes with varying quantities of ether linkages incorporated into its structure. Simulations could then be run to investigate how the presence of the ether linkages affects the mechanical properties of the tapes, most notable the strain to failure.

A study of the elements evolved from mesophase pitch-based tapes which have been stabilised under varying conditions during carbonisation could be carried out using a TGA mass spectrometer simulated carbonisation conditions. This accompanied by CHNO chemical analysis, carried out at different temperatures throughout the course of the carbonisation process may well help to further understand the changes that are occurring in the material as a result different stabilisation conditions. This in turn may lead to opportunity to put forward a firm mechanism for the stabilisation reaction.

13 References

- Adams, P. M., Katzman, H. A., (1998). "Characterization of high thermal conductivity carbon fibres and a self-reinforced graphite panel." Carbon 36(3): 233-245.
- Angell, C. L., Lewis I. C. (1978). "Raman spectroscopy of mesophase pitches." Carbon 16(6): 431-432.
- Anton-Arulrajah, A. (2002). "Fabrication and fracture characterisation of carbon/carbon composites". Institute for materials research. Leeds, University of Leeds.
- Anton-Arulrajah, A. Westwood., A. Rand, B. (2006). "The influence of mesophase pitch melt-spinning condition on the cross-sectional geometry and bulk packing properties of carbon tapes". Carbon 06, Aberdeen, Scotland.
- Aslam, Z. (2006). "Carbon nanotubes production by the catalytic method." PhD Thesis, Institute for Material Research. Leeds, University of Leeds.
- Bacon, R.. (1979). "Carbon Fibres from Mesophase Pitch" Phil. Trans. Roy. Soc. London Ser A. January 21, 1980, 294:437-442.
- Benn, M. (1989). "Pitch - mesophase - carbon transformation diagrams and the fabrication of carbon materials". PhD Thesis, Sheffield, University of Sheffield.
- Birleson, R. (2004). "The Stabilisation of pitch based carbon tapes using NMR." Undergraduate project, Leeds, University of Leeds.
- Blanco, C. (2001). "Application of scanning thermal microscopy and micro-thermal analysis to the study of carbon materials and their precursors." Departmental report, Leeds, University of Leeds.
- Blanco, C., Lu, S. (2002). "Micro-thermal analysis as a technique for in situ characterisation of the softening behaviour of the isotropic phase and mesophase in thermally treated pitches." Carbon 40(1): 132-135.
- Blanco, C., Lu, S. (2003). "The stabilisation of carbon fibres studied by micro-thermal analysis." Carbon 41(1): 165-171.
- Bradley, R. H., Ling, X. (1993). "An investigation of carbon fibre surface chemistry and reactivity based on XPS and surface free energy." Carbon 31(7): 1115-1120.
- Brooks, J. D. Taylor, G. H. (1965). "The formation of graphitizing carbons from the liquid phase." Carbon 3(2): 185-186.
- Cato, A. D., Edie, D. D. (2003). "Flow behaviour of mesophase pitch." Carbon 41(7): 1411-1417.
- Cervantes-Uc, J. M., Cauich-Rodriguez, J. V., (2006). "TGA/FTIR study on thermal degradation of polymethacrylates containing carboxylic groups." Polymer Degradation and Stability 91(12): 3312-3321.
- Chioujones, K. M., Ho, W. (2006). "Microstructural analysis of in situ mesophase transformation in the fabrication of carbon-carbon composites." Carbon 44(2): 284-292.
- Cho, D., Ha, H. S. (1996). "Microstructural evidence for the thermal oxidation protection of carbon/phenolic towpregs and composites." Carbon 34(7): 861-868.
- Cho, T., Lee, Y. S. (2003). "Structure of carbon fiber obtained from nanotube-reinforced mesophase pitch." Carbon 41(7): 1419-1424.

- Collins, S. (2005). "Advanced Biocompatible Endovascular Stents. Leeds, Leeds, University." Departmental report, Leeds, University of Leeds.
- Cornec, L. P., Fain, C. C. and Edie, D. D. (1992). Carbon, Essen Germany.
- Crespo, J. L. Arenillas, A. (2004). "A study of mesophase formation from a low temperature coal tar pitch using formaldehyde as a promoter for polymerisation." Carbon 42(12-13): 2762-2765.
- Curbishley, L. (1998). "Characterisation of high-temperature materials by mechanical testing." Institute of Materials.
- Daniels, H. R. (2003). "Novel Characterisation Techniques for Carbonaceous Materials In The FEGTEM". PhD Thesis, Institute for Materials Research. Leeds, University of Leeds.
- De la Puente, G., Pis, J. J. (1997). "Thermal stability of oxygenated functions in activated carbons." Journal of Analytical and Applied Pyrolysis 43(2): 125-138.
- Dhami, T. L., Manocha, L. M. (1991). "Oxidation behaviour of pitch based carbon fibres." Carbon 29(1): 51-60.
- Diefendorf, R. J. (2000). "Pitch Precursor Carbon Fibres" Comprehensive Composite Materials. Kelly, A. and Zweben, C. Oxford, Pergamon: 35-83.
- Dinwiddie, R. B. P., West, P. E. (1994). "Thermal conductivity 22 ed T W Tong (Lancaster PA: Technoics)." 668.
- Donnet, J. B., (1984). "Carbon Fibres."
- Drbohlav, J. Stevenson W. T. K. (1995). "The oxidative stabilization and carbonization of a synthetic mesophase pitch, part I: The oxidative stabilization process." Carbon 33(5): 693-711.
- Dresselhaus, M. S., Fung, A. W. P. (1992). "New characterization techniques for activated carbon fibres." Carbon 30(7): 1065-1073.
- Dresselhaus, M. S., Jorio, A. (2002). "Raman spectroscopy on one isolated carbon nanotube." Physica B: Condensed Matter (Amsterdam, Netherlands) 323(1-4): 15-20.
- Dumont, M., Chollon, G. (2002). "Chemical, microstructural and thermal analyses of a naphthalene-derived mesophase pitch." Carbon 40(9): 1475-1486.
- Dumont, M., Dourges, M.-A. (2005). "Carbonization behaviour of modified synthetic mesophase pitches." Carbon 43(11): 2277-2284.
- Edie, D. D. (1998). "The effect of processing on the structure and properties of carbon fibres." Carbon 36(4): 345-362.
- Edie, D. D., Fox, N. K. (1986). "Melt-spun non-circular carbon fibres." Carbon 24(4): 477-482.
- Edie, D. D., Robinson, K. E. (1994). "High thermal conductivity ribbon fibres from naphthalene-based mesophase." Carbon 32(6): 1045-1054.
- Edie, D. D. (1989). "Melt Spinning Pitch Based Carbon Fibres." Carbon 27 (5): 647-655.
- Fanjul, F., Granda, M. (2001). "Assessment of the oxidative stabilisation of carbonaceous mesophase by thermal analysis techniques." Journal of Analytical and Applied Pyrolysis 58-59: 911-926.
- Fanjul, F., Granda, M. (2002). "On the chemistry of the oxidative stabilization and carbonization of carbonaceous mesophase." Fuel 81(16): 2061-2070.

- Fathollahi, B. Didwania, A. K.J., B. Chau, P. C. White, J. L. (2005). "Mesophase stabilisation at low temperature and elevated oxygen pressure." 229th ACS National Meeting, San Diego, CA, United States.
- Fathollahi, B. W., Didwania, J. L., A. K. Chau, P. C. (2001). "Mesophase stabilisation at low temperatures and elevated oxidation pressures." International Conference on Carbon, Lexington, KY, United States.
- Fitzer, E. (1989). "Pan-based carbon fibres--present state and trend of the technology from the viewpoint of possibilities and limits to influence and to control the fiber properties by the process parameters." Carbon 27(5): 621-645.
- Fortin, F., Yoon, S.-H. (1994). "Structure and properties of thin, slit-shaped carbon fibres prepared from mesophase pitch." Carbon 32(6): 1119-1127.
- Galanopoulos, E. (2003). "Synthesis and characterisation of highly orientated mesophase pitch composites." PhD Thesis Institute for Materials. Leeds, University of Leeds.
- Gallego, N. C., Edie, D. D. (2000). "The thermal conductivity of ribbon-shaped carbon fibres." Carbon 38(7): 1003-1010.
- Gerard Lavin, J. (1992). "Chemical reactions in the stabilization of mesophase pitch-based carbon fiber." Carbon 30(3): 351-357.
- Hamada, T., Nishida, T. (1988). "Transverse structure of pitch fiber from coal tar mesophase pitch." Carbon 26(6): 837-841.
- Hamada, T., Tomioka T. (1993). "Periodic column arrangement in pitches." Carbon 31(1): 235-236.
- Hammiche, A. P., Song, H. M., Hourston, M. (1996). Meas. Sci. Technol. 7: 142.
- Hayashi, J.-I., Nakashima, M. (1995). "Rapid stabilization of pitch fiber precursor by multi-step thermal oxidation." Carbon 33(11): 1567-1571.
- Hutchenson, K. W., Roebbers, J. R., (1991). "Fractionation of petroleum pitch by supercritical fluid extraction." Carbon 29(2): 215-223.
- Jayatilaka (1979). "Fracture of brittle materials". London, Applied science publisher Ltd.
- Jones, J. M., Ross, A. B., Williams, A. (2006). "Principles and Applications of Pyrolysis-GC-MS." Encyclopaedia of Mass Spectrometry, Volume 8: Hyphenated methods. M.A.Niessen, W.
- Kanno, K., Fernandez, J. J. (1997). "Modifications to carbonization of mesophase pitch by addition of carbon blacks." Carbon 35(10-11): 1627-1637.
- Kaushik, V. K. and Bhardwaj, A. (1994). "Characterization of carbon fibre surfaces using electron spectroscopy for chemical analysis." Polymer Testing 13(4): 355-362.
- Ko, T.-H., Chiranairadul, P. (1992). "The effects of activation by carbon dioxide on the mechanical properties and structure of PAN-based activated carbon fibres." Carbon 30(4): 647-655.
- Korai, Y., Hong, S.-H. (1999). "Development of longitudinal mesoscopic textures in mesophase pitch-based carbon fibres through heat treatment." Carbon 37(2): 203-211.
- Korai, Y. and Mochida, I. (1985). "Preparation and properties of carbonaceous mesophase-i soluble mesophase produced from A240 and coal tar pitch." Carbon 23(1): 97-103.
- Kowbel, W., Wapner, P. G. (1988). "A study of the oxidation of mesophase." Journal of Physics and Chemistry of Solids 49(11): 1279-1285.

- Kwak, S.-Y., Ahn, D. U (2004). "Amelioration of mechanical brittleness in hyperbranched polymer. 1. Macroscopic evaluation by dynamic viscoelastic relaxation." Polymer 45(20): 6889-6896.
- Lavin, G. J. (1992). "Chemical reactions in the stabilization of mesophase pitch-based carbon fiber." Carbon 30(3): 351-357.
- Lewis, R. T. (1993). 22nd Conf. of the North Amer. Thermal Analysis Soc., Denver.
- Lin, S. S. (1991). "Oxidative stabilization in production of pitch based carbon fiber." Sample J 27: 9-14.
- Lu, S. (2002). Fabrication and characterisation of highly orientated mesophase based graphite (HOMG) tapes and large diameter carbon filaments. Leeds, University of Leeds.
- Lu, S., Blanco, C. (2002). "Large diameter carbon fibres from mesophase pitch." Carbon 40(12): 2109-2116.
- Lu, Y.-G., Wu, D. (1998). "Skin-core structure in mesophase pitch-based carbon fibres: causes and prevention." Carbon 36(12): 1719-1724.
- Machnikowski, J., Machnikowska, H. (2002). "Mesophase development in coal-tar pitch modified with various polymers." Journal of Analytical and Applied Pyrolysis 65(2): 147-160.
- Maeda, T., Ming Zeng, S. (1993). "Preparation of isotropic pitch precursors for general purpose carbon fibres (GPCF) by air blowing--I. Preparation of spinnable isotropic pitch precursor from coal tar by air blowing." Carbon 31(3): 407-412.
- Majumdar, A. (1998). "Thermal microscopy and heat generation in electronic devices." Microelectronics and Reliability 38(4): 559-565.
- Matsumoto, T. and Mochida, I. (1993). "Oxygen distribution in oxidatively stabilized mesophase pitches fiber." Carbon 31(1): 143-147.
- Matsumoto, T. M., I. (1992). "A structural study on oxidative stabilization of mesophase pitch fibres derived from coal tar." Carbon 30: 1041-1046.
- McHugh, J. J. and D. D. Edie (1996). "The orientation of mesophase pitch during fully developed channel flow." Carbon 34(11): 1315-1322.
- Miura, K., Nakagawa, H. (1995). "Examination of the oxidative stabilization reaction of the pitch-based carbon fiber through continuous measurement of oxygen chemisorbtion and gas formation rate." Carbon 33(3): 275-282.
- Mochida, I. (1995). Application of synthetic mesophase pitch (AR pitch) catalytically produced from aromatic hydrocarbons with a super acid HF-BF₃, Mitsubishi Gas Chemical Company Inc & Kyushu University.
- Mochida, I., Korai, Y. (2000). "Chemistry of synthesis, structure, preparation and application of aromatic-derived mesophase pitch." Carbon 38(2): 305-328.
- Mochida, I., Kudo, K. (1975). "Carbonization of pitches--IV : Carbonization of polycyclic aromatic hydrocarbons under the presence of aluminium chloride catalyst." Carbon 13(2): 135-139.
- Mochida, I., Zeng, S.-M. (1991). "The introduction of a skin-core structure in mesophase pitch fibres through a successive stabilization by oxidation and solvent extraction." Carbon 29(1): 23-29.
- Mochida, I., Zeng, S.-M. (1990). "The introduction of a skin-core structure in mesophase pitch fibres by oxidative stabilization." Carbon 28(1): 193-198.

- Montes-Moran, M. A., Crespo, J. L. (2002). "Mesophase from a coal tar pitch: a Raman spectroscopy study." Fuel Processing Technology **77-78**: 207-212.
- Mora, E., Santamaria, R. (2003). "Mesophase development in petroleum and coal-tar pitches and their blends." Journal of Analytical and Applied Pyrolysis **68-69**: 409-424.
- Moreton, R. and Watt W. (1974). "The spinning of polyacrylonitrile fibres in clean room conditions for the production of carbon fibres." Carbon **12(5)**: 543-554.
- Moriyama, R., Hayashi, J.-I. (2004). "Effects of quinoline-insoluble particles on the elemental processes of mesophase sphere formation." Carbon **42(12-13)**: 2443-2449.
- Moriyama, R., Hayashi, J.-I. (2002). "Analysis and modeling of mesophase sphere generation, growth and coalescence upon heating of a coal tar pitch." Carbon **40(1)**: 53-64.
- Otain, S., Y. Koitabashi, T. (1970). Bull Chem. Soc Jpn: 3291-2.
- Paiva, M. C., Bernardo, C. A. (2001). "A comparative analysis of alternative models to predict the tensile strength of untreated and surface oxidised carbon fibres." Carbon **39(7)**: 1091-1101.
- Paiva, M. C., Bernardo, C. A. (2000). "Mechanical, surface and interfacial characterisation of pitch and PAN-based carbon fibres." Carbon **38(9)**: 1323-1337.
- Paiva, M. C., Kotasthane, P. (2003). "UV stabilization route for melt-processible PAN-based carbon fibres." Carbon **41(7)**: 1399-1409.
- Park, Y. D., Mochida, I. (1988). "Extractive stabilization of mesophase pitch fiber." Carbon **26(3)**: 375-380.
- park, Y. D. T., Koria, H. Mochida, Y. (1988). "Rapid stabilisation of mesophase pitch based carbon fibre by solvent extraction and successive oxidation." Journal of Material Science: 1318-1320.
- Pelletier, M. J. (1999). "Analytical applications of Raman spectroscopy", Blackwell Science.
- Pimenta, M. A., Jorio, A. (2001). "Diameter dependence of the Raman D-band in isolated single-wall carbon nanotubes." Physical Review B: Condensed Matter and Materials Physics **64(4)**: 041401/1-041401/4.
- Pollock, H. M. H., A. (2001). "Micro-thermal analysis: techniques and applications." Journal of Physics D: Applied Physics **34**: R23-R53.
- Rand, B. (1985). "Carbon fibres from mesophase pitch in strong fibres". Handbook of composites, vol Strong Fibres, editors W, Watt & B, V, Perov, Elsevier. Amsterdam. Chapter 13, 495-570
- Reich, S., Thomsen, C. (2004). Carbon Nanotubes: Basic Concepts and Physical Properties.
- Richardson, J. H. (1971). "Optical microscopy for material sciences", Marcel Dekker, N.Y.
- Rogovoi, V. N. and Y. B. Amerik (1993). "Raman scattering study of mesophase pitch." Vibrational Spectroscopy **4(2)**: 167-173.
- Sansom, J. (2004). "Development of highly orientated carbon tapes." undergraduate report Leeds, University of Leeds.



- Singer, L. S., Barr, J. B., Chwasriak, S., Didchenko, R., Lewis, I.C. (1976). Applied Polymer Symposium 29: 161.
- Singer, L. U. and Mitchell S. (1997). "Diffusion of oxygen into pitch." Carbon 35(5): 599-604.
- Smith, G. W., White, J. L. (1985). "Mesophase/isotropic phase interfacial energy: Determination from coalescence kinetics of mesophase pitch." Carbon 23(1): 117-121.
- Stevens, W. C., Diefendorf, R. J. (1986). Carbon 86 Proceedings of International Conference on Carbon Baden-Baden Der Deutschen Keramische Gesellschaft, Bad Honnef: 37-42.
- Strehlow, R., A. (1970). US Oak Ridge National Laboratory Report No ORNL-4622 Molten Salt Reaction: 135-141.
- Trollsas, M. H., J. L. (1998). Macromolecules 31:4390.
- Van Krevelen, D., W. Schuyer, J. (1957). "Coal Science: Aspects of coal constitution", Elsevier Publishing Co, Princeton NJ.
- Vilaplana-Ortego, E., Alcaniz-Monge. J. (2003). "Stabilisation of low softening point petroleum pitch fibres by HNO₃." Carbon 41(5): 1001-1007.
- Wang, Y., Alsmeyer, D. C. (1990). "Raman spectroscopy of carbon materials: structural basis of observed spectra." Chemistry of Materials 2(5): 557-63.
- Wang, Y.-G., Korai, Y. (2001). "Modification of synthetic mesophase pitch with iron oxide, Fe₂O₃." Carbon 39(11): 1627-1634.
- Wickramasinghe, H. K. (2000). "Progress in scanning probe microscopy." Acta Materialia 48(1): 347-358.
- Wilkie, C. A. (1999). "TGA/FTIR: an extremely useful technique for studying polymer degradation." Polymer Degradation and Stability 66(3): 301-306.
- Williams, C. C. and Wickramasinghe H. K. (1986). "Scanning thermal profiler." Microelectronic Engineering 5(1-4): 509-513.
- Xie, Y., M., Wang, T, J., Franklin, O. Sherwood, P, M, A., (1992). "X-ray photoelectron spectroscopic studies of carbon-fiber surfaces. 15. core-level and valence-band studies of pitch-based fibres electrochemically treated in ammonium carbonate solution." Applied Spectroscopy 46(4): 645-651.
- Yamada, Y., M, S. Fukuda, N. Honda, H. (1981). TANSO 107: 135-139.
- Yan, J. and Rey A. D. (2002). "Theory and simulation of texture formation in mesophase carbon fibres." Carbon 40(14): 2647-2660.
- Yanagida, K. Y., H. Take, K. (1989). "Preprint of the 16th annual meeting Carbon Society of Japan."
- Yang, C. Q. Simms J. R. (1993). "Infrared spectroscopy studies of the petroleum pitch carbon fiber--I. The raw materials, the stabilization, and carbonization processes." Carbon 31(3): 451-459.
- Yang, K. S., Kim, Y. A. (1997). "Modification of naphthalene-derived mesophase pitch with benzoquinone." Carbon 35(7): 923-928.

14 Publications resulting from this work

Anton-Arulrajah, A. Westwood, A. Galanopoulos, E. Eagles, A. Sansom, J. Rand, B. "Wide, highly oriented mesophase pitch-based carbon tapes: Mechanical properties of the tapes and of tape-derived carbon springs", "Carbon 2004", Providence RI, USA, July 2004, Extended Abstract CD-ROM (file M070.pdf), Session 35, Precursor chemistry: pitch behavior, Paper M070 (2004).

Westwood, A. Collins, S. Sansom, J. Clarenc, R. Anton-Arulrajah, A. Rand, B. "The oxidative stabilisation process in mesophase pitch-derived tapes and tracking of its effect on their mechanical properties", "Carbon 2005", Gyeongju, Korea, July 2005, Extended Abstract CD-ROM (file S05-05-EX.pdf), Session E, Industrial carbons, Paper S05-05 (2005).

Sansom, J. A. Collins, S. Westwood, A. Clarenc, R. Anton-Arulrajah, A. and Rand, B. "Effect of oxidative stabilisation conditions on the carbon yield from mesophase pitch-based fibres and tapes", "Carbon 2006", Aberdeen, Scotland, July 2006, Extended Abstract CD-ROM (file 9D5_Sansom.pdf), Session 9D, Pyrolysis and thermal processes, Oral 9D5 (2006).

Sansom, J.A. Westwood, A.V.K. and Rand, B. "Surface analytical characterisation of the oxidative stabilisation process in mesophase pitch-based carbon tapes", The International Carbon Conference, July 2007, Seattle, USA, Extended Abstract CD-ROM (file A154.pdf), Session A, Characterization of Carbon Materials Properties – Fibres and Composites, Paper A154 (2007).

Ross, A.B. Sansom, J.A. Westwood, A.V.K. Rand, B. and Jones, J.M. "Investigation of pitch stabilisation using pyrolysis-gas chromatography-mass spectrometry", , The International Carbon Conference, July 2007, Seattle, USA, Extended Abstract CD-ROM (file P097.pdf), Poster Session 2, Poster P097 (2007).

15 Appendix

15.1 raw data for elemental change in weight with stabilisation at 160°C, 180°C 200°C, 240°C and 300°C with respect to time of oxidative stabilisation. The discrepancy between the weight change calculated by addition of elemental constituents from CHNO analysis and that arrived at by direct weighing is due to the fact that the CHNO component analyses although close to 100%, never totaled 100% exactly.

Table 31 Raw data for CHO weight change for stabilisation at 160°C with respect to time of oxygen stabilised samples

| Temperature | Time (hrs) | C % Weight Change | H % Weight Change | O % Weight Change | Overall % Weight Change |
|-------------|------------|-------------------|-------------------|-------------------|-------------------------|
| 160°C | 0 | 0 | 0 | 0 | 0 |
| 160°C | 5 | -0.1 | -0.1 | 4.9 | 4.7 |
| 160°C | 10 | -3.1 | -0.7 | 9.0 | 5.2 |
| 160°C | 15 | -2.2 | -0.7 | 10.1 | 7.2 |
| 160°C | 20 | -1.9 | -0.8 | 11.5 | 8.8 |
| 160°C | 25 | -2.0 | -0.8 | 12.7 | 9.9 |

Table 32 Raw data for CHO weight change for stabilisation at 180°C with respect to time of oxygen stabilised samples

| Temperature | Time (hrs) | C % Weight Change | H % Weight Change | O % Weight Change | Overall % Weight Change |
|-------------|------------|-------------------|-------------------|-------------------|-------------------------|
| 180°C | 0 | 0 | 0 | 0 | 0 |
| 180°C | 5 | -2.4 | -0.4 | 7.0 | 4.2 |
| 180°C | 10 | -6.9 | -1.1 | 13.7 | 5.7 |
| 180°C | 15 | -7.0 | -1.4 | 16.2 | 7.7 |
| 180°C | 20 | -7.2 | -1.4 | 16.4 | 7.9 |
| 180°C | 25 | -7.1 | -1.3 | 17.5 | 9.1 |

Table 33 Raw data for CHO weight change for stabilisation at 200°C with respect to time of oxygen stabilised samples

| Temperature | Time (hrs) | C % Weight Change | H % Weight Change | O % Weight Change | Overall % Weight Change |
|-------------|------------|-------------------|-------------------|-------------------|-------------------------|
| 200°C | 0 | 0 | 0 | 0 | 0 |
| 200°C | 5 | -3.9 | -0.4 | 10.1 | 5.8 |
| 200°C | 10 | -4.8 | -0.8 | 13.6 | 8.1 |
| 200°C | 15 | -6.1 | -1.0 | 16.9 | 9.9 |
| 200°C | 20 | -6.9 | -1.2 | 18.4 | 10.4 |
| 200°C | 25 | -7.2 | -1.3 | 19.2 | 10.7 |

Table 34 Raw data for CHO weight change for stabilisation at 240°C with respect to time of oxygen stabilised samples

| Temperature | Time (hrs) | C % Weight Change | H % Weight Change | O % Weight Change | Overall % Weight Change |
|-------------|------------|-------------------|-------------------|-------------------|-------------------------|
| 240°C | 0 | 0 | 0 | 0 | 0 |
| 240°C | 5 | -4.3 | -1.2 | 13.9 | 8.72 |
| 240°C | 10 | -3.2 | -1.7 | 16.4 | 11.8 |
| 240°C | 15 | -5.9 | -2.0 | 21.2 | 13.73 |
| 240°C | 20 | -8.6 | -2.2 | 23.6 | 13.08 |
| 240°C | 25 | -10.5 | -2.3 | 25.5 | 13.02 |

Table 35 Raw data for CHO weight change for stabilisation at 300°C with respect to time of oxygen stabilised samples

| Temperature | Time (hrs) | C % Weight Change | H % Weight Change | O % Weight Change | Overall % Weight Change |
|-------------|------------|-------------------|-------------------|-------------------|-------------------------|
| 300°C | 0 | 0 | 0 | 0 | 0 |
| 300°C | 5 | -13.3 | -2.0 | 22.5 | 7.3 |
| 300°C | 10 | -14.4 | -2.0 | 25.0 | 8.6 |
| 300°C | 15 | -17.7 | -2.1 | 28.0 | 8.3 |
| 300°C | 20 | -20.5 | -2.4 | 29.3 | 6.4 |
| 300°C | 25 | -22.5 | -2.5 | 29.4 | 4.4 |